MENDEL UNIVERSITY IN BRNO
FACULTY OF AGRISCIENCES

DISSERTATION THESIS

Brno 2017 **Ing. Vedran Milosavljević**

Mendel University in Brno
Faculty of AgriSciences
Department of Chemistry and Biochemistry

Synthesis of peptides and their application for cell penetration and drug delivery

Dissertation thesis
Branch of study: 4106V017 Agricultural Chemistry

Supervisor:
Doc. RNDr. Pavel Kopel, Ph.D.

Specialist supervisor:
Prof. RNDr. Vojtěch Adam, Ph.D.

Author:
Ing. Vedran Milosavljević

Brno 2017

Declaration

I hereby declare that, this thesis entitled “Synthesis of peptides and their application for cell penetration and drug delivery” was written and completed by me. I also declare that all the sources and information used to complete the thesis are included in the list of references. I agree that the thesis could be made public in accordance with Article 47b of Act No. 111/1998 Coll., Higher Education Institutions and on Amendments and Supplements to Some Other Acts (the Higher Education Act), and in accordance with the current Directive on publishing of the final thesis.

I am aware that my thesis is written in accordance to Act. 121/2000 Coll., on Copyright and therefore Mendel University in Brno has the right to conclude licence agreements on the utilization of the thesis as a school work in accordance with Article 60(1) of the Copyright Act.

Before concluding a licence agreement on utilization of the work by another person, I will request a written statement from the university that the licence agreement is not in contradiction to legitimate interests of the university, and I will also pay a prospective fee to cover the cost incurred in creating the work to the full amount of such costs.

In Brno date:……..

……
signature

Tato práce vznikla v rámci CEITEC - Středoevropského technologického institutu s pomocí výzkumné infrastruktury financované projektem CZ.1.05/1.1.00/02.0068 z Evropského fondu regionálního rozvoje.

EUROPEAN UNION
EUROPEAN REGIONAL DEVELOPMENT FUND
INVESTING IN YOUR FUTURE

OP Research and
Development for Innovation

Acknowledgements

I would like to express my gratitude to all the people who have supported and helped me through my PhD work.

I would like to thank to Professor **Vojtech Adam** for accepting me into the group and giving me the opportunity to gain more knowledge and professional experience.

I would like to thank to Docent **Pavel Kopel** for valuable advices, help, support and professional guidance in processing of this thesis.

I would like to thank to all my colleagues (past and present members of the group) from Department of Chemistry and Biochemistry (DCB), their cooperation and professionalism.

I would like to thank to my wife and best friend **Katarina Milosavljević** for her patience, constant support and belief in me and my dreams!

Anotace

Biologická funkce a přežití buněk jsou spojeny s ničím nerušenou funkcí buněčné membrány. Hydrofobní povaha její lipidové dvojvrstvy chrání buňky před nežádoucím vstupem molekul. To také omezuje příjem terapeutických molekul, včetně nukleových kyselin, proteinů, nano-sloučenin, drobných léčiv (doxorubicin, cisplatina, taxol a cyklosporin). Dodání terapeutických molekul ke konkrétním intracelulárním cílům a neomezené zvýšení propustnosti membrány může být dosaženo použitím transportérů. Použití penetračních peptidů (CPP) pro dodávání léčiv představuje bezpečný způsob, jak dodat léky s minimálním toxickým účinkem a zároveň obejít problém biologické dostupnosti léčiva. CPP jsou schopny dodat různé kovalentně nebo nekovalentně konjugované léčiva, jež samy nemají schopnost proniknout do buněk, k široké škále intracelulárních a dokonce i intranukleárních cílů. Cílem této práce bylo navrhnout a zkonstruovat naložený nanotransportér složený z penetračních peptidů a známého nebo nového, potenciálně terapeutického léčiva, popsat tvorbu vazby mezi penetračním peptidem a terapeutickými molekulami a účinně doručit léčiva. CPP byly vyrobeny syntézou na pevném nosiči za použití mikrovlnné metody, přičemž čištění bylo provedeno rychlou proteinovou kapalinovou chromatografií (FPLC). Kapacita vázaní a uvolňování léčiva byla pozorována za podmínek, které odpovídají těm v extracelulárním a intracelulárním prostředí. Interakce mezi CPP a léčivy byla zkoumána za použití MALDI-TOF MS, Fourierovy infračervené spektroskopie (FTIR) a elektrochemické metody. Účinky konjugátů byly testovány na lidských a bakteriálních buňkách. Tato studie ukazuje aplikaci penetračních peptidů s cílem popsat strategii buněčně specifického doručení léků a zvýšenou aktivaci léčiv změnou fyziologických podmínek. Také bylo ukázáno, že existuje značný potenciál peptidů jako transportérů léčiva, které by mohly být užitečné v budoucnu jako multifunkční činidlo v selektivní terapii různých nemocí.

Klíčová slova: penetrační peptidy, syntéza na pevné fázi, transport léčiv, vazebná kapacita, uvolňování léků, terapeutické molekuly

Annotation

Biological function and survival of cells is connected with undisturbed function of cellular membrane. The cells are protected from unwanted molecules entry by hydrophobic nature of cell membrane lipid bilayer. This also limits the uptake of therapeutics molecules including nucleic acids, proteins, nano-compounds, small drugs (doxorubicin, cisplatin, taxol, and cyclosporine). Delivery of therapeutics molecules to specific intracellular targets and increasing of membrane permeability without limitations can be accomplished by using delivery vectors. Application of cell penetrating peptides (CPPs) for drug delivery represent a safety way how to deliver drug with minimal toxicity effect and bypass the problem of drug bioavailability. CPPs are able to deliver various cell-impermeable covalently or non-covalently conjugated cargos to a wide range of intracellular and even intranuclear targets. The purpose of this work was to design and construct a loaded nanocarrier composed of CPPs and known or new potentially new therapeutic drugs, to describe the formations of bonds between CPPs and therapeutic molecule and effective delivering of drugs. Production of CPPs was done by solid phase synthesis using microwave assisted method and purification was done by fast protein liquid chromatography (FPLC). Drug binding capacity and release was observed under the conditions corresponding to the ones in extracellular and intracellular environment. Interaction between CPPs and drugs was investigated by using MALDI-TOF MS, FTIR and electrochemical method. The delivery effects of conjugates were tested on human and bacterial cells. The present study demonstrates applications of cell penetrating peptides for cell-specific delivery strategies and increasing the activation of drugs by changing physiological conditions. Moreover, we show the considerable potential of peptides as carriers for drug-delivery, which could be helpful in the future as multifunctional agent in selective therapy for various disease treatments.

Key words: Cell penetrating peptides, solid phase synthesis, drug delivery, binding capacity, drug release, therapeutic molecules.

CONTENTS

1. INTRODUCTION

The normal function and survival of cells is highly dependent on effectivity of semi permeable cellular membrane. The cells are protected from unwanted molecules entry by hydrophobic nature of cell membrane lipid bilayer. Delivery of different molecule types to cells is often limited by high selectivity of cell membrane and the size of molecules. Small molecules have the ability to enter the cell without limitation through channels and pores of membrane. However, this mode of access cannot be used for macromolecules, due to their size, which can limit their usage for biomedical research and application.

During the last two decades of search for new drug delivery systems, it has been found that various peptides have excellent possibilities for intracellular delivery of a wide range of macromolecules. One of the first peptide was discovered by Frankel & Pabo in 1988, who indicated that 86 amino acid sequences from Human Immunodeficiency Virus (HIV) Trans-activator of transcription (Tat) protein possess ability to internalize live cells. In 1991 Joliot and his group discovered 60 amino acid homeodomain from Antennapedia protein of *Drosophila* with the same ability of membrane translocation. Further investigations on this homeodomain have led to discovery that the third helix in the structure does not influence membrane translocation, which resulted in amino acid number reduction to 16 and producing of the first cell penetrating peptide (CPPs) called penetratin or pAntp. Besides penetratin and TAT discovery, a large number of peptides has been found and added to CPPs family, which includes classes of cationic, amphipathic, hydrophobic, and anionic CPPs. Today, CPPs represent promising delivery vectors, which do not exceed more than 30 residues in length and can easily translocate over cell membrane in non-toxic concentrations, carrying various cargo without limitation. CPPs sequences are mostly chosen from protein transduction domains and they can be either naturally derived, designed, or chimera sequences. However, naturally derived peptides show limitation due to poor expression in bacteria. Therefore, solid phase peptide synthesis (SPPS) pioneered by Robert Bruce Merrifield, represents nowadays the standard in peptide synthesis in controlled conditions. SPPS is renowned method due to its low time consumption, high yield and purity of synthetized peptide, ability to incorporate unnatural amino acids, peptide modification and desired peptide sequence.

2. AIMS

- Summarization of the literature about cell penetrating peptide.
- Investigation of cell penetrating peptide usage in drug delivery.
- The conjugation of cell penetrating peptide with potential drugs and their in vitro study
- Studying modification of cell penetrating peptide on the toxicity effect and mode of action on human cells.

3. LITERARY OVERVIEW

3.1. Cell penetrating peptides (CPPs)

Cell penetrating peptides (CPPs) are defined as amphiphilic peptides with typically 3 to 30 amino acids in sequence, which are able to pass cell membrane in energy-independent manner, by receptor mediated mechanism [1, 2]. CPPs are mostly rich with net of positively charged amino acids (Arginine and Lysine), that allows them to interact with negatively charged cell membrane surface components (Glycosaminoglycan's (GAGs) and sialic acids) by electrostatic force, in order to pass cell membrane [3, 4]. Depending on author, CPPs can also be described with the name "protein transduction domain (PTD)" or "membrane translocation sequence (MTS)". These alternative names explain that most of the CPPs are derived from protein sequence responsible for its membrane translocation, in comparison with designed CPPs [5-7]. However, although there are several mechanisms of CPPs membrane translocation proposed, it is still not clear how CPPs translocation through membrane occurs. The greatness of the CPPs is reflected in the variety of their application [8], exceptionally as carrier for delivery of various materials across cell membrane such us siRNA [9], nucleic acid [10], small molecule therapeutic agents [11], proteins [12], quantum dots [13], and MRI contrast agents [14]. Moreover, many studies have shown low toxicity of CPPs in comparison with other transporters, regardless of cell line [15]. Due to the low toxicity and potential for variable modification design, CPPs present excellent biological material for medical application. Therefore, application of CPPs, especially in the field of drug delivery, will be a subject of great interest in the future.

3.2. Classification of CPPs

The final classification and terminology for CPPs has not yet been established. However, per non-official classification, established by different authors in their publications, CPPs can be classified according to their individual properties such as: origin, function, sequence, mechanism of uptake, and biomedical application. Alongside with this classification, most of publications divide CPPs into two groups - by origin and physical-chemical properties [16-18].

3.2.1. Classification of CPPs by origin

The discovery of 86 amino acid sequences Trans-activator of transcription (Tat) protein from Human Immunodeficiency Virus (HIV) and their ability to internalize live cells without any limitation, has opened a new door for use of natural proteins domains for medical purposes [19]. These have led to discovery of 60-amino-acid-homeodomain from Antennapedia protein of Drosophila, with the same ability of membrane translocation [20]. Further investigations on this homeodomain lead to discovery that the third helix in structure does not have any influence on membrane translocation, which resulted in reducing of amino acid number to 16 and synthetizing of the first cell penetrating peptide (CPPs), called penetratin or pAntp [21]. Thus, CPPs are being divided into two groups: protein-derived CPPs and designed/chimeric CPPs.

3.2.1.1. Protein-derived CPPs

Natural protein motifs present a large source of protein-derived CPPs. The protein-derived CPPs are isolated from protein transduction domains or membrane translocation sequences. Usually, motifs consist of the minimal effective partial sequence of the translocation protein [22]. Many of the protein-derived CPPs have ability to bind protein on membrane surface, for instance to glycosaminoglycan (GAGs). Protein-derived CPPs can be isolated from heparin-binding protein, belonging to glycosaminoglycan (GAGs) family of carbohydrates, such as superoxide dismutase (DPV3 and DPV3/10), epidermal-like growth factors (DPV7–DPV7b), platelet derived growth factor (DPV6), intestinal mucin (DPV10/6), apolipoprotein B (DPV1047), and CAP 37 (DPV15–DPV15b) [23]. Deoxyribonucleic acid (DNA) and ribonucleic acid (RNA) binding proteins also have the ability to bind to GAGs, thanks to their cationic motifs. The most famous protein-derived CPPs from DNA/RNA binding proteins are Tat, Rev and FHC [24]. Penetratin or pAntp is a CPPs, which also belongs among DNA binding proteins (homeoproteins), contains binding motif called homeodomain [25]. Secreted proteins are also source of protein-derived CPPs called signal peptides. Signal peptides are short amino acid sequences (5-30 amino acids) located on the end of N-terminus, which serves as the targeting site of secreted proteins sequences in order to interact with the nascent protein (protein formed by a ribosome) [26]. Signal peptides have hydrophobic character, which allows them to pass the cell membrane by endocytosis and receptor-independent pathway. BPrPr(1–28) and MPrPr(1–30) belong

in the group of signal peptide [27, 28]. Protein-derived CPPs isolated from toxin venoms have lethal effect on wide range of microorganisms, and they belong to the group called antimicrobial peptides (AMPs). AMPs are amphipathic/cationic CPPs produced on the surface of epithelial tissue and phagocytic cells as results of the organisms' response to infection. Most of the AMPs have destructive nature on the microorganisms' cell membrane, which they achieve by compromising its integrity. CPPs derived from the motif of viral protein have developed mechanisms for membrane translocation. It is well known that positively charged residues in these peptides have the main role in CPPs internalization. By losing arginine from sequence, viral proteins lose the ability to pass the cell membrane, which indicates that interaction with negatively charged membrane parts is the first step in viral protein internalization [27].

Table 1: Protein derived CPPs

PEPTIDE	SEQUENCE	STRUCTURE	REF.
Heparin proteins			
HIP	CRPKAKAKAKAKDQTK	Cationic	[29]
HBD	RKKNPNCRRH	Cationic	[30]
DPV3	RKKRRRESRKKRRRES	Cationic	[31]
DPV6	GRPRESGKKRKRKRLKP	Cationic	[31]
DNA/RNA proteins			
HMG-1	TPKRPRGRPKK	Cationic	[32]
HIV1-TAT	RKKRRQRRR	Cationic	[19]
FHV coat	RRRRNRTRRNRRRVR	Cationic	[33]
REV	TRQARRNRRRRWRERQR	Cationic	[34]
Homeoproteins			
Penetratin	RQIKIWFQNRRMKWKK	Cationic	[35]
Knotted-1	KQINNWFINQRKRHWK	Cationic	[35]
HoxA-13	RQVTIWFQNRRVKEKK	Cationic	[35]
PDX-1	RHIKIWFQNRRMKWKK	Cationic	[36]
Signal peptides			
Ig(v)	MGLGLHLLVLAAALQGAKKKRKV	Amphipathic	[37]
BPrPp(1–30)	MVKSKIGSWILVLFVAMWSDVGLCKKRPKP	Amphipathic	[27]
MPrPp(1–28)	MANLGYWLLALFVTMWTDVGLCKKRPKP	Amphipathic	[28]
Antimicrobial peptides			
Bac7	RRIRPRPPRLPRPRPRPLPFPRPG	Pro-rich	[38]
Pyrrhocoricin	VDKGSYLPRPTPPRPIYNRN	Pro-rich	[39]
Melittin	GIGAVLKVLTTGLPALISWIKRKRQQ	Amphipathic	[40]
Buforin 2	TRSSRAGLQWPVGRVHRLLRK	Amphipathic	[41]
Viral protein			
Inv3	TKRRITPKDVIDVRSVTTEINT	Unknown	[42]
PreS2-TLM	PLSSIFSRIGDP	Amphipathic	[43]
VT5	DPKGDPKGVTVTVTVTVTGKGDPKPD	Amphipathic (β-sheet)	[44]

3.2.1.2. Design/chimeric CPPs

Design/chimeric peptides usually present combination of two or more motifs (hydrophilic and hydrophobic domain) from peptides which have different origins [45]. Majority of these peptides are designed using known peptide library, by screening peptides with characteristic hydrophobic or hydrophilic structure. Transportan presents one of design/chimeric peptide derived by fusion of mastoparan and neuropeptide galanin. Fusion between mastoparan and neuropeptide galanin occurs on the carboxyl terminus via lysine [46]. DNA-encoded and phylomers (gene-encoded) natural peptide library also present a large source of design/chimeric peptide. Peptides that are connected to their encoded DNA, such as phage display or plasmid display, directly increase the affinity of peptide for the protein of interest. By sequencing of encoded DNA, new selective peptides for various types of cells have been discovered, such as SG3 or 439a and 435b. Compared with DNA-encoded peptide, phylomers represent big library of structurally stable peptide subdomains, which are used as CPPs [47-50].

Table 2: Design/chimeric peptide

PEPTIDE	SEQUENCE	STRUCTURE	REF.
Peptide library			
Polyarginine (8, 9, 10, 12)	RRRRRRRR	Cationic	[51]
tp10	AGYLLGKINLKALAALAKKIL	Amphipathic	[52]
Pep-1	KETWWETWWTEWSQPKKRKV	Amphipathic	[53]
MAP	KLALKALKALKAALKLA	Amphipathic	[54]
CADY	GLWRALWRLLRSLWRLLWRA	Amphipathic	[55]
DNA-encoded, Phylomers			
SG3	RLSGMNEVLSFRWL	Amphipathic	[48]
439a	GSPWGLQHHPPRT	Hydrophobic	[49]
435b	GPFHFYQFLFPPV	Hydrophobic	[49]
CAYHRLRRC	CAYHRLRRC	Unknown	[56]
BEN_1079	RCGRASRCRVRWMRRRRI	Cationic	[57]
BEN_0805	PYSRPHVQLWYPNRESCRSLIRSLGP	Unknown	[57]

3.2.2. Physical–chemical classification of CPPs

As mentioned before, CPPs translocation over membrane mostly depends on positively charged sequence at physiological pH and their electrostatic interaction with negatively charged parts of membrane (glycoproteins). Positively charged CPPs sequence predominantly contains arginine and lysine. Arginine in CPPs sequence is able to interact with cell surface and form hydrogen bridge between guanidine head group of arginine and negatively charged phosphates and sulfates of cells membrane. On the

other hand, lysine is amino acid with the same charge as arginine, but without guanidine group in structure, which directly affects weaker internalization of membrane. This leads to conclusion that number and order of positively charged amino acids in the sequence, together with pH is critical for membrane translocation. However, at the same time, it is clear that the most of CPPs are not specific for various cell types [58, 59]. Moreover, it is reported that 83% of CPPs have net positive charge, where 44% include cationic and anionic and 15% are hydrophobic CPPs [23]. Due to this fact, CPPs can be divided in three groups: cationic, amphipathic and hydrophobic.

3.2.2.1. Cationic CPPs

Cationic peptides are mostly isolated from naturally occurring protein sequences. They represent a group of peptides with high net positive charge of sequence. HIV-1 protein Tat and penetratin are the first cationic peptides derived from natural proteins [19, 20]. However, with the possibility of controlled synthesis of peptides, artificial cationic peptides have gained more attention. Octa-arginine peptide (R8) is artificial cationic peptide with fully net positive charge sequence. Studies have shown that poly-arginine peptide with eights arginine in sequence is critical for effective membrane translocation, and with increasing number of arginine, the level of translocation is more efficient. On the other hand, peptide with only positive charged lysine shows similar behavior, but lower translocation efficiency [51, 60]. Studies also have shown that decreasing the number of amino acids to less than eight, or increasing the number of amino acids to more than 12, reduce membrane translocation efficiency of poly-arginine and poly-lysine CPPs [61]. CPPs structured from arginine, lysine or proline rich motifs, with ability of translocation through nuclear pore complex, represents a special type of cationic CPPs, called nuclear localization sequences (NLSs) [62]. NLSs are peptides that have less than eight amino acids in sequence, and most of them show lower penetrating properties, however in combination with hydrophobic peptide they form excellent amphipathic cell penetrating peptides [63].

3.2.2.2. Amphipathic CPPs

Amphipathic peptides refer to a large variety of CPPs with highly hydrophilic N-terminus and mainly hydrophobic C-terminus. Amphipathicity is a function of the primary structure of peptide, but it can also depend on secondary structure, with a clear side distinction between polar and non-polar residues [64, 65].

Primary amphipathic peptides are chimeric peptides with hydrophilic domain responsible for carying the cargo to desired position, and hydrophobic domain needed for membrane anchoring [64]. Fusion between hydrophobic MPG peptides, derived from HIV glycoprotein 41 and hydrophilic Pep-1 tryptophan-rich cluster responsible for delivery of protein to nucleus of the cell, typically represents primary amphipathic peptide [66]. Based on the same model, several other primary amphipathic peptides are reported: pVEC, ARF(1–22), and BPrPr(1–28) [67-69].

Secondary amphipathic peptides have α-helix structure with hydrophobic and hydrophilic residues separately on the opposite side of helix [70]. Amphipathicity has the main role in membrane translocation. Studies conducted on different secondary amphipathic peptides such as: MAP, GALA, p28 and KALA show that penetrating properties of peptide are preserved only in case where amphipathicity remained unchanged. By replacing alanine with lysine, the amphipathic character of mentioned peptides is not changed [54, 71, 72].

3.2.2.3. Hydrophobic CPPs

Hydrophobic CPPs belong to a small group of peptides structured from non-polar and low net charge residues [23]. The majority of conducted researches suggested that hydrophobic CPPs can be divided in several groups; linear hydrophobic peptides (BIP pentapeptides) [73, 74]; stapled peptides (p53 peptide, BH3-SG3) [48, 75, 76]; prenylated peptides (farnesyl (C15) or geranylgeranyl (C20) isoprenoid moiety) [77]; and pepducins (GPCRs, MMPs) [78]. However, only several peptides have a fully hydrophobic nature. Pep-7 is hydrophobic peptide derived from pVII–pIX phage-displayed random peptide library [79]. Pep-7 peptide has secondary α-helical character, which is able to bind to receptor site and provide receptor base for entry into cells. Fibroblast growth factor-12 (FGF12) has hydrophobic domain CPP-M and CPP-C, able to translocate into cytoplasm of a rat intestinal epithelial cell line (IEC6). It is found that deficiency of CPP-C domain reduces internalization of FGF12 into cells and inhibitory effect on apoptosis [80].

3.3 Mechanisms of CPPs membrane translocation

CPPs mechanism of cells membrane translocation is still under ongoing research [81]. Translocations of CPPs over cells membrane are mostly connected with

different properties (pH, peptide sequences and length, charge, concentration, cargo molecules, membrane lipids and proteoglycans), what makes it difficult for researcher to fully understand mechanisms of internalization [59, 82]. However, depending on the mentioned properties, CPPs are capable of translocation across the cellular membrane via multiple pathways, which are separated into two uptake mechanisms; direct penetration and the endocytotic pathways [83].

3.3.1. Direct penetration

Direct penetrations via energy-independent pathways present diffusion of CPPs through cells membrane that depend on plasma membrane potential, CPPs concentration and sequence. Direct penetration of CPPs is beginning with electrostatic interaction between peptides and negatively charged membrane components (phospholipids and heparan sulfate), involving permanent or temporary destabilization of cell membrane [84, 85]. This results in formation of cavities that enable translocation and direct penetration of CPPs via several pathways; inverted micelle model [86], toroidal pore model [87], barrel-stave pore model [88], and carpet model [89].

The inverted micelle model involves interaction of positively charged CPPs with negative charge phospholipids of membrane. By attaching to negative phospholipids head on membrane surface, CPPs are starting to rearrange lipid bilayer by hydrophobic residues. These results in entry of CPPs into lipid bilayers and entrapping in an inverted micelle, after which CPPs hydrophobic residues is again attracted by inner part of bilayer and released into cytosol. Membrane translocation by inverted micelle model requires CPPs, which contain hydrophobic residues [86]. This model of membrane translocation was proposed in a case of cell penetration peptide penetratin by Lindberg et al. [90].

Barrel-stave pore model describes CPPs membrane translocation by depolarization of membrane. Barrel-stave pore model occurs after interaction of amphipathiα-helical CPPs and lipid bilayer, which results in the formation of ion-conducting bundles. This process involves interaction of hydrophobic residues with negative phospholipids' head on membrane surface, while hydrophilic residues rearrange lipid bilayer and form pore by helical dipole moment [91]. Mastoparan X induces ion flow after interaction with lipid bilayer which leads to formation of barrel-stave pore [92].

Toroidal pore model is acting in the way that CPPs aggregate on the cell membrane surface, in order to rearrange the bilayer and expand the head-group region by disrupting polar and nonpolar parts of membrane. Result of this aggregation is distortion of lipid hydrocarbon and head-group, which leads to merging of upper and lower layers, allowing formation of toroidal pore by interacting of CPPs with bilayer [93]. Sengupta et al., describe translocation of melittin peptide trough membrane by toroidal pore model [87].

Carpet model is described as translocation of CPPs across biological membranes, where positively charged CPPs cover large surface of cell membrane like carpet. CPPs on the surface of negatively charged membrane start to change secondary structure, which results in rotation of hydrophobic residues towards hydrophobic membrane core. Interaction between hydrophobic elements goes on, until it reaches a critical concentration of CPPs on membrane surface and starts to locally disrupt bilayer structure. This leads to attraction of CPPs by hydrophobic residues from inner part of membrane bilayer and their penetration into cytosol. Dermaseptin is 34 amino acid peptide, being generated on the surface of cell membrane, which, by reaching critical concentration, penetrates cell membrane by carpet model [94, 95].

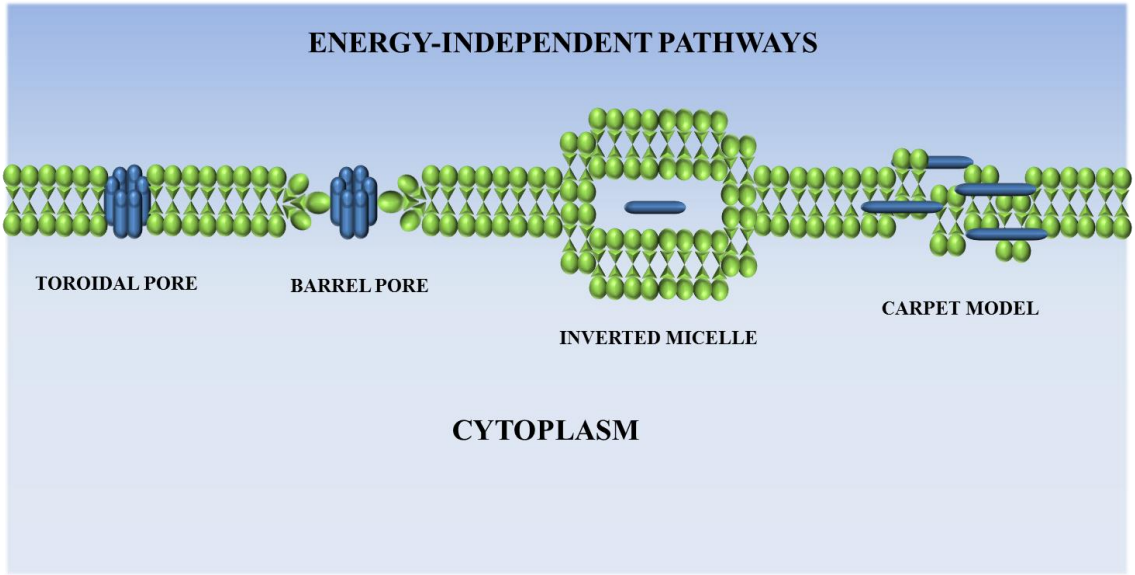

Figure 1. Direct penetrations of CPPs via energy independent pathways.

3.3.2. Endocytosis-mediated pathways

Endocytosis is a mechanism of molecule active transport into the cell via energy-dependent/independent pathways. In comparison with energy-independent pathways (direct penetration), endocytosis is able to transport large particles (phagocytosis) and uptakes of solute (pinocytosis). CPPs belong to a group of molecules which can also be transported into cell by endocytosis (pinocytosis), and this by several mechanisms such as; macropinocytosis, caveolae-mediated endocytosis, clathrin-dependent endocytosis, caveolin/clathrin endocytosis [81].

Macropinocytosis is a signal dependent process, in which outer surface of plasma membrane is actin-mediated folded, leading to formation of vesicle called macropinosomes, mostly triggered by growth factor substances. Formed macropinosomes have structure very similar to cell membrane, with ability to transfer large quantities of solute into cell. Macropinosomes is released from cell membrane under the influence of protein called dynamin [96]. Macropinocytosis is mostly being activated in case that large biological molecule with cargo has intention to internalize into cell. Kaplan et al., describe internalization of 30 kDA TAT-fusion proteins and TAT PTD peptides into cells by micropinocytosis. They found that internalization is mostly connected with total charge of peptide [97]. On the other hand, Rejman et al., suggest that micropinocytosis is in the direct correlation with the size of delivered molecules.

Caveolae-mediated endocytosis is signal-mediated process connected with expression caveolin-1 protein. The formation of cholesterol or sphingolipid-rich caveolae vesicle is connected with disruption of actin cytoskeleton by tyrosine kinase inhibitor and invagination of plasma membrane by expression of caveolin-1 protein. By activity of dynamin, caveolae is released from plasma membrane into cytosol. Amphipathic Pro-rich CPPs internalize cell membrane by caveolae-mediated endocytosis and show excellent potential for delivery of cargo into nucleus without disruption of lysosome [98].

Clathrin-dependent endocytosis is receptor-mediated endocytosis, trigger by expression of adaptor proteins (APA2). Adaptor proteins have ability to bind clathrin protein and force them to assembly into a lattice-like network, which results in bending of plasma membrane and formation of coated-pit vesicle. Clathrin and adaptor proteins also bind

other proteins such as dynamin and synaptojanin. Dynamin has the main role in release of vesicle from plasma membrane into cytosol, while synaptojanin decoats the vesicle [99, 100]. Richard et al., describe internalization of unconjugated TAT peptide by clathrin-dependent endocytosis. They have found that internalization of TAT peptide into cell by clathrin-dependent endocytosis depends on temperature and presence of heparan sulfate receptors [101].

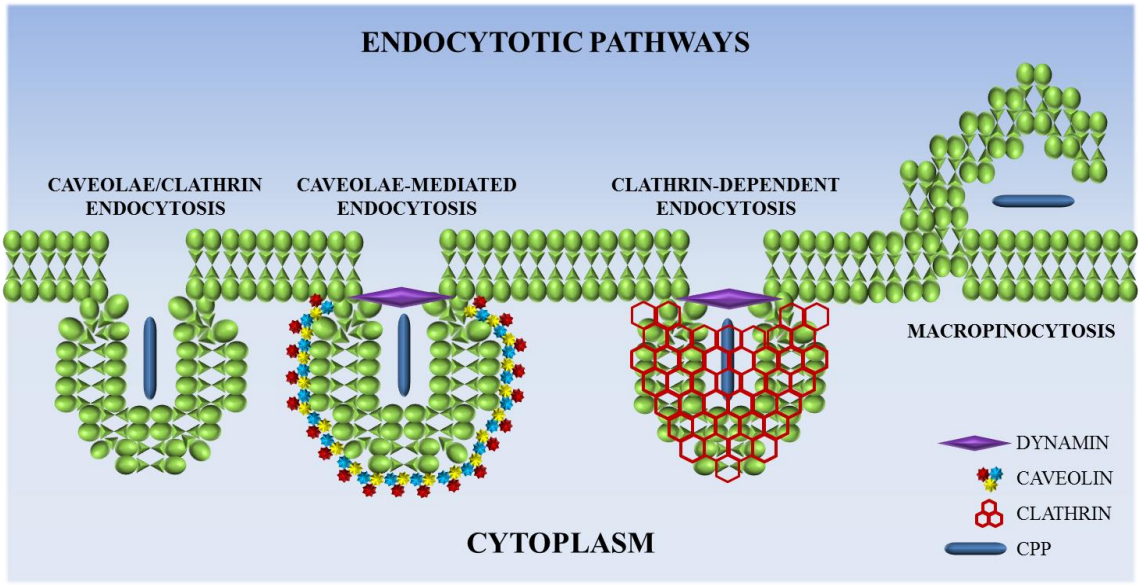

Figure 2. Model of endocytosis-mediated pathways.

3.4. Application of CPPs in delivery of therapeutics molecules

When using CPPs as drug delivery vector, several limitation have to be overcome, i.e., the fact that most of CPPs are not specific for type of cells or special target inside of the cell line; possibility of CPPs to easily decompose in the biological fluids; and toxicity of CPPs [102-104]. Moreover, formation of a stable bond between CPPs and therapeutic molecule also have to be taken into account as possible limitation. In order to form a stable drug carrier, CPPs can be conjugated with therapeutic molecule by covalent bond (chemical cross-linking), e.g., TAT, penetratin and polyarginine peptide R8 conjugation with doxorubicin for cancer treatment [105, 106]. On the other hand, stable conjugation between CPPs and therapeutic molecules can be accomplished through non-covalent bond. This is possible due to amphipathic nature of CPPs, which enables formation of conjugate through electrostatic or hydrophobic interaction, e.g., Pep-1 and MPG are used for delivery of protein and oligonucleotide for therapeutic purposes. It is also

reported that CPPs CADY is able to form non-covalent complex with doxorubicin, which is used in cancer treatments [107, 108]. Till now, more than 300 scientific reports related to drug delivery by CPPs are published [109]. Delivery of drugs by CPPs presents excellent tools for the non-invasive cellular delivery of various types of therapeutics molecules such as; small molecules, nucleic acid, peptide, protein and nanoconstructs [8].

3.4.1. CPPs delivery of small molecules

Due to enhanced permeability of small molecules into the cytosol and retaining of their activity, CPPs present excellent delivery vectors. Regardless of the fact that conjugation between CPPs and chemotherapeutic molecules reduces drugs activity, high cellular delivery by CPPs compensates this disadvantage. However, CPPs show high capacity for binding of small chemotherapeutic molecules, such as; Doxorubicin [110], Taxol [111], Cyclosporine A [112], and Methotrexate [113]. Lin et al. [110], reported new doxorubicin delivery system called CD13, based on interaction between NGR peptide and ultrasound-sensitive nanobubbles (NBs). After conjugation with CPPs, Doxorubicin was encapsulated into NGR-NBs delivery system, which temporary suppressed penetration properties of delivery peptide. By ultrasound stimulation doxorubicin conjugate with CPPs was released from CD13, which has again triggered penetration properties of peptide. Encapsulation rate of doxorubicin was 90%, while 85% was released from complex under ultrasound effect.

To overcome limitation in delivery of doxorubicin to tumor cell lines (HT-1080 and MCF-7), active able cell-penetrating peptides (ACPPs) sensitive to matrix metalloproteinase 2 and 9 were used as delivery vector. Doxorubicin was conjugated to ACPPs by linker *N*-succinimidyl 3-maleimidopropionate. In the presence of matrix, metalloproteinase 2 and 9 overexpressed in HT-1080 complex was activated, inhibiting cell proliferation, while in MCF-7 cell line, enzyme was downregulated leading to inability of peptide to be activated and to penetrate into cell [114]. Blood-brain barrier (BBB) also limited the delivery of doxorubicin, mostly because of the efflux activity of P-glycoprotein on the membrane surface. To bypass the blockade effect of P-glycoprotein, doxorubicin was covalently bound to two CPPs (D-penetratin and SynB1). Results have shown that in the presence of CPPs, uptake rate is increasing 20-fold, in comparison with free doxorubicin confirming low uptake rate [115].

P-glycoprotein does not only limit entry of doxorubicin through membrane, but it also limits other chemotherapeutic molecules due to their hydrophobic nature. Treatment of ovarium cancer by chemotherapeutic Taxol is ineffective due to efflux mechanisms of P-glycoprotein. To overcome this limitation Taxol is conjugated with cationic R8 peptide by disulfide linker on position C2 and C7, producing highly water soluble conjugate, which enables unlimited delivery of Taxol into ovarium cancer cells [116]. It is well known that arginine based CPPs have high penetration properties due to their cationic nature. Cyclosporine A is an immunosuppressive agent which is able to suppress inflammatory diseases. However, this drug shows poor penetration ability in the case of the tissue barriers. Poor absorption of cyclosporine A through barriers can be overcome by using arginine base peptide as delivery vector. It is reported that conjugation of cyclosporine A by pH sensitive linker (N-hydroxy succinimide ester) to R7 peptide increases the uptake rate of drug trough human skin. R7- cyclosporine A conjugate effectively targets dermal T lymphocytes and suppresses the occurred inflammation [112].

Methotrexate (MTX) is a chemotherapy agent used in therapy against breast, skin, head and neck, or lung cancer. Multidrug resistance (MDR) mechanisms limited application of methotrexate in cancer therapy. Lindgren et al. [117], reported alternative model, to bypass multidrug resistance mechanisms, by designing conjugate between methotrexate and two types of peptide (YTA2 and YTA4) for intracellular delivery [117]. The human breast cancer isolate MDA-MB-231 was chosen due to high level of resistance to chemotherapeutics drugs. Results show that YTA2 has higher delivery potential and lower hemolytic activity, which leads to inhibition of dihydrofolate reductase (target enzyme of MTX) and stops proliferation process. KIF20A-derived peptide conjugates with gemcitabine (inhibiting DNA synthesis) [118] were used in treatment of patient with advanced pancreatic cancer. Exposure of patient with KIF20A-derived peptide-gemcitabine conjugate resulted in increase of IFN-γ-producing cells in 4 out of 9 patients. The control of cancer progression was achieved in 4 out of 9 patients, together with antigen-specific T-cell response in the presence of KIF20A-derived peptide [119].

3.4.2. CPPs delivery of biologically active peptide and proteins

Macromolecules are usually limited by physicochemical properties, which can obstruct their internalization and accumulation in cells. Physicochemical limitation can be overcome by coupling macromolecules to CPPs, which are able to deliver cargo into cells without limitations. However, carefulness is mandatory due to ability of CPPs to interference with the biological function of conjugated macromolecules, or to cause steric hindrance.

It is well established that interaction between CPPs and other short motifs could provide new selective peptides, able to penetrate and activate specific cellular mechanisms. McCusker et al. [120], reported synthesis of a new anti-inflammatory peptide STAT-6-IP, used in treatment of allergic rhinitis and asthma. Testing on murine model has shown that appearance of acute asthma is in the direct correlation with activation of STAT-6 transcription factor, triggered by Th2 cytokines IL-4 and IL-13. To avoid the limitations of cell internalization, STAT-6-IP peptide was conjugated with protein transduction domain (HIV-Tat-derived PTD4). Results show that after internalization, a new peptide suppresses production of Th2 cytokines IL-4 and IL-13 from cultured murine splenocytes, which limits production of STAT-6 transcription factor.

The role of p53 tumor suppressor protein in genomic stability of cells induced by cellular stress is well known. Inducing apoptosis, p53 protein is able to reduce appearance of cancer. On the other side, mutation or loss of p53 protein is directly connected with development of various types of cancer [121]. Activation of endogenous p53 protein in cancer cells can be an alternative way used in cancer anti-proliferation and destruction treatments. Snyder et al. [122], reported treatment of preclinical cancer models (TA3/St, H1299, Namalwa, human foreskin fibroblast), with p53C′ parent peptide modified by D-isomer residues. To overcome the penetration limit p53C′ was fused with TAT protein transduction domain. Results have shown that new RI-TATp53C′ peptide expresses p53, reduces number of TA3/St tumor cell and extends survival of mouse model for 70 days in comparison to vehicle-treated mice. In a case of mice harboring peritoneal lymphoma cells Namalwa, mouse model lives more than 200 days after treatment with RI-TATp53C′ with higher expression of p53 in comparison with vehicle-treated mice, where survival time was around 30 days. However, after treatment with RI-TATp53C′, human foreskin fibroblast and H1299 lung adenocarcinoma cells

did not suppresses proliferation of cells and expressed p53. The authors concluded that proliferation is related to applied dose and specificity of peptide action. Similar results were reported by Michl et al. [123], where PNC-28 peptide derived from p53 mdm-2-binding domain induced necrosis in different cell lines. PNC-28 was fused with penetratin, in order to overcome membrane translocation. New peptide was tested on Athymic Nu/Nu mice model with xenotransplanted pancreatic carcinoma cells. Results have shown those two weeks after tumor transplantation, peptide induced necrosis in all tumor cells and blocked further tumor proliferation. Sepsis is medical condition mostly caused by bacterial infection. In these conditions lymphocytes and dendritic cells activate programmed suicide process apoptosis. This leads to suppression of immune system, which can results in death of patients [124]. Hotchkiss et al. [125], investigated treatment of sepsis by using of anti-apoptotic proteins and peptide. The investigation was conducted on two mice models - Bcl-xL transgenic mice and wild-type mice infected with *E. coli*. They observed the effect of TAT-Bcl-xL fusion protein and TAT-BH4 peptide on sepsis trigger apoptosis, induced by E. coli. The in vitro experiment has shown that human lymphocyte treated with TAT-Bcl-xL fusion protein and TAT-BH4 significantly decreases *E. coli* induced apoptosis, while treatment with free Bcl-xL protein has shown lack of apoptosis decrease. In vitro results show that antiapoptotic TAT-BH4 peptide reduces the presence of CD3 T cell and B cell apoptosis in both mice models. Proposed Tat-BH4 mechanism of action suggest that obtained results involve post-transcriptional protein-protein interaction.

VP22 herpes simplex virus protein fused with GATA4 transcription factor (GATA4 -viability and hypertrophic response of cardiac myocytes) shows therapeutic effect on myocardial response to injury [126]. Cardiac fibroblasts transfected with conjugate VP22-GATA4 complex transplanted into Lewis rat, suffering from ischemic cardiomyopathy, results in expression of cardiac myosin involved in normal cardiac function, after 1 month of exposure. After two months of exposure mice model with VP22-GATA4 complex expression stabilized cardiac function. Reported results show that treatment of rat group with VP22-GATA4 complex have 100% surviving rate, while rats used as control group show 30% mortality rate. This suggests that VP22-GATA4 complex could reduce fibrosis of infarcted myocardium and prevent the effect of ischemic cardiomyopathy [127].

Stimulation of immune system to respond to specific pathogen is well established and enabled through usage of antigenic material in form of vaccine. Protein vaccination applied for activation of immune system in C57BL/6 and OT-I mice model, EL-4 thymoma cell and OVA-transfected EL-4 cell lines was reported by Bleifuss et al. [128]. To provoke immune system response, ovalbumin was conjugated to cell penetrating motif (TLM) obtained from PreS2 domain of the human hepatitis B virus and applied as protein vaccine. They observed influence of TLM peptide as vaccine to immunization effect. Results have shown the response of immune system in both mice models after treatment of TLM-ovalbumin vaccine, in comparison with model treated with ovalbumin. Vaccination with TLM-ovalbumin triggers anti-tumor effects and delays tumor proliferation in both models. The mechanisms mode of action is not described; however they have found high production of IgG2a antibody and CD8+T cell as result of immune response.

3.4.3. CPPs delivery of nucleic acid

Delivery of nucleic acid into the cells for purposes of treatment of genetic and non-genetic disorders (cancer, infectious disease, cardiovascular disease) is a promising therapeutic approach in human medicine [129, 130]. Expression or regulation of a deficiently expressed gene is connected with delivery of therapeutic nucleic acid into nucleus. However, nucleic acid is a large molecule with hydrophilic backbone, which limits its free permeability through plasma membrane of eukaryotic cells [131]. Limited therapeutic effect of nucleic acid, caused by poor permeability, can be overcome by using viral or non-viral delivery vectors [132]. Viral vectors (retrovirus, adenovirus) usually have limitations due to poor cargo capacity and high toxicity, while non-viral vectors (liposomes, cationic polymers and dendrimers) suffer from low transfection efficiency [130, 133]. Solution to this problem can be provided by using cationic CPPs, which are able to interact electrostatically with negatively charged nucleic acid and deliver the same nucleic acid through plasma membrane without limitations [134].

It is reported that arginine/lysine rich peptides have excellent ability to deliver nucleic acid for therapeutic purposes [135]. Liu et al. [136], studied delivery of plasmid DNA into adenocarcinoma human alveolar basal epithelial cells (A549 cells) using arginine rich CPPs as delivery vector. The study was conducted by using three arginine-rich CPPs (SR9, HR9, and PR9).

Using mammalian EGFP reporter gene for gene expression assay purposes, they have found that plasmid DNA was expressed after cell treatment with CPPs/DNA complexes. In cells treated only with DNA or CPPs, plasmid expression is not detected. To prove that CPPs have the main role in delivery of DNA, cells where incubated with CPPs/DNA complexes at 4°C and treated with endocytic inhibitor nocodazole. The authors have found that lower temperature and endocytic inhibitors did not limit delivery of plasmid, which leads to conclusion that CPPs/ DNA conjugate involves direct translocation through the plasma membrane. However, use of hydrophobic peptides for delivery of biologically active cargo into the cells has also been proposed. Veiman et al. [137], describe delivery effect of new negatively charged nanoparticles based on conjugation of PF14 peptide with plasmid DNA. PF14 peptide is hydrophobic peptide obtained by modification of stearyl-transportan 10 (TP10). To confirm that new complex has biological activity CHO, U2OS, U87 and HEK293 cell lines were incubated with luciferase-encoding plasmid (pGL3) and complex, resulting in expression of pGL3 after 24 hours and confirmation of biological activity. Their results show that A scavenger receptors (SCARA) and caveolae-mediated endocytosis have the main role in complex delivery into the cells. Treatment of cell lines with SCARA inhibitors results in complete knockdown of luciferase activity, while control ligand does not stop delivery, suggesting that internalization of complex is stopped.

As ATP-dependent drug efflux pump, P-glycoprotein plays a role in decreasing of drug presence in multidrug-resistant cells, which limits cellular uptake of drugs [138]. Tat and Antp arginine/lysine rich peptide conjugate with phosphorothioate oligonucleotide was used as antisense strategy for inhibition of P-glycoprotein [139]. Conjugates have ability to bind AUG site of the P-glycoprotein message, which lead to inhibition of *MDR1* gene. Both conjugates have induced inhibition of expression of P-glycoprotein. However, it is interesting that conjugates have more potential in serum than in serum free conditions, which opens possibility to usage of this conjugate for in vivo therapeutic applications. A similar result was published by Antopolsky et al. [140], where 17 amino acid signal motifs from Kaposi fibroblast growth factor (MPM) and 27 amino acids from transcription nuclear factor kB containing MPM motif were conjugated with phosphorothioate oligonucleotide, in order to inhibit luciferase gene expression.

Messenger RNA (mRNA) has the main role in delivery of DNA genetic information to ribosomes in order to synthesize new proteins. Knocking out mRNA synthesis or stopping protein expression, leads to degradation of the mRNA transcript or blocking of mRNA translation. Inhibition of protein expression can have an important therapeutic potential in curing various diseases, especially in cancer treatment. Small interfering RNA (siRNA) has ability to stop protein expression, by degradation of mRNA, manifesting its potential as therapeutic agent. However, treatment of diseases with siRNA has therapeutic limitations due to its poor cellular permeability, strong charges and relatively large sizes [141, 142]. Davidson et al. [143], studied protein function in hippocampal and sympathetic neurons cultures after application of siRNA. Delivery of siRNA into the cell cultures was achieved by conjugation of siRNA to cell penetrating peptide Penetratin-1 via disulfide bond. They have proven that formed complex penetrates the entire cell population after 2 hours, while the applied concentration of 80 nM of conjugate causes knockdown of SOD1 or Casp3 proteins, with cytotoxicity lower than 8 %. The obtained results lead to conclusion that complex targets cell nucleus in order to interact with RNA-induced silencing complex (RISC), and induce silencing of gene by mRNA degradation. Chiu et al. [144], reported localization, uptake and activity of siRNA in HeLa cell line by using TAT peptide as delivery vector. Determination of gene silencing was done by dual fluorescence assay, using enhanced green fluorescent protein (EGFP) and red fluorescent protein (RFP). siRNA was conjugated to TAT peptide with oligo-carbamate modified backbone, or cysteine via disulfide bond. Results show that at 400 nM concentration 70 % of EGFP and 82 % of Cyclin-dependent kinase 9 (CDK9) were knocked down, while at the same concentration using only siRNA or TAT, peptide knockdown was not confirmed. Localization of siRNA was confirmed using lipofectamine transfection protocols, which represent the standard for siRNA delivery into the cells and their interaction with RISC. Protocol confirmed internalization of siRNA into the HeLa cells and their perinuclear localization. siRNA-TAT conjugate localization was identical to one in the case of lipofectamine transfection protocols, leading to conclusion that conjugate induces silencing of gene by mRNA degradation. Similar result was obtained by Moschos et al. [145], where siRNA was conjugated with TAT and penetratin peptide, in order to deliver and knock down p38 MAP kinase mRNA in mouse lung.

3.5. Stability and toxicity of CPPs

3.5.1. Stability of CPPs

Cell penetrating peptides show excellent potential as vector for drug delivery. However, delivery by CPPs can be limited due to chemical instability, which usually leads to degradation of cell penetrating peptides by extracellular and intracellular enzymes. On one hand, this will lead to decrease in concentration of applied CPPs limiting penetration properties in the case of direct penetration, but on the other hand, degradation of CPPs is a desirable feature when CPPs are used as delivery vector, related to safety of patients and toxicity control [146]. For *in vivo* application, stability and preservation of penetration properties of CPPs is highly recommended. Improving the stability of CPPs can be achieved by changing the amino acid stereochemistry, modification of sequences on specific locations or using β- and γ-peptoid residues [146].

Incorporation of unnatural D-form amino acids in known peptide sequences will result in change of the unstable peptide stereochemistry. Modification of peptides with D-amino acids increases the stability and life of CPPs in biological fluids. Nielsen et al. [147], studied oral delivery of insulin based on CPPs delivery. For this purposes, D-penetratin and L-penetratin were synthesized and incubated with rat gastrointestinal fluid. They have found that incorporation of D-amino acids into penetratin structure increases half-life of peptide, in comparison with fast degradation of L-penetratin. Due to application of D-penetratin, the half-life of insulin was increased from 25 min to 90 min, respectively. On the other side, it is also reported that changes in the stereochemistry of CPPs leads to decrease of penetration and delivery properties. Khafagy et al. [148], investigated effect of novel antidiabetic therapeutics (glucagon-like peptide-1 (GLP-1), exendin-4, interferon-β (IFN-β) protein) delivered with D-penetratin and L-penetratin vectors across nasal and intestinal epithelia. They have discovered that nasal route is more efficient in delivery of new drugs, in comparison with restricted delivery in intestinal route. It is however interesting that D-penetratin increases concentration of INF-β in plasma, in comparison with L-penetratin. In the case of GLP-1 and exendin-4, D-penetratin shows insignificant increase of concentration in plasma, while L-penetratin significantly increases concentration in plasma and viability, in comparison with D-penetratin. This shows that replacing L-amino acids with D-amino acids does not necessarily increase the delivery of drugs and stability of peptide.

The CPPs stability increase can be achieved by replacing the existing amino acid in peptide sequences at specific position with new amino acid, to enhance the resistance to proteolytic activity. Rennert et al. [149], studied resistance of modified C-terminal fragment of human calcitonin (hCT 9-32) to proteolytic activity. By replacing amino acid at position 12 and 16 with N-methylphenylalanine or D-phenylalanine, six new peptides were synthesized. Proteolytic degradation and stability of new peptide were observed in HEK 293T cell culture supernatant and blood plasma. In comparison with original hCT, modified hCT shows high proteolytic resistance. This suggests that increase of proteolytic resistance is connected to stabilization of peptide N-terminal part and use of N-methylated amino acids or D-amino acids, which are not compatible with native enzymes. Similarly, *in vitro* experiment on HeLa, MDCK or Calu-3 epithelial cell cultures was done by Foerg et al. [150], where they investigated stability of four peptides; SAP, hCT(9-32)-br, [Pα] and [Pβ]. Proteolytic activity between cell lines is found to be variable, while peptides express the same proteolytic cleavage. However, SAP and hCT show poor membrane translocation, which excludes effect of enzymatic degradation, while modified [Pα] and [Pβ] show good proteolytic resistance. They have concluded that modification of N-terminus with N-methylated or D-amino acids increases the stability of modified peptides.

Stabilization of CPPs backbone by incorporating β- and γ-peptoid residues increases the stability of peptide structure. Jing et al. [151], reported synthesis of N-terminal-labeled α-peptide/β-peptoid and N-acetylated peptidomimetics modified with achiral N-benzyl-β-alanine, in order to investigate interaction and penetration properties of new peptides. They reported that by increasing the number of α-peptide/β-peptoid in sequences, the absorption of peptide by HeLa cells also gets higher. They have supposed that due to presence of the benzyl side chains in peptidomimetics, adsorption rate is increasing, which is connected with net positive charge and hydrophobicity of peptides. However, they have also found that modification of N-terminus with α-peptide/β-peptoid and N-benzyl-β-alanine increases the stability of peptide, due to proteolytic stability of mentioned residues [152].

3.5.2. Toxicity of CPPs

CPPs used as delivery vectors require minimal toxicity, if they want to be applied in drug delivery. Toxicity induced by CPPs depends on the mechanism of membrane translocation and selectivity for specific components inside of cells. Toxicity of CPPs is also in direct correlation with concentration, sequence and net charge of applied peptide [153, 154]. Toxicity mostly arises from membrane disruption, which leads to leaking of cytoplasm or disruption of protein membrane function, on the other side, some peptides do not disturb the function of membrane, but they can restrict the cellular function e.g. disturb the activity of GTPase activity by transportan [155]. A brief study of CPPs effect to membrane toxicity was reported by Saar et al. [153]. Toxicity effect of five most documented CPPs (pAntp(43–58), pTAT(48–60), pVEC(615–632), model amphipathic peptide (MAP), and transportan 10 (TP 10)), were observed on three cell lines (K562-erythroleukemia, S40-transformed human AECs and MDA-MB-231-breast cancer), by testing of lactate dehydrogenase leakage (LDH leakage assay) and decreasing of bis-oxonol incubate plasma membrane fluorescence. LDH leakage assay results show non-significant leakage in all three lines after application of pAntp, pVEC and pTAT peptides. On the other hand MAP and transportan 10 show similar and significant leakage of LDH, about 40% in K562 and MDA-MB-231 cell lines. They reported that stronger LDH activity of MAP and transportan 10 is connected with higher amount of lysine in sequences which have stronger membrane activity, in comparison with arginine rich peptide pAntp, pVEC and pTAT which have a different uptake model. The similar results were obtained by observing the fluorescence intensity of plasma membrane in K562 and MDA-MB-231 cell lines. In the case of S40-transformed human cell line, leaking is not detected after treatment with all five peptides.

Moreover, disturbance and leakage of cells membrane is not connected only with concentration and net charge, the attached cargo also plays a significant role in the internalization of peptides. El-Andaloussi et al. [156], studied the influence of concentration and attached cargo of CPPs on cell membrane translocation. Cytotoxicity of TP10, penetratin and Tat was studied in HeLa and CHO cell lines. Membrane integrity of HeLa and CHO cell lines was investigated by LHD assay. Penetratin and Tat do not affect the function of membrane cell lines, while TP10 induces leaking of LDH in concentration-dependent manner.

At applied concentration of 10 μM, leaking of LDH was around 20%, while at concentration of 50 μM, leaking reached the maximal 100 % in both cell lines. In comparison to unconjugated peptide, conjugations of TP10 N-terminus with cargo molecule fluorescein increase the leaking of membrane and toxicity. On the other side, orthogonal conjugation of TP10 with fluorescein decreases the toxicity of peptide. The authors have assumed that conjugation of fluorescein on N-terminus increases the hydrophobicity of TP10, which leads to stronger membrane destabilization, while conjugation of fluorescein orthogonally to cationic part of TP10 reduces its amphipathic nature, resulting in toxicity decrease. Conjugation of penetratin and Tat with dsDNA shows the lack of membrane leaking at concentration of 50 μM, while in the case of TP10; membrane leaking is decreasing at concentration of 10 μM in comparison with unconjugated TP10. Conjugation between DNA and TP10 leads to lower exposure of cell membrane to peptide, which results in decreasing of toxicity. Hansen et al. [157], investigated membrane integrity of SH-SY5Y cell line after treatment by proline rich peptide attached on penetratin. They have found that internalization of peptide depends on concentration. With higher concentration (160 μg/mL), peptide shows intracellular localization and perinuclear localization, while at lower concentration (40 μg/mL) intercellular localization is not observed. However, morphology of cell line is disturbed at higher concentration, indicating leaking of cytoplasm and disruption of membrane integrity.

3.6. Chemical synthesis of CPPs

Synthesis of peptides by chemical methods was established in 1881 by Theodor Curtius. Curtius used benzoyl-chloride to treat silver salt of glycine, in order to produce first N-protected dipeptide by azide-coupling method. In 1901, Emil Fischer published the first work on chemically synthetized dipeptide glycine-glycine by hydrolysis, using diketopiperazine [158]. However, the real progress in chemical synthesis of peptide was reached by introducing of protecting group to amino acids. Bergmann and Zerwas in 1931 protected amino acid with carbobenzoxy (Cbz) group, followed by Carpino, McKay and Albertson, who introduced *tert*-butyloxycarbonyl (Boc) group in 1957. Based on protective techniques, Merrifield produced the first peptide from solid support called solid phase peptide synthesis (SPPS) in 1963 [159, 160]. Today, two chemical

techniques are used for production of synthetic peptide: solution phase synthesis (SPS) and solid phase peptide synthesis (SPPS).

3.6.1. Solution phase synthesis

Synthetic synthesis of peptide is the opposite process of the natural synthesis of peptide, which starts from amino group side of amino acid (N-terminus). Synthesis of peptides by solution phase synthesis begins from the carbonyl group side of amino acid (C-terminus) to amino group side of other amino acid (N-terminus) in solution, without using the first building block, like in the case of solid phase peptide synthesis. Solution phase synthesis was not regarded as suitable method for peptide synthesis at first, due to isolation and purification limitations. However, by de-protection and purification of intermediate products, highly purified peptides were synthetized, attracting more interest for this method. Benefits of this method can be found in large scale production and low chemical volumes in relation to obtained amount of peptide, which is beneficial for industrial scale production and specialized laboratory applications. Pharmaceutical companies use solution phase synthesis for production of various types of hormones, such as Oxytocin (sexual reproduction hormone), Porcine (gastrin releasing peptide) and Insulin (hormone regulating carbohydrate metabolism) [161-165]. On the other hand, long reaction time usually limits the use of this method for scientific research. Solid phase synthesis combined with microwave has demonstrated an ability to increase reaction rates, decrease the time and side reactions, and to use different types of solvents, presenting more suitable method for scientific research [166, 167].

3.6.2. Solid phase peptide synthesis

Solid phase peptide synthesis is a method based on use of anchored insoluble polymeric support, called resin, as the first building block. The first amino acid with protected reactive side chain is attached to anchored resin by covalent attachment step via its C-terminus. After the first amino acid is added, the protecting group is removed and washed, in order to unprotect the amine group of anchored amino acid and to attach the next amino acid by their carboxylic group [160]. This procedure is repeated until the sequence is completed. Amino acids used in peptide synthesis are masked with protecting group, in order to prevent unwanted side reactions. The two main synthesis strategies used in peptide production are named after protecting group Fmoc (Fluorenylmethyloxycarbonyl chloride) and Boc (tert-Butyloxycarbonyl) [159, 168].

Selection of protecting strategy influences the choice of solid support (resin) and other chemicals used in peptide synthesis. Fmoc group is unstable in the presence of base conditions, while Boc is unstable in the presence of acid conditions. Due to that fact, Fmoc strategy requires the base stable solid support and side chain protection group, in order to protect the peptide during the synthesis, while Boc strategy requires the acid stable support and protecting group [169, 170]. Various types of solid support are available on the market, adopted for requirement of protecting strategy, such as polystyrene, hydroxymethyl, phenylacetamidomethyl, Wang ([4-(Hydroxymethyl)phenoxymethyl] polystyrene) and 4-methylbenzhydrylamine resins [171, 172]. Releasing the peptide from solid support and removing the side chain protecting groups is being done by using strong acid, trifluoroacetic acid in the case of Fmoc strategy and hydrofluoric acid in the case of Boc strategy [173].

Benefits of solid phase peptide synthesis were found in mitigation of cleavage conditions by Fmoc and Boc chemistry, reducing of side reactions by using different protecting groups and minimization of side reactions by cleavage of peptides with strong acids [173]. However, the full potential of solid phase peptide synthesis has been reached by involving microwave-assisted method in peptide synthesis [174]. Using microwave irradiation in peptide synthesis has enabled high yield of synthetized peptide, low racemization, protection of long peptides from aggregation, control of the temperature and pressure while the synthesis is in progress, and minimization of time and energy used in synthesis [175]. The first application of domestic microwave in the synthesis of ACP peptide resulted in acceleration of the coupling reaction up to 2-4 fold from standard coupling [176]. Using single mode microwave cavity in the deprotection and coupling steps, the speed of one cycle in peptide synthesis has been shortened to only 3 minutes [177].

As in this research only the Fmoc method was used, this method will be described more detailed in the following chapter.

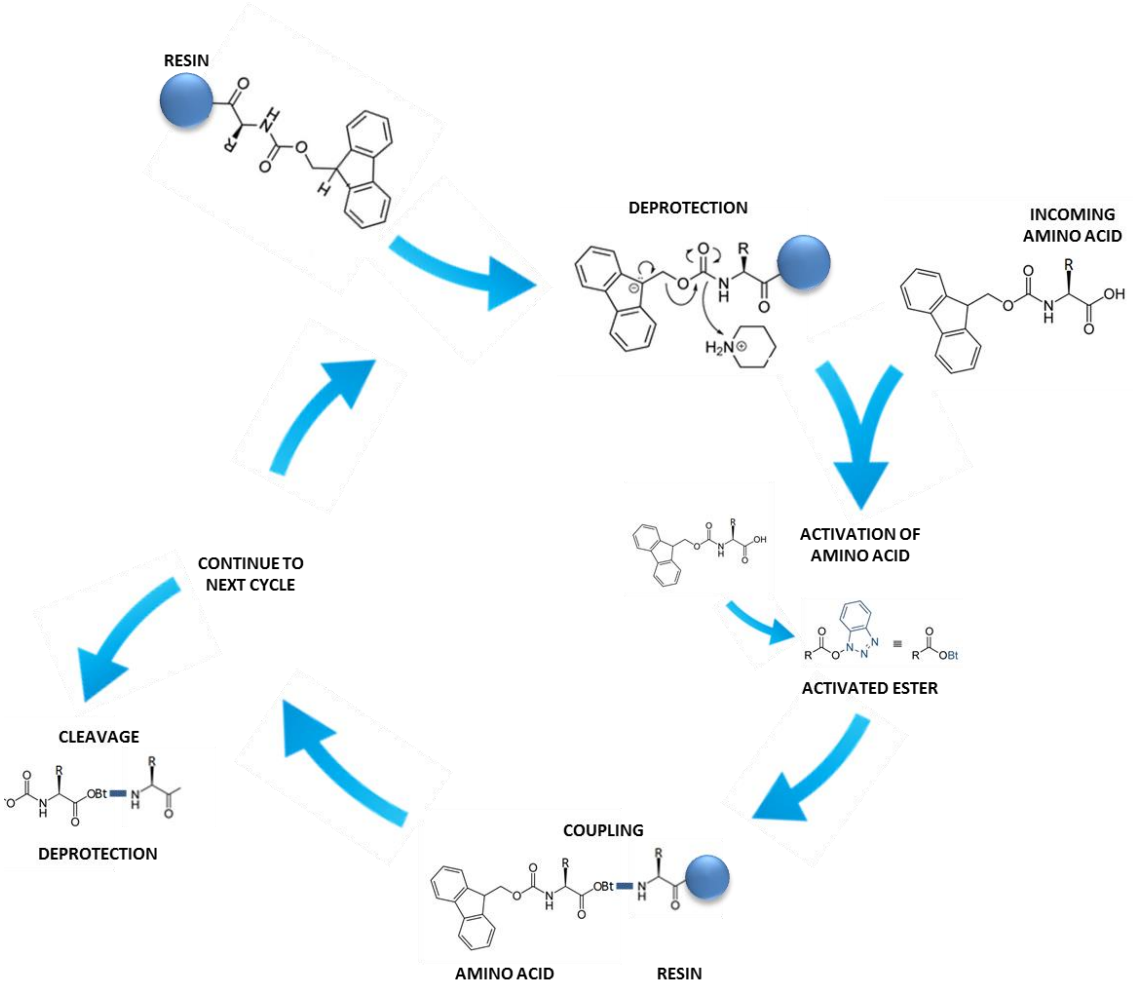

Scheme 1. Schematic representation of solid phase peptide synthesis.

3.6.2.1. Chemistry behind the Fmoc solid phase peptide synthesis

The Fmoc solid phase peptide synthesis is a method containing several steps joined in one cycle. Usually, depending of amino acid, one cycle contains the following steps; deprotection, 3x washing, deprotection, 3x washing, coupling, washing and cleavage of peptides.

The first and the crucial step in peptide synthesis is deprotection of Fmoc from amino acid, in order to free protected amine for decarboxylation process. Deprotection is usually done by strong base piperidine, but piperazine can also be used. Using strong base, the acidic hydrogen atom on 9 position of fluorene ring is easily removed, which triggers β-elimination mechanism. As a consequence of this process, the Fmoc group converts to dibenzofulvene, while the amine group becomes deprotected. Produced dibenzofulvene is usually scavenged by base and removed from synthesis by washing [178, 179].

Formation of peptide bond between free amino acid and peptide chain requires activation or coupling step. Coupling of incoming amino acid to the peptide chain is usually mediated by activators, such as carbodiimides or onium salt [180-183]. Carboiimides triggers the activation of amino acid through the formation of highly reactive O-acylisourea. Highly reactive O-acylisourea is formed after interaction of carboiimides nitrogen atoms with carboxylic side of amino acid in peptide chain. The peptide bond is fromed by interaction between amine part of incoming amino acid and highly reactive O-acylisourea. However, using carboiimides can also lead to formation of less reactive N-acylisourea, or formation of oxazolone, which can epimerize activated amino acid [177]. To avoid the possible undesirable conversion, using the so called additives is highly recommended. The most common additives today used in combination with carboiimides are HOBt (Hydroxybenzotriazole) or HOAt (1-Hydroxy-7-azabenzotriazole). The additives' function is to convert highly reactive O-acylisourea to reactive OBt ester, in order to avoid formation of oxazolone or N-acylisourea [184, 185].

Onium salt application requires additional activator base, in order to activate amino acids, as onium salt is interacting with carboxylate ion. Due to the fact that incoming amino acid is in highly reactive ester state, the purposes of activator base are to control unwanted reactions. Benzotriazols phosphonium salts, such as BOP (Benzotriazol-1-yloxy)tris(dimethylamino)phosphonium hexafluorophosphate) and PyBOP (benzotriazol-1-yl-oxytripyrrolidinophosphonium hexafluorophosphate) are the first activator bases used in cyclization reaction [186, 187]. However, using BOP is restricted due to production of secondary product hexamethylphosphoramide (HMPA) during cyclization reaction [187]. Toxicity of HMPA produced in cyclization reaction is limited by introduction of PyBOP activator base, which is a product of replacing dimethylamino groups of BOP with pyrrolidine. Benzotriazoles amonium salts HBTU (2-(1H-benzotriazol-1-yl)-1,1,3,3-tetramethyluronium hexafluorophosphate) and TBTU O-(Benzotriazol-1-yl)-N,N,N′,N′-tetramethyluronium tetrafluoroborate present the next generation of activator bases used in peptide synthesis. Activator bases, based on HBTU or TBTU show higher reactivity than PyBOP, however, they can limit synthesis of peptide by production of guanidine as side product [188, 189].

Synthesis of peptides finishes with cleavage of peptide from solid support and isolation by precipitation. As mentioned before, cleavage of peptide from solid support and removal of side chain protecting group is done by trifluoroacetic acid (TFA), due to acid instability of Fmoc group. To protect the new peptide from free radicals and reattaching of free protecting group after cleavage, trifluoroacetic acid is mixed with scavenger molecules [190]. Various types of scavenger molecules are used in Fmoc strategy, depending of synthetizing peptide, such as; triisopropyl silane, ethane dithiol, dioxa-1,8-octane-dithiol, thioanisole. Isolation of new peptide is usually done by precipitation, using cold diethyl ether. Precipitation allows washing and removing of cleavage solution from new peptide [191].

3.7. Book chapter

P. Kopel, D. Wawrzak, **V. Milosavljevic**, A. Moulick, M. Vaculovicova, R. Kizek, V. Adam, NANOTRANSPORTERS FOR ANTICANCER DRUG DELIVERY, Nanotechnology Research Journal, 8 (2015) 1, Advances in Nanotechnology. Book edited by Zacharie Bartul and Jérôme Trenor, ISBN: 978-1-63482-971-7.

Participation in the work of the author Vedran Milosavljevic literature research 40% and manuscript preparation 40%.

Nanotransportes are powerful tool for delivery of various types of biologically active molecules. Among them, peptides attract specially attention due to inability of cell membrane to prevent their internalization. Peptides has potential not only to change the cancer diagnosis method, but also to open a new opportunity in drug delivery.

In: Advances in Nanotechnology. Volume 14 ISBN: 978-1-63482-971-7
Editors: Zacharie Bartul and Jérôme Trenor

Chapter 1

NANOTRANSPORTERS FOR ANTICANCER DRUG DELIVERY

Pavel Kopel[1,2], Dorota Wawrzak[3], Vedran Milosavljevic[1], Amitava Moulick[2], Marketa Vaculovicova[1,2], Rene Kizek[1,2] and Vojtech Adam[*1,2]

[1]Department of Chemistry and Biochemistry, Mendel University in Brno, Brno, Czech Republic
[2]Central European Institute of Technology, Brno University of Technology, Technicka, Brno, Czech Republic
[3]Institute of Chemistry, Envoronmental Protection and Biotechnology, Jan Dlugosz University of Czestochowa, Czestochowa, Poland

ABSTRACT

Nanomedicine is a relatively new field of medicine aiming to overcome usual problems that appear in disease treatment. Natural or artificial nanodevices, with dimensions similar to those of biological molecules in human body, can carry drugs more efficiently and mostly with no side effects on healthy tissue than drugs alone. Nowadays, there is a huge interest in nanotechnology for detection, imaging and cancer treatment because cancer causes death of millions people every year. There are already some nanoparticle based drugs, mostly in liposomes, approved for clinical use or under clinical investigation. Many attempts are made to improve nanoparticles sizes, shapes and surface modifications that lead to prolongation of drug circulation in blood stream and targeting to cancer cells. Thus small molecules like polyethylene glycol and targeting ligands like folic acid, peptides, antibodies, aptamers and nucleic acids are bound on the surface of nanoparticles with the aim to increase specific cell uptake. Very promising are multifunctional nanoparticles that combine both diagnostic as well as delivery role together.

In this chapter, we describe recent progress on utilization of different nanotransporters including dendrimers, micelles, liposomes, protein-based carriers,

[*] Corresponding author, e-mail: vojtech.adam@mendelu.cz.

graphene, graphene oxide, carbon nanotubes, silica, gold and iron oxides nanoparticles, for transport of anticancer drugs.

INTRODUCTION

Nanotechnology deals with the creation and testing of structures, the size of which at least one dimensions is less than 100 nm. Nanomaterials beyond the specific sizes have different characteristics and properties of the same material with a lower degree of fragmentation. You cannot reduce the size of infinity, because the matter has different properties in the macro and the subatomic world, and crossing the border nano, redefine the way that appliances. Here was born the concept of nanomaterials. Nanotechnology is not only chemistry and technology of manufacture of small molecules, but also the formation and use of molecules with nano dimensions having unique properties which can be used for the preparation of new materials or construction of miniature systems. Nanomaterials have different chemical, physical and biological substances forming them than particles of larger sizes. This is due to the fact that most of the molecules forming the nanomaterial are close to the surface, and thus their electronic structure, energy levels, and the reactivity is different than if the classical form a crystal network.

Nanomaterials and nanoparticles retain characteristic physicochemical properties of these materials at the macro level, but also have a range of original features, occurring only in the nanoscale. The main reasons for the unique properties of nano-objects are their dimensions, as well as the related disclosure of quantum phenomena. The small size allows them to penetrate through most barriers, and also mean that in their case the observed effects resulting from the laws of quantum physics. Dualism of nature nanoparticles is one of their biggest advantages. Compared to the material in the macro-nano characterized inter alia: more developed specific surface area, greater hardness, greater strength and increasing plasticity occurring at the same time, sliding properties or greater biocompatibility of nano biomaterials [1]. Most of nanomaterials have a dual character: a percentage of the property does not make their use in biology, chemistry, environmental engineering and medicine becomes attractive especially in the transport and delivery of drugs and bioactive substances. The concept of using a particle measured in the nanoscale as carriers of drugs and vaccines appeared over three decades ago. Advances in nano medicine has evolved and has raised hopes for the implementation methods of striking antitumor therapy selectively in tumor mass, while reducing the risk of a wide range of side effects, which are encumbering modern pharmacology. Nanoparticles are attractive as drug delivery platforms because it is relatively easy to influence their properties and modify their features, so that they can be useful in creation of effective and precise medicine carriers. Meaningful are not only dimensions of the carrier enabling tissue penetration, but also their shape, and developed different functionalities of surface.

Current progress in the field of nanobiotechnology has led to the development of a new area of nanomedicine, associated with the application of nano biomaterials, both for diagnostic and therapeutic aims creating a new category of nano particles called theranostics. The main expectations and challenges in this regard relate to nano-magnetic properties, received bioengineering methods, with potential used in the transport of drugs, particularly anticancer drugs used in therapy determined using molecular targets. Unique physicochemical

properties of magnetic nanoparticles promise hope for the development of modern cancer nanomedicine, acting, inter alia, technological breakthrough in the area of targeted drug delivery and gene therapy of cancer using magnetic hyperthermia, tissue engineering, marking the tumor cells and the molecular magnetic resonance imaging. Along with a broad interest in magnetic nanoproducts and bioengineering, in the area of special attention is the toxic potential. A considerable amount of scientific evidence to date suggests that certain properties of nanoparticles magnetic (e.g. increased surface activity, ability to penetrate cell membranes, resistance biodegradation processes) may enhance their cytotoxic potential compared to the corresponding materials lacking the size in the nanoscale. In other words, the safety evaluation conducted with respect to standard magnetic materials, may be of limited use in the risk assessment of health and environmental exposure in the case of new nano-magnetic received bioengineering methods.

In this chapter we discuss the main directions of research conducted in experimental models in vitro and in vivo to nanoparticles (NPs), paying particular attention to the nanotransporters for anticancer drug delivery. The chapter presents also new directions in the field of research conducted in area of nanotransporters in clinical use and investigation, drug release from nanoparticles, proteins as a natural nanotransporters, liposomes and their modifications, dendrimers and polymer nanoparticles, inorganic nanoparticles as well as carbon based nanomaterials (see. Figure 1).

Nanotechnology in medicine and health care was initiated over forty years ago with deliverance of the first therapeutic and diagnostic agents in a safer and more efficient manner [2]. Convergention of diagnosis and therapy carried out through exploitation of nanoparticles resulted with increasing number of theradiagnostics went out from research stage and being commercialized or having reached clinical stage. Unique structures and physical properties which are characteristic for nanoparticles are originated because a large fraction of their volume is within “hailing distance” of the surface.

Such a structure of nanoparticles makes them useful as carriers of “heavy loads” of surface coatings, area that is structurally and compositionally different from the bulk. Coating material can rearrange all or parts of the nanoparticle structure themselves, provide a shell of different composition, or adsorb layers inorganic or organic molecules. External layers of nanoparticle are highly flexible in ability to initiate creation or building novel structures with different properties both of the core structure as adsorbed layers [3].

The fundamental complexities in structure, bonding, and interfacial interactions between a particle, its coating, and its neighboring environment, can be exploited to derive unique properties for many potential applications. The development of functional, inorganic nanoparticles (NPs) has progressed exponentially over the past two decades. Magnetic nanocrystals, luminescent particles and sophisticated systems such as up-converting NPs are some of examples from the diverse range of availabilities [4, 5]. Attainable functionalities enable the realisation of different diagnostic and therapeutic applications [6]. Although only a relatively small number of nanosized drug delivery carriers have been approved for human use so far, it is now accepted that nanotechnologies will likely constitute a growing share of the oncologist's therapeutic arsenal over the next decades to come [7-9]. There are many nanoparticle technologies under development and a great majority are still without clinical proof of concept, but advances on clinical stage show how promising and limitless is nanotechnology especially in medicine.

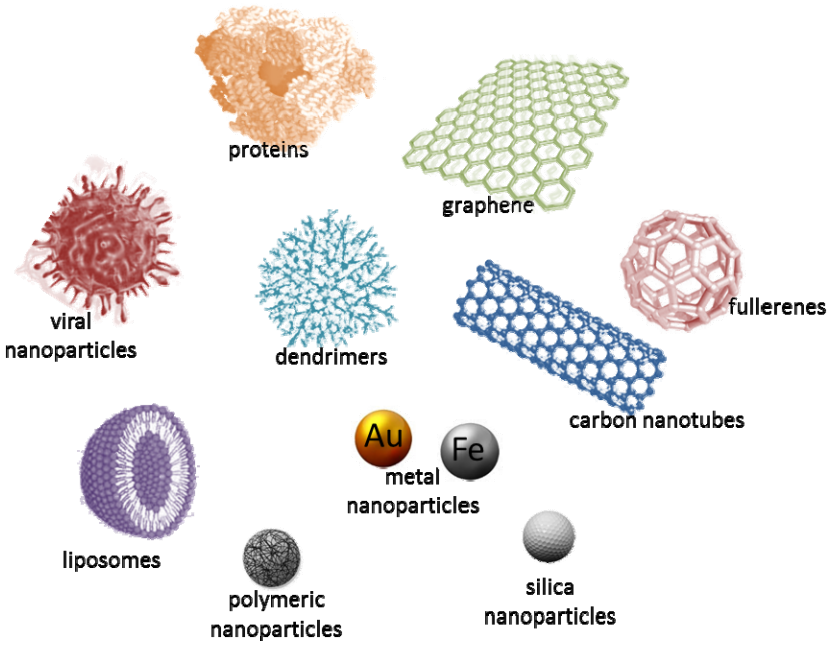

Figure 1. Different types of nanotransporters.

1. NANOTRANSPORTERS IN CLINICAL USE AND INVESTIGATION

There is observed rapid development of various branches of nanotechnology in the very beginning of 21st century, among which outstanding is nanomedicine. Its characteristic future is use of nanoparticles and nanomaterials in areas such as: nanodiagnostics, nanooncology or nanopharmacology. In nanodiagnostics nanoparticles help in the rapid diagnosis of disease as markers and indicators. One of the fastest growing areas of nanomedicine is nanopharmacology, which is based upon creation of nanosystems of the carrier to enable selective delivery of drug and its controlled release in pathological cells or tissues. It also deals with the creation of nanomedicines and improving existing ones. Nanotechnology applied in medicine has vast the potential to revolutionize cancer diagnosis and therapy. Protein engineering and materials science have contributed to novel nanoscale targeting new hope to cancer patients. Several therapeutic nanocarriers have been approved for clinical use. However, to date, there are only a few clinically approved nanocarriers that incorporate molecules to selectively bind and target cancer cells [8].

1.1. Nanomaterials in Medicine

Nanoparticles are referred to as "zero-dimensional" because they all fit the dimensions at the nanoscale [8]. They are characterized by a high ratio of surface atoms to the number of atoms in the core of the particle which changes its physicochemical characteristics compared

to materials with the same chemical composition, but a normal size. This results in a change in the behavior of nanoparticles under the influence of external forces and contributes, among others, to their increased chemical reactivity and biological and other electrical and optical properties [10]. Due to the small size nanoparticles enter the body through the skin, inhalation, ingestion and can accumulate in various organs. Nanomaterials are materials which at least one dimensions less than 100 nm. They are divided into zero-dimensional nanomaterials such. Quantum dots, one-dimensional - wires and tubes, two-dimensional forming layer and forming three-dimensional materials composed of nano-crystals [10]. Due to their size they acquire new characteristic properties that differ from those obtained in the macro scale. Additional features specific for these materials include high specific surface area, the tendency to agglomerate and the ability to high specific activity [11].

1.2. Nanoparticles a Core-shell Type

These nanoparticles are composed of silica core coated with a thin layer of gold, which can be further integrated by biological ligands. Because of the ability of absorption and scattering of electromagnetic waves from the visible to near IR may be used in optical and medical imaging. Another advantage is the ability to change the scope of radiation absorbed by modifying the core thickness and number of coats. They are used mainly targeted therapy by means of photodynamic methods. In a study conducted by Hirsch et al. used in the treatment of tumor on mice in vivo and in vitro cell line SKBR3. Nanoparticles were injected interstitially to the lesion and then irradiated with low doses of near infrared radiation (820 nm; 4W/cm^2). This caused high heat up of the tumor cells and eventually their destruction, while preserving all functions of the surrounding healthy tissue. The same result was obtained in studies conducted in vitro [12]. These nanoparticles, coated with antibodies were also used for the delivery of drugs in the hydrogel coating; under the effect of laser radiation dissolved and released the active drug in tumor tissue while reducing the toxicity of chemotherapy. Such nanostructures are also important in medical diagnostics for example the detection of a variety of molecules, e.g. immunoglobulin in the blood or plasma [13].

1.3. Nanoparticles of Metallic Materials

Novel properties of nanoscale metallic materials, also called nanomaterials, have attracted enormous interest compared to conventional (microcrystalline) materials. In recent years nanoscale magnetic materials showed the potential for use in many different biological and medical applications. For example, super paramagnetic iron oxide nanoparticles having an average particle diameter of about 10 nm, suspended in suitable liquid carriers are commonly referred to as ferrofluids and have excellent properties. In these materials, a wide range of both metallic and oxide magnetic nanoparticles were synthesized. Magnetic nanoparticles can be used for testing due to their high surface area and the interaction with different tissues. The main applications are the detection and analysis of bio particles directed transport of drugs, contrast during magnetic resonance imaging and hyperthermia. Effect of controlled heating of cells and tissues is one of surprising futures of ferrofluids. Each cycle of a hysteresis loop of any magnetic material involves an energy loss proportional to the area of

the loop. Hence if magnetic nanoparticles having the required coercivity are remotely positioned at a given site in the body, perhaps the site of a malignancy, then the application of an alternating magnetic field can be used to selectively warm a given area. It has been proposed that this simple physical effect could be used both to destroy cells directly and to induce a modest increase in temperature so as to increase the efficiency either in chemotherapy or radiotherapy [14].

Rapid immunization of microorganisms to antibiotics induced intensive research of new substances with antibacterial properties. Intensive development of nanotechnology enabled the creation of nanoparticles of metals such as silver, gold and copper, which are characterized by antimicrobial properties. The largest application has silver nanoparticles due to its homogeneity, stability and functionality. From the earliest years were characterized by silver antibacterial properties, which by means of nanotechnology have been strengthened. Each silver nanoparticle contains 20 – 15 000 atoms and due to the different structures (beads, rods, cubes or wires) are generally less than 100 nm. Toxic effects of nanosilver as a germicide, antifungal and antiviral are mainly based on disruption of cell membranes, protein denaturation, the production of oxygen radicals and interference with DNA replication and inhibition of expression of proteins and enzymes constituting the respiratory chain [15]. The nano-silver antibacterial important is the construction of the bacterial cell wall. Gram-positive bacteria, for example *Staphylococcus aureus*, because of the thicker layer of peptidoglycan, are less sensitive to the toxic influence of nanosilver than gram-negative bacteria [16]. Combination of nanosilver with antibiotics enhances the effect of antibacterial agents such as amoxicillin, erythromycin, clindamycin, penicillin G and vancomycin as was proved by Shaverdi et al. [17]. They are also exploited as an antibacterial agent in the manufacture of bandages, dressings and surgical masks, and the coating of medical implants and ensure a long antimicrobial activity by slow release of silver ions. Silver nanoparticles are also used in medical diagnostics as biosensors, optical signal through the use of localized, surface plasmon resonance (LSPR). The method has been used in the diagnosis head and neck squamous-cell carcinoma or squamous cell cancer (SCC or SqCC), by coating with nanosilver mouse monoclonal antibody against the protein p53, which underwent overexpression in patients studied [18]. Other nanostructures used in medicine are nanoparticles of gold. Gold nanoparticles, which can be shaped and obtain different shapes, with their ease of attachment on the surface of nanoparticles additional ligands, they fulfil specific functions. For diagnostic purposes, such ligands are used as lipids or antibodies that are used for imaging tumor cells and to determine the risk of atherosclerosis - macrophages [19]. Gold nano particles are also used in the treatment of cancer using photothermal therapy (PPT). The treatment utilizes electro- magnetic radiation which is directed to nanoparticles contained in pathological tissues. They convert the radiation into heat, causing a temperature increase in pathological tissues and cell death. Nanoparticles of gold nanorods have high absorption in the near infrared and visible range, and effective generation of heat, so that the arms are promising in the treatment of cancer and other diseases [20].

Core-shell nanoparticles are of a particular interest. They comprise of a core made from one material, and a shell (or coating) made from the second one. The core/shell nanoparticles are always made from an inorganic core (i.e. oxide, nitride, carbide). The shell is made from another oxide, nitride, carbide, or an organic material (monomer, surfactant, surface active organic molecule, and organic dye). By proper selection of core and shell materials properties of nanoparticles can be combined, or the surface can be functionalized. Low toxicity of these

types of nanoparticles made of gold and ease of synthesis of such nanoparticles implies that they are used as carriers for drugs and biological macromolecules such as peptides, proteins and nucleic acids. Nanoparticles such as these provide pharmaceuticals to specific sites in the body (e.g. to tumor cell), thereby increasing the effectiveness of therapy. Nanoparticles of gold can be used as a carrier of insulin according to a study by Bhumkar et al. [21]. Gold also perfectly absorbs X-rays, which can be used to assist radiation therapy [22]. Although radiotherapy is still being improved, including the use of a radiation beam with a high voltage in order to avoid damage to the skin, tomotherapy and modulating the intensity of the therapeutic beam, is still an unresolved issue is the protection of normal cells against radiation beam [23]. The solution to this problem is to use nanoparticles of gold that are accumulated in the site of the tumor and absorbing ionizing radiation allowing the use of lower therapeutic doses, which protects normal tissues. It is estimated that the strengthening of therapeutic doses using the nanoparticles of gold before the radiation reaches up to 200%. Studies Hainfeld et al. [24] showed that gold nanoparticles do not cause growth inhibition of neoplastic lesions, and irradiation causes only slow down the development of the tumor. In contrast, irradiation after the administration of nanoparticles of gold resulted in substantial reduction in tumor size or total eradication. However, in some instances, this therapy did not give positive results and tumor renew. Copper is another metal used in nanomedicine. The research results have shown that copper oxide nanoparticles (CuONPs) can be used in nosocomial infections, but their antibacterial activity is less than the nanosilver. Additionally, antiviral qualities can be used against influenza virus A and SARS virus [25]. CuONP good solubility in a low pH gives the possibility of using them in the treatment of neoplastic diseases. A study conducted by Studer et al. [26] has shown toxicity of nanoparticles on HeLa cells. Probably penetrating into the cells are located in the lysosomes and changing the osmotic pressure or to produce radicals cause the release of their contents into the lumen of the cell [26]. Another research group has demonstrated that CuONPs inhibit the proliferation of melanoma cancer cells and HeLa cells via cell cycle arrest at G0 / G1 phase, and the damage of the mitochondrial membrane to induce apoptotic pathways [27].

1.4. Fullerenes, Graphene and Carbon Nanotubes

A fullerene is a molecule of carbon in the form of a hollow sphere, ellipsoid, tube, and many other shapes. Spherical fullerenes are also called buckyballs, and they resemble the balls used in football. Cylindrical ones are called carbon nanotubes or buckytubes. Fullerenes are similar in structure to graphite, which is composed of stacked graphene sheets of linked hexagonal rings; but they may also contain pentagonal (or sometimes heptagonal) rings. Fullerenes are nanostructures with a shape similar to the sphere shell consisting of a conjugated ring consisting of five or six carbon atoms. The most popular are sixty-atomic nanostructures on the shape of a truncated icosahedron. Fullerenes are used for imaging tumors during surgery and to observe the lymph nodes closest to the tumor foci. In addition to the interior of the nanostructures can be made radioactive isotopes used in radiation therapy. The discovery of fullerenes significantly expanded the number of known carbon allotropes, which until recently were limited to graphite, diamond, and amorphous carbon such as soot and charcoal. Unique chemistry and technological applications made buckyballs and buckytubes the subject of intense research, especially in materials science, electronics, and

nanotechnology. For the past decade, the chemical and physical properties of fullerenes have been a hot topic in the field of research, development are likely to continue to be for a long time. Fullerenes were under study for potential medicinal use: binding specific antibiotics to the structure to target resistant bacteria and even target certain cancer cells such as melanoma [28]. Fullerenes have been extensively used for several biomedical applications including the design of high-performance MRI contrast agents, X-Ray imaging contrast agents, photodynamic therapy and drug and gene delivery, summarized in several comprehensive reviews [29].

Graphene is a two-dimensional layer of carbon atoms with a thickness of single atom, of a hexagonal arrangement of atoms in a shape of *honeycomb*, and is often visualized as a homogeneous network of a large size. It is the basic structural element of other allotropes, including graphite, charcoal, carbon nanotubes and fullerenes. In real life, such an ideal structure does not exist, however it is possible to produce such a structure as small adjacent monolayers. Graphene has many extraordinary properties such as an extremely high mechanical strength and flexibility, good thermal and electrical conductivity, is nearly transparent. There was the bipolar transistor effect identified as a quality of graphene as well as ballistic transport of charges and large quantum oscillations in the material. Graphene is impermeable to virtually all substances, biological properties, the ability of sensory, high electron mobility and hydrophobicity (repulsion of water molecules). Of course, all these characteristics are present together only in theory. In practice, graphene is produced by various methods. The two main ones are: carbon deposition on metals and substrates of crystalline and multi-splitting (exfoliation) to a maximum of thin graphite flakes. The first process allows the fabrication of graphene monolayers mononuclear about the maximum size of the order of tens of microns. In the second one slightly thicker flakes made of several atomic layers on their surface are formed with significant amounts of oxygen. This results in formation of graphene oxide (GO), which in subsequent stages is subject to reduction (removal of oxygen) forms of reduced graphene oxide (rGO).

Medical applications of graphene are built around its bacteriostatic and bactericidal properties, which are pledged with selected other features open extremely wide field of possibilities. Biomedical applications relate to the whole family of graphene derivatives. Antibacterial properties of graphene and graphene oxide correspond to two phenomena. The first is a purely mechanical effect of destroying cell membranes by the sharp edges of graphene flakes and GO. The second is destructive to many strains of bacterial interaction of oxygen introduced into the cells on the surface of the GO [30].

Medical uses of carbon materials are intensively researched especially carbon nanotubes (CNTs). Carbon nanotubes (CNTs) take the form of a hollow cylinder with a rolled-up graphene built. It may form a structure having a diameter of several nanometers and a length of a few centimeters. Due to the number of layers that build the wall nanotubes, divided into single-wall carbon nanotubes (SWNT) and multi-walled (MWNT). CNTs are used as drug carriers enable the continuous and constant dosing of pathological cells. It may additionally comprise an antibody or specifically targeting the enzyme activity [31]. An example would be the use of MWNTs containing cisplatin, the use of which resulted in inhibition of tumor cell growth [32]. Similar results were obtained by combining doxorubicin with carbon nanotubes in breast cancer [33], or the attachment of carboplatin in the treatment of bladder cancer [34]. Nanotubes are also excellent semiconductors, with strong fluorescence and Raman scattering, can also be used as a scaffold for the immobilization of biomolecules. Such scaffolds are used

in the diagnosis of biological protein microarrays in nanomatrices with high sensitivity of detection of 1 fmol / l [35, 36]. Use of the biosensor can be based on detecting changes in glucose concentration in the interstitial fluid, which is due to the increased quantity of sugar in the body which affects the fluorescence in the infrared nanotubes [36]. Carbon nanotubes are characterized by diverse morphology and unique physicochemical properties. These factors have been decided about rapid development of experimental works in the last twenty years exploring carbon nanostructures and their prospective applications. Nanomedicine is an extremely important area in which nanotubes can find a variety of uses, both in therapy and diagnosis. One of the directions is the development of biosensors, and nano-scale bioreactors, where the base is the protein or enzyme immobilization on the surface of carbon nanotubes or in the interior of the graphite cylinder [37, 38]. There are reports of electro-analytical devices based on nanotubes, which can be effectively used for the diagnosis of antigens and catalyze the enzymatic reaction [38]. By attaching specific ligand at the end of the carbon nanotube for example may be obtained useful nano diagnostic probes. Carbon nanotubes can also become a breakthrough in tissue engineering by mapping receptors on the cell surface. There are preliminary studies conducted suggesting the possibility of nanotubes acting as an electromechanical starter for artificial muscles and works on a suitable bio-functionalization of nanotubes, which are intended to provide a substrate for neuronal growth [39, 40]. Efforts are also made in attempts to combine carbon nanotubes with active particles to create modern target drug transporters, which are particularly important for the pharmaceutical industry [41, 42]. The pharmaceutical industry, and particularly the process of new drugs development, is faced with some problems, underpinned should be two important causes. First is the expiration of patents on essential drugs pharmacologically original so called *blockbuster drugs*. The second is inadequate bio-availability or the high toxicity of the newly discovered active substances. This forces pharmaceutical companies to take creative action to "refresh" programs of exploration and development of new drugs [42].

One strategy is to implement nanotechnology at an early stage of the process. Pharmaceutical industry offers as drug carriers liposomes, surfactants or polymeric structures [43]. Clinical studies have shown an increase in efficacy while reducing toxicity associated with doxorubicin liposomal carrier and polyethylene glycol. Systems transporting the drug substance may also affect other properties of the drug, solubility in water, allow to obtain sustained release or controlled release of the active ingredient addition can protect the drug substance against chemical degradation (hydrolysis and enzymatic), photo degradation and improve its bioavailability. The use of carbon nanotubes as a carrier is possible thanks to the progress of research on the chemical modification [44]. Carbon nanotubes can be subjected to functionalization with different active particles responsible for target recognition (targeted therapy), imaging and treatment. In this way, a multifunctional system for transporting a drug can greatly improve the pharmacological profile [44, 45]. Carbon nanotubes are also used as nanocontainers. Nanotubes filled with different chemical substances can be used in tumor therapy, diagnostic, and as contrast agents [45].

Research is carried out on "clean", efficient and reproducible synthesis of carbon nanotubes filled with iron for the treatment of cancer, using method of overheating by ferromagnetic fluid [46, 47]. The first clinical tests are run on coating with nanotubes metal or metal oxide nanoparticles, and at the same time obtaining a surface ligands (folic acid or the corresponding glycoprotein) providing transport of nanoparticles to the tumor cells. Such particles after intravenous administration to achieve the target are subjected to an external

magnetic field, which leads to a controlled heating of the metal particles and, consequently, destruction of the transformed cells. The results indicate that this method is more accurate than chemotherapy, carries also less risk of side effects and generates lower costs.

Carbon nanotubes also fulfill a role of gene carrier. Gene therapy is a promising treatment for cancer and genetic disorders. For the transport of viral genes there are special and non-viral carriers (e. g. liposomes, polymers, micro- and nanoparticles). The first ones carry a risk of side effects such as immune response, inflammation and oncogenesis. In contrast, no viral carriers, but more secure, do not always provide the appropriate level of gene expression. Therefore, researchers are making efforts to seek new, more efficient vehicles [41]. High molecular weight and a cationic nature of functionalized carbon nanotubes (f-CNT) allow electrostatic interaction with plasmid DNA. In order to test the ability of f-CNTs to form complexes with nucleic acids and their translocation were combined in various ratios f-CNT and the plasmid DNA containing the gene of β-galactosidase marker. Obtained images demonstrated the presence of CNT-DNA complexes. F-SWCNT nanotubes were present in the form of beams, between which there plasmids in the form of annular clusters or super-coiled structures. The study of gene expression level of β-galactosidase showed penetration of these complexes to the cells. Furthermore, it was found that 5-10 times greater levels of gene expression for f-SWCNT complexes and DNA than for the same helix [48, 49].

Carbon nanotubes have also been used as carriers of antigens. Connection of the external walls of the nanotubes with synthetically produced peptides, as for example. Epitopes of antigens create a system which can induce an immune response in a living body [50].

Recently intensive research was focused on fullerenols, the water-soluble derivatives of fullerenes. Fullerenols are being intensively studied in the context of the possibility of their application in the biomedicine due to their hydrophilic properties and the ability to eliminate free radicals. Fullerenols may in the future provide a solid alternative to currently used pharmacological methods in chemotherapy, treatment of neurodegenerative diseases and radiobiology. Depending on the research protocol applied, fullerenols may also act as pro oxidants. The dualistic nature of fullerenols may contribute to finding new biomedical applications of these agents in the future, by exerting a cytotoxic or protective effect respectively against cancer cells or healthy cells [51].

1.5. Hydroxyapatite Composites

Great importance for medicine has hydroxyapatite nano composite – occurring naturally as a substrate of bone and teeth. This is flexible-HA composite hydrogel, which has a mineral-to-matrix organic ratio approximating to that of human bone. Due to the high percentage of rejection of artificial implants for hydroxyapatite is used as the coating of metal medical implants. Given its natural character it reduces the immune response and promotes healing of wounds. Additionally, it can be used as a drug carrier for bone tissue for the treatment of inflammatory or post-operation complications. Research is also progressing on the use of nanohydroxyapatite in tumor therapy by combining nanohydroxyapatite Fe^{3+} ions exploiting their magnetic properties [52].

1.6. Magnetic Nanoparticles

Magnetic nanoparticles (MNPS) are made of an inorganic core, e.g. iron oxide, cobalt or nickel coated with substances being compatible with respect to the tissue, to which has been implemented [53]. One of the most important features is the MNPS to *superparamagnetism* used in clinical diagnostic techniques. Introduction of MNPS to the tested tissue bears effect of disorder of the local magnetic field in the tissue resulting in decrease of the relaxation time, the phenomenon used in magnetic resonance imaging [54, 55]. Using MNPS significantly improves possibilities of distinction between tumor and healthy tissue. Among the available contrast agents using nanoparticles there are superparamagnetic iron oxide (SPIO), used for liver imaging, or ultra small SPIO called Combidex used in the diagnosis of metastases with a diameter of 5-10 nm in the lymph nodes [56]. In addition to tumor tissue imaging MNPS are used to observe the cardiovascular system, especially in the detection of atherosclerotic plaques, and other diseases of the cardiovascular system. MNPS can be further combined with organic dyes and fluorescent like rhodamine or fluorescein isothiocyanate (FITC), allowing to define the extent of tumor resection intraoperative study.

Other application of MNPS is delivery of medicine to specific pathological tissue by utilizing the affinity of the ligands used in surface and magnetism which allows manipulating with pharmaceuticals through the external magnetic field. Biocompatibility, non-toxicity and high level of accumulation in tumors cause that magnetic nanoparticles are also used in intracellular hyperthermia. This therapy involves the use of MNPS and alternating magnetic field to produce a significant amount of heat in tumor cells. Depending on the temperature and time of generated heat it causes death of the tumor cell or at least increase their sensitivity to radiotherapy or chemotherapy [14].

1.7. Quantum Dots

Quantum dots (QDs) are nanostructured semiconductors, in which the motion of electrons is suppressed in three directions and creating by this way so-called potential barrier forming *potential box*. Single QD nanoparticle is composed of a core consisting of 100 - 100 000 atoms of carbon mainly telluride or cadmium selenide with futures of a semiconductor. The core is surrounded by a protective coat of zinc sulfide, which can be connected to various ligands, i.e. nucleic acids, proteins and antibodies having an affinity to specific structures in the body, e.g. tumors. Additionally coat can be enriched by a variety of chemical compounds, e.g. polyethylene glycol (PEG) or dihydrolipoic acid (DHLA), which protects the QDs from the action of enzymes and hydrolysis. To reduce aggregation of the quantum dots in the suspension, additional outer layer of trioctylphosphine oxide (TOPO) is added giving nanostructure hydrophobic character. TOPO is an organophosphorus compound $OP(C_8H_{17})_3$, frequently referred to as TOPO, this compound is used as an extraction or stabilizing agent. It is an air-stable, white and solid at room temperature [57]. QDs are the result of a complex process that can be matched to obtain a different size and shape of the nanostructures. This is an important property of quantum dots, since the length of the emitted electromagnetic waves depends on the size of the nanoparticles [58] used in the multidimensional detection, which gives opportunity to use QDs of different colors. QDs have a wide range of radiation from the ultraviolet absorption (400 nm) to infrared (2 000

nm), a narrow, symmetric emission spectrum and a powerful, deep and constant intensity of light [59]. It has been shown that a combination of 6 colors at 10 intensities is sufficient to encode more than one million combinations. Due to its characteristics of QDs are widely used in medicine, for detection of tumor cells with the aid of fluorescence microscope [60]. Tumor markers are detected by specific antibody attached to the quantum dots shell which, when injected into a patient prior to surgery, facilitate the work of the surgeon, thereby improving the visibility of treated surgically tumor. In vitro studies have shown a higher specificity of antibody-coated QDs to tumor cells than the melanocytes, resulting in high specificity of detection, which is very important in the diagnosis of tumors with the difficult cytological examination [60]. Using quantum dots coated with specific biomolecules can detect and track the journey of parasites, viruses and bacteria within the host. They are also used for marking the DNA and create nanosensors to determine the kinetics of biochemical reactions in the cells and the concentration of various toxic chemicals in determining the degree of poisoning of the body. Quantum dots may be used as contrast agents in computed tomography and magnetic resonance imaging.

1.8. Dendrimers

Dendrimers are nanoparticles which adopt a three dimension, spherical shape with a diameter ranging from 1 nm to several tens of nanometers. Inside comprise of a core which is surrounded by a radially radiating dendrons forming the central portion of the nanoparticle. As a result, the external layers are formed in a branch called generation. They contain free functional groups which by increasing the amount of layers surface and modifications affect the size of the nanoparticles as well as physical and chemical properties. A characteristic feature of the dendrimers is the presence of voids between their arms, which can be used to transport different substances, including antitumor compounds. As a result of the combination with cytotoxic drugs dendrimer obtains nanostructure reducing significantly skin tumors in mice, whereas the combination of ibuprofen dendrimer increased the concentrations of drug in lung cancer cells [61]. As a result of the use of polyamidoamine dendrimers (PAMAM) as carriers for sulfamethoxazole, demonstrated a significant increase in antibacterial activity and increased the solubility of the antibiotic in water [62]. PAMAM dendrimers of specific modifications adopted antiviral activity against HSV-1 and HSV-2 in vitro cultures of HFF cell line and in vivo in mice as topical antiviral agent HSV-2 [63]. Another research team demonstrated modified dendrimers called vivaGel® (SPL7013 gel) tested by ex vivo against HIV in humans adopting strong virucidal properties. The obtained results show that after administration of intravaginal gel exhibits potent antiviral activity to three hours of application. Probably such properties were gained by binding virus to the surface protein envelope gp120, which is responsible for viral entry into cells [63]. Dendrimers due to the positive charge derived from the amine groups can connect with the negatively charged phosphate groups to serve as a non-viral vector of nucleic acid. Due to the high rate of removal from a human body dendrimers may be used as contrast compounds in the magnetic resonance imaging e.g. PAMAM of the 2nd and 6th generation enriched with gadolinium salts enhancing properties exploited in blood vessels imaging [64]. In clinical use dendrimers play considerable role depending on construction and the nature of dendrimer in use. For example, nanoparticles of less than 60 kDa are suitable for imaging of kidney, while larger, of

hydrophilic character, are much proper and useful to analyze the lymphatic system. Dendrimers containing antibodies can also be used as tumor markers [65].

1.9. Nanomaterials Produced by Microorganisms

Bacterial cellulose (BC) is nano biomaterial consisting of β-1,4-glucan produced by *Gluconoacetobacter xylinus* (formerly *Acetobacter xylinum*). The resulting polymer is skin look-alike with micro fibriles below 100 nm thickness, and given the appropriate spatial structure, flexible and with ability to retain water is used as bandage. In addition, BC is not mutagenic and does not cause allergic reactions. The dressing made of BC protects the wound from external factors at the same time does not adhere to the wound tissue, relieving pain and its properties can be enhanced by the addition of nano-silver or antibiotics. Tubular implants or vascular trachea can be obtained from bacterial cellulose with any length and diameter [66].

2. DRUG RELEASE FROM NANOPARTICLES

Nanoparticles are able to enter various types of cells and can interact with subcellular structures. The size, shape and chemistry of the nanoparticles affect cellular uptake, subcellular localization, and ability to catalyze oxidative products [67]. The nanoparticles are internalized by the cells using a possible mechanism of passive uptake or adhesive interaction. Van der Waals forces, steric interactions, electrostatic charges, or interfacial tension effects can initiate this uptake which does not result in the formation of vesicles [68, 69]. After this uptake, the nanoparticles are not needed to be placed within a phagosome. Porter et al. suggested that C_{60} molecules enter cells and can be found along the nuclear membrane, and within the nucleus [70]. Non-phagocytic uptake and free movement within the cell can cause very problematic situation by having direct access to cytoplasm proteins and organelles. Nanoparticles can be found in different locations inside cell, such as the cytoplasm, outer-cell membrane [71], mitochondria [67], lipid vesicles, along the nuclear membrane or within the nucleus [67, 71].

Cells generally use two main endocytic pathways to internalize nanoparticles: Phagocytosis and pinocytosis. Phagocytosis is generally found in neutrophils, dendritic cells, and macrophages [72] whereas Pinocytosis can be found in almost all types of cells. There different types of pinocytosis: clathrin-mediated endocytosis, caveolae-mediated endocytosis, clathrin/caveolae-independent endocytosis, and macropinocytosis (see Figure 2).

A number of researches are carried out to explore the internalization of nanoparticle via phagocytosis. The cellular uptake of nanoparticles through phagocytosis in macrophages employs attractive forces (i.e., ionic, electrostatic, hydrophobic/ hydrophilic, van der Waals) between the surfaces of the cells and nanoparticle. The phagocytosis can be initiated by the receptor-mediated recognition of opsonins adsorbed on the nanoparticle surfaces.

The geometry of the particle can help in controlling their cellular uptake through phagocytosis. Because of different shapes, the particles can generate different angles between the membrane and themselves at the point of cell attachment and this angle of contact shows

substantial effects on the ability of macrophages to uptake particles via actin-driven movement of the membrane of macrophages [73, 74]. Champion and Mitragotri reported that the shape of the particle, not size, plays a dominant role in phagocytosis. They studied six different geometric shapes of nanoparticles, such as, spheres (radius 1.0–12.5 μm), oblate ellipsoids (major axis 4 μm, aspect ratio 4), prolate ellipsoids (major axis 2–6 μm, aspect ratio 1.3– 3), elliptical disks (major axis 3–14 μm, aspect ratio 2–4, thickness 400–1000 nm), rectangular disks (major axis 4–8 μm, aspect ratio 1.5–4.5), and UFOs (sphere radius 1.5 μm, ring radius 4 μm). They confirmed that the elongated particles with higher aspect ratios are less prone to phagocytosis [74]. A similar finding was also described by Geng and coworkers [75]. Harguindey et al. suggested that a higher aspect ratio can be associated with preferential localization into endosomes and lysosomes [76]. So it can be concluded that the shape of the particles should be designed properly to modulate intracellular targeting and phagocytosis.

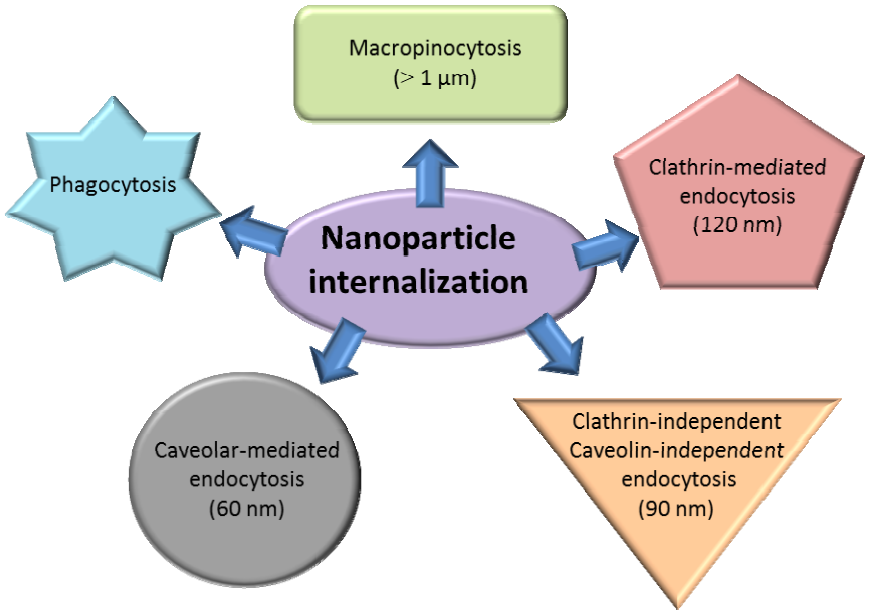

Figure 2. Internalization of nanotransporters in cell.

Nanoparticles are generally internalized by cells via more than one endocytic pathway. Zhang et al. [77] carried out an experiment on lapatinib-loaded nanoparticles formulated with a core of albumin and a lipid corona made by egg yolk lecithin. Results showed that the size and zeta potential of the nanoparticles were ~62 nm and 22.80 mV respectively. The nanoparticles were taken up by BT-474 cells via energy-dependent endocytosis including clathrin-dependent pinocytosis and macropinocytosis.

An important aspect of nanoparticles drug delivery systems is the mechanism by which drugs are released to the target cancer cell upon entry of the nanoparticle-drug conjugate. The main aim of release kinetics control is to regulate the drug level in blood within the therapeutic window, between the minimum toxic concentration (MTC) and the minimum effective concentration (MEC) [78]. Upon administration of a drug as a single large dose, the drug level is raised above MTC, causing toxic side effects, and then rapidly drops below the MEC. Multiple dosing with a certain interval can decrease the instability of drug levels in

plasma but can cause non-compliance issues in patient. For this reason, it is needed to develop specific drug carriers that provide controlled release of a drug with a low dosing frequency. Hence, a constant drug release rate (zero-order drug release profile) is frequently followed [78, 79]. On the other hand, pulsatile or stimuli-responsive drug release became interesting topic of research also to achieve timely drug release [80-82].

Several factors regulate the release of drugs from carrier such as the composition (drug, polymer, and additives), their ratio, physical and/or chemical interactions among the components, and the preparation methods. The drug release can be classified into four categories on the basis of the mechanism by which a drug escapes a carrier (solvent, diffusion, chemical reaction, and stimuli controlled release) [83, 84].

Solvent transport into a drug carrier can affect the release behaviour of the drug from carriers. There are two types of solvent-controlled release: swelling-controlled release and osmosis-controlled release [83].

If glassy hydrophilic polymeric systems are put in aqueous solutions (eg. body fluids), water diffuses into the system. The uptake of the water causes the swelling of the polymeric particles followed by drug release (swelling-controlled release). The rate of the release of the drug can be determined by the diffusion rate of water and the chain relaxation rate of polymers [85]. Different groups of researchers reported that the swelling-controlled systems can be made by polymeric materials with three dimensionally crosslinked network such as hydrogels, where the mesh size plays a central role in controlling the behaviour of drug release [85, 86]. It was found that the swelling-controlled systems can achieve a zero-order drug release, depending on the polymer composition [87] or initial drug distribution in the system [88].

Osmosis-controlled release can be found in a carrier covered with a semi-permeable polymeric membrane. Water can flow through this membrane from outside of the carrier (with a low drug concentration) to the drug-loaded core (with a high drug concentration). It has been reported that this mechanism can show a zero-order release profile as long as a constant concentration gradient is maintained across the membrane [89].

In case of diffusion-controlled drug release, a drug can be dissolved or dispersed in a core surrounded by polymeric membrane [90]. The different concentrations of the drugs across the membrane drive this diffusion. In this case, the drug initially dissolves in the core then diffuses through the membrane. The diffusion-controlled release profile can also be found in matrix-type nanospheres, where drug molecules are dispersed throughout the polymer matrix. Here, no membrane acts as a diffusion barrier. As a result, this matrix-type system generally shows high initial release, followed by a decreasing release rate with the increasing diffusion distance for drug molecules located inside of the carrier.

Different types of biodegradable polymeric drug carriers such as polyamides, polyesters, poly(amino acids), and polysaccharides release drugs by hydrolytic and/or enzymatic degradation of amide, ester, and hydrazone bonds in their backbones [91-93]. Bulk degradations are found from matrices made of polymers like poly(lactic-co-glycolic acid) (PLGA), polylactic acid (PLA), and polycaprolactone (PCL). This process can result in simultaneous degradation of entire matrices. In a small-dimension matrix like nanoparticls, the distance of water diffusion is short and the domain size of crystallization is found to be restricted. In this case, the polymer degradation is significantly enhanced, and these polymers do not necessarily follow the typical surface erosion behaviour but can show a bulk degradation (constant particle size during polymer degradation) [94].

The behaviour of the release of the drug from stimuli-responsive nanocarriers is regulated by internal or external factors such as pH, temperature, ionic strength, sound, and electric or magnetic fields [80]. As the stimuli can be localized, these carriers were explored for target-specific drug delivery. Researchers have developed some nanocarriers with pH-sensitive linkers for tumor-specific drug delivery [95, 96]. To increase the contrast between intracellular and extracellular drug release pH-sensitive carriers have been developed [96-98]. In case of thermosensitive drug carriers, the temperature-induced phase transition of the polymer causes the release of the drugs [99, 100].

3. LIPOSOMES AND THEIR MODIFICATIONS

Nanotransporters have been explored for delivering drugs for over 35 years. Liposomes have been the most successful drug delivery carriers. Liposomes are extensively used as carriers for numerous molecules in cosmetic and pharmaceutical industries. Additionally, liposomes can entrap unstable compounds (for example, antimicrobials, antioxidants, flavors and bioactive elements) and can trap both hydrophobic and hydrophilic compounds, avoid decomposition of the entrapped compounds and release the entrapped at designated targets. Because of their biocompatibility, biodegradability, low toxicity and possibility to trap both hydrophilic and lipophilic drugs and simplify site-specific drug delivery to tumor tissues, liposomes have increased rate of both as an investigational system and commercially as a drug delivery system. The drugs inside the liposomes are protected from oxidation and degradation during circulation in bloodstream. This protective phospholipid shield or barrier remains undamaged until the contents of the liposome are delivered to the exact target gland, organ, or system where the contents will be utilized [101]. Since the introduction of Doxil (a PEGylated liposomal doxorubicin), several products have been approved worldwide [102]. Doxil was approved by the US FDA in 1995 [103]. Liposomes are mostly used for the passive targeting having blood lifetime one or two days. It is required that the size of liposomes is less than 200 nm to facilitate fenestration through the leaky blood vessels around the tumour site. In general, the release of drug from liposome has to be slow enough not to let free drug to be removed quickly from the bloodstream. Liposome involves an aqueous core entrapped ba one or more bilayers composed of natural or synthetic lipids. Drugs with different lipophilicity can be encapsulated into liposomes i.e. lipophilic drugs are located in the lipid bilayer whereas hydrophilic drugs are in the core and those intermediary between lipid and aqueous phases.

Doxorubicin was loaded into the aqueous core of the liposome at a concentration exceeding saturation. This high loading (~ 12.5% by weight of the lipids) was achieved through a special technique called active loading using an ammonium sulphate gradient [104]. Undissolved doxorubicin is in the core in the form of crystals. This method of preparation serves to prolongation of the drug release beyond the circulation halftime.

Most of the liposomes for cancer treatment were approved on the basis of reduced side effects due to their passive targeting capabilities. Other liposomal anticancer products, such as DaunoXome and Myocet were primarily used to reduce toxicity in comparison to free doxorubicin and not to sustained release of encapsulated drug [105].

Except of conventional liposomes there are modified ones called stealth liposomes. These were designed to improve properties of transporters. The main reason for modification of liposomes is that although they behave like biomembranes they are still foreign objects of the body. Therefore, liposomes are known by the mononuclear phagocytic system (MPS) after contact with plasma proteins. Accordingly, liposomes can be removed from the blood stream. These stability difficulties are solved through the use of synthetic phospholipids, particle coated with amphipathic polyethylene glycol (PEG), coating liposomes with chitin derivatives, freeze drying, polymerization, micro-encapsulation of gangliosides [106]. Coating liposomes with PEG reduces the percentage of uptake by macrophages and leads to a prolonged circulation and, therefore, make available abundant time for these liposomes to leak from the circulation. Stealth liposomes are transporters with a membrane composed of phospholipid bilayer used to deliver drugs into a cell. A liposome can be made of naturally phospholipids with mixed lipid chains coated by polymers of PEG and colloidal in nature. Stealth liposomes are a new generation of compounds used for controlled drug release [107]. This stealth principle has been used to develop the successful doxorubicin-loaded liposome product that is presently marketed as Doxil (Janssen Biotech, Inc., Horsham, USA) or Caelyx (Schering-Plough Corporation, Kenilworth, USA) for the treatment of solid tumors [108].

Very often, poly(ethylene glycol) molecules (PEG) (molar mass ~ 2000 Da) are situated on to the surface of the liposomes by mixing the PEGylated lipids with the main lipids that form liposome [103]. The combination of properties (PEGylation, active loaded crystallized drug and small size) enables some selectivity of action towards tumor tissue, thus reducing side effects of the drug. For example, the biodistribution characteristics of liposomes surface-modified with the mixture of polyethylene glycol (PEG) and polyvinyl alcohol (PVA) as a drug carrier for passive targeting of drugs was studied [109]. The liposomes were made of (egg phosphatidylcholine: cholesterol = 55:40, molar ratio) modified with both PEG and PVA (4:1 molar ratio).

Clinically have been approved these drugs in liposomes – Doxil (Caelyx in Europe), Myocet, DaunoXome and DepoCyt [101]. Doxorubicin is known for its cardiotoxicity which is minimized by closing in the first two liposomal drugs. Doxil is a PEGylated liposome and it was already mentioned that use of PEG increases circulation time, which result in delaying of capture by the reticuloendothelial system [110]. Doxil is used for treatment of metastatic breast cancer, ovarian cancer, multiple myeloma and also in treatment of AIDS-related Kaposi's sarcoma (KS).

It was also shown that taxane-resistant breast cancer patients treated with PEGylated liposomal doxorubicin exhibited slightly increased survival results compared to those treated with vinorelbine or vinblastine in combination with mitomycin C [111]. The effectiveness of doxorubicin and its PEGylated form is nearly the same but cardiotoxicity, myelosuppression, vomiting and alopecia was decreased in the groups of patients treated with Doxil [112]. The same result was obtained for Kaposi's sarcoma treatment [113, 114]. Doxil was also compared with topotecan used for ovarian cancer. Doxil show much lower toxicity and effectiveness of therapy is comparable [115]. Increased efficiency gives Doxil in combination with other chemotherapeutic drugs docetaxel or bortezomib but unfortunately this combination leads to higher toxicity [116, 117]. Doxil, in combination with radiotherapy, has shown increased anticancer effect [118]. Myocet is a liposomal doxorubicin used for the treatment of breast cancer in combination with cyclophosphamide. In the trials and in comparison with free doxorubicin it was found that Myocet show lower cardiotoxicity and

neutropenia and has the same effectiveness of cancer treatment [119, 120]. Another liposomal product DaunoXome containing daunorubicin was showing better results than doxorubicin, bleomycin and vincristine, in Kaposi's sarcoma treatment [121]. DepoCyt is commercially available non-PEGylated liposomal form for cytarabine, which belong to a group of hydrophilic chemotherapeutic drugs. It can be used for treatment of lymphomatous meningitis, leukaemia and glioblastoma.

There are plenty of anticancer liposomes under clinical trials. To the group belong PEGylated lipoplatin, S-CKD602 [122] and NL CPT-11 containing cisplatin, CKD-602 (a camptothecin analogue) and irinotecan (CPT-11), respectively. From the trials it follows that lipoplatin is less toxic and of the same activity like cisplatin applicable for various cancers [123, 124, 125].

Drug irinotecan was encapsulated in liposomes and products are under names NL CPT-11, CPX-1 and LE-SN38. The drugs are tested for glioma and colorectal cancer treatment [126]. Liposomes can be modified for specific targeting. Such example can be MBP-426 containing oxaliplatin and transferrin which is bonded to phosphatidylethanolamine of liposome [127]. MCC-465 is a PEGylated liposome encapsulating doxorubicin with surface modification with a fragment of the human monoclonal antibody, able to identify cell surface molecules of different cancer cells [128, 129]. CPX-351 is a liposome encapsulated formulation of cytarabine and daunorubicin that exploits molar ratio-dependent drug-drug synergy to enhance antileukemic efficacy. The phase II study shows on lower mortality of patients [130]. Trastuzumab combined with sequential chemotherapy with taxanes and anthracyclines as primary systemic therapy achieved high rates of pathologic complete response. Non-pegylated liposome-encapsulated doxorubicin has shown equal efficacy but minor cardiotoxicity compared to doxorubicin. This phase II study aimed to evaluate the activity and safety of trastuzumab with sequential chemotherapy for early or locally advanced HER2 positive BC.

No cardiac toxicity or discontinuation of trastuzumab was reported. This study confirms that integrating anti-HER2 therapy in primary treatment for HER2 positive breast cancer is active [131].

3.1. Modified Liposomes

To improve efficacy of cancer treatment by liposomes it is necessary to modify either liposomes or their surface by peptides, RNA or antibodies which also serve for targeted delivery to specific cancer tissue. Some examples of recent development in the field are mentioned hereinafter.

Dual-ligand liposomal delivery system for targeting the delivery of paclitaxel to lung cancer was prepared. The specific ligand peptide HAIYPRH (T7) and the cationic cell-penetrating peptide TAT were connected with phospholipid via a polyethylene glycol (PEG) spacer to prepare the dual-ligand liposomes (T7/TAT-LP-PTX) [132].

Active targeting molecules displayed better cell selectivity but were shadowed by the poor tumor penetration effect. Cell penetrating peptides could increase the uptake of the carriers but were limited by their non-specificity. Dual-ligand system may possess a synergistic effect and create a more ideal drug delivery effect. Thus, liposome system modified with RGD, TAT and cleavable PEG was designed. The RGD specifically

recognized the integrins overexpressed on various malignant tumors and mediated efficient internalization in the synergistic effect of the RGD and TAT. In vitro cellular uptake and 3D tumor spheroids penetration studies demonstrated that the system could not only be selectively and efficiently taken up by cells overexpress ingintegrins but also penetrate the tumor cells to reach the depths of the avascular tumor spheroids. In vivo imaging and fluorescent images of tumor section further demonstrated that this system achieved profoundly improved distribution within tumor tissues, and the RGD and TAT ligands on C-R/T liposomes produced a strong synergistic effect that promoted the uptake of liposomes into cells after the systemic administration of L-cysteine. The results of this study demonstrated a tremendous potential of this multistage liposomes for efficient delivery to tumor tissue and selective internalization into tumor cells [133].

Liposomal drug delivery system conjugated with cyclic arginine-glycine-aspartic acid-tyrosine-lysine peptide (cRGDyk) was developed to improve therapeutic efficacy in a mice model of bone metastasis from prostate cancer. Compared with free cisplatin and cRGDyk-free liposomes, cRGDyk conjugated liposomes showed significantly higher cellular uptake and higher cytotoxicity of loaded cisplatin, as evidenced by in vitro cell experiments. In vivo results revealed that free cisplatin and free cRGDyk could relieve tumor-induced pain but had no contributions to tumor regression and overall survival improvement. cRGDyk-free liposomal drug system with prolonged blood circulation time could accumulated in the tumor sites in the bone through enhanced permeability and retention (EPR) effects (see Figure 3) and however, did not exhibit desirable therapeutic efficacy superior to free cisplatin and free cRGDyk. Inspired by their enhanced therapeutic efficacy and low organ toxicity, cRGDyk conjugated liposomes could serve as an effective drug system for targeted and synergistic therapy of bone metastases [134].

Novel, acid-sensitive liposomes that respond to physiopathological pH for tumour targeting applications were obtained by surface modification with 1,2-distearoyl-sn-glycero-3-phosphoethanolamine-N-[methoxy(polyethyleneglycol)] (mPEG-DSPE) and stearoyl-poly(ethyleneglycol)-poly(methacryloylsulfadimethoxine) copolymer (stearoyl-PEG-polySDM). All of the liposome formulations were stable at pH 7.4, even in the presence of foetal bovine serum, but they underwent rapid size increase at pH 6.5. At pH 6.5, these liposomes displayed higher cytotoxicity than at pH 7.4 or compared to non-responsive control liposomes at both incubation pH. Notably, treatment with free gemcitabine did not yield cytotoxic effects, indicating that the carrier can efficiently deliver the anticancer drug to the cytosolic compartment [135].

The cancer treatment through the combination of chemotherapy and thermotherapy using doxorubicin-loaded magnetic liposomes is reported. The citric acid-coated magnetic nanoparticles (CAMNP, ca. 10 nm) and doxorubicin were encapsulated into the liposome (HSPC/DSPE/cholesterol = 12.5:1:8.25) by rotary evaporation and ultrasonication process. In vitro cytotoxicity of the liposome was investigated through 3-(4,5-dimethylthiazol-2-yl)-2,5-diphenyltetrazolium bromide (MTT) assay using L-929 cells, as the mammalian cell model. In vitro cytotoxicity and hyperthermia (inductive heating) studies were evaluated against colorectal cancer (CT-26 cells) with high-frequency magnetic field (HFMF) exposure. MTT assay revealed that these drug carriers exhibited no cytotoxicity against L-929 cells, suggesting excellent biocompatibility. When the magnetic liposomes with doxorubicin was used to treat CT-26 cells in combination with HFMF exposure, approximately 56% cells were killed and found to be more effective than either hyperthermia or chemotherapy treatment

individually. Therefore, these results show that the synergistic effects between chemotherapy (drug-controlled release) and hyperthermia increase the capability to kill cancer cells [136].

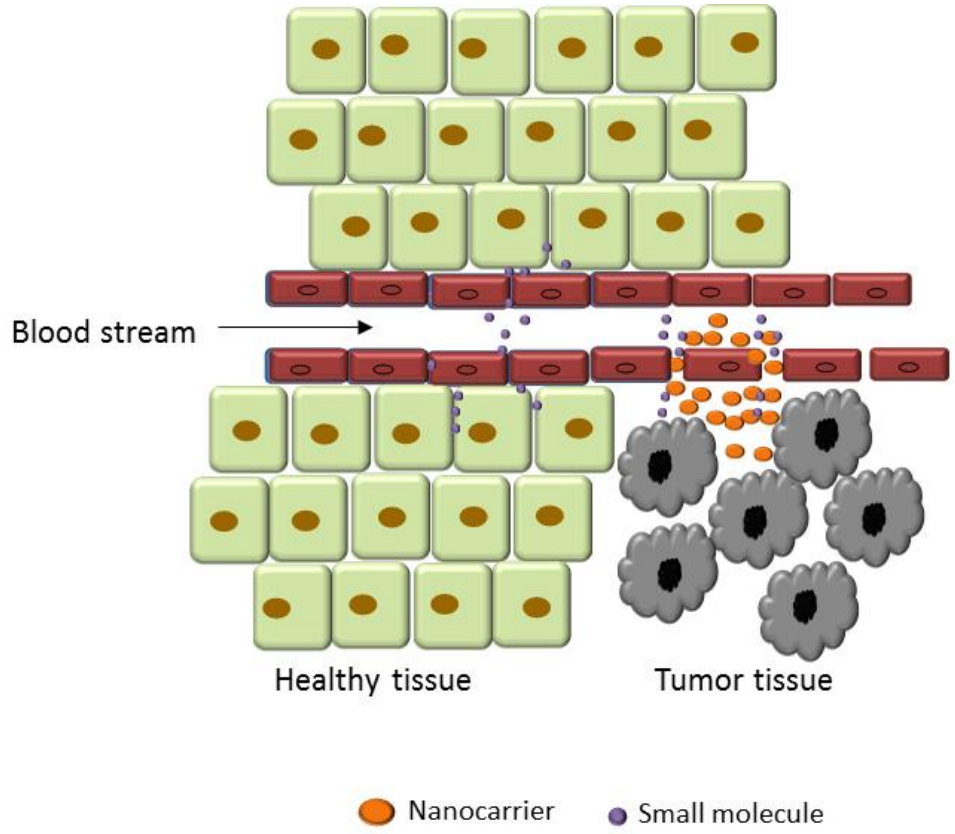

Figure 3. Enhanced permeability and retention (EPR) effect (targeting by leaky vessels in cancer).

Thermally enhanced drug delivery using low temperature liposomal doxorubicin (LTLD), given with mild local hyperthermia (MLHT) for breast cancer was developed. The phase I trials shown that the use is safe and that this combined therapy produces objective responses in heavily pre-treated breast cancer patients. Future work should test thermally enhanced LTLD delivery in a less advanced patient population [137].

Combining chemotherapeutics is a promising method of improving cancer treatment; however, the clinical success of combination therapy is limited by the distinct pharmacokinetics of combined drugs, which leads to nonuniform distribution. New approach to load two drugs with different hydrophilicities into a single cross-linked multilamellar liposomal vesicle (cMLV) to precisely control the drug ratio that reaches the tumor in vivo is reported. The stability of cMLVs improves the loading efficiency and sustained release of doxorubicin and paclitaxel, maximizing the combined therapeutic effect and minimizing the systemic toxicity [138].

Liposome mediated anticancer drug delivery has the advantage of reducing cytotoxicity in healthy tissues but slow drug release decreases the therapeutic efficacy of PEGylated liposomal doxorubicin. To increase the efficacy a combination of stealth thermosensitive

liposomes and local mild hyperthermia was investigated to increase bioavailable doxorubicin levels in tumors. It was found that the combination of PEGylated thermosensitive liposome and local mild hyperthermia offers promising clinical opportunities to improve liposomal doxorubicin delivery to solid tumors [139].

A single nanoparticle platform has been developed through the modular and controlled layer-by-layer process to codeliver siRNA that knocks down a drug-resistance pathway in tumor cells and a chemotherapy drug to challenge a highly aggressive form of triple-negative breast cancer. Layer-by-layer films were formed on nanoparticles by alternately depositing siRNA and poly-L-arginine; a single bilayer on the nanoparticle surface could effectively load up to 3500 siRNA molecules, and the resulting nanoparticles exhibit an extended serum half-life of 28 h. In animal models, one dose via intravenous administration significantly reduced the target gene expression in the tumors by almost 80%. By generating the siRNA-loaded film on doxorubicin-loaded liposome, the efficacy was enhanced by 4 fold in vitro and led to up to an 8 fold decrease in tumor volume compared to the control treatments with no observed toxicity [140].

Liposomal drug delivery has expanded considerably over the past few decades, and several liposomal drugs are already providing improved clinical outcomes. Liposomes have now progressed beyond simple, inert drug carriers and can be designed to be highly responsive in vivo, with active targeting, increased stealth, and controlled drug-release properties. Ligand targeted liposomes have the potential to revolutionize the treatment of cancer. Recent challenges in ligand targeted liposomes are described [141].

4. NATURAL NANOTRANSPORTERS – PROTEINS

Ferritin belongs to proteins with cage like structure, which can be used to bind molecules in its cavity. Ferritin molecules are present in most living organisms and are used to store iron ions as their hydrated hydroxide-oxide Fe(III) to avoid their toxicity due to free radicals that can be generated with Fe(III), which is readily reduced to Fe(II). There are two kinds of ferritins namely maxiferritins and miniferritins. These have distinctly different inner and outer diameters and molecular weights. Maxiferritins are formed from 24 subunits 12 nm in diameter with 8 nm cavities with MW = 480 kDa and miniferritins formed from 12 subunits 8 nm in diameter with 5 nm diameter cavities of MW = 240 kDa [142]. Mostly maxiferritins are used, especially horse spleen ferritin for its commercial availability. Ferritin wide occurrence as well as its ability to reversibly store and release iron ions to the living cells has attracted the interest of researchers worldwide.

It was found that the cavity can be utilized for storage of other ions and molecules and can be utilized for synthesis of nanoparticles with defined size. Apart from interior cavity, the surface of apoferritin can be modified. This offers further possibility of delivering encapsulated drug to a target cell in more effective way and minimalizing thus side effects particularly toxicity to nontarget organs by drugs.

There are two possible ways for preparation of apoferritin loaded compounds. These routes can be called reassembly and nanoreactor routes. Reassembly route comprise of disassembly of the apoferritin shell into protein subunits at low pH by addition of an acid. Then the solution of complex, drug or nanoparticles is added. Afterwards, pH of the solution

is adjusted with addition of a base to pH around 8. Protein subunits are reassembled again to form apoferritin with loaded compounds in the cavity [143]. Nanoreactor route comprise of utilization of ion or nanoparticles diffusion through channels in apoferritin structure. Mostly, ions are added to the apoferritin solution and mixture is shaken, afterwards, anions are added which form nanoparticles in the cavity. Reactants and precipitates outside of apoferritin are than removed by centrifugation, dialysis or ultrafiltration.

Selective dose-dependent antitumor activity of horse spleen apoferritin encapsulated PbS quantum dots against two human-derived colorectal carcinoma cell lines is reported (GI_{50} similar to 70 μg mL^{-1}) [144]. Following in vitro exposure to PbS, CRC cells fail to recover proliferative capacity, and undergo apoptosis triggered by the generation of reactive oxygen species (ROS). In contrast, the apoferritin-PbS nanocomposites do not affect the growth and cell cycle of non-tumor human endothelial HMEC-1 cells. Neither adverse health nor behavioral indicators were observed throughout the 15 day study in mice. The photoluminescence combined with selective antitumor activity offer potential for simultaneous non-invasive imaging and treatment of malignant tissue. Apoferritin was employed to encapsulate anticancer drugs cisplatin and carboplatin [145, 146]. It is well known, that clinical application of platinum-based anticancer drugs is largely limited by severe general toxicity and drug resistance. Drug delivery systems with tumor-targeting potential are highly desired for improving the efficacy and applicability of these drugs. The delivery of platinum drugs cisplatin, carboplatin and oxaliplatin by encapsulating each of them in the cavity of apoferritin was studied. The encapsulation was achieved through reassembly route at pH 2.0 and 7.4, respectively, in saturated drug solution. UV-vis spectrometry, circular dichroism spectrometry, dynamic light scattering, and inductively coupled plasma mass spectrometry were used to characterize the apoferritin-drug complexes. The loading capacity of apoferritin varies with respective drugs and the structural integrity of the protein shell remains intact after encapsulation. In vitro assays on the rat pheochromocytoma cell line (PC12) show that cisplatin inhibits the cells in a slow but sustaining mode and the cellular uptake of platinum drug is enhanced by apoferritin. Carboplatin and oxaliplatin complexes in apoferritin exhibit a marginal cytotoxicity towards this cell line under similar concentrations [146]. A novel antibody-drug conjugate was synthesized incorporating ferritin cisplatin nanoparticles [147]. An average of three molecules of monoclonal antibody (mAb) Ep1 to the human melanoma-specific antigen CSPG4 were conjugated to a single ferritin cage encapsulating about 50 cisplatin molecules. The flow cytometry demonstrated specific binding to a CSPG4(+) melanoma cell line, but not to a CSPG4(-) breast carcinoma cell line. As compared to the cisplatin-containing ferritin nanoparticle alone, which inhibited thymidine incorporation more efficiently in breast carcinoma than melanoma cells, the mAb-derivatized nanoparticle had a 25-fold preference for the latter. Anticancer activity was also studied on a methylene blue-encapsulated apoferritin complex. The complex shows cytotoxic effects on MCF-7 human breast adenocarcinoma cells when irradiated at the appropriate wavelength [148].

Ferritin can be genetically modified to present a peptide sequence on the surface [149]. Thus Cys-Asp-Cys-Arg-Gly-Asp-Cys-Phe-Cys (RGD4C)-modified ferritin can efficiently target tumors through RGD-integrin interaction. It was shown that after being precomplexed with Cu(II), doxorubicin can be loaded onto RGD modified apoferritin with high efficiency (up to 73.49 wt %). These doxorubicin-loaded ferritin nanocages showed on U87MG subcutaneous tumor models a longer circulation half-life, higher tumor uptake, better tumor

growth inhibition, and less cardiotoxicity than free doxorubicin. Such a technology might be extended to load a broad range of therapeutics and holds great potential in clinical translation [149]. RGD4C-modified ferritin can also serve as a safe and efficient photosensitizer vehicle [150]. Zinc hexadecafluorophthalocyanine (ZnF16Pc), a potent photosensitizer with a high quantum yield but poor water solubility, can be encapsulated into ferritin and tests on U87MG subcutaneous tumor models, P-RFRTs showed a high tumor accumulation rate and minimal toxicity to the skin and other major organs.

Ma-Ham et al. [151] studied daunomycin, an anthracycline antibiotic drug that is used for specific types of cancer treatment such as acute myeloid leukemia and acute lymphocytic leukemia, encapsulated within apoferritin cage. They used reassembly route to load the therapeutic compound daunomycin into the cavity of apoferritin. At experimental pH 5 conditions the interaction between the apoferritin interior cage and daunomycin was weak making it difficult to encapsulate the drug effectively within the protein cage. The incorporation of poly-L aspartic acid, a polypeptide and biodegradable material that does not increase the toxicity of the drug delivery system and is negatively charged at pH 5.0, into the drug delivery system resulted in a substantial improvement in the drug encapsulation. The binding properties of free daunomycin with DNA were compared to the synthesized apoferritin protein based drug delivery system. Encapsulation of the daunomycin within the apoferritin protein cage had little effect upon the intrinsic binding constant, K(i), or the exclusion parameter n as compared to the free daunomycin model. The study resulted in the design and optimization of a unique protein based drug delivery platform using the protein cage apoferritin for potential therapeutic administration of the anticancer agent daunomycin.

Doxorubicin belongs to the group of anthracycline antibiotics with very effective anticancer properties. On the other hand, the cardiotoxic effects limit its application. To overcome this obstacle, encapsulation of this drug into the protective nanotransporter such as apoferritin is beneficial. The apoferritin-doxorubicin complex has been formed by reassembly of the apoferritin sphere in the presence of doxorubicin [152]. The doxorubicin encapsulation was carried out using direct and step-wise change of pH of the solution from 2.5 to 7.4. Non-denaturing polyacrylamide gels showed that the protein cage of the complex successfully self-assembles into its nanosphere form. It was found that up to 28 molecules of doxorubicin can be capsulated per apoferritin protein and no significant drug leakage occurs during the first two days.

Magnetic particle mediated transport in combination with nanomaterial based drug carrier has a great potential for targeted cancer therapy. Doxorubicin encapsulated into the apoferritin was conjugated with magnetic particles and investigated by capillary electrophoresis with laser-induced fluorescence detection (CE-LIF). This combination of magnetic particles and drug encapsulated in apoferritin can be potentially used for magnetic resonance imaging, thermotherapy and chemotherapy [153].

Voltammetry was used for detection of doxorubicin (DOX) and encapsulated doxorubicin in apoferritin structure at a carbon paste electrode [154]. The samples were measured by differential pulse voltammetry in phosphate buffer (pH 5.5). The experimental conditions as time of accumulation and deposition potential were optimized. The study also shows on the release of doxorubicin at different pH which is very important for cancer treatment. Fluorescent behaviour of doxorubicin in various solvents was studied [155]. Ethanol, acetonitrile and dimethyl sulfoxide were tested and the best linearity of the calibration curve was obtained when above 50 % of the solvent was present in the binary mixture with water.

Moreover, pH influence on the DOX fluorescence was also observed within the range of 4-10. Further, the DOX behavior in capillary electrophoresis (CE) was investigated. Electrophoretic mobilities (CE) in various pH of the background electrolyte were determined and CE was also used to monitor the encapsulation of DOX into the cavity of apoferritin as well as the pH-triggered release [155]. Apoferritin and liposome encapsulated forms of doxorubicin were prepared and their toxicity were compared with doxorubicin alone and Myocet on prostate cell lines [156]. Three different prostatic cell lines PNT1A, 22Rv1, and LNCaP were chosen. The toxicity was compared using the MTT assay, real-time cell impedance-based cell growth method (RTCA), and flow cytometry. The efficiency of doxorubicin entrapment was 56% in apoferritin cages and 42% in the liposome carrier. Apodox IC50 was determined as follows: 603.1, 1344.2, and 931.2 nM for PNT1A, 22Rv1, and LNCaP, respectively. Ferritin nanocages can carry high doses of doxorubicin for tumor-specific targeting and killing without any targeting ligand functionalization or property modulation [157]. Doxorubicin loaded apoferritin specifically bound and subsequently internalized into tumor cells via interaction with overexpressed transferrin receptor 1 and released doxorubicin in the lysosomes. In vivo in the mouse, it exhibited more than 10-fold higher intratumoral drug concentration than free doxorubicin and significantly inhibited tumor growth after a single-dose injection. It also displayed an excellent safety profile that significantly reduced healthy organ drug exposure and improved the maximum tolerated dose by fourfold compared with free doxorubicin [157].

Ferritins can be used not only for drug transport but can be applied for magnetic resonance imaging, optical imaging and cell tracking. The progress in the field can be also found in some reviews that appeared just recently [158-161].

5. DENDRIMERS AND POLYMER NANOPARTICLES

5.1. Polymeric Nanoparticles

Polymeric nanoparticles represent biomaterial widely used for drug delivery application, which arise from their remarkable biodegradability and biocompatibility with other molecules. Compared with other drug delivery materials (especially with liposome) the polymeric nanoparticles demonstrate higher stability, sharper size distribution, more tunable physicochemical properties, sustained and more controllable drug-release profiles, and higher loading capacity for poorly water soluble drugs. The applications of the polymers in drug delivery have been investigated extensively for group of natural and as well as for synthetic polymers [162, 163]. Natural polymers such as albumin, chitosan and heparin have been a material of choice for the delivery of oligonucleotides, DNA, protein and drugs. The clinical application of natural polymers as transporter for anticancer drug delivery were reported in the case of metastatic breast cancer, non–small-cell lung cancer (phase II trial) and advanced nonhematologic malignancies (phase I and pharmacokinetics trials using abraxane which represents nanometer-sized albumin-bound paclitaxel [164-166]. However, the synthetic polymers enable the delivery of various drugs due to their great modification potential allowing particles to be tailored for specific needs. *N*-(2-hydroxypropyl)-methacrylamide copolymer (HPMA), poly(lactico-glycolic acid) (PLGA) and polycaprolactone (PCL),

polystyrene-maleic anhydride copolymer (PMA), polyethylene glycol (PEG), and poly-L-glutamic acid (PGA) are reported as more common synthetic nanoparticle used in drug delivery [167]. For clinical trials of cancer various polymeric nanoparticles are known (Table 1).

Table 1. Polymer drugs nanoparticles

Name	*Drug*	Polymers	Indication	Reference
Xyotax	*Paclitaxel*	PGA	Ovarium cancer and non–small-cell lung cancer	[168, 169]
CT-2016	*Camptothecin*	PGA	Lung and breast cancer	[170]
FCE-28069	*Doxorubicin*	HMPA	Various cancer	[171]
PNU-166945	*Paclitaxel*	HMPA	Various cancer	[172]
Prothecan	*Camptothecin*	PEG	Various cancer	[173]
NKTR-102	*Irniotecan*	PEG	Ovarium and cervical cancer	[174]
NKTR-105	*Docetaxel*	PEG	Solid tumors	[174]
AD-70	*Doxorubicin*	Dextran	Various cancer	[175]
XMT-1001	*Camptothecin*	Polyacetal polymer	Advanced cancer	[176]

The functional properties of polymeric nanoparticles are based on amphiphilic block copolymers that self-assemble into nanoparticles in aqueous solutions, where the hydrophobic core region serves as a reservoir for hydrophobic drugs, whereas the hydrophilic shell region stabilizes the hydrophobic core and renders the polymers water-soluble [177].

For clinical applications, different types of chemotherapeutics conjugate with various polymers are used widely for *in vitro* and *in vivo* testing showing great potential in drug delivery. Among the synthetic polymers PLGA and PEG represent widely used transporters for *in vivo* drug delivery, due to their hydrophobic and hydrophilic properties. PLGA as polymers can easily hydrolyze into lactic acid and PEG can significantly reduce nonspecific cellular uptake by forming a stealth layer [178, 179].The interactions of polymers with drugs take a place during polymeric nanoparticles preparation where the drugs are easily encapsulated. It is reported that organic solvent diffused into the aqueous phases can be applied for encapsulation of the drug into polymers, which can lead to the evaporation of the organic solvent where hydrophobic polymers are self-assembled and form nanoparticles with drugs encapsulated inside [180-182]. However, different approaches have been established for co-encapsulate multiple therapeutic agents into a single polymeric nanoparticle. One of these approaches is to directly encapsulate multiple drugs into the hydrophobic polymeric core where multiple therapeutic agents are mixed with the polymer solution during the particle synthesis. This approach is widely adopted for the co-delivery of anticancer drugs. Typically the examples of directly polymer-drug encapsulation were reported by Xiang et al. [183], for the treatment of multidrug resistant (MDR) cancer using combinations of encapsulated cytotoxic drugs. They reported that the interaction of PLGA polymer nanoparticles formulations was capable of delivering a cytotoxic drug, vincristine, verapamil and their combination prepared via acetone–dichloromethane emulsion solution at predetermined concentrations before solvent displacement and particle precipitation. The

preparation of polyalkylcyanoacrylate (PACA) nanoparticles in combination with cyclosporin A and doxorubicin were reported by Soma et al. [184], as direct encapsulation of drug into polymer by emulsion polymerization process in which the hydrophobic cyclosporin A was added together with doxorubicin to the polymerization medium to achieve dual drug loading. Both of this studies show *in vitro* cytotoxicity for multidrug resistant cancer cell, enabling the use of a great potential of polymeric particles for the drug transports and cancer treatment. However, the problem is that it can limit this way of encapsulation come from little possibility to control the release of different drugs.

The drug releasing problem of direct encapsulation method can be avoided using alternative multicompartment approach. This approach is conceived using the advantages of highly functional surface of polymeric nanoparticles. Zhang et al. [162], reported a delivery of hydrophobic and hydrophilic drugs by aptamer-nanoparticles. They produced PLGA targeted polymeric nanoparticles which were conjugate with docetaxel (Dtxl) as a hydrophobic drug and doxorubicin (Dox) as a hydrophilic drug. PLGA polymer nanoparticles ware surface modified with oligonucleotides which was use as targeting ligands and as intercalation sites for a hydrophilic doxorubicin. The efficiency of PLGA nanoparticles was demonstrated against prostate cancer cell resulting in high targeting delivery of docetaxel and doxorubicine as well as effective drug releasing kinetics. The release profiles of Dtxl and Dox from the PLGA nanoparticles-aptamer bioconjugates showed a high releasing efficiency of 80 % after 6 hours for doxorubicin comparing with lower efficiency of docetaxel where after 6 hours it was released only 50 %. These pathways provide excellent opportunities for the delivery of two different class of drug for cancer treatment allowing application of combined therapy. This targeted co-delivery system may also allow for temporally distinct release of drugs, which may have implications for delivery to distinct anatomical locations [180].

The control of drug releasing was reported by Sengupta et al. [180], who synthesized a nanocell consisting of a PLGA core and a lipid envelope to demonstrate the potential of differential drug release in combination with anticancer therapy. The particles were fabricated by encapsulating doxorubicin after the conjugation with PLGA to achieve a slow release profile. Combretastatin from the other side were conjugated with PLGA-liposome allowed optimal loading of drug by partitioning into the lipid bilayer. Since doxorubicin is linked to the PLGA polymer, its release was determined by the hydrolytic degradation rate of the polymer and was much slower than the release of combretastatin resulted in a complete ablation of the tumor cells without affecting the endothelial cells. In compare with PLGA-liposomal co-encapsulation of combretastatin, liposomal shell faster degradation and releasing of drug resulted in a rapid collapse of the vascular network without affecting the tumor cells. The therapeutic efficacy of this treatment were examines on B16/F10 melanomas and Lewis lung carcinoma cell resulting in better tumor reduction, longer median survival time, as well as lower systemic toxicity. Thus, the concept can enables a significant advance in cancer therapy over current approaches.

One more approach for encapsulating and delivering drug by polymer is to capture multiple drugs into single polymeric nanoparticles by conjugation of multiple drugs to the polymer backbone. Bea et al. [185] reported the conjugation of doxorubicin and wortmannin to PEG–poly(aspartate hydrazide) which blocks copolymers through an acid-labile hydrazone bond where the hydrazone linker allows the release of the functional moieties by undergoing rapid hydrolysis in the acidic endosomal and lysosomal environments. According to the authors, the benefits of this approach lies in the fact that the ratio of the drugs can be precisely

controlled by varying the drug content during the conjugate synthesis process. The temporal control on anticancer drug releasing has been reported by Lammers et al. [181], using peptide linkers that are susceptible to intracellular proteases. In this experiment, the chemotherapeutic agents gemcitabine and doxorubicin interact with HPMA polymer nanoparticle by Gly-Phe-Leu-Gly peptide linker. This peptide sequence is a known substrate to a lysosomal cysteine protease, cathepsin B, where on this substrate drug release kinetics is observed at pH 6 indicating that after 10 hours 100 % of gemcitabine was released compared with doxorubicin were after 30 hours only 30 % was released increasing its toxicity, and it more strongly inhibited angiogenesis and induced apoptosis. According to the author, the poor doxorubicin releasing is directly connected with their structure which might hinder the cathepsin activity by blocking the peptide substrate. However, these findings demonstrate that passively tumor-targeted polymeric drug carriers can be used for delivering two different chemotherapeutic agents to tumors simultaneously.

The selective control of drug concentration and distribution within the tumor microenvironment is one of the most important factors to achieve effective and safe cancer chemotherapy. Controlled drug delivery systems using macromolecular bioconjugates have been shown to offer benefits for improving the delivering of two different pharmacologically active agents to tumors simultaneously. Among all the polymeric nanoparticles, polymeric micelles from amphiphilic which block copolymers are considered as the most promising drug carriers, and characterized by excellent biocompatibility, high drug-loading content, and markedly improved biodistribution.

5.2. Dendrimers Nanoparticles

Dendrimers are a novel class of nanoparticles widely used in cancer therapy composed of multiple highly branched monomers that emerge radially from the central core. Dendrimer-based drug delivery systems have been developed in order to improve the biodistribution of a drug in the body and to allow the controlled release of the drug at its target site. Their high aqueous solubility, low toxicity, compact globular shape and controlled surface functionalities with defined structure of initiator core, layers of branched repeating units and functional end groups on the outermost layer made them ideal carriers for water soluble and insoluble anti-cancer drugs [186]. The internal cavity of the dendrimers could be used for the encapsulation of hydrophobic anti-cancer drugs, offering the advantage of subsequent controlled release of the drug to the tumors and on the other hand multivalent surface of the dendrimers allows conjugation with hydrophilic drugs. However, it is reported that dendrimers are suitable for small anticancer drugs, where solubility and toxicity of the anticancer drugs against cancer cells can increase the encapsulation into dendrimers [187]. The dendrimer-drug conjugates generally consist of an anti-neoplastic agent covalently attached to the peripheral groups of the dendrimer and various types of this conjugates are reported. Among the dendrimers PGLSA poly(glycerol succinic acid) represent widely used transporters for delivery of camptothecins drugs, who are naturally-derived hydrophobic compounds with anticancer activity. Morgan et al. [188], reported an use of two dendrimes transporters, G4-PGLSA dendrimers with hydroxyl (G4-PGLSA-OH) peripheral groups and G4-PGLSA dendrimers with carboxylate (G4-PGLSA-COONa) peripheral groups, for encapsulation of 10-hydroxycamptothecin (10-HCPT) applied on MCF-7 human breast cancer cells. However, the

results showed that G4-PGLSA dendrimers with hydroxyl group after mixing with 10-HCPT was precipitated, which was explain as lower water solubility of dendrimers and they reported that the unloaded dendrimer didn't show any anticancer effect. In contrary to the dendrimers with hydroxyl group, the dendrimers with carboxylate group are excellent soluble in water. 10-HCPT was successfully encapsulated into dendrimer, which showed a significant reduction of cell viability, demonstrating that 10-HCPT retains the activity upon encapsulation. Similar results ware reported by same group [189], only in this experiment they synthesized dendrimer modified with PEG $(G4\text{-}PGLSA\text{-}OH)_2\text{-}PEG_{3400}$, and the anti-cancer activity was examined using HT-29 human colon cancer cells. In this case the same cytotoxicity was reported for encapsulated 10-HCPT as well as for non-encapsulated 10-HCPT. This lead to the conclusion that G4-PGLSA-COONa dendrimer show better abilities for delivering a highly potent lipophilic camptothecin derivative.

Poly(amido amine)-PAMAM dendrimer transporters for delivering of anticancer drugs modified with PEG and poly(γ-caprolactone) were reported by Wang et al. [190]. Doxorubicin and etoposide were successfully encapsulated into a formation of micelle dendrimer and applied on kidney epithelial cells. The results showed that the unloaded dendrimer didn't cause any cytotoxicity in comparison with loaded drugs, where they showed similar cytotoxicity for the cell at the same concentration. A cytotoxicity assay demonstrated that the star-PCL-PEG copolymer is nontoxic in cell culture. This type of block copolymer can be used as a drug delivery carrier. The anticancer drug delivery by PAMAM dendrimer was also reported by Malik et al., [191], where his group encapsulat cisplatin after interaction with carboxylate surface of dendrimer, enabling synthesis of highly water soluble dendrimer-platinate which slowly released cisplatinum. In vivo experiment was conducted on B16F10 melanomas resulting in an accumulation of cisplatin in tumor cells with high cytotoxicity and less toxicity in normal tissues by 3-to 15-fold compared to the free drug in the solution. This model can open the way for delivery of anticancer drugs. To avoid the solubility problem of doxorubicine and secondary effect on health tissue Kojima and his group encapsulated doxorubicin into PEGylated PAMAM dendrimers with chain end of third or fourth generation via urethane bond [192]. They reported that the encapsulation efficacy of the drug are increasing with dendrimer generation and chain length of poly(ethylene glycol) grafts, where the highest ability have dendrimer of fourth generation with 6.5 doxorubicin molecules per dendrimer molecule and 100 % of drug releasing after 2 hours. PEGylated-PAMAM dendrimers for delivery of anti-cancer drug 5-fluorouracil was studied byBhadra and his group [193]. They reported the synthesis of PAMAM dendrimers, using ethylenediamine as a core and methylmethacrylate as a propagating agent and *N*-hydroxysuccinimide-activated carboxymethyl MPEG-5000 for PEGylation. The drug loading capacity into the dendrimer was increased by this formulation, but it was also found that the releasing rate and hemolytic activity of the drugs reduced. The PEGylation systems were found suitable for prolonged delivery of an anti-cancer drug in in vitro and for the reduction of drug leakage and hemolytic toxicity, providing excellent system for drug loading in body.

As it is mentioned above many of the drugs have water solubility problem, especially paclitaxel is limited by its poor solubility in water. Wu et al. [194] overcome this problem encapsulating paclitaxel with poly(glycerol) dendrimer formulations which led to a drug water solubility 400-fold higher than that of the free drug. The results showed that the fifth-generation of poly(glycerol) dendrimers increased paclitaxel solubility. They suggested that paclitaxel is not incorporated within the core of these dendrimer, but instead of that methyne

groups and aromatic rings of the paclitaxel are surrounded by the dendrimer structure leading to hydrotropic solubilization.

To improve its bioavailability and its poor water solubility Neerman and his group [195], used melamine-based dendrimers to solubilize and reduce toxicity of anticancer drugs methotrexate and 6-mercaptopurine. They reported that the intraperitoneal injection of the known hepatotoxic drug methotrexate and 6-mercaptopurine into mice liver significantly reduce hepatotoxicity and decrease the levels of alanine transaminase for 27% in case of methotrexate and 36% of 6-mercaptopurine compared to those obtained with the free drug.

The delivery of anticancer drugs by the encapsulation into denrimers is limited by the very small capacity of the void spaces within the dendrimers and the problem with long time releasing of encapsulated anticancer drugs. For this reason, drug-encapsulated dendrimer systems may be the best to utilized via direct intra-tumor injection or conjugate then to the surface of the dendrimers.

6. INORGANIC NANOPARTICLES FOR ANTICANCER DRUG DELIVERY

Inorganic nanoparticles as drug carrier for cancer treatment can be defined as particles of metal oxide or metallic composition possessing great opportunity due to their advantages such us easy modification of targeting molecules, drugs or other molecules on them, effective delivery to target sites, resulting in high therapeutic efficacy and controlling drug release by external/internal stimuli. Inorganic nanoparticles provide significantly chemical, physical, and biological properties, and functionality due to their nanoscale size, which is connect high surface area per unit volume and the ability to be functionalized with a large number of ligands to enhance their affinity towards target molecules, local delivery of the drug, reducing of side effect, and provide higher efficiency of the therapeutic molecule. However, synthesis of inorganic nanoparticles offers different ways of preparation depending on the applying drugs [196, 197]. One of the traditional methods for synthesis of inorganic nanoparticles is by sol-gel route, where producing of inorganic nanoparticles are directly connected with influence on pH or thermal conditions in solution. Controlling the hydrolysis and condensation reaction by mineralizers metal oxide species can be synthesis using different type of inorganic precursor such as metal salts, metal halides, and inorganic alkoxides [196]. However, it is also reported more friendly synthesis such us spray-drying process, enabling by spraying homogenization of inorganic precursors solution in special chamber at temperatures bellows then boiling point of the solvent. Using flowing gas, solution is sprayed into chamber as droplet leading to fast evaporation of solution by hot air or nitrogen enable formation of nanoparticles [198]. Using of gas-phase methods can be effective rout for synthesis of inorganic nanoparticles, which can include the use of a combustion flame, laser ablation, chemical vapor deposition, and spray-pyrolysis [199]. Microemulsions present one of thermodynamically stable method for preparation of inorganic nanoparticles without significant mechanical agitation making it a rather simple technique [200]. Among, inorganic nanoparticles, we focus on iron based nanoparticles.

6.1. Iron Based Nanoparticles

Iron based nanoparticles have been actively investigated as the next generation of nanoparticles systematically administered but directed towards a specific target in the human body while remaining ultimately localized, by means of an applied magnetic field. Benefit of iron based NPs is, the use of localized magnetic field gradients to attract the particles to a chosen site, and the possibility to hold them there until the therapy is complete and then to remove them. It is reported different ways of iron based nanoparticles synthesis in different form such as γ-Fe_2O_3 (maghemite), Fe_3O_4 (magnetite), α-Fe_2O_3 (hermatite), magnetite-based, silica-coated MNP (SiMNP), superparamagnetic Fe_3O_4 poly ε-caprolactone (PCL), silica-coated iron–carbon nanoparticles, $MgFe_2O_4$ magnetic nanoparticle and other form iron oxide nanoparticles [201-204]. Superparamagnetic nanoparticle ferumoxtran using as drug delivery system for the lymphatic biodistribution were reported by Rety et al., [205]. Ferumoxtran was applied on rat subdiaphragmatic lymph nodes for investigation of uptake mechanism, were 0.3 ml of lymph was collected over 45 minutes for 24 hours. Cytology results demonstrated that immediately after injection high concentrations of nanoparticles were found in the thoracic lymph, but without any nanoparticles in lymph cells indicating that ferumoxtran was extracellular in the lymph fluid, concluding that transcapillary pathway and subsequent lymph drainage have a main roll to drug pathway into lymph node.

Conjugations of magnetic nanoparticles with anticancer drug doxorubicin were reported by Sadighian et al., [206], demonstrated that the doxorubicin-magnetic nanoparticles can be applied on tumor-bearing tissues with dual targeting effect using magnetic attraction and the pH-sensitive cleavage of the drug–nanoparticle. Also releasing of drug was longer then in case of not loaded drug directly reduces the side effect of anticancer drug. Magnetic field and pH were effective in increasing the DOX-nanoparticle bioavailability in acidic condition then in neutral pH, enabling using this conjugate for targeting and increasing therapeutic efficiency of anticancer drug. The biodistribution of doxorubicin and methotrexate conjugate with magnetite nanoparticles are reported by Samra et al., [207]. Immunosorbent assay and FTIR spectroscopy demonstrated that the doxorubicin 18 % and methotrexate 27 % were immobilization with magnetic nanoparticles respectively. Result showed that modified magnetic nanoparticles with anticancer drug applied on Hella cells binding between 41 and 45 % comparing with B cells which binding 20 to 26 %, with higher releasing of anticancer drug in acid condition (pH-5) of 45 %, than in neutral condition (pH-7.4) of 10 %. These indicate that this methodology can be effective as mechanism for anticancer drug delivery.

Superparamagnetic Fe_3O_4 poly ε-caprolactone (PCL) nanoparticles may provide therapeutic effect on xenografts of human HPAC pancreatic adenocarcinoma cells [208]. Gang and his group reported pharmacokinetic behavior of superparamagnetic poly ε-caprolactone nanoparticles conjugated with gemcitabine on tumor cells, resulting in drug loading content of 18.6 % with entrapment efficiency of 52.2%. They were found widely distribution of anticancer drug with 15-fold higher dose in comparison with free gemcitabine in tumor cells, indicating the efficiency of magnetic PCL nanoparticles in drug delivery. Poly-(N-isopropylacrylamide-methyl methacrylic acid, (PNIPAAm-MAA) grafted magnetic nanoparticles as anticancer drug delivery transporter are reported by Akbarzadeh et al. [209], were polymerization of N-isopropylacrylamide and methacrylic acid was conduct using silan coated magnetic nanoparticles. Block copolymer-coated magnetite nanoparticles conjugate with doxorubicin were applied on A549 lung cancer cell line for investigation of targeting and

controlled drug delivery. Results show that polymer chains were effectively grafted onto the surface of the Fe_3O_4 nanoparticles and encapsulate doxorubicin with loading efficiency of 75%, which results in longer time of drug release at pH 5.8 comparing with neutral pH at 7.4. These nanoparticles show potential as anticancer drug delivery system.

6.2. Iron Based Nanoparticles with Silica

Modification of iron carbon magnetic nanoparticles with silica are used as an anticancer drug delivery platform, were chemoadsorptive properties of activated carbon are provide drug loading and magnetic Fe are used for targeting [210]. Silica-coated iron–carbon composite nanoparticles are loaded with doxorubicin and biodistributed in the left hepatic lobe of pigs under external magnetic field. Results show that nanoparticles loaded with doxorubicin was 24 times higher in hepatic tissue then in tissue that is not targeted, leading to penetration of magnetic nanoparticles trough capillary wall encircling the tissue interstitium and hepatic cells. These indicating that the novel silica-coated iron-carbon composite particles could be a potential application in targeted treatment for some kinds of tumor as an effective drug carrier. Applications of arsenic trioxide Mg-Fe ferrite magnetic nanoparticles as anticancer drug delivery system were reported by Yang et al., [211], where their effect was evaluated by *in vivo* experiment. Particles were prepared by solvent-displacement method using Poly-D,L-lactic-co-glycolic acid (PLGA) in process of synthesis. Cytotoxicity of nanoparticles was investigated on Saos-2 cells showing no significant toxicity, also they investigated concentration of As_2O_3–MNPs in liver resulting in four time higher concentration then non-magnetically vectored group and kidney where concentration was lower than in non-magnetically vectored group leading to conclusion that polymer-loaded magnetic nanoparticle composed of arsenic trioxide show great possibility for targeting and drug delivery.

7. CARBON BASED NANOMATERIALS

Among the several types of nanomaterials invented in recent years, carbon based materials have attracted tremendous attention due to their unique properties as one of the most promising nanomaterials for a variety of biomedical applications. Different types of carbon based nanomaterials such as graphene, carbon nanotubes, fullerene, nanodiamond and carbon nanoparticles (CNPs) have been developed especially as delivery vehicles for drugs.

In 1960s, nanodiamond was first studied by researchers and recently started to be highlighted in different medical applications [212]. The fullerene was discovered in 1985 as a new type of carbon molecules [213]. The carbon nanotube (CNT) was first discovered by Iijima in 1991 [214]. In comparison with other nanomaterials, CNTs (an allotrope of carbon) can be considered as more dynamic nanomaterials in their biological application. For example, not like other nanomaterials, CNTs have the potential to be used not only in imaging but also for drug delivery and thermal ablation [215]. Generally, it is prepared using three main techniques: laser ablation, thermal or plasma enhanced chemical vapour deposition and electric arc discharge [216]. The application of CNTs in drug delivery to their cite of action has become one of the main areas of interest for different researchers due to their

special characteristics including their unique physical, chemical, and biological properties, hollow monolithic structure, nanoneedle shape, and their ability to acquire the desired functional groups on their surface [217]. The shape of CNTs allows them to penetrate cells using various methods including endocytosis or passive diffusion across the lipid bilayer. In case of endocytosis, the CNT attaches to the cell surface and is subsequently engulfed by the cell membrane [217, 218]. The factors which make CNTs as a promising drug carrier are the hollow monolithic structure of CNTs and their ability to bind desired functional groups on the surface [217, 219].

CNTs can be mainly classified into two categories on the basis of the number of cylindrical graphene layers: single-walled carbon nanotubes (SWCNTs) and multi-walled carbon nanotubes (MWCNTs). SWCNTs have a single cylindrical carbon layer whose diameter varies from 0.4 to 2 mm depending on the temperature at which they have been prepared [220]. It has been reported that a higher growth temperature is responsible to give a larger diameter. On the other hand, MWCNTs are usually consists of several cylindrical carbon layers with diameters in the range of 2–100 nm for the outer tubes and 1–3 nm for the inner tubes [221].

Different research groups reported that functionalized water soluble CNTs can enter cells. The exact uptake mechanism may depend on the size and surface chemistry of CNTs and the type of the cells. The majority of reports have revealed that CNTs functionalized by oxidization, wrapped by DNA, and coated by surfactants or amphiphilic polymers can be engulfed by cells using an energy-dependent endocytosis pathway [222-227]. The similar entryway can be found for other nanomaterials used in biomedicine.

Some researchers also showed that CNTs can enter cells via passive diffusion owing to the needle-like structure of nanotubes after functionalization by the 1,3-dipolar cycloaddition, or Prato reaction [228-230]. The interactions of CNTs and cell depend not only the surface chemistry but also the size of them. Kang et al. reported that the endocytosis pathway for SWNTs with length of 100 – 200 nm was mainly via clathrin-coated pits, whereas shorter SWNTs (50 – 100 nm) were internalized through clathrincoated vesicles as well as the caveolae pathway [231]. Another experiment suggested that individual MWCNT is able enter cells through direct penetration while the bundles of MWCNTs are taken up by cells through endocytosis [232].

After the process of endocytosis, CNTs generally stays inside cell lysosomes and endosomes. CNTs can also move away from these membrane-bound compartments inside cells depending on their sizes and surface modifications. SWCNTs and MWCNTs show difference in nature inside the cells. Various reports suggested that SWCNTs functionalized by DNA or PEG are mostly retained inside endosomes and lysosomes [224, 225, 233, 234]. On the other hand, it has been found that individualized MWCNTs are able to travel through various cellular barriers and even entered the nucleus [230, 232]. In a different experiment, Zhou et al. showed that by conjugating different molecules to PEG functionalized SWCNTs, nanotubes show the ability to localize in specific subcellular organelles like mitochondria [235].

Chemotherapeutic agents show some limitations after their application to body due to their toxic side effects. So it is needed to develop cell-targeting drug formulations with a wide therapeutic index. Drug delivery can be considered as one of the most widely explored applications of CNTs in biomedicine. CNTs have the ability to deliver drugs directly to cancer cells [219, 236]. Anticancer drugs can be attached on the outer surface of the CNTs

through two main ways: covalent bonding and noncovalent bonding (hydrophobic, π-π stacking, and electrostatic interactions) [237-239].

In case of covalent conjugation, the drug molecules are linked to the functional groups on the CNT surface or to the polymer coating of CNTs, generally using cleavable bonds. The 1, 3-dipolar cycloaddition is used to functionalize CNTs via amide bonds to link anti-cancer drugs [240, 241].

Liu et al. studied paclitaxel (PTX), a widely used cancer chemotherapy drug, with SWCNTs. In this experiment the paclitaxel had been delivered to cancer cells via covalent attachment of paclitaxel to the outer surface of the SWCNT. The paclitaxel was initially reacted with succinic anhydride, which helped to add carboxylic acid groups on the surface of paclitaxel. Then, a sonication was carried out for 30 minutes for SWCNTs in a 0.2 mmol/L solution of DSPE-PEG 5000-4-arm-(PEG-amine) and they were centrifugation at 24,000 g for 6 hours. This process helped in formation of SWCNTs noncovalently attached to PEG-NH_2. Subsequently, the carboxylic acid-coated paclitaxel was reacted with the product in presence of coupling agents: 1-ethyl-3-(3-dimethylaminopropyl) carbodiimide hydrochloride (EDC) 5 mmol/L and N- ydroxysulfosuccinimide (NHS) 5 mmol/L. A filtration process was carried out to remove unconjugated paclitaxel. Then, UV-visible near infrared spectra of SWCNTs were recorded before and after the conjugation with paclitaxel. In vitro delivery of the drug samples showed that paclitaxel attached to SWCNTs can suppress tumor growth more efficiently than paclitaxel alone. This experiment suggested that a higher concentration of paclitaxel can be delivered to breast cancer cells using SWCNT-paclitaxel conjugates compared to the delivery of paclitaxel alone [242].

Another group of researcher have showed that platinum (IV) can also be delivered to cancer cells by conjugation to SWCNTs. In this experiment, SWCNTs were initially sonicated with platinum (IV)-PEG-NH_2 for 1 hour followed by a centrifugation at 2.4 × 104 g for 6 hours to remove catalysts and large aggregates. Then an ultrafiltration was carried out to remove excess free platinum (IV)-PEG-NH_2. Result showed that the platinum (IV) conjugated with SWCNTs, was able to kill cancer cells at higher rates than platinum alone. Platinum (IV)-SWCNT complex showed an enhanced cytotoxicity which suggests that SWCNTs can successfully deliver platinum (IV) improving the cellular uptake of the drug [243].

Wu et al. reported that 10-hydroxy camptothecin (HCPT) (an antitumor agent) can be attached to the outer surface of the MWCNTs by covalent bonding. Succinic anhydride was used to obtain carboxylic groups on the surface of HCPT. They were then reacted together in the presence of NHS and EDC as coupling agents. The linkage of the MWCNTs to HCPT was confirmed by UV-visible near infrared spectrometry [238].

Besides covalent linkage, it has been found that some aromatic molecules with a flat structure can also be attached to the surface of CNTs using non-covalent π-π stacking, hydrophobic interaction, or electrostatic adsorption. Liu et al. reported that doxorubicin can be loaded on the surface of PEGylated SWCNTs with a significantly high loading capacity of up to 4 grams of drug per 1 gram of nanotubes. The ultrahigh surface area of SWCNTs allowed the drug to be loaded at amount [244]. It has been suggested that that the pH-dependent drug binding and releasing behaviors can be useful for drug release in lysosomes and endosomes, as well as in tumor micro-environments with acidic pH. Different groups of researchers suggested that this π-π stacking based drug loading strategy can be applied to MCWNTs and nano-graphene also [245-248]. However, the main limitation of the

noncovalent bonding is the lack of efficient attachment, which can result in release of the drug before it reaches its site of action. [249, 250].

Graphene is an sp^2-bonded novel 2D carbon material with unique physical and chemical properties. It has gained tremendous attention since researchers isolated a graphene sheet from graphite crystal in 2004 [251]. From that time, graphene and graphene oxide (GO) have been used in different ways in the field of biomedicine [252, 253]. Graphene shares a similar chemical structure with CNTs and thus can be used as a carrier for drug delivery. Yang et al. studied the in vivo behaviours of nanographene sheets (NGS) with polyethylene glycol (PEG) coating by a fluorescent labelling method. Results showed that NGS has several interesting in vivo behaviours including highly efficient tumour passive targeting and relatively low retention in reticuloendothelial systems. The strong optical absorbance of NGS in the near-infrared (NIR) region was employed for *in vivo* photothermal therapy. They showed that the intravenous administration of NGS and low-power NIR laser irradiation can cause ultraefficient tumour ablation [254].

Yang et al. studied multi-functionalized graphene oxide as an anticancer drug-carrier. Initially they prepared a superparamagnetic GO–Fe_3O_4 nanohybrid. Then, folic acid, a targeting agent toward some tumour cells, was attached with the Fe_3O_4 nanoparticles. This chemical linkage was formed with amino groups of the 3-aminopropyl triethoxysilane (APS) modified superparamagnetic GO–Fe_3O_4 nanohybrid. Doxorubicin hydrochloride (Dox) was attached on the surface of this multi-functionalized GO using π–π stacking. This experiment suggested that this multi-functionalized GO can be used as a potential carrier for targeted delivery and the controlled release of anticancer drugs [255].

CONCLUSION

The main objective of research in recent years is to provide a multifunctional nanoparticles and nanomaterials whose properties can be controlled in the body through the local environment and external factors, e. g. external magnetic field. Many pharmaceutical companies have their own research programs aimed at the introduction of new products based on nanoparticles and nanomaterials and improve current pharmaceuticals. As a result of intensive and lengthy analysis the structure and properties of nano materials and nano particles were examined what let find out a lot of new qualities of nanocels. Nanosubstances appeared to be commercially and started to be used widely in the diagnosis or treatment of cancer, among others. Intensive nanotechnology research in the future will lead to extend the functions of nanoparticles in nanodiagnostics, in nanopharmacology and in many new medical applications. Now nanoparticles are mainly used as carriers of drugs and substances with antibacterial and anti-virus. Also play a major role in diagnosis, where they are used in immunohistochemistry, genetic studies and for the detection of pathogens and cancer. They increase the speed, accuracy and sensitivity bioassays with of small sample volumes. In addition to the use of nanoparticles for diagnostic imaging, the future nanotechnologies also involve the targeted treatment of cancer. Despite the many advantages and applications not only in the medical field and in the protection of the environment and in various technologies, it is important to test the nanoparticles and nanosubstances for cytotoxicity.

ACKNOWLEDGMENTS

The financial support of NANOSEMED KAN208130801 is highly acknowledged.

REFERENCES

[1] Zhao, JS, and Castranova, V (2011). Toxicology of nanomaterials used in nanomedicine. *J. Toxicol. Env. Health-Pt b-Crit. Rev., 14*, 593-632.

[2] Strebhardt, K, and Ullrich, A (2008). Paul Ehrlich's magic bullet concept: 100 years of progress. *Nat. Rev. Cancer, 8*, 473-480.

[3] Navrotsky, A (2003). Energetics of nanoparticle oxides: interplay between surface energy and polymorphism. *Geochem. Trans., 4*, 34-37.

[4] Reiss, P, Protiere, M, and Li, L (2009). Core/Shell Semiconductor Nanocrystals. *Small, 5*, 154-168.

[5] Wang, HQ, and Nann, T (2009). Monodisperse Upconverting Nanocrystals by Microwave-Assisted Synthesis. *ACS Nano, 3*, 3804-3808.

[6] Bear, J, Charron, G, Fernandez-Arguelles, MT, Massadeh, S, McNaughter, P, and Nann, T (2011). In Vivo Applications of Inorganic Nanoparticles. In Betasys: Systems Biology of Regulated Exocytosis in Pancreatic Beta-Cells, Volume 2, B. BoossBavnbek, B. Klosgen, J. Larsen, F. Pociot and E. Renstrom, eds. (New York: Springer), pp. 185-220.

[7] Scheinberg, DA, Villa, CH, Escorcia, FE, and McDevitt, MR (2010). Conscripts of the infinite armada: systemic cancer therapy using nanomaterials. *Nat. Rev. Clin. Oncol., 7*, 266-276.

[8] Peer, D, Karp, JM, Hong, S, FaroKhzad, OC, Margalit, R, and Langer, R (2007). Nanocarriers as an emerging platform for cancer therapy. *Nat. Nanotechnol., 2*, 751-760.

[9] Kim, BYS, Rutka, JT, and Chan, WCW (2010). Current Concepts: Nanomedicine. *N. Engl. J. Med., 363*, 2434-2443.

[10] Murthy, SK (2007). Nanoparticles in modern medicine: State of the art and future challenges. *Int. J. Nanomed., 2*, 129-141.

[11] Oberdorster, E (2004). Manufactured nanomaterials (Fullerenes, C-60) induce oxidative stress in the brain of juvenile largemouth bass. *Environ. Health Perspect., 112*, 1058-1062.

[12] Hirsch, LR, Stafford, RJ, Bankson, JA, Sershen, SR, Rivera, B, Price, RE, Hazle, JD, Halas, NJ, and West, JL (2003). Nanoshell-mediated near-infrared thermal therapy of tumors under magnetic resonance guidance. *Proc. Natl. Acad. Sci. U. S. A., 100*, 13549-13554.

[13] Freitas, RA (2005). Current status of nanomedicine and medical nanorobotics. *J. Comput. Theor. Nanosci., 2*, 1-25.

[14] Maier-Hauff, K, Rothe, R, Scholz, R, Gneveckow, U, Wust, P, Thiesen, B, Feussner, A, von Deimling, A, Waldoefner, N, Felix, R, et al. (2007). Intracranial thermotherapy using magnetic nanoparticles combined with external beam radiotherapy: Results of a feasibility study on patients with glioblastoma multiforme. *J. Neuro-Oncol., 81*, 53-60.

[15] Kim, JS, Kuk, E, Yu, KN, Kim, JH, Park, SJ, Lee, HJ, Kim, SH, Park, YK, Park, YH, Hwang, CY, et al. (2007). Antimicrobial effects of silver nanoparticles. *Nanomed.-Nanotechnol. Biol. Med., 3*, 95-101.

[16] Shrivastava, S, Bera, T, Roy, A, Singh, G, Ramachandrarao, P, and Dash, D (2007). Characterization of enhanced antibacterial effects of novel silver nanoparticles. *Nanotechnology, 18*.

[17] Shahverdi, AR, Fakhimi, A, Shahverdi, HR, and Minaian, S (2007). Synthesis and effect of silver nanoparticles on the antibacterial activity of different antibiotics against Staphylococcus aureus and Escherichia coli. *Nanomed.-Nanotechnol. Biol. Med., 3*, 168-171.

[18] Zhou, W, Ma, YY, Yang, HA, Ding, Y, and Luo, XG (2011). A label-free biosensor based on silver nanoparticles array for clinical detection of serum p53 in head and neck squamous cell carcinoma. *Int. J. Nanomed., 6*, 381-386.

[19] Thaxton, CS, Daniel, WL, Giljohann, DA, Thomas, AD, and Mirkin, CA (2009). Templated Spherical High Density Lipoprotein Nanoparticles. *J. Am. Chem. Soc., 131*, 1384-1385.

[20] Huang, XH, Jain, PK, El-Sayed, IH, and El-Sayed, MA (2008). Plasmonic photothermal therapy (PPTT) using gold nanoparticles. *Lasers Med. Sci., 23*, 217-228.

[21] Bhumkar, DR, Joshi, HM, Sastry, M, and Pokharkar, VB (2007). Chitosan reduced gold nanoparticles as novel carriers for transmucosal delivery of insulin. *Pharm. Res., 24*, 1415-1426.

[22] Ahn, S, Jung, SY, and Lee, SJ (2013). Gold Nanoparticle Contrast Agents in Advanced X-ray Imaging Technologies. *Molecules, 18*, 5858-5890.

[23] Dong, P, Yu, V, Nguyen, D, Demarco, J, Woods, K, Boucher, S, Low, DA, and Sheng, K (2014). Feasibility of using intermediate x-ray energies for highly conformal extracranial radiotherapy. *Med. Phys., 41*, 1-12.

[24] Hainfeld, JF, Dilmanian, FA, Slatkin, DN, and Smilowitz, HM (2008). Radiotherapy enhancement with gold nanoparticles. *J. Pharm. Pharmacol., 60*, 977-985.

[25] Ren, GG, Hu, DW, Cheng, EWC, Vargas-Reus, MA, Reip, P, and Allaker, RP (2009). Characterisation of copper oxide nanoparticles for antimicrobial applications. *Int. J. Antimicrob. Agents, 33*, 587-590.

[26] Studer, AM, Limbach, LK, Van Duc, L, Krumeich, F, Athanassiou, EK, Gerber, LC, Moch, H, and Stark, WJ (2010). Nanoparticle cytotoxicity depends on intracellular solubility: Comparison of stabilized copper metal and degradable copper oxide nanoparticles. *Toxicol. Lett., 197*, 169-174.

[27] Wang, Y, Zi, XY, Su, J, Zhang, HX, Zhang, XR, Zhu, HY, Li, JX, Yin, M, Yang, F, and Hu, YP (2012). Cuprous oxide nanoparticles selectively induce apoptosis of tumor cells. *Int. J. Nanomed., 7*, 2641-2652.

[28] Tegos, GP, Demidova, TN, Arcila-Lopez, D, Lee, H, Wharton, T, Gali, H, and Hamblin, MR (2005). Cationic fullerenes are effective and selective antimicrobial photosensitizers. *Chem. Biol., 12*, 1127-1135.

[29] Montellano, A, Da Ros, T, Bianco, A, and Prato, M (2011). Fullerene C-60 as a multifunctional system for drug and gene delivery. *Nanoscale, 3*, 4035-4041.

[30] Geim, AK, and Novoselov, KS (2007). The rise of graphene. *Nat. Mater., 6*, 183-191.

[31] Terranova, ML, Sessa, V, and Rossi, M (2006). The world of carbon nanotubes: An overview of CVD growth methodologies. *Chem. Vapor Depos., 12*, 315-325.

[32] Tripisciano, C, Kraemer, K, Taylor, A, and Borowiak-Palen, E (2009). Single-wall carbon nanotubes based anticancer drug delivery system. *Chem. Phys. Lett., 478*, 200-205.

[33] Ali-Boucetta, H, Al-Jamal, KT, and Kostarelos, K (2008). Multi-Walled Carbon Nanotube-Doxorubicin Supramolecular Complexes for Cancer Therapeutics, (Boca Raton: Crc Press-Taylor & Francis Group).

[34] Hampel, S, Kunze, D, Haase, D, Kramer, K, Rauschenbach, M, Ritscbel, M, Leonbardt, A, Thomas, J, Oswald, S, Hoffmann, V, et al. (2008). Carbon nanotubes filled with a chemotherapeutic agent: a nanocarrier mediates inhibition of tumor cell growth. *Nanomedicine, 3*, 175-182.

[35] Liu, Z, Tabakman, S, Welsher, K, and Dai, HJ (2009). Carbon Nanotubes in Biology and Medicine: In vitro and in vivo Detection, Imaging and Drug Delivery. *Nano Res., 2*, 85-120.

[36] Barone, PW, Baik, S, Heller, DA, and Strano, MS (2005). Near-infrared optical sensors based on single-walled carbon nanotubes. *Nat. Mater., 4*, 86-U16.

[37] Baughman, RH, Cui, CX, Zakhidov, AA, Iqbal, Z, Barisci, JN, Spinks, GM, Wallace, GG, Mazzoldi, A, De Rossi, D, Rinzler, AG, et al. (1999). Carbon nanotube actuators. *Science, 284*, 1340-1344.

[38] Rege, K, Raravikar, NR, Kim, DY, Schadler, LS, Ajayan, PM, and Dordick, JS (2003). Enzyme-polymer-single walled carbon nanotube composites as biocatalytic films. *Nano Lett., 3*, 829-832.

[39] Lin, Y, Taylor, S, Li, HP, Fernando, KAS, Qu, LW, Wang, W, Gu, LR, Zhou, B, and Sun, YP (2004). Advances toward bioapplications of carbon nanotubes. *J. Mater. Chem., 14*, 527-541.

[40] Mattson, MP, Haddon, RC, and Rao, AM (2000). Molecular functionalization of carbon nanotubes and use as substrates for neuronal growth. *J. Mol. Neurosci., 14*, 175-182.

[41] Bianco, A, Kostarelos, K, and Prato, M (2005). Applications of carbon nanotubes in drug delivery. *Curr. Opin. Chem. Biol., 9*, 674-679.

[42] Prato, M, Kostarelos, K, and Bianco, A (2008). Functionalized carbon nanotubes in drug design and discovery. *Accounts Chem. Res., 41*, 60-68.

[43] Malmsten, M (2006). Soft drug delivery systems. *Soft Matter, 2*, 760-769.

[44] Cui, DX, Tian, FR, Ozkan, CS, Wang, M, and Gao, HJ (2005). Effect of single wall carbon nanotubes on human HEK293 cells. *Toxicol. Lett., 155*, 73-85.

[45] Pastorin, G, Wu, W, Wieckowski, S, Briand, JP, Kostarelos, K, Prato, M, and Bianco, A (2006). Double functionalisation of carbon nanotubes for multimodal drug delivery. *Chem. Commun.*, 1182-1184.

[46] Costa, S, Borowiak-Palen, E, Bachmatiuk, A, Rummeli, MH, Gemming, T, and Kalenezuk, RJ (2007). Filling of carbon nanotubes for bio-applications. *Phys. Status Solidi B-Basic Solid State Phys., 244*, 4315-4318.

[47] Gooding, JJ, Wibowo, R, Liu, JQ, Yang, WR, Losic, D, Orbons, S, Mearns, FJ, Shapter, JG, and Hibbert, DB (2003). Protein electrochemistry using aligned carbon nanotube arrays. *J. Am. Chem. Soc., 125*, 9006-9007.

[48] Pantarotto, D, Singh, R, McCarthy, D, Erhardt, M, Briand, JP, Prato, M, Kostarelos, K, and Bianco, A (2004). Functionalized carbon nanotubes for plasmid DNA gene delivery. *Angew. Chem.-Int. Edit., 43*, 5242-5246.

[49] Singh, R, Pantarotto, D, McCarthy, D, Chaloin, O, Hoebeke, J, Partidos, CD, Briand, JP, Prato, M, Bianco, A, and Kostarelos, K (2005). Binding and condensation of plasmid DNA onto functionalized carbon nanotubes: Toward the construction of nanotube-based gene delivery vectors. *J. Am. Chem. Soc., 127*, 4388-4396.

[50] Ito, A, Shinkai, M, Honda, H, and Kobayashi, T (2005). Medical application of functionalized magnetic nanoparticles. *J. Biosci. Bioeng., 100*, 1-11.

[51] Grebowski, J, Kazmierska, P, and Krokosz, A (2013). Fullerenols as a New Therapeutic Approach in Nanomedicine. *Biomed Res. Int.*, 1-10.

[52] Vedakumari, WS, Priya, VM, and Sastry, TP (2014). Deposition of superparamagnetic nanohydroxyapatite on iron-fibrin substrates: Preparation, characterization, cytocompatibility and bioactivity studies. *Colloid Surf. B-Biointerfaces, 120*, 208-214.

[53] Mnneil, SE (2005). Nanotechnology for the biologist. *J. Leukoc. Biol., 78*, 585-594.

[54] Jain, TK, Richey, J, Strand, M, Leslie-Pelecky, DL, Flask, CA, and Labhasetwar, V (2008). Magnetic nanoparticles with dual functional properties: Drug delivery and magnetic resonance imaging. *Biomaterials, 29*, 4012-4021.

[55] Sun, C, Lee, JSH, and Zhang, MQ (2008). Magnetic nanoparticles in MR imaging and drug delivery. *Adv. Drug Deliv. Rev., 60*, 1252-1265.

[56] Harisinghani, MG, Barentsz, J, Hahn, PF, Deserno, WM, Tabatabaei, S, van de Kaa, CH, de la Rosette, J, and Weissleder, R (2003). Noninvasive detection of clinically occult lymph-node metastases in prostate cancer. *N. Engl. J. Med., 348*, 2491-U2495.

[57] Watson, EK, and Rickelton, WA (1992). A review of the industrial and recent potential applications of trioctylphosphine oxide. *Solvent Extr. Ion Exch., 10*, 879-889.

[58] Gao, XH, Cui, YY, Levenson, RM, Chung, LWK, and Nie, SM (2004). In vivo cancer targeting and imaging with semiconductor quantum dots. *Nat. Biotechnol., 22*, 969-976.

[59] Jaiswal, JK, Mattoussi, H, Mauro, JM, and Simon, SM (2003). Long-term multiple color imaging of live cells using quantum dot bioconjugates. *Nat. Biotechnol., 21*, 47-51.

[60] Chan, WCW, Maxwell, DJ, Gao, XH, Bailey, RE, Han, MY, and Nie, SM (2002). Luminescent quantum dots for multiplexed biological detection and imaging. *Curr. Opin. Biotechnol., 13*, 40-46.

[61] Kolhe, P, Misra, E, Kannan, RM, Kannan, S, and Lieh-Lai, M (2003). Drug complexation, in vitro release and cellular entry of dendrimers and hyperbranched polymers. *Int. J. Pharm., 259*, 143-160.

[62] Ma, ML, Cheng, YY, Xu, ZH, Xu, P, Qu, H, Fang, YJ, Xu, TW, and Wen, LP (2007). Evaluation of polyamidoamine (PAMAM) dendrimers as drug carriers of anti-bacterial drugs using sulfamethoxazole (SMZ) as a model drug. *Eur. J. Med. Chem., 42*, 93-98.

[63] Price, CF, Tyssen, D, Sonza, S, Davie, A, Evans, S, Lewis, GR, Xia, S, Spelman, T, Hodsman, P, Moench, TR, et al. (2011). SPL7013 Gel (VivaGel (R)) Retains Potent HIV-1 and HSV-2 Inhibitory Activity following Vaginal Administration in Humans. *PLoS One, 6*, 1-12.

[64] Wiener, EC, Auteri, FP, Chen, JW, Brechbiel, MW, Gansow, OA, Schneider, DS, Belford, RL, Clarkson, RB, and Lauterbur, PC (1996). Molecular dynamics of ion-chelate complexes attached to dendrimers. *J. Am. Chem. Soc., 118*, 7774-7782.

[65] Svenson, S, and Tomalia, DA (2005). Commentary - Dendrimers in biomedical applications - reflections on the field. *Adv. Drug Deliv. Rev., 57*, 2106-2129.

[66] Czaja, W, Krystynowicz, A, Bielecki, S, and Brown, RM (2006). Microbial cellulose - the natural power to heal wounds. *Biomaterials, 27*, 145-151.

[67] Xia, T, Kovochich, M, Brant, J, Hotze, M, Sempf, J, Oberley, T, Sioutas, C, Yeh, JI, Wiesner, MR, and Nel, AE (2006). Comparison of the abilities of ambient and manufactured nanoparticles to induce cellular toxicity according to an oxidative stress paradigm. *Nano Lett, 6*, 1794-1807.

[68] Peters, A, Veronesi, B, Calderon-Garciduenas, L, Gehr, P, Chen, LC, Geiser, M, Reed, W, Rothen-Rutishauser, B, Schurch, S, and Schulz, H (2006). Translocation and potential neurological effects of fine and ultrafine particles a critical update. *Part Fibre Toxicol, 3*, 13.

[69] Geiser, M, Rothen-Rutishauser, B, Kapp, N, Schürch, S, Kreyling, W, Schulz, H, Semmler, M, Hof, VI, Heyder, J, and Gehr, P (2005). Ultrafine Particles Cross Cellular Membranes by Nonphagocytic Mechanisms in Lungs and in Cultured Cells. *Environ Health Persp, 113*, 1555-1560.

[70] Porter, AE, Muller, K, Skepper, J, Midgley, P, and Welland, M (2006). Uptake of C-60 by human monocyte macrophages, its localization and implications for toxicity: Studied by high resolution electron microscopy and electron tomography. *Acta Biomater, 2*, 409-419.

[71] Garcia-Garcia, E, Andrieux, K, Gil, S, Kim, HR, Le Doan, T, Desmaele, D, d'Angelo, J, Taran, F, Georgin, D, and Couvreur, P (2005). A methodology to study intracellular distribution of nanoparticles in brain endothelial cells. *Int J Pharmaceut, 298*, 310-314.

[72] Aderem, A, and Underhill, DM (1999). Mechanisms of phagocytosis in macrophages. *Annu. Rev. Immunol., 17*, 593-623.

[73] Champion, J, and Mitragotri, S (2009). Shape Induced Inhibition of Phagocytosis of Polymer Particles. *Pharm Res, 26*, 244-249.

[74] Champion, JA, and Mitragotri, S (2006). Role of target geometry in phagocytosis. *P Natl Acad Sci USA, 103*, 4930-4934.

[75] Geng, Y, Dalhaimer, P, Cai, S, Tsai, R, Tewari, M, Minko, T, and Discher, DE (2007). Shape effects of filaments versus spherical particles in flow and drug delivery. *Nat Nano, 2*, 249-255.

[76] Harguindey, S, Arranz, JL, Wahl, ML, Orive, G, and Reshkin, SJ (2009). Proton transport inhibitors as potentially selective anticancer drugs. *Anticancer Res, 29*, 2127-2136.

[77] Zhang, L, Zhang, S, Ruan, S-b, Zhang, Q-y, He, Q, and Gao, H-l (2014). Lapatinib-incorporated lipoprotein-like nanoparticles: preparation and a proposed breast cancer-targeting mechanism. *Acta Pharmacol Sin, 35*, 846-852.

[78] Siegel, R, and Rathbone, M (2012). Overview of Controlled Release Mechanisms. In Fundamentals and Applications of Controlled Release Drug Delivery, J. Siepmann, R.A. Siegel and M.J. Rathbone, eds. (Springer US), pp. 19-43.

[79] Bajpai, AK, Shukla, SK, Bhanu, S, and Kankane, S (2008). Responsive polymers in controlled drug delivery. *33*, 1088-1118.

[80] Abouelmagd, SA, Hyun, H, and Yeo, Y (2014). Extracellularly activatable nanocarriers for drug delivery to tumors. *Expert Opin Drug Del, 11*, 1601-1618.

[81] Ehrbar, M, Schoenmakers, R, Christen, EH, Fussenegger, M, and Weber, W (2008). Drug-sensing hydrogels for the inducible release of biopharmaceuticals. *Nat Mater, 7*, 800-804.

[82] Mura, S, Nicolas, J, and Couvreur, P (2013). Stimuli-responsive nanocarriers for drug delivery. *Nat Mater, 12*, 991-1003.

[83] Langer, R, and Peppas, N (1983). Chemical and Physical Structure of Polymers as Carriers for Controlled Release of Bioactive Agents: A Review. *J Macrom Sci C, 23*, 61-126.

[84] Siegel, RA, and Rathbone, MJ (2012). Overview of Controlled Release Mechanisms. In Fundamentals and Applications of Controlled Release Drug Delivery, J. Siepmann, R.A. Siegel and M.J. Rathbone, eds., pp. 19-43.

[85] Peppas, NA, Bures, P, Leobandung, W, and Ichikawa, H (2000). Hydrogels in pharmaceutical formulations. *Eur J Pharm Biopharm, 50*, 27-46.

[86] Lin, C-C, and Metters, AT (2006). Hydrogels in controlled release formulations: Network design and mathematical modeling. *Adv Drug Del Rev, 58*, 1379-1408.

[87] Kaity, S, Isaac, J, and Ghosh, A (2013). Interpenetrating polymer network of locust bean gum-poly (vinyl alcohol) for controlled release drug delivery. *Carbohyd Polym, 94*, 456-467.

[88] Lee, PI (1984). Novel approach to zero-order drug delivery via immobilized nonuniform drug distribution in glassy hydrogels. *J Pharm Sci, 73*, 1344-1347.

[89] Herrlich, S, Spieth, S, Messner, S, and Zengerle, R (2012). Osmotic micropumps for drug delivery. *Adv Drug Del Rev, 64*, 1617-1627.

[90] Cauchetier, E, Deniau, M, Fessi, H, Astier, A, and Paul, M (2003). Atovaquone-loaded nanocapsules: influence of the nature of the polymer on their in vitro characteristics. *Int J Pharmaceut, 250*, 273-281.

[91] Lee, SH, Mok, H, Lee, Y, and Park, TG (2011). Self-assembled siRNA–PLGA conjugate micelles for gene silencing. *J Control Release, 152*, 152-158.

[92] Prabaharan, M, Grailer, JJ, Pilla, S, Steeber, DA, and Gong, S (2009). Amphiphilic multi-arm-block copolymer conjugated with doxorubicin via pH-sensitive hydrazone bond for tumor-targeted drug delivery. *Biomaterials, 30*, 5757-5766.

[93] Yoo, HS, and Park, TG (2001). Biodegradable polymeric micelles composed of doxorubicin conjugated PLGA-PEG block copolymer. *J Control Release, 70*, 63-70.

[94] Lee, W-C, and Chu, IM (2008). Preparation and degradation behavior of polyanhydrides nanoparticles. *J Biomed Mater Res, 84B*, 138-146.

[95] Min, KH, Kim, J-H, Bae, SM, Shin, H, Kim, MS, Park, S, Lee, H, Park, R-W, Kim, I-S, Kim, K, et al. (2010). Tumoral acidic pH-responsive MPEG-poly(β-amino ester) polymeric micelles for cancer targeting therapy. *J Control Release, 144*, 259-266.

[96] Talelli, M, Iman, M, Varkouhi, AK, Rijcken, CJF, Schiffelers, RM, Etrych, T, Ulbrich, K, van Nostrum, CF, Lammers, T, Storm, G, et al. (2010). Core-crosslinked polymeric micelles with controlled release of covalently entrapped doxorubicin. *Biomaterials, 31*, 7797-7804.

[97] Lai, P-S, Lou, P-J, Peng, C-L, Pai, C-L, Yen, W-N, Huang, M-Y, Young, T-H, and Shieh, M-J (2007). Doxorubicin delivery by polyamidoamine dendrimer conjugation and photochemical internalization for cancer therapy. *J Control Release, 122*, 39-46.

[98] Yuba, E, Harada, A, Sakanishi, Y, Watarai, S, and Kono, K (2013). A liposome-based antigen delivery system using pH-sensitive fusogenic polymers for cancer immunotherapy. *Biomaterials, 34*, 3042-3052.

[99] Chang, C, Wei, H, Quan, C-Y, Li, Y-Y, Liu, J, Wang, Z-C, Cheng, S-X, Zhang, X-Z, and Zhuo, R-X (2008). Fabrication of thermosensitive PCL-PNIPAAm-PCL triblock copolymeric micelles for drug delivery. *J Polym Sci Pol Chem, 46*, 3048-3057.

[100] Li, W, Li, J, Gao, J, Li, B, Xia, Y, Meng, Y, Yu, Y, Chen, H, Dai, J, Wang, H, et al. (2011). The fine-tuning of thermosensitive and degradable polymer micelles for enhancing intracellular uptake and drug release in tumors. *Biomaterials, 32*, 3832-3844.

[101] Hofheinz, RD, Gnad-Vogt, SU, Beyer, U, and Hochhaus, A (2005). Liposomal encapsulated anti-cancer drugs. *Anti-Cancer Drugs, 16*, 691-707.

[102] Allen, TM, and Cullis, PR (2013). Liposomal drug delivery systems: From concept to clinical applications. *Adv. Drug Deliv. Rev., 65*, 36-48.

[103] Barenholz, Y (2012). Doxil (R) - The first FDA-approved nano-drug: Lessons learned. *J. Control. Release, 160*, 117-134.

[104] Haran, G, Cohen, R, Bar, LK, and Barenholz, Y (1993). Transmembrane ammonium-sulfate gradients in liposomes produce efficient and stable entrapment of amphipathic weak bases. *Biochim Biophys Acta, 1151*, 201-215.

[105] Huynh, NT, Passirani, C, Saulnier, P, and Benoit, JP (2009). Lipid nanocapsules: A new platform for nanomedicine. *Int. J. Pharm., 379*, 201-209.

[106] Sharma, A, and Sharma, US (1997). Liposomes in drug delivery: progress and limitations. *Int. J. Pharm., 154*, 123-140.

[107] Gabizon, AA (2001). Stealth liposomes and tumor targeting: One step further in the quest for the magic bullet. *Clin. Cancer Res., 7*, 223-225.

[108] Romberg, B, Hennink, WE, and Storm, G (2008). Sheddable coatings for long-circulating nanoparticles. *Pharm. Res., 25*, 55-71.

[109] Shehata, T, Ogawara, K, Higaki, K, and Kimura, T (2008). Prolongation of residence time of liposome by surface-modification with mixture of hydrophilic polymers. *Int. J. Pharm., 359*, 272-279.

[110] Gaitanis, A, and Staal, S (2010). Liposomal Doxorubicin and nab-Paclitaxel: Nanoparticle Cancer Chemotherapy in Current Clinical Use. In Cancer Nanotechnology: Methods and Protocols, Volume 624, S.R. Grobmyer and B.M. Moudgil, eds. (Totowa: Humana Press Inc), pp. 385-392.

[111] Keller, AM, Mennel, R, Georgoulias, VA, Nabholtz, JM, Erazo, A, Lluch, A, Vogel, CL, Kaufmann, M, von Minckwitz, G, Henderson, IC, et al. (2004). Randomized phase III trial of pegylated liposomal doxorubicin versus vinorelbine or mitomycin C plus vinblastine in women with taxane-refractory advanced breast cancer. *J. Clin. Oncol., 22*, 3893-3901.

[112] O'Brien, MER, Wigler, N, Inbar, M, Rosso, R, Grischke, E, Santoro, A, Catane, R, Kieback, DG, Tomczak, P, Ackland, SP, et al. (2004). Reduced cardiotoxicity and comparable efficacy in a phase III trial of pegylated liposomal doxorubicin HCl (CAELYX (TM)/Doxil (R)) versus conventional doxorubicin for first-line treatment of metastatic breast cancer. *Ann. Oncol., 15*, 440-449.

[113] Northfelt, DW, Dezube, BJ, Thommes, JA, Miller, BJ, Fischl, MA, Friedman-Kien, A, Kaplan, LD, Du Mond, C, Mamelok, RD, and Henry, DH (1998). Pegylated-liposomal doxorubicin versus doxorubicin, bleomycin, and vincristine in the treatment of AIDS-related Kaposi's sarcoma: Results of a randomized phase III clinical trial. *J. Clin. Oncol., 16*, 2445-2451.

[114] Stewart, S, Jablonowski, H, Goebel, FD, Arasteh, K, Spittle, M, Rios, A, Aboulafia, D, Galleshaw, J, Dezube, BJ, and Int Pegylated Liposomal Doxorubicin Study, G (1998). Randomized comparative trial of pegylated liposomal doxorubicin versus bleomycin and vincristine in the treatment of AIDS-related Kaposi's sarcoma. *J. Clin. Oncol., 16*, 683-691.

[115] Gordon, AN, Fleagle, JT, Guthrie, D, Parkin, DE, Gore, ME, and Lacave, AJ (2001). Recurrent epithelial ovarian carcinoma: A randomized phase III study of pegylated liposomal doxorubicin versus topotecan. *J. Clin. Oncol., 19*, 3312-3322.

[116] Sparano, JA, Makhson, AN, Semiglazov, VF, Tjulandin, SA, Balashova, OI, Bondarenko, IN, Bogdanova, NV, Manikhas, GM, Oliynychenko, GP, Chatikhine, VA, et al. (2009). Pegylated Liposomal Doxorubicin Plus Docetaxel Significantly Improves Time to Progression Without Additive Cardiotoxicity Compared With Docetaxel Monotherapy in Patients With Advanced Breast Cancer Previously Treated With Neoadjuvant-Adjuvant Anthracycline Therapy: Results From a Randomized Phase III Study. *J. Clin. Oncol., 27*, 4522-4529.

[117] Orlowski, RZ, Nagler, A, Sonneveld, P, Blade, J, Hajek, R, Spencer, A, Miguel, JS, Robak, T, Dmoszynska, A, Horvath, N, et al. (2007). Randomized phase III study of pegylated liposomal doxorubicin plus bortezomib compared with bortezomib alone in relapsed or refractory multiple myeloma: Combination therapy improves time to progression. *J. Clin. Oncol., 25*, 3892-3901.

[118] Davies, CDL, Lundstrom, LM, Frengen, J, Eikenes, L, Bruland, OS, Kaahus, O, Hjelstuen, MHB, and Brekken, C (2004). Radiation improves the distribution and uptake of liposomal doxorubicin (Caelyx) in human osteosarcoma xenografts. *Cancer Res., 64*, 547-553.

[119] Harris, L, Batist, G, Belt, R, Rovira, D, Navari, R, Azarnia, N, Welles, K, Winer, E, and Grp, TDS (2002). Liposome-encapsulated doxorubicin compared with conventional doxorubicin in a randomized multicenter trial as first-line therapy of metastatic breast carcinoma. *Cancer, 94*, 25-36.

[120] Batist, G, Ramakrishnan, G, Rao, CS, Chandrasekharan, A, Gutheil, J, Guthrie, T, Shah, P, Khojasteh, A, Nair, MK, Hoelzer, K, et al. (2001). Reduced cardiotoxicity and preserved antitumor efficacy of liposome-encapsulated doxorubicin and cyclophosphamide compared with conventional doxorubicin and cyclophosphamide in a randomized, multicenter trial of metastatic breast cancer. *J. Clin. Oncol., 19*, 1444-1454.

[121] Gill, PS, Wernz, J, Scadden, DT, Cohen, P, Mukwaya, GM, vonRoenn, JH, Jacobs, M, Kempin, S, Silverberg, I, Gonzales, G, et al. (1996). Randomized phase III trial of liposomal daunorubicin versus doxorubicin, bleomycin, and vincristine in AIDS-related Kaposi's sarcoma. *J. Clin. Oncol., 14*, 2353-2364.

[122] Zamboni, WC, Ramalingam, S, Friedland, DM, Edwards, RP, Stoller, RG, Strychor, S, Maruca, L, Zamboni, BA, Belani, CP, and Ramanathan, RK (2009). Phase I and Pharmacokinetic Study of Pegylated Liposomal CKD-602 in Patients with Advanced Malignancies. *Clin. Cancer Res., 15*, 1466-1472.

[123] Boulikas, T (2009). Clinical overview on Lipoplatin (TM): a successful liposomal formulation of cisplatin. *Expert Opin. Investig. Drugs, 18*, 1197-1218.

[124] Canta, A, Chiorazzi, A, Carozzi, V, Meregalli, C, Oggioni, N, Sala, B, Crippa, L, Avezza, F, Forestieri, D, Rotella, G, et al. (2011). In vivo comparative study of the

cytotoxicity of a liposomal formulation of cisplatin (lipoplatin (TM)). *Cancer Chemother. Pharmacol., 68*, 1001-1008.

[125] Casagrande, N, De Paoli, M, Celegato, M, Borghese, C, Mongiat, M, Colombatti, A, and Aldinucci, D (2013). Preclinical evaluation of a new liposomal formulation of cisplatin, lipoplatin, to treat cisplatin-resistant cervical cancer. *Gynecol. Oncol., 131*, 744-752.

[126] Batist, G, Gelmon, KA, Chi, KN, Miller, WH, Chia, SKL, Mayer, LD, Swenson, CE, Janoff, AS, and Louie, AC (2009). Safety, Pharmacokinetics, and Efficacy of CPX-1 Liposome Injection in Patients with Advanced Solid Tumors. *Clin. Cancer Res., 15*, 692-700.

[127] Sankhala, KK, Mita, AC, Adinin, R, Wood, L, Beeram, M, Bullock, S, Yamagata, N, Matsuno, K, Fujisawa, T, and Phan, A (2009). A phase I pharmacokinetic (PK) study of MBP-426, a novel liposome encapsulated oxaliplatin. *J. Clin. Oncol., 27*, 1-2.

[128] Matsumura, Y, Gotoh, M, Muro, K, Yamada, Y, Shirao, K, Shimada, Y, Okuwa, M, Matsumoto, S, Miyata, Y, Ohkura, H, et al. (2004). Phase I and pharmacokinetic study of MCC-465, a doxorubicin (DXR) encapsulated in PEG immunoliposome, in patients with metastatic stomach cancer. *Ann. Oncol., 15*, 517-525.

[129] Egusquiaguirre, SP, Igartua, M, Hernandez, RM, and Pedraz, JL (2012). Nanoparticle delivery systems for cancer therapy: advances in clinical and preclinical research. *Clin. Transl. Oncol., 14*, 83-93.

[130] Cortes, JE, Goldberg, SL, Feldman, EJ, Rizzeri, DA, Hogge, DE, Larson, M, Pigneux, A, Recher, C, Schiller, G, Warzocha, K, et al. (2015). Phase II, Multicenter, Randomized Trial of CPX-351 (cytarabine: daunorubicin) Liposome Injection Versus Intensive Salvage Therapy in Adults With First Relapse AML. *Cancer, 121*, 234-242.

[131] Saracchini, S, Foltran, L, Tuccia, F, Bassini, A, Sulfaro, S, Micheli, E, Del Conte, A, Bertola, M, Gion, M, Lorenzon, M, et al. (2013). Phase II study of liposome-encapsulated doxorubicin plus cyclophosphamide, followed by sequential trastuzumab plus docetaxel as primary systemic therapy for breast cancer patients with HER2 overexpression or amplification. *Breast, 22*, 1101-1107.

[132] Wang, RH, Cao, HM, Tian, ZJ, Jin, B, Wang, Q, Ma, H, and Wu, J (2015). Efficacy of dual-functional liposomes containing paclitaxel for treatment of lung cancer. *Oncol. Rep., 33*, 783-791.

[133] Mei, L, Fu, L, Shi, KR, Zhang, QY, Liu, YY, Tang, J, Gao, HL, Zhang, ZR, and He, Q (2014). Increased tumor targeted delivery using a multistage liposome system functionalized with RGD, TAT and cleavable PEG. *Int. J. Pharm., 468*, 26-38.

[134] Wang, FF, Chen, L, Zhang, R, Chen, ZP, and Zhu, L (2014). RGD peptide conjugated liposomal drug delivery system for enhance therapeutic efficacy in treating bone metastasis from prostate cancer. *J. Control. Release, 196*, 222-233.

[135] Bersani, S, Vila-Caballer, M, Brazzale, C, Barattin, M, and Salmaso, S (2014). pH-sensitive stearoyl-PEG-poly(methacryloyl sulfadimethoxine) decorated liposomes for the delivery of gemcitabine to cancer cells. *Eur. J. Pharm. Biopharm., 88*, 670-682.

[136] Hardiansyah, A, Huang, LY, Yang, MC, Liu, TY, Tsai, SC, Yang, CY, Kuo, CY, Chan, TY, Zou, HM, Lian, WN, et al. (2014). Magnetic liposomes for colorectal cancer cells therapy by high-frequency magnetic field treatment. *Nanoscale Res. Lett., 9*, 1-13.

[137] Zagar, TM, Vujaskovic, Z, Formenti, S, Rugo, H, Muggia, F, O'Connor, B, Myerson, R, Stauffer, P, Hsu, IC, Diederich, C, et al. (2014). Two phase I dose-

escalation/pharmacokinetics studies of low temperature liposomal doxorubicin (LTLD) and mild local hyperthermia in heavily pretreated patients with local regionally recurrent breast cancer. *Int. J. Hyperthermia, 30*, 285-294.

[138] Liu, YR, Fang, JX, Kim, YJ, Wong, MK, and Wang, P (2014). Codelivery of Doxorubicin and Paclitaxel by Cross-Linked Multilamellar Liposome Enables Synergistic Antitumor Activity. *Mol. Pharm., 11*, 1651-1661.

[139] Li, L, ten Hagen, TLM, Hossann, M, Suss, R, van Rhoon, GC, Eggermont, AMM, Haemmerich, D, and Koning, GA (2013). Mild hyperthermia triggered doxorubicin release from optimized stealth thermosensitive liposomes improves intratumoral drug delivery and efficacy. *J. Control. Release, 168*, 142-150.

[140] Deng, ZJ, Morton, SW, Ben-Akiva, E, Dreaden, EC, Shopsowitz, KE, and Hammond, PT (2013). Layer-by-Layer Nanoparticles for Systemic Codelivery of an Anticancer Drug and siRNA for Potential Triple-Negative Breast Cancer Treatment. *ACS Nano, 7*, 9571-9584.

[141] Noble, GT, Stefanick, JF, Ashley, JD, Kiziltepe, T, and Bilgicer, B (2014). Ligand-targeted liposome design: challenges and fundamental considerations. *Trends Biotechnol., 32*, 32-45.

[142] Theil, EC, Liu, XFS, and Tosha, T (2008). Gated pores in the ferritin protein nanocage. *Inorg. Chim. Acta, 361*, 868-874.

[143] Hennequin, B, Turyanska, L, Ben, T, Beltran, AM, Molina, SI, Li, M, Mann, S, Patane, A, and Thomas, NR (2008). Aqueous Near-Infrared Fluorescent Composites Based on Apoferritin-Encapsulated PbS Quantum Dots. *Adv. Mater., 20*, 3592-3596.

[144] Bradshaw, TD, Junor, M, Patane, A, Clarke, P, Thomas, NR, Li, M, Mann, S, and Turyanska, L (2013). Apoferritin-encapsulated PbS quantum dots significantly inhibit growth of colorectal carcinoma cells. *J. Mat. Chem. B, 1*, 6254-6260.

[145] Yang, Z, Wang, XY, Diao, HJ, Zhang, JF, Li, HY, Sun, HZ, and Guo, ZJ (2007). Encapsulation of platinum anticancer drugs by apoferritin. *Chem. Commun.*, 3453-3455.

[146] Xing, RM, Wang, XY, Zhang, CL, Zhang, YM, Wang, Q, Yang, Z, and Guo, ZJ (2009). Characterization and cellular uptake of platinum anticancer drugs encapsulated in apoferritin. *J. Inorg. Biochem., 103*, 1039-1044.

[147] Falvo, E, Tremante, E, Fraioli, R, Leonetti, C, Zamparelli, C, Boffi, A, Morea, V, Ceci, P, and Giacomini, P (2013). Antibody-drug conjugates: targeting melanoma with cisplatin encapsulated in protein-cage nanoparticles based on human ferritin. *Nanoscale, 5*, 12278-12285.

[148] Yan, F, Zhang, Y, Yuan, HK, Gregas, MK, and Vo-Dinh, T (2008). Apoferritin protein cages: a novel drug nanocarrier for photodynamic therapy. *Chem. Commun.*, 4579-4581.

[149] Zhen, ZP, Tang, W, Chen, HM, Lin, X, Todd, T, Wang, G, Cowger, T, Chen, XY, and Xie, J (2013). RGD-Modified Apoferritin Nanoparticles for Efficient Drug Delivery to Tumors. *ACS Nano, 7*, 4830-4837.

[150] Zhen, ZP, Tang, W, Guo, CL, Chen, HM, Lin, X, Liu, G, Fei, BW, Chen, XY, Xu, BQ, and Xie, J (2013). Ferritin Nanocages To Encapsulate and Deliver Photosensitizers for Efficient Photodynamic Therapy against Cancer. *ACS Nano, 7*, 6988-6996.

[151] Ma-Ham, AH, Wu, H, Wang, J, Kang, XH, Zhang, YY, and Lin, YH (2011). Apoferritin-based nanomedicine platform for drug delivery: equilibrium binding study of daunomycin with DNA. *J. Mater. Chem., 21*, 8700-8708.

[152] Kilic, MA, Ozlu, E, and Calis, S (2012). A Novel Protein-Based Anticancer Drug Encapsulating Nanosphere: Apoferritin-Doxorubicin Complex. *J. Biomed. Nanotechnol., 8*, 508-514.

[153] Blazkova, I, Nguyen, HV, Dostalova, S, Kopel, P, Stanisavljevic, M, Vaculovicova, M, Stiborova, M, Eckschlager, T, Kizek, R, and Adam, V (2013). Apoferritin Modified Magnetic Particles as Doxorubicin Carriers for Anticancer Drug Delivery. *Int. J. Mol. Sci., 14*, 13391-13402.

[154] Tmejova, K, Hynek, D, Kopel, P, Dostalova, S, Smerkova, K, Stanisavljevic, M, Nguyen, HV, Nejdl, L, Vaculovicova, M, Krizkova, S, et al. (2013). Electrochemical Behaviour of Doxorubicin Encapsulated in Apoferritin. *Int. J. Electrochem. Sci., 8*, 12658-12671.

[155] Konecna, R, Nguyen, HV, Stanisavljevic, M, Blazkova, I, Krizkova, S, Vaculovicova, M, Stiborova, M, Eckschlager, T, Zitka, O, Adam, V, et al. (2014). Doxorubicin Encapsulation Investigated by Capillary Electrophoresis with Laser-Induced Fluorescence Detection. *Chromatographia, 77*, 1469-1476.

[156] Gumulec, J, Fojtu, M, Raudenska, M, Sztalmachova, M, Skotakova, A, Vlachova, J, Skalickova, S, Nejdl, L, Kopel, P, Knopfova, L, et al. (2014). Modulation of Induced Cytotoxicity of Doxorubicin by Using Apoferritin and Liposomal Cages. *Int. J. Mol. Sci., 15*, 22960-22977.

[157] Liang, MM, Fan, KL, Zhou, M, Duan, DM, Zheng, JY, Yang, DL, Feng, J, and Yan, XY (2014). H-ferritin-nanocaged doxorubicin nanoparticles specifically target and kill tumors with a single-dose injection. *Proc. Natl. Acad. Sci. U. S. A., 111*, 14900-14905.

[158] Fan, KL, Gao, LZ, and Yan, XY (2013). Human ferritin for tumor detection and therapy. *Wiley Interdiscip. Rev.-Nanomed. Nanobiotechnol., 5*, 287-298.

[159] Bellini, M, Mazzucchelli, S, Galbiati, E, Sommaruga, S, Fiandra, L, Truffi, M, Rizzuto, MA, Colombo, M, Tortora, P, Corsi, F, et al. (2014). Protein nanocages for self-triggered nuclear delivery of DNA-targeted chemotherapeutics in Cancer Cells. *J. Control. Release, 196*, 184-196.

[160] Heger, Z, Skalickova, S, Zitka, O, Adam, V, and Kizek, R (2014). Apoferritin applications in nanomedicine. *Nanomedicine, 9*, 2233-2245.

[161] Zhen, ZP, Tang, W, Todd, T, and Xie, J (2014). Ferritins as nanoplatforms for imaging and drug delivery. *Expert Opin. Drug Deliv., 11*, 1913-1922.

[162] Zhang, L, Radovic-Moreno, AF, Alexis, F, Gu, FX, Basto, PA, Bagalkot, V, Jon, S, Langer, RS, and Farokhzad, OC (2007). Co-delivery of hydrophobic and hydrophilic drugs from nanoparticle-aptamer bioconjugates. *Chemmedchem, 2*, 1268-1271.

[163] Putnam, D, and Kopecek, J (1995). Polymer conjugates with anticancer activity. In Advances in Polymer Science; Biopolymers II, Volume 122, N.A. Peppas and R.S. Langer, eds., pp. 55-123.

[164] Gradishar, WJ, Tjulandin, S, Davidson, N, Shaw, H, Desai, N, Bhar, P, Hawkins, M, and O'Shaughnessy, J (2005). Phase III trial of nanoparticle albumin-bound paclitaxel compared with polyethylated castor oil-based paclitaxel in women with breast cancer. *J Clin Oncol, 23*, 7794-7803.

[165] Green, MR, Manikhas, GM, Orlov, S, Afanasyev, B, Makhson, AM, Bhar, P, and Hawkins, MJ (2006). Abraxane((R)), a novel Cremophor((R))-free, albumin-bound particle form of paclitaxel for the treatment of advanced non-small-cell lung cancer. *Ann Oncol, 17*, 1263-1268.

[166] Nyman, DW, Campbell, KJ, Hersh, E, Long, K, Richardson, K, Trieu, V, Desai, N, Hawkins, MJ, and Von Hoff, DD (2005). Phase I and pharmacokinetics trial of ABI-007, a novel nanoparticle formulation of paclitaxel in patients with advanced nonhematologic malignancies. *J Clin Oncol, 23*, 7785-7793.

[167] Li, C (2002). Poly(L-glutamic acid) - anticancer drug conjugates. *Adv Drug Del Rev, 54*, 695-713.

[168] Auzenne, E, Ghosh, SC, Khodadadian, M, Rivera, B, Farquhar, D, Price, RE, Ravoori, M, Kundra, V, Freedman, RS, and Klostergaard, J (2007). Hyaluronic acid-paclitaxel: Antitumor efficacy against CD44(+) human ovarian carcinoma xenografts. *Neoplasia, 9*, 479-486.

[169] Sabbatini, P, Aghajanian, C, Dizon, D, Anderson, S, Dupont, J, Brown, JV, Peters, WA, Jacobs, A, Mehdi, A, Rivkin, S, et al. (2004). Phase II study of CT-2103 in patients with recurrent epithelial ovarian, fallopian tube, or primary peritoneal carcinoma. *J Clin Oncol, 22*, 4523-4531.

[170] Bhatt, RL, de Vries, P, Tulinsky, J, Bellamy, G, Baker, B, Singer, JW, and Klein, P (2003). Synthesis and in vivo antitumor activity of poly(L-glutamic acid) conjugates of 20(S)-camptothecin. *J Med Chem, 46*, 190-193.

[171] Seymour, MT, Maughan, TS, Ledermann, JA, Topham, C, James, R, Gwyther, SJ, Smith, DB, Shepherd, S, Maraveyas, A, Ferry, DR, et al. (2007). Different strategies of sequential and combination chemotherapy for patients with poor prognosis advanced colorectal cancer (MRC FOCUS): a randomised controlled trial. *Lancet, 370*, 143-152.

[172] Atkins, JH, and Gershell, LJ (2002). Selective anticancer drugs. *Nat Rev Cancer, 2*, 645-645.

[173] Rowinsky, EK, Schwartz, GH, Gollob, JA, Thompson, JA, Vogelzang, NJ, Figlin, R, Bukowski, R, Haas, N, Lockbaum, P, Li, YP, et al. (2004). Safety, pharmacokinetics, and activity of ABX-EGF, a fully human anti-epidermal growth factor receptor monoclonal antibody in patients with metastatic renal cell cancer. *J Clin Oncol, 22*, 3003-3015.

[174] Pasut, G, and Veronese, FM (2009). PEG conjugates in clinical development or use as anticancer agents: An overview. *Adv Drug Del Rev, 61*, 1177-1188.

[175] Watanabe, T, Komuro, Y, Kiyomatsu, T, Kanazawa, T, Kazama, Y, Tanaka, J, Tanaka, T, Yamamoto, Y, Shirane, M, Muto, T, et al. (2006). Prediction of sensitivity of rectal cancer cells in response to preoperative radiotherapy by DNA microarray analysis of gene expression profiles. *Cancer Res, 66*, 3370-3374.

[176] Yurkovetsky, Z, Skates, S, Lomakin, A, Nolen, B, Pulsipher, T, Modugno, F, Marks, J, Godwin, A, Gorelik, E, Jacobs, I, et al. (2010). Development of a Multimarker Assay for Early Detection of Ovarian Cancer. *J Clin Oncol, 28*, 2159-2166.

[177] Adams, ML, Lavasanifar, A, and Kwon, GS (2003). Amphiphilic block copolymers for drug delivery. *J Pharm Sci, 92*, 1343-1355.

[178] Bazile, D, Prudhomme, C, Bassoullet, MT, Marlard, M, Spenlehauer, G, and Veillard, M (1995). Stealth Me.PEG-PLA nanoparticles avoid uptake by the mononuclear phagocytes system *J Pharm Sci, 84*, 493-498.

[179] Allemann, E, Brasseur, N, Benrezzak, O, Rousseau, J, Kudrevich, SV, Boyle, RW, Leroux, JC, Gurny, R, and Vanlier, JE (1995). PEG-coated poly(lactic acid) nanoparticles for the delivery of hexadecafluoro zinc phthalocyanine to ETM-6 mouse mammary-tumors. *J Pharm Pharmacol, 47*, 382-387.

[180] Sengupta, S, Eavarone, D, Capila, I, Zhao, GL, Watson, N, Kiziltepe, T, and Sasisekharan, R (2005). Temporal targeting of tumour cells and neovasculature with a nanoscale delivery system. *Nature, 436*, 568-572.

[181] Lammers, T, Subr, V, Ulbrich, K, Peschke, P, Huber, PE, Hennink, WE, and Storm, G (2009). Simultaneous delivery of doxorubicin and gemcitabine to tumors in vivo using prototypic polymeric drug carriers. *Biomaterials, 30*, 3466-3475.

[182] Abeylath, SC, Turos, E, Dickey, S, and Lim, DV (2008). Glyconanobiotics: Novel carbohydrated nanoparticle antibiotics for MRSA and Bacillus anthracis. *Bioorgan Med Chem, 16*, 2412-2418.

[183] Song, XR, Cai, Z, Zheng, Y, He, G, Cui, FY, Gong, DQ, Hou, SX, Xiong, SJ, Lei, XJ, and Wei, YQ (2009). Reversion of multidrug resistance by co-encapsulation of vincristine and verapamil in PLGA nanoparticles. *Eur J Pharm Sci, 37*, 300-305.

[184] Soma, CE, Dubernet, C, Bentolila, D, Benita, S, and Couvreur, P (2000). Reversion of multidrug resistance by co-encapsulation of doxorubicin and cyclosporin A in polyalkylcyanoacrylate nanoparticles. *Biomaterials, 21*, 1-7.

[185] Bae, Y, Diezi, TA, Zhao, A, and Kwon, GS (2007). Mixed polymeric micelles for combination cancer chemotherapy through the concurrent delivery of multiple chemotherapeutic agents. *J Control Release, 122*, 324-330.

[186] Liu, MJ, and Frechet, JMJ (1999). Designing dendrimers for drug delivery. *Pharmaceut Sci Technol Today, 2*, 393-401.

[187] Wolinsky, JB, and Grinstaff, MW (2008). Therapeutic and diagnostic applications of dendrimers for cancer treatment. *Adv Drug Del Rev, 60*, 1037-1055.

[188] Morgan, MT, Carnahan, MA, Immoos, CE, Ribeiro, AA, Finkelstein, S, Lee, SJ, and Grinstaff, MW (2003). Dendritic molecular capsules for hydrophobic compounds. *J Am Chem Soc, 125*, 15485-15489.

[189] Morgan, MT, Carnahan, MA, Finkelstein, S, Prata, CAH, Degoricija, L, Lee, SJ, and Grinstaff, MW (2005). Dendritic supramolecular assemblies for drug delivery. *Chem Commun*, 4309-4311.

[190] Wang, F, Bronich, TK, Kabanov, AV, Rauh, RD, and Roovers, J (2005). Synthesis and evaluation of a star amphiphilic block copolymer from poly(epsilon-caprolactone) and poly(ethylene glycol) as a potential drug delivery carrier. *Bioconjugate Chem, 16*, 397-405.

[191] Malik, N, Evagorou, EG, and Duncan, R (1999). Dendrimer-platinate: a novel approach to cancer chemotherapy. *Anti-Cancer Drug, 10*, 767-776.

[192] Kojima, C, Kono, K, Maruyama, K, and Takagishi, T (2000). Synthesis of polyamidoamine dendrimers having poly(ethylene glycol) grafts and their ability to encapsulate anticancer drugs. *Bioconjugate Chem, 11*, 910-917.

[193] Bhadra, D, Bhadra, S, Jain, S, and Jain, NK (2003). A PEGylated dendritic nanoparticulate carrier of fluorouracil. *Int J Pharmaceut, 257*, 111-124.

[194] Wu, G, Barth, RF, Yang, WL, Kawabata, S, Zhang, LW, and Green-Church, K (2006). Targeted delivery of methotrexate to epidermal growth factor receptor-positive brain

tumors by means of cetuximab (IMC-C225) dendrimer bioconjugates. *Mol Cancer Ther, 5*, 52-59.

[195] Neerman, MF, Chen, H-T, Parrish, AR, and Simanek, EE (2004). Reduction of drug toxicity using dendrimers based on melamine. *Mol Pharmaceut, 1*, 390-393.

[196] Lee, EJH, Ribeiro, C, Longo, E, and Leite, ER (2006). Growth kinetics of tin oxide nanocrystals in colloidal suspensions under hydrothermal conditions. *Chem Phys, 328*, 229-235.

[197] Mann, S, Burkett, SL, Davis, SA, Fowler, CE, Mendelson, NH, Sims, SD, Walsh, D, and Whilton, NT (1997). Sol-gel synthesis of organized matter. *Chem Mater, 9*, 2300-2310.

[198] Vasiliev, PO, Faure, B, Ng, JBS, and Bergstroem, L (2008). Colloidal aspects relating to direct incorporation of TiO2 nanoparticles into mesoporous spheres by an aerosol-assisted process. *J Colloid Interf Sci, 319*, 144-151.

[199] Tenne, R, Remskar, M, Enyashin, A, and Seifert, G (2008). Inorganic nanotubes and fullerene-like structures (IF). In Carbon Nanotubes, Volume 111, A. Jorio, G. Dresselhaus and M.S. Dresselhaus, eds., pp. 631-671.

[200] Kishida, M, Fujita, T, Umakoshi, K, Ishiyama, J, Nagata, H, and Wakabayashi, K (1995). Novel preparation of metal-supported catalysts by colloidal microparticles in a water-in-oil microemulsion - catalytic-hydrogenation of carbon-dioxide. *Chem Commun*, 763-764.

[201] Mu, Q, Yang, L, Davis, JC, Vankayala, R, Hwang, KC, Zhao, J, and Yan, B (2010). Biocompatibility of polymer grafted core/shell iron/carbon nanoparticles. *Biomaterials, 31*, 5083-5090.

[202] Corot, C, Robert, P, Idee, J-M, and Port, M (2006). Recent advances in iron oxide nanocrystal technology for medical imaging. *Adv Drug Del Rev, 58*, 1471-1504.

[203] Chang, Y, Meng, X, Zhao, Y, Li, K, Zhao, B, Zhu, M, Li, Y, Chen, X, and Wang, J (2011). Novel water-soluble and pH-responsive anticancer drug nanocarriers: Doxorubicin-PAMAM dendrimer conjugates attached to superparamagnetic iron oxide nanoparticles (IONPs). *J Colloid Interf Sci, 363*, 403-409.

[204] Jiang, W, Zhang, X, Sun, Z, Fang, Y, Li, F, Chen, K, and Huang, C (2011). Preparation and mechanism of magnetic carbonaceous polysaccharide microspheres by low-temperature hydrothermal method. *J Magn Magn Mater, 323*, 2741-2747.

[205] Rety, F, Clement, O, Siauve, N, Cuenod, CA, Carnot, F, Sich, M, Buisine, A, and Frija, G (2000). MR lymphography using iron oxide nanoparticles in rats: Pharmacokinetics in the lymphatic system after intravenous injection. *J Magn Reson Imaging, 12*, 734-739.

[206] Sadighian, S, Rostamizadeh, K, Hosseini-Monfared, H, and Hamidi, M (2014). Doxorubicin-conjugated core-shell magnetite nanoparticles as dual-targeting carriers for anticancer drug delivery. *Colloid Surface B, 117*, 406-413.

[207] Samra, ZQ, Ahmad, S, Javeid, M, Dar, N, Aslam, MS, Gull, I, and Ahmad, MM (2013). Anticancer medicines (doxorubicin and methotrexate) conjugated with magnetic nanoparticles for targeting drug delivery through iron. *Prep Biochem Biotech, 43*, 781-797.

[208] Gang, J, Park, S-B, Hyung, W, Choi, EH, Wen, J, Kim, H-S, Shul, Y-G, Haam, S, and Song, SY (2007). Magnetic poly epsilon-caprolactone nanoparticles containing Fe3O4

and gemcitabine enhance anti-tumor effect in pancreatic cancer xenograft mouse model. *J Drug Target, 15*, 445-453.

[209] Akbarzadeh, A, Zarghami, N, Mikaeili, H, Asgari, D, Goganian, AM, Khiabani, HK, Samiei, M, and Davaran, S (2012). Synthesis, characterization, and in vitro evaluation of novel polymer-coated magnetic nanoparticles for controlled delivery of doxorubicin. *Nanotech sci appl, 5*, 13-25.

[210] Cao, H, Gan, J, Wang, S, Xuan, S, Wu, Q, Li, C, Wu, C, Hu, C, and Huang, G (2008). Novel silica-coated iron-carbon composite particles and their targeting effect as a drug carrier. *J Biomed Mater Res A, 86A*, 671-677.

[211] Yang, G-f, Li, X-h, Zhao, Z, and Wang, W-b (2009). Preparation, characterization, in vivo and in vitro studies of arsenic trioxide Mg-Fe ferrite magnetic nanoparticles. *Acta Pharmacol Sin, 30*, 1688-1693.

[212] Schrand, AM, Hens, SAC, and Shenderova, OA (2009). Nanodiamond Particles: Properties and Perspectives for Bioapplications. *Crit Rev Solid State 34*, 18-74.

[213] Kroto, HW, Heath, JR, O'Brien, SC, Curl, RF, and Smalley, RE (1985). C60: Buckminsterfullerene. *Nature, 318*, 162-163.

[214] Iijima, S (1991). Helical microtubules of graphitic carbon. *Nature, 354*, 56-58.

[215] Utreja, P, Jain, S, and Tiwary, AK (2010). Novel Drug Delivery Systems for Sustained and Targeted Delivery of Anti-Cancer Drugs: Current Status and Future Prospects. *Curr Drug Deliv, 7*, 152-161.

[216] Baughman, RH, Zakhidov, AA, and de Heer, WA (2002). Carbon Nanotubes--the Route Toward Applications. *Science, 297*, 787-792.

[217] Sahoo, NG, Bao, H, Pan, Y, Pal, M, Kakran, M, Cheng, HKF, Li, L, and Tan, LP (2011). Functionalized carbon nanomaterials as nanocarriers for loading and delivery of a poorly water-soluble anticancer drug: a comparative study. *Chem Commun, 47*, 5235-5237.

[218] Lamprecht, C, Liashkovich, I, Neves, V, Danzberger, J, Heister, E, Rangl, M, Coley, HM, McFadden, J, Flahaut, E, Gruber, HJ, et al. (2009). AFM imaging of functionalized carbon nanotubes on biological membranes. *Nanotechnology, 20*.

[219] Beg, S, Rizwan, M, Sheikh, AM, Hasnain, MS, Anwer, K, and Kohli, K (2011). Advancement in carbon nanotubes: basics, biomedical applications and toxicity. *J Pharm Pharmacol, 63*, 141-163.

[220] Klumpp, C, Kostarelos, K, Prato, M, and Bianco, A (2006). Functionalized carbon nanotubes as emerging nanovectors for the delivery of therapeutics. *Biochim Biophys Acta, 1758*, 404-412.

[221] Bekyarova, E, Ni, Y, Malarkey, EB, Montana, V, McWilliams, JL, Haddon, RC, and Parpura, V (2005). Applications of Carbon Nanotubes in Biotechnology and Biomedicine. *J Biomed Nanotechnol, 1*, 3-17.

[222] Liu, Z, and Qian, L (2009). Changepoint Estimation in a Segmented Linear Regression via Empirical Likelihood. *Commun Stat - Simul C, 39*, 85-100.

[223] Tans, SJ, Devoret, MH, Dai, H, Thess, A, Smalley, RE, Geerligs, LJ, and Dekker, C (1997). Individual single-wall carbon nanotubes as quantum wires. *Nature, 386*, 474-477.

[224] Kam, NWS, Liu, Z, and Dai, H (2006). Carbon Nanotubes as Intracellular Transporters for Proteins and DNA: An Investigation of the Uptake Mechanism and Pathway. *Angew Chem Int Edit, 45*, 577-581.

[225] Jin, H, Heller, DA, and Strano, MS (2008). Single-Particle Tracking of Endocytosis and Exocytosis of Single-Walled Carbon Nanotubes in NIH-3T3 Cells. *Nano Lett, 8*, 1577-1585.

[226] Wu, P, Chen, X, Hu, N, Tam, UC, Blixt, O, Zettl, A, and Bertozzi, CR (2008). Biocompatible Carbon Nanotubes Generated by Functionalization with Glycodendrimers. *Angew Chem Int Edit, 47*, 5022-5025.

[227] Chen, X, Tam, UC, Czlapinski, JL, Lee, GS, Rabuka, D, Zettl, A, and Bertozzi, CR (2006). Interfacing Carbon Nanotubes with Living Cells. *J Am Chem Soc, 128*, 6292-6293.

[228] Pantarotto, D, Briand, J-P, Prato, M, and Bianco, A (2004). Translocation of bioactive peptides across cell membranes by carbon nanotubes. *Chem Commun*, 16-17.

[229] Bianco, A, Kostarelos, K, Partidos, CD, and Prato, M (2005). Biomedical applications of functionalised carbon nanotubes. *Chem Commun*, 571-577.

[230] Kostarelos, K, Lacerda, L, Pastorin, G, Wu, W, WieckowskiSebastien, Luangsivilay, J, Godefroy, S, Pantarotto, D, Briand, J-P, Muller, S, et al. (2007). Cellular uptake of functionalized carbon nanotubes is independent of functional group and cell type. *Nat Nano, 2*, 108-113.

[231] Kang, B, Chang, S, Dai, Y, Yu, D, and Chen, D (2010). Cell Response to Carbon Nanotubes: Size-Dependent Intracellular Uptake Mechanism and Subcellular Fate. *Small, 6*, 2362-2366.

[232] Mu, Q, Broughton, DL, and Yan, B (2009). Endosomal Leakage and Nuclear Translocation of Multiwalled Carbon Nanotubes: Developing a Model for Cell Uptake. *Nano Lett, 9*, 4370-4375.

[233] Kam, NWS, and Dai, H (2005). Carbon Nanotubes as Intracellular Protein Transporters: Generality and Biological Functionality. *J Am Chem Soc, 127*, 6021-6026.

[234] Kam, NWS, Liu, Z, and Dai, H (2005). Functionalization of Carbon Nanotubes via Cleavable Disulfide Bonds for Efficient Intracellular Delivery of siRNA and Potent Gene Silencing. *J Am Chem Soc, 127*, 12492-12493.

[235] Zhou, F, Xing, D, Wu, B, Wu, S, Ou, Z, and Chen, WR (2010). New Insights of Transmembranal Mechanism and Subcellular Localization of Noncovalently Modified Single-Walled Carbon Nanotubes. *Nano Lett, 10*, 1677-1681.

[236] Jin, H, Heller, DA, and Strano, MS (2009). Single-particle tracking of endocytosis and exocytosis of single-walled carbon nanotubes in NIH-3T3 cells. *Abstr Am Chem Soc, 237*.

[237] Liu, Z, Chen, K, Davis, C, Sherlock, S, Cao, Q, Chen, X, and Dai, H (2008). Drug delivery with carbon nanotubes for in vivo cancer treatment. *Cancer Res, 68*, 6652-6660.

[238] Wu, W, Li, R, Bian, X, Zhu, Z, Ding, D, Li, X, Jia, Z, Jiang, X, and Hu, Y (2009). Covalently Combining Carbon Nanotubes with Anticancer Agent: Preparation and Antitumor Activity. *ACS Nano, 3*, 2740-2750.

[239] Li, Y, Cousins, BG, Ulijn, RV, and Kinloch, IA (2009). A Study of the Dynamic Interaction of Surfactants with Graphite and Carbon Nanotubes using Fmoc-Amino Acids as a Model System. *Langmuir, 25*, 11760-11767.

[240] Pastorin, G, Wu, W, Wieckowski, S, Briand, J-P, Kostarelos, K, Prato, M, and Bianco, A (2006). Double functionalisation of carbon nanotubes for multimodal drug delivery. *Chem Commun*, 1182-1184.

[241] Wu, W, Wieckowski, S, Pastorin, G, Benincasa, M, Klumpp, C, Briand, J-P, Gennaro, R, Prato, M, and Bianco, A (2005). Targeted Delivery of Amphotericin B to Cells by Using Functionalized Carbon Nanotubes. *Angew Chem Inter Edit, 44*, 6358-6362.

[242] Liu, Z, Chen, K, Davis, C, Sherlock, S, Cao, QZ, Chen, XY, and Dai, HJ (2008). Drug delivery with carbon nanotubes for in vivo cancer treatment. *Cancer Res., 68*, 6652-6660.

[243] Dhar, S, Liu, Z, Thomale, J, Dai, H, and Lippard, SJ (2008). Targeted single-wall carbon nanotube-mediated Pt(IV) prodrug delivery using folate as a homing device. *J Am Chem Soc, 130*, 11467-11476.

[244] Liu, Z, Sun, X, Nakayama-Ratchford, N, and Dai, H (2007). Supramolecular Chemistry on Water-Soluble Carbon Nanotubes for Drug Loading and Delivery. *ACS Nano, 1*, 50-56.

[245] Liu, Z, Robinson, JT, Sun, X, and Dai, H (2008). PEGylated Nanographene Oxide for Delivery of Water-Insoluble Cancer Drugs. *J Am Chem Soc, 130*, 10876-10877.

[246] Sun, X, Zhang, Y, Zhang, X, Yu, J, Li, Y, Yang, X, Dai, Z, and Li, M (2008). The clinical evaluation of Iressa first-line treatment of senium advanced-stage non-small cell lung cancer. *Chin. -Ger. J. Clin. Oncol., 7*, 203-206.

[247] Ali-Boucetta, H, Al-Jamal, KT, McCarthy, D, Prato, M, Bianco, A, and Kostarelos, K (2008). Multiwalled carbon nanotube-doxorubicin supramolecular complexes for cancer therapeutics. *Chem Commun*, 459-461.

[248] Robinson, JT, Tabakman, SM, Liang, Y, Wang, H, Sanchez Casalongue, H, Vinh, D, and Dai, H (2011). Ultrasmall Reduced Graphene Oxide with High Near-Infrared Absorbance for Photothermal Therapy. *J Am Chem Soc, 133*, 6825-6831.

[249] Kam, NWS, Jessop, TC, Wender, PA, and Dai, HJ (2004). Nanotube molecular transporters: Internalization of carbon nanotube-protein conjugates into mammalian cells. *J Am Chem Soc, 126*, 6850-6851.

[250] Gottesman, MM, Fojo, T, and Bates, SE (2002). Multidrug resistance in cancer: Role of ATP-dependent transporters. *Nat Rev Cancer, 2*, 48-58.

[251] Geim, AK, and Novoselov, KS (2007). The rise of graphene. *6*, 183-191.

[252] Zhang, Y, Nayak, TR, Hong, H, and Cai, W (2012). Graphene: a versatile nanoplatform for biomedical applications. *Nanoscale, 4*, 3833-3842.

[253] Yang, K, Feng, L, Shi, X, and Liu, Z (2013). Nano-graphene in biomedicine: theranostic applications. *Chem Soc Rev, 42*, 530-547.

[254] Yang, K, Zhang, S, Zhang, G, Sun, X, Lee, S-T, and Liu, Z (2010). Graphene in Mice: Ultrahigh In Vivo Tumor Uptake and Efficient Photothermal Therapy. *Nano Lett, 10*, 3318-3323.

[255] Yang, X, Wang, Y, Huang, X, Ma, Y, Huang, Y, Yang, R, Duan, H, and Chen, Y (2011). Multi-functionalized graphene oxide based anticancer drug-carrier with dual-targeting function and pH-sensitivity. *J Mater Chem, 21*, 3448-3454.

4. MATERIALS AND METHODS

4.1. Synthesis of peptide by solid phase

Synthesis of all peptides was performed by Liberty Blue peptide synthesizer (CEM, Matthews, NC, USA). Syntheses of peptides were conducted on a solid-phase, by using 9-Fluorenylmethoxycarbonyl (Fmoc) protected MBHA resin and amino acids. The Fmoc protecting groups were removed with 20 % piperidine *v/v* in *N*,*N*-dimethylformamide (DMF). Amino acids were coupled by combination of *N*,*N*,*N´*,*N´*-tetramethyl-*O*-(1*H*-benzotriazol-1-yl)uronium-hexafluorophosphate (HBTU), *N*,*N*-diisopropylethylamine (DIEA), and DMF. The cleavage of the side chain protecting groups was performed by treating the peptides resin with 95 % trifluoroacetic acid (TFA) *v/v*, 2.5 % H_2O *v/v*, and 2.5 % triisopropylsilane *v/v* for 30 min at 38°C under microwave irradiation. Precipitation and purification of peptides were performed by centrifugation (6000 rpm, 3 x 5 min) using cold diethyl ether (- 20°C).

4.2. Oxidation of MWCNTs and Fullerenes

1 mg MWCNTs and 1 mg fullerenes (Sigma-Aldrich, St. Louis, MO, USA) were separately mixed with 0.5 mL of concentrated HNO_3. Also 4 mg of fullerenes was mixed with trimesic acid. Prepared mixtures were sonicated using an ultrasonic bath (Bandelin, Berlin, Germany) for 15 min and then heated on Thermo-mixer (Eppendorf, Hamburg, Germany) for 20 min at 80°C, 800 rpm. Oxidized mixtures were centrifuged at 25000 rpm at 20 °C for 10 min using a table top centrifuge (Eppendorf, Hamburg, Germany) in order to remove excess of acid. Product was washed by centrifugation with MilliQ water, until the pH became neutral.

4.3. Ion Exchange Chromatography

Ion exchange chromatography was conducted by AAA 400 (Ingos, Prague, Czech Republic). The system consisting of a glass filling chromatographic column and steel pre-column, two chromatographic pumps for transport of elution buffers and derivatization reagent, a cooled carousel for 25 Eppendorf tubes, a dosing valve, a heat reactor, a Vis detector, and a cooled chamber for derivatization reagent. The volume of

the injected sample was 100 μL with RSD 1%. A two-channel Vis detector with a 5 μL flow volume cuvette operated at wavelengths of 440 and 570 nm was used. A solution of ninhydrin was prepared in 75% methyl cellosolve (v/v) and 25% 4 M acetic buffer (v/v, pH 4.0). Tin chloride was used as reducing reagent. Prepared solution of ninhydrin was stored under an inert atmosphere (N_2) with cooling at 4 °C. Flow rate was 0.25 mL·min−1. Pressure ranged from 4.5 to 6.0 MPa. Reactor temperature was set to 120°C. The amino acids were eluted with a gradient increasing with increasing pH 0-7 min (pH 2.7), 7-20 min (pH 3), 20 to 31 min (pH 4.25), 31-90 min (pH 9.7)

4.4. Purification of peptide by FPLC and HPLC

Fast protein liquid chromatography (FPLC) was performed by Biologic DuoFlow system (Biorad, USA), equipped with two chromatographic pumps for elution buffers, a gel-filtration column (HiLoad 26/60, 75 PG, GE healthcare Sweden), 2 mL sample loop injection valve system and UV-VIS detector. Mobile phase flow was set to 4 mL/min, while mobile phase solution was prepared by mixing 150 mM of NaCl in 10 mM Tris-HCl buffer (pH 8.6). Isocratic elution was used for peptide separation. Column was washed for 60 min by mobile phase. Fractions were collected in elution tube with volume of 2 ml for each eluent.

Purification of peptide was also performed by high-performance liquid chromatography (HPLC). The HPLC system is equipped with two chromatographic pumps Model 582 ESA (ESA Inc., Chelmsford, MA, USA) and chromatographic column with reverse phase Kinetex 5 lm EVO C18 (150 9 4.6 mm, Phenomenex, Inc., Torrance, CA, USA). The mobile phase flow rate was 1 cm^3 min^{-1}. The mobile phase consisted of A: 0.01 % TFA and B: acetonitrile with 0.01 % TFA.

4.5. Matrix-assisted laser desorption/ionization-time-of-flight mass spectrometry (MALDI-TOF MS)

The mass spectrometry experiments were performed on MALDI-TOF MS Bruker Ultraflextreme (Bruker Daltonik GmbH, Bremen, Germany) equipped with a laser, operating at wavelength of 355 nm with an accelerating voltage of 25 kV, cooled with nitrogen and maximum energy of 43.2 μJ with repetition rate of 2000 Hz in linear and positive mode, and with software for data acquisition and processing of mass spectra flexControl version 3.4 and flexAnalysis version 2.2. The matrix used in the MALDI method was 2,5-dihydroxybenzoic acid matrix (DHB) (Bruker Daltonik GmbH).

The matrix was prepared in TA30 (30% acetonitrile, 0.1% TFA solution). Mixture was thoroughly vortexed and ultrasonicated using Bandelin 152 Sonorex Digital 10P ultrasonic bath (Bandelin electronic GmbH, Germany) for 2 min, 50% of intensity at ambient temperature. Working standard solutions were prepared daily by dilution of the stock solutions. The sample solutions were TA30. The solutions for analysis were mixed in ratio of 1:1 (matrix/substance). After obtaining a homogeneous solution, 1 µL was applied on the target and dried under atmospheric pressure and ambient temperature. A mixture of peptide calibrations standard (Bruker Daltonik GmbH) was utilized to externally calibrate the instrument. The MS spectra were typically acquired by averaging 20 sub spectra from a total of 500 shots of the laser.

4.6. Spectroscopy analysis

Fluorescence and absorbance were detected by Tecan Infinite 200 PRO multifunctional microplate reader (Tecan, Männedorf, Switzerland). The fluorescence and absorbance measurement was measure within the range 230 to 850 nm with detector gain set to 100%. Costar Corning® transparent 96 well microplates with flat bottom (Thermo Scientific, Waltham, MA, USA), were used for samples analysis. Data was collected and processed by Microplate Reader software i-control™ 1.9 (Tecan, Männedorf, Switzerland).

4.7. Attenuated total reflectance-Fourier transforms infrared spectroscopy (ATR-FT-IR)

Nicolet iS10 FT-IR spectrometer with diamond ATR attachment (Thermo Electron Inc., San Jose, USA) was used for recording of FT-IR spectra in a range from 4000 to 650 cm^{-1} and resolution of 4 cm^{-1}. Each spectrum was acquired by adding together 32 interferograms. Spectra were measured at 22 °C. The OMNIC™ software was used for IR spectra recording and JDXview v0.2 software was used for further spectra evaluation.

4.8. Adsorptive transfer technique coupled with differential pulse voltammetry (AdT-DPV)

Sample analyses were performed with adsorptive transfer technique, coupled with differential pulse voltammetry using 663 VA Stand instrument (Metrohm, Switzerland).

Hanging mercury drop electrode was used as working electrode, while Ag/AgCl/3M KCl as reference electrode, and platinum as auxiliary electrode. Measurements were conducted under pure argon (99.999 %) saturated with water for 10 s. Brdicka supporting electrolyte containing 1 mM $[Co(NH_3)_6]Cl_3$ and 1 M ammonia buffer (NH_3(*aq*) and NH_4Cl, pH = 9.6) and acetate buffer (0.2 M CH_3COONa + CH_3COOH, pH 5) were used for all AdT-DPV analyses. The measurement parameters were set as follows: initial potential −0.50 V, end potential −1.75 V, adsorption time 60 s; modulation time 0.03 s; interval time 0.8 s; step potential 3.5 mV; modulation amplitude 25 mV. Data were processed by VA Database 2.2 by Metrohm.

4.9. Atomic absorption spectrometry (AAS)

Element content in samples was analyzed by using a 280Z Agilent Technologies atomic absorption spectrometer (Agilent, USA) with electro-thermal atomization. As radiation source, the arsenic ultrasensitive hollow cathode lamp (lamp current 10 mA) was applied. The spectrometer was operated at a resonance of 193.7 nm with a spectral bandwidth of 0.5 nm.

4.10. CHNS elemental analysis

Organic elements content analysis of samples was performed by CHNS organic elemental analyzer Flash 2000 (Thermo-Fisher Scientific Inc., Waltham, MA, USA). 2 mg of dried sample were added in soft tin containers and burned on 950 ºC under helium flow. Contents of elements were detected by thermal conductive detector (TCD). Data were processed by software Eager 300.

4.11. Particle size distribution

The size distributions and zeta potential of samples were analyzed by quasi-elastic laser light scattering with a Malvern Zetasizer (NANO-ZS, Malvern Instruments Ltd., Worcestershire, United Kingdom). Measuring was conducted in a polystyrene latex cell and measured at a detector angle of 173, a wavelength of 633 nm, temperature of 25 C, refractive index of 0.30, and a real refractive index of 2.2.

4.12. Optical microscopy

Optical behaviors of samples were observed by inverted microscope system Olympus UIS2 series (Tokyo, Japan). The 100 time increasing magnification was conducted by

objective CPlanFLN 10× (N.A. 0.3, W.D. 9.5 mm, F.N. 22) and for 400 time magnification increasing objective LUCPlanFLN 40× (N.A. 0.6, W.D. 2.7 – 4 mm, F.N. 22) was used. The images were captured by Camera Olympus DP73 and processed by Stream Basic 1.7 Software; the resolutionof the images was 1600 × 1200 pixels, ISO 200.

4.13. Prostate cell line cultivation

PNT1A human cell prostatic line and the PC3 human prostate cancer cell line used for testing were purchased from Health Protection Agency Culture Collections (Salisbury, UK). PNT1A cells were cultured in RPMI-1640 with 10% FBS. PC3 cells were cultured in Ham's F12 medium with 7% FBS. Cells containing media treated with penicillin (100 U/mL) and streptomycin (0.1 mg/mL) where stored at 37°C ina humidified incubator (Sanyo, Moriguchi, Japan) with 5% CO_2. Casy model TT system was used for cell counting (Roche Applied Science, Penzberg, Germany). 100-µL cell suspension mixed with 10 mL of Casy Tone was used as viable cell standard. All subsequent measurements were performed with a 100 µL cell suspension diluted 100×.

4.14. Determination of cytotoxicity by MTT and XTT assay

For experiment purposes, 5000 cells suspension was added to each well of microtiter plates (E-plates 16). Cell growth was maintained and incubated for 2 days at 37°C in both cultures. Medium containing tested samples was added to both cultures with previous discharging incubation medium. After 24 hours of incubation, the medium containing samples was replaced with fresh medium three times per day. Additionally, the medium was replacedwith 200 µL of fresh medium containing 50 µL of 3-(4,5-dimethylthiazol-2-yl)-2,5-diphenyltetrazolium bromide (MTT [5 $mgmL^{-1}$ in PBS]) and incubated for 4 h at 37°C. To dissolve the MTT-formazan crystals, the medium was replaced with 200 µL of 99.9 % dimethylsulfoxide, following by addition of 25 µL of glycine buffer to each well. The absorbance was measured at 570 nm (VersaMax microplate reader, Molecular Devices, Sunnyvale, CA, USA).

In the case of XTT, assay procedure is similar to MTT assay with the following difference: XTT [(2,3-bis-(2-methoxy-4-nitro-5-sulfophenyl)-2H-tetrazolium-5-carboxanilide)] and phenazine methosulfate were added directly to each well and the mixture was incubated for 2 h at 37 °C. In the case of XTT assay, the absorbance was measured at 450 nm (Infinite 200PRO, Tecan, Männedorf, Switzerland).

4.15. Hemolysis analysis

The red blood cells (RBCs) suspension obtained according to Evans *et al.* [192], were washed three time by iso-osmotic PBS (pH 7.4). RBCs were diluted by iso-osmotic PBS (500 µL) and stored at 4 °C for not more than 24 h. 500 µL of erythrocyte suspension were mixed with samples at various doses with following incubation for 1h at 37°C. The haemolysis expression was determined by measuring the absorbance of the supernatant at 540 nm after centrifugation and calculated according the following equation: $\%hemolysis = [(A_t - A_c)/A_{100\%} - A_c)] \times 100$, where A_t is the absorbance of the supernatant from samples incubated with the samples; A_c is the absorbance of the supernatant from negative control (PBS, pH 7.4); $A_{100\%}$ is the absorbance of the supernatant of positive control (0.1% Triton X-100), which causes complete lysis of RBCs.

4.16. Quantitative RT-PCR

Gene expression analysis has been conducted by using quantitative RT-PCR Mastercycler pro S instrument (Eppendorf, Hamburg, Germany). The design primers set were used to amplify the coding region of different genes. 2 µL of RNA was applied for each of 20 µL reaction. The final concentration for each primer was set at 2 µM. The PCR cycle used in analysis consists of a reverse transcription at 44 °C for 30 min, initial denaturation at 94 °C for 2 min; 35 cycles of denaturation at 94 °C for 15 s, annealing-extension at 60 °C for 1 min; with the final extension at 68 °C for 7 min. To confirm the specificity of the PCR amplification, procedure was controlled by using melting curves and 1% agarose gel electrophoresis. The results obtained for the different treatments were standardized to the 18S ribosomal RNA (GenBank Accession X03205.1). The relative levels of transcription were calculated by using the $2-\Delta\Delta CT$ method.

4.17. SDS-PAGE and Western blotting

Isolation of proteins was conducted using the following steps; each 200 mL culture plate was homogenized with 2 mL of lysis buffer (150 mM NaCl, 1.0% Triton X-100, 50 mM Tris, pH 8.0, and10 µL protease inhibitor cocktail (Sigma-Aldrich, USA)). Incubation of culture samples was done with occasional shaking for 30 min in ice, and

then centrifuged at 20000× g for 10 min to remove the debris. Samples were stored at −80 °C until analysis. The SDS-PAGE was done by electrophoresis Mini Protean Tetra apparatus with gel dimension of 8.3 × 7.3 cm (Bio-Rad, USA). First 12.5 % running gel, then 5 % stacking gel was prepared. The gels were prepared from 30 % (w/v) acrylamide stock solution with 1 % (w/v) bisacrylamide. The polymerization of the running or stacking gels was carried out at room temperature for 45 min. The samples were loaded in 5 μL Sample Buffer (20 % glycerol, 0.1 % bromophenol blue, 50 mM Tris, 2 % SDS) in 2:1 ratio. For determination of the molecular mass, the protein ladder P7703S from New England Biolabs (Ipswich, MA, USA) was used. The electrophoresis was run at 200 V for 33 min at 20 °C (Power Basic, Bio-Rad USA) in Tris-Glycine running buffer (0.025 M Trizma-base, 0.19 M glycine and 3.5 mM SDS, pH = 8.3). Western blotting was done by conducting next steps: activation of PVDF membranes for 30 s with methanol following incubated with blotting paper, and gel for 5 min in blotting buffer (25 mM Tris-base, 150 mM glycine and 10 % (v/v) methanol). Blotting sandwich included 3 layers of soaked blotting paper, PVDF membrane, gel, and another 3 layers of soaked blotting paper. Transfer was performed for 1 hour at voltage of 0.9 mA per 1 cm2 of the membrane. Blotting process was as follows: blocking for 30 min (1 % dried skimmed milk in PBS (137 mM NaCl, 2.7 mM KCl, 1.4 mM NaH_2PO_4, a 4.3 mM Na_2HPO_4, pH 7.4)), followed by primary antibody (diluted 1:200 in solution of 1 mg/mL BSA in PBS), followed by washing 3 × PBS-T (0.05 % v/v Tween-20 in PBS) for 5 min. Then secondary antibody (diluted 1:1000 in solution of 1 mg/mL BSA in PBS) followed by washing 3 × PBS-T for 5 min. Solution for calorimetric detection for 1 membrane (5 mL of 0.01 M acetate buffer pH 5.4, 5 μL of hydrogen peroxide and 50 μL of 3-Amino-9-ethyl-carbazole in DMF). Blot was then washed by water, dried and scanned.

4.18. Microarray analyses

The cDNA was isolated following the manufacturer's protocol: 1 μg of total DNase-treated RNA in a 20 μL reaction containing 200 units of Super-Script II Reverse Transcriptase (Invitrogen, Carlsbad, CA, USA) and 100 ng of random hexamers. Isolated cDNA according manufacturer's instruction was biotinylated on its 3' end using Biotin 3' End DNA labeling kit (Thermo Scientific, Waltham, MA, USA). Microarray was carried out according to Roth *et al.* [193]. For hybridization Human

Cancer 3711 ElectraSense 4×2k array slides were utilized with 1609 DNA probes (Custom Array, Bothell, WA, USA). Briefly, fresh pre-hybridization solution (2 × Hyb solution stock, 6 × saline–sodium phosphate–EDTA (SSPE), 0.05% Tween-20, 20 mM EDTA, nuclease-free water, 5 × Denhardt's solution, 100 $ng \cdot \mu L^{-1}$ salmon sperm DNA, and 0.05% SDS) was prepared. The hybridization chamber was filled with the pre-hybridization solution, and the microarray was loaded onto the rotisserie in the hybridization oven and incubated at the desired hybridization temperature for 30 min with gentle rotation. Hybridization solution containing 10 to 40 $ng \cdot \mu L^{-1}$ labeled targets was prepared and denatured at 95 °C for 3 min and then cooled for 1 min on ice. The hybridization chamber was filled with hybridization solution, and the microarray was loaded onto the rotisserie in the hybridization oven and incubated at 50 °C for 16 h with gentle rotation. The hybridization chamber was rinsed using 6 × SSPETween (SSPET), 3 × SSPET, 0.5 × SSPET, and PBSTween wash solution to remove weakly bound DNA. Subsequently, post-hybridization the CombiMatrix ElectraSense™ Detection Kit was used. The PBSTween wash solution was removed from the hybridization chamber, then the blocking buffer was added to the hybridization chamber and the array was incubated at room temperature for 15 min. The Blocking Buffer was removed, and the Biotin Labeling Solution was added to the hybridization chamber, the array was incubated at room temperature for 30 min, the Biotin Labeling Solution was removed from the hybridization chamber, the hybridization chamber was rinsed using the Biotin Wash Solution. The hybridization chamber was filled, and incubated at room temperature for 5 min (repeated two more times for a total of three washes). The Biotin Wash Solution was retained in the hybridization chamber during preparation of the ElectraSense™ Reader and until electrochemical detection was done. Preparation of the hybridized ElectraSense™ for electrochemical detection was with TMB (3, 3', 5, 5'–tetramethylbenzidene) substrate solution. The ElectraSense™ Reader performed amperometric detection of this current flux for each individual spot through the underlying platinum microelectrode. The resultant data provided direct numeric quantification of the hybridization signals for all spots. Thus, in contrast to fluorescent imaging, image data extraction is not required for the ElectraSense™ detection system.

5. RESULTS AND DISCUSION

Results and Discussion part of this Ph.D. thesis is presented as five publications in scientific journals and supplemented by the comments of the author. For each work author's contribution on the creation of publication is also marked.

5.1. Optimization and detection of cargo interaction with cell penetrating peptide

The next step of the study shows synthesis of peptide by solid phase, using Fmoc strategy, and demonstrates the promising technique for screening and characterization of ideal peptide binding conditions.

5.1.1. Research article I

N. Cernei, Z. Heger, P. Kopel, **V. Milosavljevic**, M. Kominkova, A. Moulick, O. Zitka, L. Trnkova, V. Adam, R. Kizek, Spectroscopic and Electrochemical Characterization of CD4 Binding Site of HIV-1 Exterior Envelope gp120, Int. J. Electrochem. Sci, 9 (2014) 3386-3397.

Participation in the work of the author Vedran Milosavljevic: experimental part 30% and manuscript preparation 20%.

Human immunodeficiency virus (HIV) destroys the human immune system and triggers acquired immune deficiency syndrome (AIDS) with lethal outcome. Chemokine receptor family and interaction of CD4 receptors on the CD4+ T cells plays the main role in HIV-1 cell entry [194]. Cell internalization of HIV-1 is mediated by the glycoproteins viral envelope. Association of glycoprotein (gp120 obtained by proteolysis of gp160 in Golgi apparatus) subunit with the CD4 receptor and the CCR5 co-receptor induce conformational changes in variable loop regions V1/V2 and V3, resulting in HIV-1 and host cell membrane fusion [195-197]. The final cell entry of HIV-1 trough membrane is achieved by releasing gp 41, while the hydrophobic fusion of peptide is extended more towards the host cell membrane [198]. Understandings of HIV-1 cells internalization open possible opportunities for the development of effective drugs against HIV-1. Blocking conservative CD4 binding site on gp120 will lead to limitation of HIV-1 cells internalization.

The aim of this work was synthesis of peptide which will bind the CD4 binding site and block the binding of CD4 receptors. Spectroscopic characterization and electrochemical measurements were carried out, in order to optimize the conditions for rapid and accurate monitoring of various peptide-protein interactions, helpful for development of new potential peptides with antiviral or other effects.

Synthesis of peptide, which will bind to CD4 binding site of gp120, was successfully confirmed by MALDI-TOF MS. Ion exchanging chromatography, electrochemistry and flow injection analysis confirmed that synthetized peptide successfully imitates the CD4 binding site of exterior envelope glycoprotein 120 of HIV-1, responsible for affinity towards CD4 receptor localized on membrane of CD4+ T-cells.

Influence of organic solvent, buffer type and influence of its pH on peptide current response were also determined. Results show that Acetonitrile (ACN) with 3% of TFA has the best response of detector, after new peptide is bound to gp120-CD4 binding site. On the other side, among various buffers used, Britton-Robinson shows the greatest effect on peptide detection. The ideal conditions were found at pH 7 with peak height 44.8 μA and pH 8 with peak height 45.9 μA. Electrochemical analysis confirmed that current response increases relatively slowly, up to reaching the interval of redox potential (800 mV). However, by reaching "inflection point", the current response increases rapidly to high oxidation potential, where maximal detection potential (1100 mV) was achieved as the ideal for peptide analyses (peak height 45.9 μA).

Obtained results show that artificially made peptide is able to block conservative CD4 binding site of gp120 and to exclude the ability of HIV-1 virions to induce the fusion with the host cells. It was found that optimized approach shows great potential for rapid and simple method for detection of peptide-peptide or protein-peptide interactions. Moreover, this can be an important pathway for development of new therapeutic agents.

Int. J. Electrochem. Sci., 9 **(2014)** 3386 - 3397

International Journal of
ELECTROCHEMICAL
SCIENCE
www.electrochemsci.org

Spectroscopic and Electrochemical Characterization of CD4 Binding Site of HIV-1 Exterior Envelope gp120

Natalia Cernei[1,2], *Zbynek Heger*[1], *Pavel Kopel*[1,2], *Vedran Milosavljevic*[1], *Marketa Kominkova*[1], *Amitava Moulick*[2], *Ondrej Zitka*[1,2], *Libuse Trnkova*[2], *Vojtech Adam*[1,2], *Rene Kizek*[1,2*]

[1] Department of Chemistry and Biochemistry, Faculty of Agronomy, Mendel University in Brno, Zemedelska 1, CZ-613 00 Brno, Czech Republic, European Union
[2] Central European Institute of Technology, Brno University of Technology, Technicka 3058/10, CZ-616 00 Brno, Czech Republic, European Union
[*]E-mail: kizek@sci.muni.cz

Received: 18 January 2014 / *Accepted:* 17 March 2014 / *Published:* 14 April 2014

Glycoprotein 120 (gp120) is essential biomolecule for HIV-1 entry into cells as it plays a vital role in attachment to specific cell surface receptors. Exterior envelope glycoprotein 120 contains conservative CD4 binding site in its structure that may be one of target molecules for development of HIV therapeutic agents, able to inhibit the viral entry steps into the host cells. The present study describes the solid-phase, Fmoc-based synthesis of CD4 binding site (SSGGD PEIVMH), and its subsequent spectroscopic characterization, with determined purity over 90 %. Moreover; electrochemical analyses were carried out to optimize the conditions for peptide determination. Using the optimized conditions as Britton-Robinson buffer with pH 8 and 3% addition of acetonitrile (*v*/*v*) as a mobile phase, potential 1100 mV, limit of detection of 0.04 μg.mL^{-1} and limit of quantification of 0.1 μg.mL^{-1} were estimated.

Keywords: CD4 binding loop; gp120; Human immunodeficiency virus-1; Peptide synthesis

1. INTRODUCTION

Human immunodeficiency virus type 1 (HIV-1) is characterized by extensive genetic variability, as a consequence of high replication and mutation rates and frequent recombination [1,2]. HIV destroys the human immune system and causes lethal diseases such as acquired immune deficiency syndrome (AIDS) [3], one of the most devastating disease, attacking humanity today, affecting 65 million people with 11 000 new cases per day [4].

HIV-1 entry depends on the sequential interaction with the CD4 receptors on the $CD4^+$ T cells and the members of the chemokine receptor family [5]. The entry of HIV-1 into cell is mainly mediated by the viral envelope glycoproteins [6], which are synthesized as an ~850- amino acid

precursor. After trimerization and posttranslational modification by carbohydrate, 160-kDa glycoprotein (gp160) is formed. Proteolysis of gp160, processed in the Golgi apparatus, provides a creation of gp120 exterior envelope glycoprotein containing relatively conserved CD4 binding site and gp41 *trans*-membrane envelope glycoprotein [7-9]. In the mature HIV-1 envelope glycoprotein trimer, the three gp120 subunits are noncovalently bound to three membrane-anchored gp41 subunits [10], as it can be seen in Fig. 1.

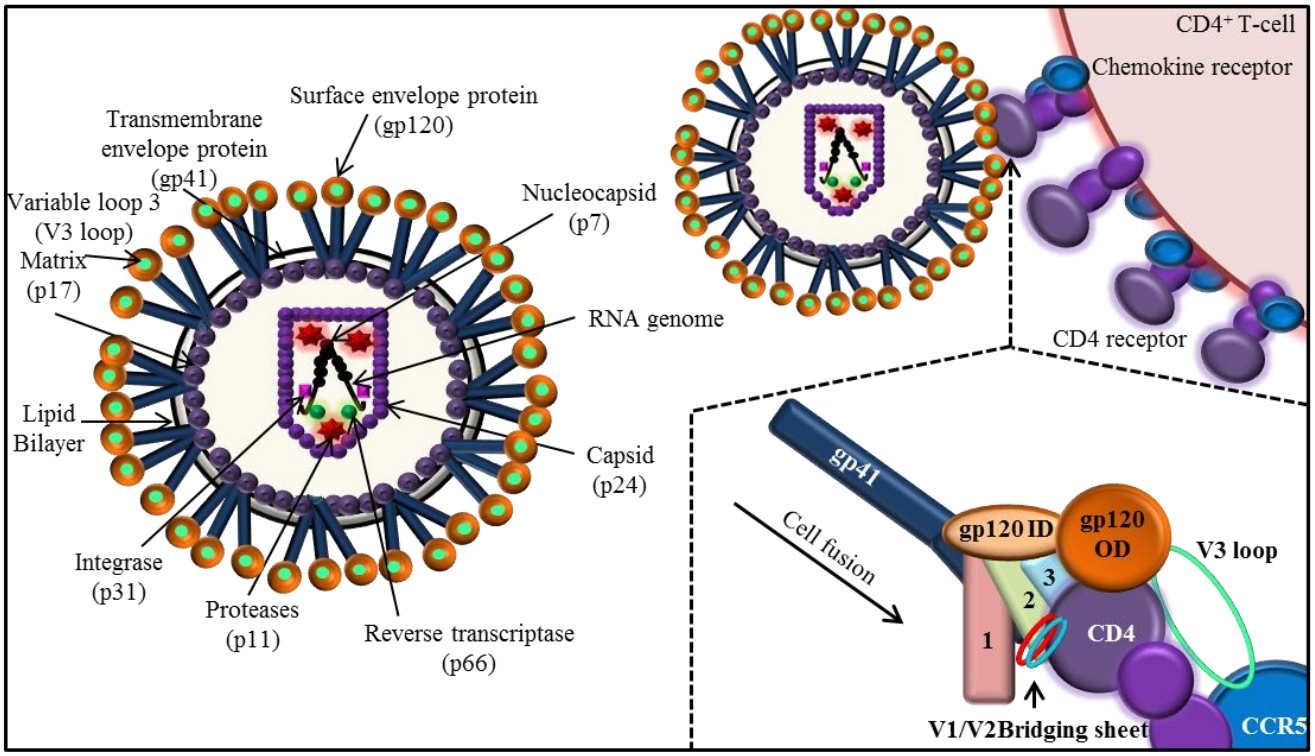

Figure 1. Overall scheme of HIV-1 virion with the expression of interaction between HIV-1 envelope glycoproteins with CD4 receptor binding site. One of the subunit of gp41 is depicted. Binding with CD4 results in the apposition of layer 1 and layer 2, the formation of the bridging sheet and the projection of the V3 loop away from the gp120 core towards coreceptor. This rearrangement of gp120 allows the gp41 ectodomain to undergo additional conformational changes, necessary for HIV-1 entry. The **gp120 OD** stays for outer domain of glycoprotein 120, **gp120 ID** stays for inner domain of glycoprotein 120, **1**; **2**; **3** stays for loops that form three topological layers and **CCR5** stays for coreceptor (chemokine receptor).

For entry of HIV-1 into a host cell, the gp120 subunit associates with the CD4 receptor and the CCR5 coreceptor, and this induces series of conformational changes culminating in virus and host cell membrane fusion. Most primary HIV-1 strains use the chemokine receptor CCR5 as coreceptor in conjunction with CD4 for virus entry. However, some strains has evolved to use related receptors [11]. Binding of gp120 to CD4 causes conformational changes observable in variable loop regions V1/V2 and V3, causing the V3 loop to evaginate, thus becoming exposed to the co-receptors [12], which is shown in Fig. 1. The precise mechanisms of interaction between V1/V2, V3 and chemokine receptors are not well understood [13]. The final step of viral entry, fusion of the viral

components with target membrane, is achieved by gp 41 [14,15]. After binding of gp120 to CD4 and coreceptors, conformational changes occur, leading to gp41 unfolding and the hydrophobic fusion peptide sequence extends towards the host cell membrane [16]. The insertion of the peptide leads to fold into a hairpin-like structure, believed to be responsible for the fusion of the HIV to the host cell [17].

Due to the nature of fusion, there are several possible targets for the development of drugs with synergistic effects on inhibition of viral entry steps, at which the interference can be attempted. Generally, these targets may affect viral entry by the inhibition of CD4 binding due to a blocking of conservative CD4 binding site of gp120. Hence, glycoprotein cannot interact with receptors and coreceptors and process of conformational changes, whereas the triggering the fusion is stopped.

Therefore, the aim of this study was a synthesis of CD4 binding site and its subsequent spectroscopic characterization. Moreover, electrochemical measurements were carried out to optimize the conditions for analyses serving for rapid and accurate monitoring of various peptide-peptide interactions helpful for development of new potential peptides with antiviral or other effects.

2. EXPERIMENTAL PART

2.1. Chemicals and pH measurement

Working solutions like buffers and standard solutions were prepared daily by diluting the stock solutions. Standards and other chemicals were purchased from Sigma-Aldrich (St. Louis, MO, USA) meets the specification of American Chemical Society (ACS), unless noted otherwise. Methyl cellosolve as well as tin chloride were purchased from Ingos (Prague, Czech Republic). Deionised water underwent demineralization by reverse osmosis using the instruments Aqua Osmotic 02 (Aqua Osmotic, Tisnov, Czech Republic) and then it was subsequently purified using Millipore RG (Millipore Corp., USA, 18 MΩ) – MiliQ water.

2.2. Synthesis of CD4 binding loop of gp120

Peptide (SSGGD PEIVMH) with molecular mass of 1908 was prepared using Liberty Blue peptide synthesizer (CEM, Matthews, NC, USA) by standard f-moc solid-phase peptide synthesis. Fourfold excess of f-moc amino acid was used with respect to the resin. As the first step 167 mg of rink amide was swelled in 10 mL of N,N-dimethylformamide (DMF) for 1 hour. For preparation of activator 9.48 g of N,N,N′,N′-tetramethyl-O-(1H-benzotriazol-1-yl)uronium hexafluorophosphate (HBTU) was dissolved in 50 mL of DMF. As an activator base 17.4 mL of N,N-diisopropylethylamine (DIEA) was mixed with 32.6 mL of DMF. Deblocking of f-moc protecting groups was carried out using 20% piperidine (*v/v*) in 80% DMF (*v/v*). For each amino acid, microwave deprotection was performed for 2 minutes at 80 ºC and 15 PSI. For each amino acid, microwave coupling was carried out for 5 minutes at 89 ºC, 15 PSI and 150 W (except of coupling of histidine, where 50 ºC was applied). Entire synthesis was carried out for 1 hour and synthesized peptides, attached with rink

amide, were taken out from reaction vessel, mixed with 10 mL of dichloromethane and replaced into a vacuum cleaner tube used for removal of the solvent and other undesired chemicals. The cleavage of groups protecting the side chains was performed by treatment of peptide resin with 95% trifluoroacetic acid (TFA) (*v/v*), 2.5% H_2O (*v/v*), and 2.5% triisopropylsilane (*v/v*) for 30 minutes in Discovery microwave (CEM, Matthews, NC, USA) at 38 ºC. Further, into solution of peptide with cleavage cocktail, diethylether used for peptide precipitation was added. Resulting solution was centrifuged (6000 rpm, 4 min, 0 ºC) and the supernatant was discarded. Peptide synthesized in this way was prepared for subsequent experiments.

2.3 UV/Vis Spectrophotometry

Absorption spectra were recorded within the range from 220 to 700 nm on spectrophotometer SPECORD 210 (Analytik Jena, Jena, Germany) using quartz cuvettes (1 cm, Hellma, Essex, UK). Cuvette space was tempered by a thermostat Julabo (Labortechnik, Wasserburg, Germany) to temperature 25 °C. After a measurement, cuvettes were rinsed with deionised water and dried with nitrogen.

2.4 Acidic hydrolysis

1 mg of peptide was mixed with 0.5 mL of 6 M HCl and solution was subsequently subjected to digestion in a microwave reactor Anton Paar (Anton Paar GmbH, Graz, Austria) using the following conditions: power 80, ramp 15 minutes, hold 90 minutes, maximum 120 °C and maximum pressure 25 bar. Further, the hydrolysed sample was diluted with the dilution buffer composed of 5 $mL.L^{-1}$ of thiodiglycol, 14 $g.L^{-1}$ of citric acid, 11.5 $g.mL^{-1}$ of sodium chloride and centrifuged using Microcentrifuge 5417R (Eppendorf AG, Hamburg, Germany) using 25,000 g at 4 °C for 10 min.

2.5 Ion-exchange chromatography

For identification of peptide and its amino acid composition, the ion-exchange liquid chromatography with post column derivatization by ninhydrin and the absorbance detector in the VIS range set to 440 nm was employed. Glass column, tempered to 60 °C with inner diameter of 3.7 mm and 350 mm length, was filled manually with strong cation exchanger in sodium cycle LG ANB with approximately 12 μm particles and 8% porosity. Experimental conditions were applied according to our preliminary study [18].

2.6 Matrix-assisted laser desorption/ionization-time of flight mass spectrometry

Confirmation of successful peptide synthesis was performed on a MALDI-TOF/TOF mass spectrometer Bruker ultrafleXtreme (Bruker Daltonik GmbH, Germany) equipped with a laser operating at wavelength of 355 nm with an accelerating voltage of 25 kV, cooled with nitrogen and

with a maximum energy of 43.2 μJ. The matrix used in the MALDI method was a 2,5-dihydroxybenzoic acid (Sigma-Aldrich). The saturated matrix solution was prepared in 50% methanol (*v*/*v*) and 0.1% trifluoroacetic acid (*v*/*v*). Mixture was vortexed and ultrasonicated using Bandelin 152 Sonorex Digital 10P ultrasonic bath (Bandelin electronic GmbH, Germany) for 2 minutes at 50 % intensity at room temperature. A dried-droplet method was used for sample preparation. Briefly, the sample solution was mixed with matrix solution in volume ratio 1:1. After the obtaining a homogeneous solution, 2 μL of mixture was applied on the target plate and dried under atmospheric pressure at room temperature. The mass spectra were acquired by averaging 2000 subspectra from a total of 2000 shots of the laser. Laser power was set 5-10 % above the threshold.

2.7 Flow injection analysis with electrochemical detection

Flow injection analysis with electrochemical detection (FIA-ED) system consisted of two chromatographic pumps Model 582 ESA (ESA Inc., Chelmsford, USA) with working range 0.001 - 9.999 $mL.min^{-1}$ and CoulArray electrochemical detector (Model 5600A, ESA, USA). Detector consisted of flow analytical chamber (Model 6210, ESA, USA). The chamber contains four analytical cells. One analytical cell contains two referent (hydrogen-palladium), and two counter electrodes and one porous graphite working electrode. Electrochemical detector is situated in control module, which is thermostated. Sample (20 μL) was injected by manual valve (Rheodyne, Oak Harbor, WA, USA). Flow rate of mobile phase was 1 $mL.min^{-1}$.

2.8 Descriptive statistics

Mathematical analysis of the data and their graphical interpretation were realized by Microsoft Excel®, Microsoft Word® and Microsoft PowerPoint®. Results are expressed as mean ± standard deviation (S.D.) unless noted otherwise. The detection limits (3 signal/noise, S/N) were calculated according to Long and Winefordner [19], whereas N was expressed as standard deviation of noise determined in the signal domain unless stated otherwise.

3. RESULTS AND DISCUSSION

HIV-1 infection is characterized by rapid and extensive $CD4^+$ T-cells depletion and immunodeficiency leading to the decreased immune response and to infection facilitating viral persistence, and increased viral loads and transmission rates [20,21]. Based upon this information, CD4 binding site of gp120 may exhibit large potential in the development of therapeutic agents able to block this structure and thus prevent the HIV virion fusion with host cell.

3.1 Synthesis of CD4 binding site-like peptide

In this study, firstly, the synthesis of peptide, comprising Ser-Ser-Gly-Gly-Asp Pro-Glu-Ile-Val-Met-His (SSGGD PEIVMH, calculated mass 1098.13 Da), was carried out. Peptide synthesis was

performed on a solid-phase, employing 9-Fluorenylmethoxycarbonyl (Fmoc) for side chains protection [22]. Resulting peptide imitates the CD4 binding site of exterior envelope glycoprotein 120 of HIV-1 responsible for affinity towards CD4 receptor localized on membrane of $CD4^+$ T-cells. Success rate of CD4 binding site peptide synthesis can be seen in Fig. 2A, where record obtained from Liberty blue synthesizer is shown. Two columns for each amino acid and resin, used in synthesis represent the initial absorbance (left column) and absorbance after synthesis (right column). Low values in the right column point at successful synthesis due to a low amount of amino acid remained in reactor (Fig. 2A). This implies that overwhelming majority of amino acid was correctly linked into peptide chain on the resin.

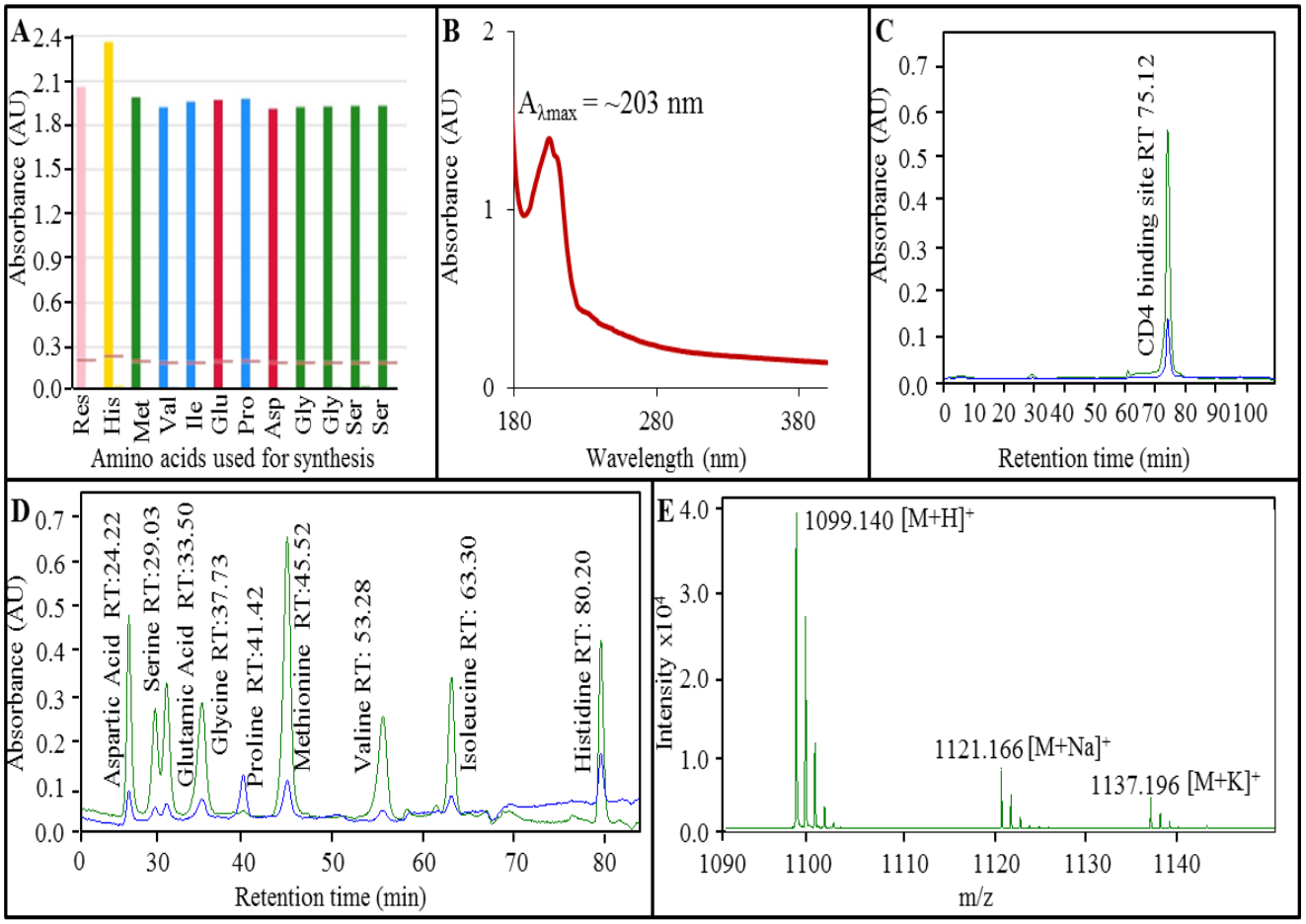

Figure 2. (**A**) Record obtained from program Liberty Blue, confirming successful synthesis of CD4 binding site (SSGGD PEIVMH), contained in region 366 – 376 of gp120 of HIV-1. (**B**) Absorption spectra of synthesized CD4 binding site with absorption maximum at 203 nm (c = 1 $mg.mL^{-1}$). (**C**) Typical chromatogram obtained on ion-exchange chromatography (IEC) showing retention time (75.12 min) of CD4 binding site peptide. (**D**) Expression of amino acid content in CD4 binding site after hydrolysis in microwave reactor MW 3000. (**E**) MALDI-TOF/TOF mass spectra of CD4 binding site peptide with calculated mass of 1098.13 Da. DHB was used as a matrix. Measurements were carried out in reflector positive mode, with laser power of 70 %. One spectrum is made as an average from 2500 subspectra. **M** stays for molecule of analyte; **H** stays for atom of hydrogen.

3.2 UV/Vis spectrophotometry

To determine the optical properties of synthesized compound, UV/Vis spectrophotometry was employed. As it can be seen in Fig. 2B, CD4 binding site-like peptide shows its absorption maxima at ~203 nm. The absorbance of radiation by intrinsic chromophores may be useful in determination of peptides/proteins, particularly at 280 nm ($A_{\lambda max}$ = 280 nm), offering high specifity, arising strictly from trypthophan (W) and/or tyrosine (Y) residues (and from a small extent from disulphide bonds if present) [23]. On the other hand, optical properties of peptides/protein, containing no W and/or Y in their structure arising primarily from absorbance of peptide backbone and peptide bond [24]. UV/Vis spectrophotometry may be easily employed to obtain the basic information about amino acid composition.

3.3 Ion-exchange chromatography

As the next step, entire CD4 binding site was dissolved in ACS water in concentration of 1 $mg.mL^{-1}$ and directly analysed using ion-exchange chromatography (IEC) using Vis detection after ninhydrin derivatization to reveal the possible presence of undesired fragments ocurred during synthesis (Fig. 2C). Although the most of peptide separations in the past 30 years have employed reverse-phase (RP) chromatography, in the past 10 years, cation exchange chromatography of peptides has developed into a significant complement to RP [25]. CD4 binding loop with pI calculated at 4.47 and net charge at 1.7 was identified at retention time of 75.12 minutes. Importantly, only very low amount of undesired fragments that belong to few unsuccessful steps in synthesis was determined, and recovery of peptide synthesis was therefore calculated up to 93.8 %. IEC was further employed for determination of amino acid composition of peptide after acidic hydrolysis using 6 M hydrochloric acid causing a destruction of the protein/peptide chain to amino acids that made up the initial molecule. As it can be seen in Fig. 2D, where entire chromatogram of IEC analysis is shown, all of amino acids (Asp; Ser; Glu; Gly; Pro; Met; Val; Ile; His) were determined in high amounts in their typical retention times. Hence, undesired fragments, observed using IEC analysis of whole peptide, are formed by amino acids used for CD4 binding site synthesis, not by other amino acids that may occur as the unwanted residues from previous syntheses or contamination. Therefore, synthesis process is not able to accomplish binding of all amino acid molecules used in synthesis and some of them form residual artefacts.

3.4 Matrix-assisted laser desorption/ionization time of flight mass spectrometry

Further, Matrix-assisted laser desorption/ionization time of flight mass spectrometry (MALDI-TOF MS) was utilized for characterization of CD4 binding site-like peptide synthesized by us (Fig. 2E). Peptide mass weight was calculated at 1098.13 Da. Using following analysis conditions: 2,5-dihydroxybenzoic acid (DHB) as the matrix, reflector positive mode with laser power of 70 %, signal at 1099.140 Da was observed and attributed to a quasimolecular ion $[M+H]^+$ formed from molecule of

peptide and proton resulted from charging through DHB matrix. Similarly, quasimolecular $[M+Na]^+$ with mass-to-charge ratio of 1121.166; and $[M+K]^+$ was also observed.

3.5 Influence of organic solvent on CD4 binding site electrochemical measurements

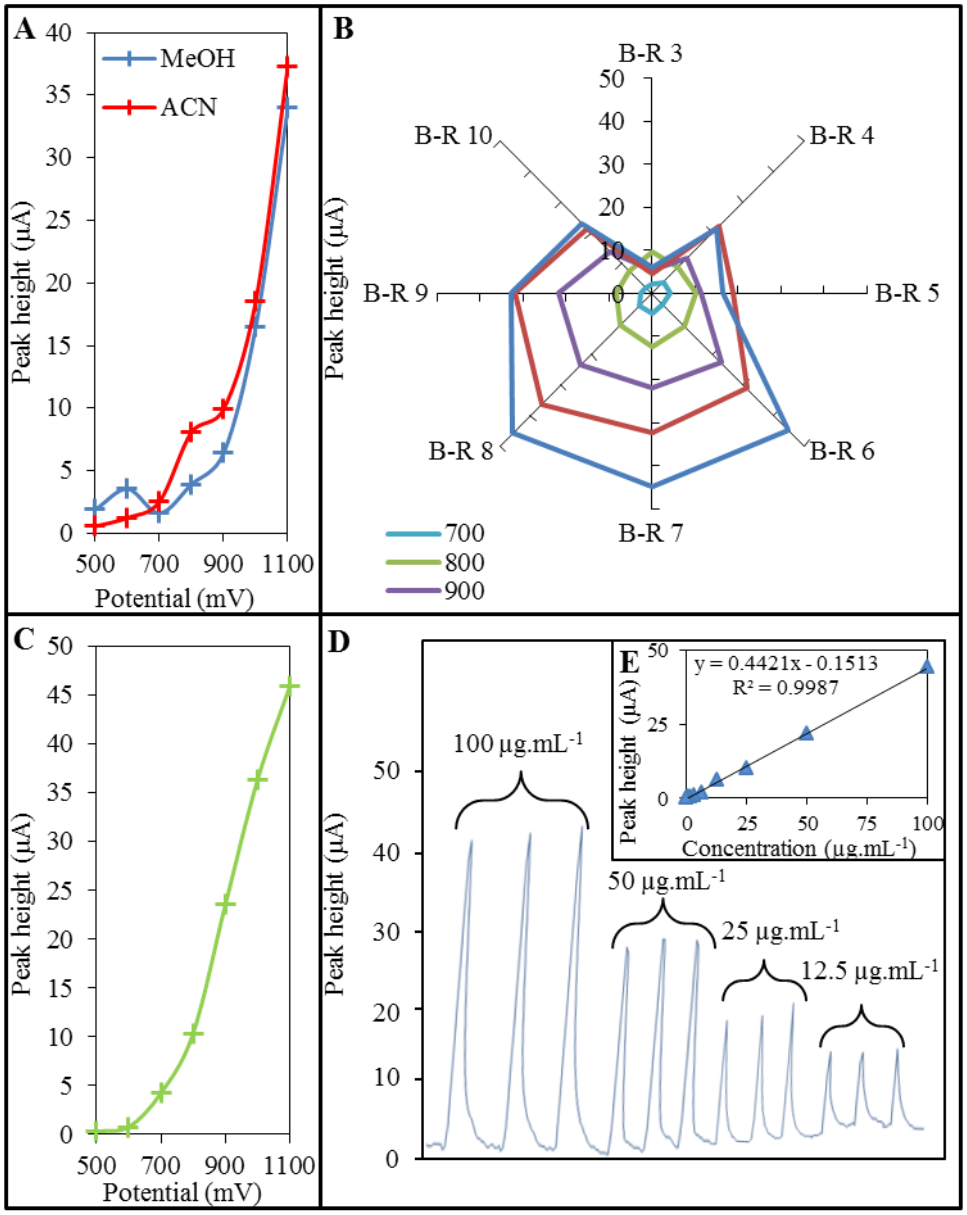

Figure 3. Optimization of Electrochemical detection of CD4 binding site of gp120 of HIV-1. Applied concentration of CD4 binding site-like peptide for analyses instead of calibration curves was 100 µg.mL^{-1}. (**A**) Expression of influence of addition of organic solvents on amperometric signal of the peptide. MeOH – methanol, ACN – acetonitrile. (**B**) Optimization of potential for detection (500 – 1100 mV) of the peptide, and its behaviour under influence of Britton-Robinson buffer (pH 3 – 10). (**C**) Hydrodynamic voltammogram of CD4 binding site measured under optimized conditions (B-R pH 8, with 3% addition of CAN (*v*/*v*) in potential range 500 – 1100 mV). (**D**) Array record of CD4 binding site calibration curve measured within the range from 12.5 to 100 µg.mL^{-1}. (**E**) Calibration curve measured within range from 12.5 to 100 µg.mL^{-1} using potential of 1100 mV.

After acquisition of basic spectroscopic characteristics, further we continued to the optimization of electrochemical detection of CD4 binding site of gp120. For electrochemical experiment, flow injection analysis (FIA) setup with electrochemical detector containing four analytical cells was employed.

Firstly, electrochemistry was utilized to monitor an effect of organic solvents in mobile phase on electrochemical response of peptide. As it can be seen in Fig. 3A, two organic solvents (MeOH – methanol, and ACN – acetonitrile) were tested in 3% addition into 80 mM trifluoroacetic acid (TFA) with pH 1.5 (*v/v*) used as a mobile phase. Analyses were performed within the potential range of 500 – 1100 mV, and it was shown that ACN supports the analysis at the ideal potential (1100 mV) more than MeOH (peak height of peptide for ACN 37.33 μA and for MeOH 33.99 μA). Therefore, 3% addition of acetonitrile to TFA (*v/v*) was chosen as beneficial to increase sensitivity in subsequent analyses.

3.6 Optimization of pH of mobile phase

Although TFA with 3% addition of ACN showed relatively good detector response of CD4 binding site-like peptide, we decided to test various pH buffers due to their ability to enhance the sensitivity of detection. Firstly, we tested various buffers as phosphate buffer, borate buffer, acetate buffer and Britton-Robinson (B-R) buffer, whereas B-R buffer was shown to have the greatest effect on peptide detection (data not shown). Hence, for further optimization experiments we utilized merely B-R buffer in pH range of 3 – 10 (3% addition of ACN (*v/v*)) and potentials within range between 700 – 1100 mV (Fig. 3B). As it is obvious from Fig. 3B, low pH maintained by B-R buffer with pH 3 was shown to influence the detection of peptide in sense of sensitivity. Ideal potential was determined at 800 mV showing peptide peak with height of 9.7 μA. After application of B-R buffer with pH 4 it was shown that ideal potential shifted to 1000 mV (peak height 21.8 μA) and the same phenomenon was observed at B-R buffer with pH 5 (peak height 16.5 μA). Interestingly, at pH 6 a significant change in electrochemical behaviour of CD4 binding site occurred. Ideal potential was determined at 1100 mV (peak height 44.7 μA) and the same trend was observed at all of B-R buffer pHs utilized (pH 7 – peak height 44.8 μA, pH 8 – peak height 45.9 μA). After application of B-R buffer, maintaining pH 9, rapid decrease of difference of peptide signal obtained when using detection potential 1000 mV (peak height 31.1 μA) and 1100 mV (peak height 32.7 μA) was observed. The same phenomenon was observed at B-R buffer of pH 10, where signal at 1100 mV was decreased to 6.0 μA (Fig. 3B). Based upon obtained data, it is obvious that B-R buffer with pH 8 shows the most beneficial effect on CD4 binding site detection, and therefore we decided to use it as mobile phase for subsequent analyses.

3.7 CD4 binding site-like peptide hydrodynamic voltammogram

Using the ideal conditions found from previous experiments (B-R buffer with pH 8, with 3% addition of ACN (*v/v*)) we carried out further analysis to obtain hydrodynamic voltammogram (HDV) of CD4 binding site. In ideal manner, the working electrode should be immersed to the supporting electrolyte and should give response only to the analysed substance in a thermodynamically defined,

potential-dependent fashion [26]. In our case hydrodynamic voltammetry was carried out within the potential range from 500 to 1100 mV (Fig. 3C). It clearly follows from the results obtained that the current response increases relatively slowly up to reaching interval of redox potential (800 mV). After reaching this "inflection point", the current response increases rapidly to high oxidation potential, where maximal detection potential (1100 mV) was achieved as the ideal for peptide analyses (peak height 45.9 μA).

3.8 Analysis of CD4 binding site-like peptide in ideal conditions

After we optimized the electrochemical analysis of the peptide fragment, calibration curve was measured within the range from 12.5 to 100 $\mu g.mL^{-1}$. The array record obtained from calibration curve measurements is shown in Fig. 3D. From these data we constructed the calibration curve, which is shown in Fig. 3E. Under concentrations in above mentioned range, linear dependence of CD4 binding site-like peptide signal on its applied concentration ($y = 0.4421x - 0.1513$, $R^2 = 0.9987$) was obtained. Using the optimal conditions, we were able to estimate the detection limit (3 S/N) of the peptide as 0.04 $\mu g.mL^{-1}$. Other analytical parameters are shown in Tab. 1. Limit of quantification (10 S/N) was estimated as 0.1 $\mu g.mL^{-1}$.

Table 1. Parameters of electrochemical analysis of CD4 binding loop of gp120, where [1] stays for molecular mass, [2] for regression coefficient, [3] for limit of detection (3 S/N), [4] for limit of quantification (10 S/N) and [5] for relative standard deviation for injection of 20 μL.

Compound	Mr[1]	Regression equation	Linear dynamic range ($\mu g.mL^{-1}$)	R^2	LOD[3] ($\mu g.mL^{-1}$)	LOQ[4] ($\mu g.mL^{-1}$)	RSD (%)
CD binding loop	1098.13	$y = 0.4421x - 0.1513$	0.8 – 100.0	0.9987	0.04	0.1	2.2

4. CONCLUSION

In our study, we carried out the synthesis of peptide imitating the CD4 binding site by its amino acid sequence. Using spectroscopic methods we carried out basic characterization of substance, resulted from synthesis and moreover; we tested its purity that was established more than 90 %. For subsequent analyses, electrochemical measurement was employed to obtain information about the ideal conditions for CD4 binding site behaviour. Influence of organic solvent, type of buffer and influence of its pH on peptide current response were determined. Furthermore, the ideal detection potential was identified to provide complex information about CD4 binding site electrochemical properties. Optimized approach in this manner may serve as a tool for rapid and cheap method able to

determinate the peptide-peptide or protein-peptide interactions, which may be important for development of new therapeutic agents, able to block conservative CD4 binding site of gp120, and thus inhibit the ability of HIV-1 virions to form fusion with the host cells.

ACKNOWLEDGEMENTS
The authors acknowledge to NanoBioMetalNet CZ.1.07/2.4.00/31.0023 for financial support. Moreover, the authors wish to express their thanks to Lukas Melichar for perfect technical assistance.

CONFLICT OF INTEREST:
The authors have declared no conflict of interest.

References

1. J. Hemelaar, E. Gouws, P. D. Ghys and S. Osmanov, *Aids*, 25 (2011) 679.
2. D. L. Robertson, J. P. Anderson, J. A. Bradac, J. K. Carr, B. Foley, R. K. Funkhouser, F. Gao, B. H. Hahn, M. L. Kalish, C. Kuiken, G. H. Learn, T. Leitner, F. McCutchan, S. Osmanov, M. Peeters, D. Pieniazek, M. Salminen, P. M. Sharp, S. Wolinsky and B. Korber, *Science*, 288 (2000) 55.
3. D. A. Cooper, P. Maclean, R. Finlayson, H. M. Michelmore, J. Gold, B. Donovan, T. G. Barnes, P. Brooke and R. Penny, *Lancet*, 1 (1985) 537.
4. A. K. Rizos, I. Tsikalas, D. Morikis, P. Galanakis, G. A. Spyroulias and E. Krambovitis, *J. Non-Cryst. Solids*, 352 (2006) 4451.
5. R. Wyatt, P. D. Kwong, E. Desjardins, R. W. Sweet, J. Robinson, W. A. Hendrickson and J. G. Sodroski, *Nature*, 393 (1998) 705.
6. R. Wyatt and J. Sodroski, *Science*, 280 (1998) 1884.
7. B. S. Stein and E. G. Engleman, *J. Biol. Chem.*, 265 (1990) 2640.
8. R. L. Willey, J. S. Bonifacino, B. J. Potts, M. A. Martin and R. D. Klausner, *Proc. Natl. Acad. Sci. U. S. A.*, 85 (1988) 9580.
9. R. L. Dewar, M. B. Vasudevachari, V. Natarajan and N. P. Salzman, *J. Virol.*, 63 (1989) 2452.
10. E. Helseth, U. Olshevsky, C. Furman and J. Sodroski, *J. Virol.*, 65 (1991) 2119.
11. V. Sundaravaradan, S. R. Das, R. Ramakrishnan, S. Sehgal, S. Gopalan, N. Ahmad and S. Jameel, *Virology Journal*, 4 (2007).
12. I. Douagi, M. N. E. Forsell, C. Sundling, S. O'Dell, Y. Feng, P. Dosenovic, Y. X. Li, R. Seder, K. Lore, J. R. Mascola, R. T. Wyatt and G. B. K. Hedestam, *J. Virol.*, 84 (2010) 1683.
13. H. B. Bernstein, S. P. Tucker, S. R. Kar, S. A. McPherson, D. T. McPherson, J. W. Dubay, J. Lebowitz, R. W. Compans and E. Hunter, *J. Virol.*, 69 (1995) 2745.
14. A. Zafiropoulos, S. Baritaki, Z. Vlata, D. A. Spandidos and E. Krambovitis, *Biochem. Biophys. Res. Commun.*, 284 (2001) 875.
15. W. Weissenhorn, A. Dessen, S. C. Harrison, J. J. Skehel and D. C. Wiley, *Nature*, 387 (1997) 426.
16. C. T. Wild, D. C. Shugars, T. K. Greenwell, C. B. McDanal and T. J. Matthews, *Proc. Natl. Acad. Sci. U. S. A.*, 91 (1994) 9770.
17. M. Lu, S. C. Blacklow and P. S. Kim, *Nat. Struct. Biol.*, 2 (1995) 1075.
18. O. Zitka, N. Cernei, Z. Heger, M. Matousek, P. Kopel, J. Kynicky, M. Masarik, R. Kizek and V. Adam, *Electrophoresis*, 34 (2013) 2639.
19. G. L. Long and J. D. Winefordner, *Anal. Chem.*, 55 (1983) 712.
20. M. D. Hazenberg, D. Hamann, H. Schuitemaker and F. Miedema, *Nat. Immunol.*, 1 (2000) 285.
21. J. B. Alimonti, T. B. Ball and K. R. Fowke, *J. Gen. Virol.*, 84 (2003) 1649.

22. G. B. Fields and R. L. Noble, *Int. J. Pept. Protein Res.*, 35 (1990) 161.
23. C. N. Pace, F. Vajdos, L. Fee, G. Grimsley and T. Gray, *Protein Sci.*, 4 (1995) 2411.
24. N. J. Anthis and G. M. Clore, *Protein Sci.*, 22 (2013) 851.
25. A. J. Alpert, K. Petritis, L. Kangas, R. D. Smith, K. Mechtler, G. Mitulovic, S. Mohammed and A. J. R. Heck, *Anal. Chem.*, 82 (2010) 5253.
26. O. Zitka, M. Kominkova, S. Skalickova, H. Skutkova, I. Provaznik, T. Eckschlager, M. Stiborova, V. Adam, L. Trnkova and R. Kizek, *Int. J. Electrochem. Sci.*, 7 (2012) 10544.

5.2. Delivery of cargo to cell by cell penetrating peptide

Cell penetrating peptides (CPP) attract great attention due to their abilities for intracellular delivery of a wide range of molecules. In this study, delivery and localization of cargoes conducted by cell penetrating peptides has been demonstrated.

5.2.1. Research article II

V. Milosavljevic, Y. Haddad, M.A.M. Rodrigo, A. Moulick, H. Polanska, D. Hynek, Z. Heger, P. Kopel, V. Adam, The Zinc-Schiff Base-Novicidin Complex as a Potential Prostate Cancer Therapy, PloS one, 11 (2016) e0163983, doi:10.1371/journal. pone.0163983.

Participation in the work of the author Vedran Milosavljevic: experimental part 55% and manuscript preparation 60%.

The male population commonly suffers from prostate carcinoma (PCa). Surgical and radiation therapy presents the standard treatment of PCa in early stage. However, metastatic cells have ability to lose androgen dependency by hormonal ablation therapy, which leads to development of hormone-independent tumor with a very low survival rate [199]. Glandular epithelial cells of the human prostate gland can accumulate a high level of zinc. Zinc is essential element required for variety of cellular activities, such as cell growth, replication, osteogenesis, enzyme, immunity and antioxidant activity. The accumulation of zinc has ability to stop oxidation of citrate in cells by inhibition of mitochondrial aconitase activity [200-202]. Malignant cells rely on low level of zinc to activate the citrate oxidation process and become more energy efficient through the completion of the Krebs cycle [203]. Hypothetically, increasing level of circulating zinc in available form for cellular uptake could be efficacious approach in restoration of zinc pathway in malignant cells and could lead to tumor suppression.

Based on this consideration, we were interested in synthesizing zinc delivery system, which could increase the availability of zinc in PCa cells. Cell penetrating peptides and Schiff bases are strong candidates for transport of zinc ions because they can both interact with metals in coordinated bonding. The mechanism of action for this complex is not yet well understood. This paper is an attempt to investigate the

molecular changes that take place after the delivery of zinc complex system by studying genes involved in zinc stress.

Interactions between cell penetrating peptide with Zn-S Schiff base complex and the complex forming where confirmed by MALDI-TOF MS, FTIR and electrochemistry analysis. Cytotoxicity test done by optical microscope and MTT assay has proven that after 12 and 24 hours of incubation, PC3 cells started to show membrane "blebbing" which was an indicator of the cell death by apoptosis, whereas PNT1A cells remained healthy. Microscopy analysis confirmed localization of peptide in cytosol. Haemolysis activity is found to be about 7.4%, indicating minimal effect of complex on blood circulation.

Molecular change in PC3 and PNT1A cell lines were observed by RT-PCR and microarray analysis. Within 40 min of exposure to Zn-S-NVC, our results show activation of *p53* more than two fold and absence of *SP1* gene activation in PC3 cell line, however in PNT1A cell line no visible change in p53 protein level was observed. However, on protein level, overexpression of SP1 protein in PC3 cell line was found, while there wasn't any in PNT1A cell line. Overexpressing SP1 protein leads to apoptosis through overexpression of p53 protein in PC3 cell line. Our results also show increasing *ZnT-1* expression in both cell lines upon treatment. This was also confirmed by zinc concentration, measured using AAS. It is possible that peptide component of complex is only internalized by PC3 cells, due to their membrane structure differences, while Zn-Schiff base are internalized in both PC3 and PNT1A cells. On the other hand, microarray shows that Zn-S-NVC complex suppressed cell proliferation in PC3 cell line. Results show overexpression of *CASP1, NR4A3* and *DNAJA1* genes in PC3 cell comparing with PNT1A cell line. Overexpressed genes cause a delay in cell proliferation, and as well, they play the main role in controlled cell death.

These data strongly suggest that Zn-S-NVC complex can be used as potent inducer of apoptosis in PCa cells, which has a great potential to be developed into novel anticancer therapy.

PLOS ONE

RESEARCH ARTICLE

The Zinc-Schiff Base-Novicidin Complex as a Potential Prostate Cancer Therapy

Vedran Milosavljevic[1], Yazan Haddad[1], Miguel Angel Merlos Rodrigo[1,2], Amitava Moulick[2], Hana Polanska[3], David Hynek[1,2], Zbynek Heger[1,2], Pavel Kopel[1,2], Vojtech Adam[1,2]*

1 Department of Chemistry and Biochemistry, Mendel University in Brno, Zemedelska 1, CZ-613 00, Brno, Czech Republic, European Union, **2** Central European Institute of Technology, Brno University of Technology, Purkynova 123, CZ-612 00, Brno, Czech Republic, European Union, **3** Department of Physiology, Faculty of Medicine, Masaryk University, Kamenice 5, CZ-625 00, Brno, Czech Republic, European Union

* vojtech.adam@mendelu.cz

Citation: Milosavljevic V, Haddad Y, Merlos Rodrigo MA, Moulick A, Polanska H, Hynek D, et al. (2016) The Zinc-Schiff Base-Novicidin Complex as a Potential Prostate Cancer Therapy. PLoS ONE 11 (10): e0163983. doi:10.1371/journal.pone.0163983

Editor: Aamir Ahmad, University of South Alabama Mitchell Cancer Institute, UNITED STATES

Received: August 7, 2016

Accepted: September 16, 2016

Published: October 11, 2016

Data Availability Statement: All relevant data are within the paper and its Supporting Information files.

Funding: This research was carried out under the project CEITEC 2020 (LQ1601) with financial support from the Ministry of Education, Youth and Sports of the Czech Republic under the National Sustainability Programme II and GACR 16-18917S.

Competing Interests: The authors have declared that no competing interests exist.

Abstract

Prostate cancer cells control energy metabolism by chelating intracellular zinc. Thus, zinc delivery has been a popular therapeutic approach for prostate cancer. Here, we propose the use of the membrane-penetrating peptide Novicidin connected to zinc-Schiff base as a carrier vehicle for the delivery of zinc to prostate cells. Mass spectrometry, electrochemistry and spectrophotometry confirmed the formation/stability of this complex and provided insight regarding the availability of zinc for complex interactions. This delivery system showed minor toxicity in normal PNT1A cells and high potency towards PC3 tumor cells. The complex preferentially penetrated PC3 tumor cells in contrast to confinement to the membranes of PNT1A. Furthermore, zinc uptake was confirmed in both cell lines. Molecular analysis was used to confirm the activation of zinc stress (e.g., *ZnT-1*) and apoptosis (e.g., *CASP-1*). Our results strongly suggest that the zinc-Schiff base-Novicidin complex has great potential as a novel anticancer drug.

Introduction

Prostate cancer (PCa) is the most common malignant tumor in males in the developed world, and its prevalence is steadily increasing [1]. PCa that is detected in early stages can be treated with curative treatment modalities, including surgical and radiation therapy. However, the hormonal ablation of metastatic cells can lead to a loss of androgen dependency of PCa cells and thus, a hormone-independent tumor with a very low survival rate [2].

Glandular epithelial cells of the human prostate gland can accumulate a high level of zinc, two- to five-fold greater than the zinc level found in other tissues [3]. Zinc is an essential element required for a variety of enzymes and cellular activities, such as cell growth [4]. Zinc accumulation inhibits mitochondrial aconitase activity, leading to an inability of cells to oxidize citrate [5]. Prostate cells can accumulate high levels of citrate to chelate intracellular zinc, whereas in other cells, 95% of zinc is mostly bound to macromolecules in the immobile form of

metalloproteins (such as metallothioneins; MTs) and nucleic acids, among others. Prostate cells acquire zinc through transporter proteins (e.g., ZIP1, ZnT-1) that take up zinc from the extracellular fluid or intracellular vesicles [6,7,8]. Malignant cells rely on low zinc levels to activate the citrate oxidation process, thereby becoming more energy efficient through the completion of the Krebs cycle to produce coupled energy (total energy ~38 ATP), whereas normal epithelial cell accumulation of zinc inhibits the m-aconitase, interrupting the Krebs cycle and eliminating coupled energy (total energy ~14 ATP) [9,10]. Hypothetically, increasing the level of circulating zinc available for cellular uptake could be an efficacious approach for restoring the zinc pathway in malignant cells and thus promote tumor suppression.

The challenge associated with zinc deficiency in malignant cells can be addressed through the use of various delivery systems. In the search for new delivery systems, cell-penetrating peptides (CPP) have attracted attention due to their ability to deliver intracellularly a wide range of molecules [11]. CPP are short peptides of fewer than 30 amino acids that are mostly enriched with positively charged amino acids (e.g., Arg, Lys and His), allowing penetration through the cell membrane via various mechanisms, including endocytosis. CPP can provide the easy delivery of various cell-impermeable covalently or non-covalently conjugated cargos [12,13]. Novicidin (NVC) peptide is a promising delivery system candidate due to several properties, such as its cell-penetrating abilities, a low hemolytic effect, a highly amphipathic alpha helix structure and a high affinity for anionic lipids that are characteristic of cancer cells [14].

To carry the metal ion cargo, Schiff bases are organic compounds with versatile biological properties. The type of metal and the complexity of the Schiff base play a major role in the potency of these compounds as chemotherapeutic agents. Schiff bases bound to metal ions interact directly with the cell membrane and cause oxidative stress damage. The binding of the Schiff base-metal ion complex with other compounds can neutralize this oxidative capability and permit delivery within biological systems [15,16]. According to the Lewis acid-base theory, the complex of Schiff base–metal ion–peptide (Zn-S-NVC) should be highly stable (Fig 1); both the Schiff base and peptide work together as electron donors to the metal ion, while the metal ion center stabilizes the entire complex [17,18].

Consequently, we were interested in synthesizing a zinc delivery system to increase zinc availability in PCa cells. Here, we investigated the molecular changes that occur after delivery by studying the genes involved in zinc stress. This delivery system showed minor toxicity in normal PNT1A cells and a high potency towards PC3 tumor cells, as shown by a preference to penetrate PC3 cells in contrast to localized confinement to membranes of PNT1A. Furthermore, zinc uptake was confirmed in both cell lines. Molecular analyses were used to confirm the activation of zinc stress (e.g., *ZnT-1*) and apoptosis (e.g., *CASP-1*) genes. For clarity, protein names were shown in normal fonts and gene names were shown in italics.

Results

Characterization of the Zn-S-NVC complex

As described below, we exploited the interaction of the Schiff base–zinc complex (Zn-S) with the NVC peptide to produce a stable complex for zinc delivery to cells. To confirm this interaction, matrix-assisted laser desorption/ionization time-of-flight mass spectrometry (MALDI-TOF MS) was applied. The observed signals for Zn-S are shown in Fig 2A and were assigned as follows: $[Zn\text{-}S+H]^+$ (m/z = 342 Da) corresponds to the ionized Zn-S complex, whereas the peak m/z = 439 Da is assigned to the perchlorate adduct of the molecular ion indicating the formation of a hydrogen bond between perchlorate ions and nitrogen donors that have been previously reported for complex ions[19,20]. Fig 2B shows the mass spectrum of ionized NVC $[NVC+H]^+$ (m/z = 2294 Da). Fig 2C shows the mass spectrum of Zn-S-NVC. The peak at m/

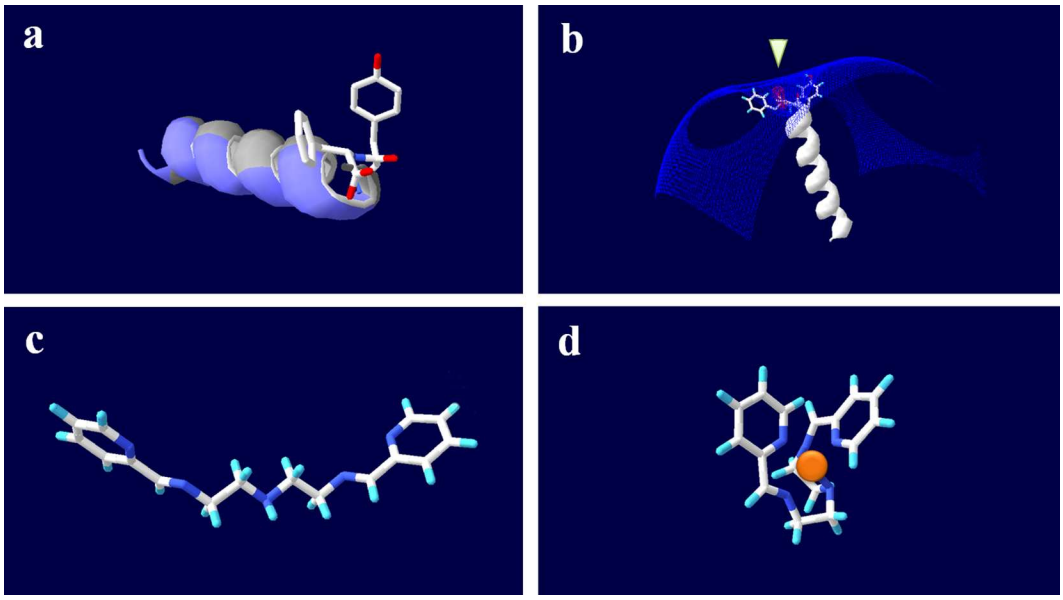

Fig 1. Molecular structure compatibility of Novicidin (NVC) and Schiff base. A) Helix NVC structure prediction using SWISS-MODEL based on the template PDB-ID: 4TQL (Biasini et al. 2014) showing the aromatic ring side chains of the *C*-terminal Tyr-Phe-COO^- on a helix ribbon. Positively charged amino acids on the ribbon are shown in blue, while neutral amino acids are shown in gray. After energy minimization (total -900 $kJ{\cdot}mol^{-1}$), the distance between the aromatic rings was 5.4–8.9 Å. The distance between the aromatic rings and the charged center was 3.4–7.0 Å. B) Electrostatic potential of NVC calculated using DeepView v 4.1 (Guex and Peitsch 1997) and showing the *C*-terminus as the only "negative pocket" in the structure (arrow), represented by the carboxylic acid group surrounded by two aromatic rings. C) Relaxed Schiff base structure without a zinc ion, drawn using Chemwriter (Metamolecular, LLC, USA). The distance between aromatic rings was ~11.4–15.7 Å. D) Zinc-Schiff base structure drawn using Chemwriter showing a positive zinc atom surrounded by two aromatic rings on nearly perpendicular planes. The five nitrogen atoms resulted in a pentahedral shape (9 edges, 6 triangular faces), allowing maximum accessibility to the zinc ion from two opposing sides (edges ~3.3±0.06 Å compared with smaller edges with an average of ~2.5±0.13 Å). One of these sides opposes one aromatic ring, while the other allows for interactions with both rings. The flexibility and directionality in the zinc-Schiff base structure suggests that zinc can be actively accessed even after complexing with peptide. The distance between aromatic rings was ~2.4–6.0 Å. The distance between aromatic rings and charged center was ~1.8 Å. (atoms: red-oxygen, white-carbon, blue-nitrogen, light-blue-hydrogen).

doi:10.1371/journal.pone.0163983.g001

z = 2648 Da corresponds to the quasimolecular ion $[Zn\text{-}S\text{-}NVC+H]^+$ and confirms the formation of the Zn-S-NVC complex. In the spectrum, there are also peaks at m/z = 2585 Da, 2548 Da, 2484 Da and 2385 Da, which are likely to be fragments of the complex and/or fragments of the complex and organic adduct originating from the matrix, which can be attributed to a high laser intensity and/or the robustness of the crystals that form the DHB matrix. The peak at m/z = 2385 Da corresponds to $[Zn\text{-}NVC+Na]^+$, where the presence of sodium ion can be due to its presence in the matrix, whereas the peaks at m/z = 2585 Da and 2484 Da are likely to be perchlorate adducts of $[Zn\text{-}NVC+Na]^+$. Although we cannot confirm the type of bonding that occurred between the metal and the peptide by MALDI-TOF, complexation between NVC and Zn-S occurred.

To better understand the Zn-S interaction with NVC peptide, FTIR measurement was conducted. In the spectrum of Zn-S-NVC, there are slight differences compared with Zn-S, which, as anticipated, occur in the areas where the peptide vibrations are most intense (Fig 3A). The change in the area of 1621 cm^{-1}, i.e., near the most intense vibration of free peptide (1647 cm^{-1}, which is the area characteristic of the so called amide I., the peak representing the response to the valence vibration C = O in the CONH group) [21]. The shift to lower frequencies could be testified for the possible involvement of atoms from the group interacting with the central zinc

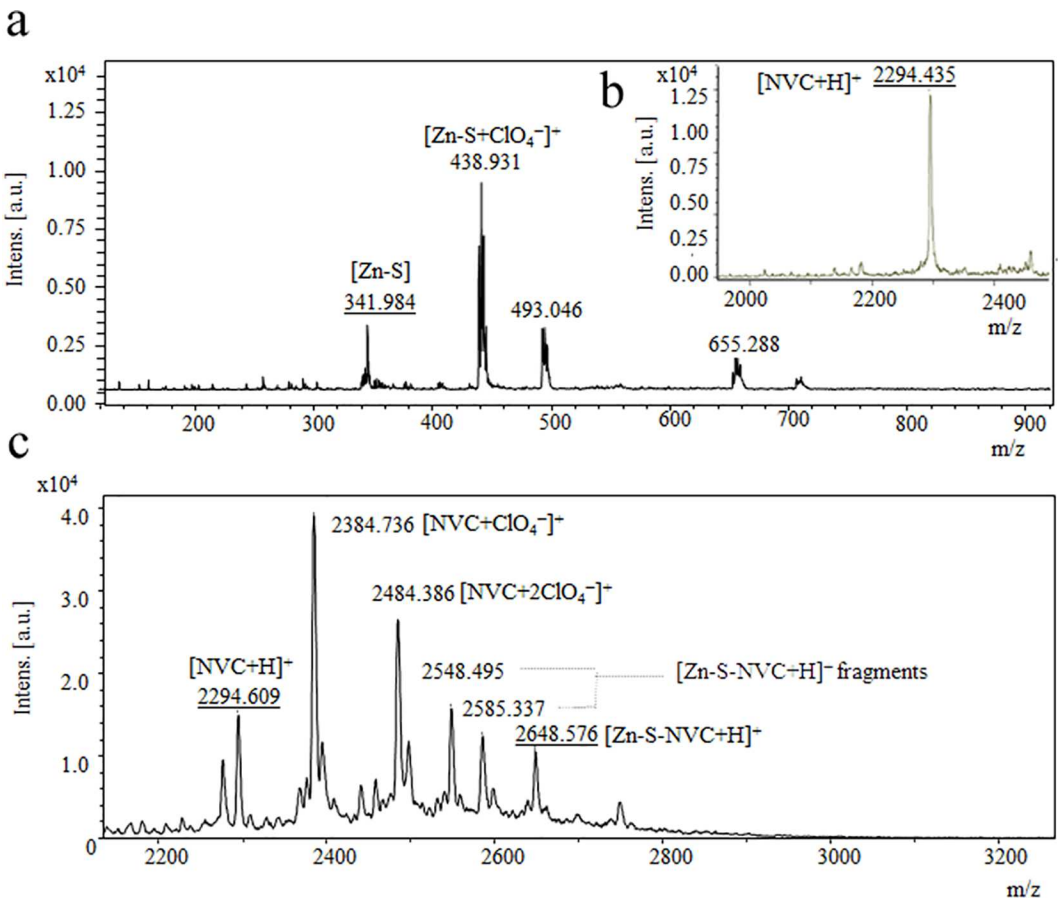

Fig 2. Matrix-assisted laser desorption/ionization time-of-flight mass spectrometry (MALDI-TOF-MS) analysis of the Zinc-Schiff base-Novicidin complex. A) Spectrum of zinc Schiff base [Zn-S]. B) Novicidin peptide [NVC+H]. C) Spectrum of [Zn-S-NVC]. All spectra were measured by MALDI-TOF MS with a 2,5-dihydroxybenzoic acid matrix in TA30 and a maximum energy of 43.2 μJ with a repetition rate of 2000 Hz and 20 subspectra.

doi:10.1371/journal.pone.0163983.g002

atom. Furthermore, as one of the most intense peptide signals in the fingerprint of the Zn-S-NVC spectrum, a signal was apparent at 1175 cm^{-1} that likely represents one of the C = O valence vibrations. The last signal demonstrates the presence of the NVC peptide in the Zn-S-NVC sample at 720 cm^{-1}. Due to the intensity of the band in the Zn-S spectrum, it was not possible to reliably identify the remaining peptide vibration in the IR spectrum of Zn-S-NVC; however, it was possible to observe an apparent signal increase in the so-called amide II 1550–1500 cm^{-1} area or even slight differences in the fingerprint area, which could be attributed to the interaction between the peptide and Zn-S. The peaks at 1597 and 1566 cm^{-1} are presented in the spectra of both complexes, and the peaks can be assigned to the ν(C = N) vibration of the Schiff base[22].

Interaction studies between Zn-S and NVC were conducted at room temperature using spectrophotometric methods. The samples were mixed at a 1:1 ratio. The maximum absorbance of all samples was observed at 266 nm. The stability of the formed complex was monitored spectrophotometrically over one week (Figure B in S1 File). An excitation wavelength of 266 nm was used to determine the maximum fluorescence emission wavelength of Zn-S and its interaction with cell-penetrating peptide. However, as shown in Fig 3B, NVC did not show an emission peak in the region of the visible spectrum. The emission spectra of Zn-S showed two

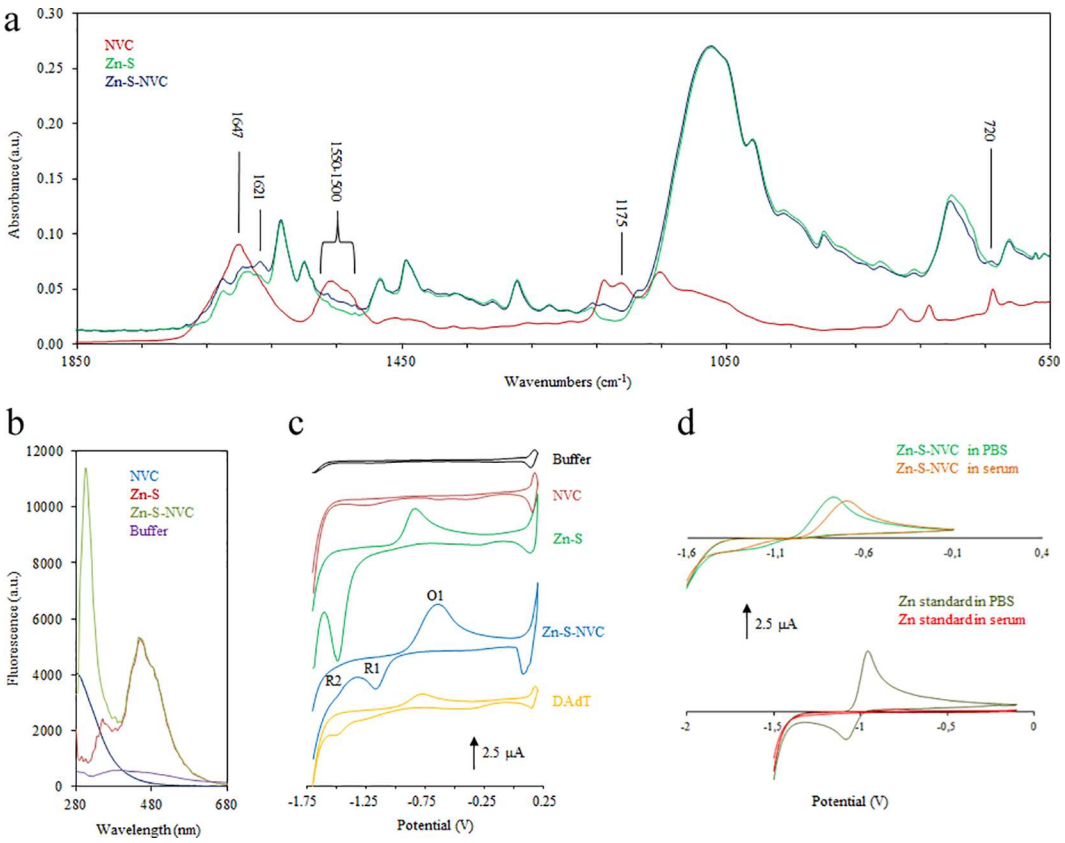

Fig 3. Characterization of Novicidin (NVC), Schiff base (Zn-S) and Zn-S-Novicidin complex (Zn-S-NVC). A) FTIR measurement. B) Fluorescence spectroscopy. C) Real cyclic voltammograms related to the Britton Robinson buffer itself (black line) and prepared complex labeled as follows: NVC (red line), Zn-S (green line), Zn-S-NVC complex determined in the cell (blue line) and Zn-S-NVC complex determined utilizing the double adsorptive transfer technique (orange line). D) Influence of the environment (phosphate buffer and human serum) on the electrochemical response represented by cyclic voltammograms of the free zinc ions (upper part of the figure) and the Zn-S-NVC complex (lower part of the figure). Real cyclic voltammograms were measured in 0.2 M acetate buffer, pH 5.

doi:10.1371/journal.pone.0163983.g003

peaks at 350 and 450 nm, which are typical for the coordination of Zn ions to Schiff base [23,24]. A comparison of the Zn-S-NVC complex with Zn-S Schiff base revealed that the peak occurred at the same position in both cases, and only the emission of Zn-S-NVC showed one additional peak at 304 nm, which we can assume belongs to the peptide-metal complex representing the Tyr amino acid present in our peptide[25,26].

Furthermore, the interaction of NVC with Zn-S was confirmed and studied using electrochemical methods (Fig 3C). A detailed analysis of data using the double adsorptive transfer technique and cyclic voltammograms is presented in S1 File. The stability of the complex and the environmental influence on Zn-S and NVC was studied in phosphate buffer and human serum. Electrochemical zinc signals (oxidation and reduction) that can be masked in serum were observed in buffer and serum (Fig 3D), suggesting that the complex was stable.

Cytotoxicity test

We selected the human prostate cell lines PC3 and PNT1A, which are commonly used in biomedical research. Approximately 1000 cells were incubated in 100 µL of a reduced-serum medium for cell culture (Opti-MEM, Life Technologies, USA) under standard conditions

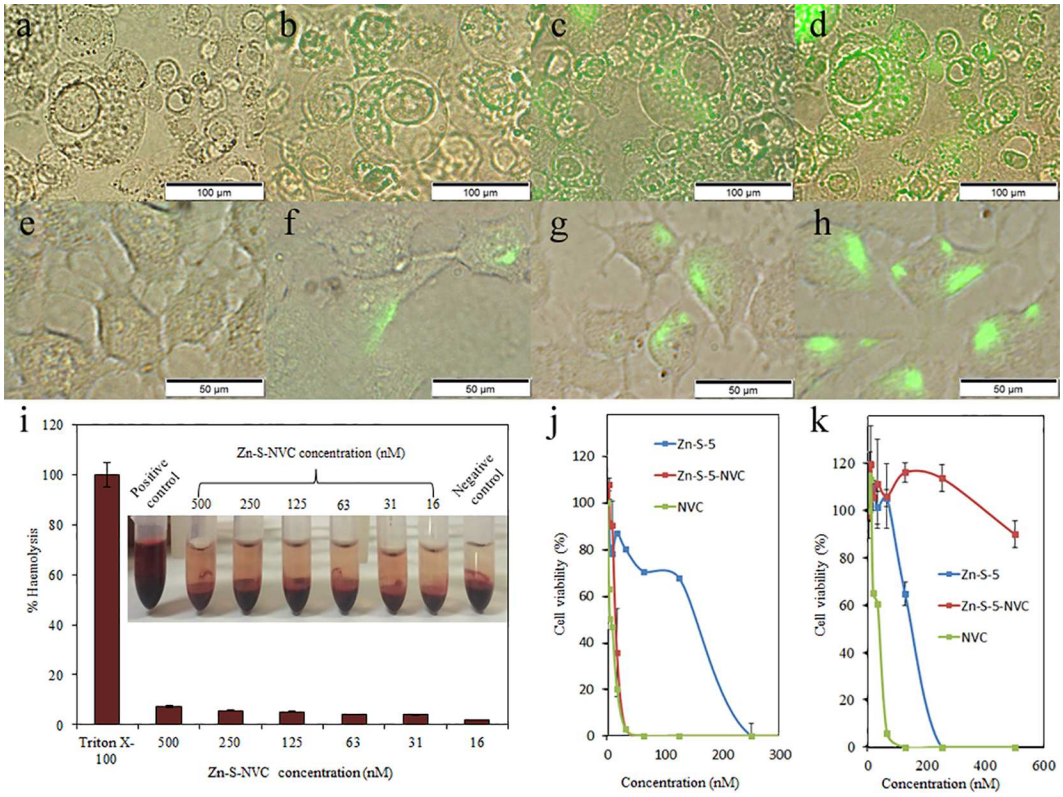

Fig 4. Fluorescence microscopy images. A) PNT1A cells exposed to Zn-S-NVC (conjugated to fluorescent dye) at 0 min. B) PNT1A cells exposed to Zn-S-NVC (conjugated to fluorescent dye) at 30 min. C) PNT1A cells exposed to Zn-S-NVC (conjugated to fluorescent dye) at 60 min. D) PNT1A cells exposed to Zn-S-NVC (conjugated to fluorescent dye) at 90 min. E) PC3 cells exposed to Zn-S-NVC (conjugated to fluorescent dye) at 0 min. F) PC3 cells exposed to Zn-S-NVC (conjugated to fluorescent dye) at 30 min. G) PC3 cells exposed to Zn-S-NVC (conjugated to fluorescent dye) at 60 min. H) PC3 cells exposed to Zn-S-NVC (conjugated to fluorescent dye) at 90 min. I) Haemocompatibility of Zn-S-NVC using human RBCs, showing negligible haemolytic activity in the selected concentration range of Zn-S-NVC (16–500 nM). Inserts show images after incubation and centrifugation. J) MTT analysis of the PC3 cell line. K) MTT analysis of the PNT1A cell line.

doi:10.1371/journal.pone.0163983.g004

(37°C, 5% CO_2) in an incubator (New Brunswick Eppendorf, USA). The Zn-S-NVC complex was applied to the cells at a final concentration of 100 μM. After different incubation periods (30: 60 and 90 min), the samples were washed three times with PBS buffer to remove the excess of Zn-S-NVC complex. The control sample was maintained under the same conditions without the addition of the Zn-S-NVC complex. PNT1A cells were also prepared using the same protocol for a comparative study of the effect of the Zn-S-NVC complex on cells. Uptake of the Zn-S-NVC complex slowly increased in PC3 cells over time (Fig 4A–4D). Attachment of the Zn-S-NVC complex to PNT1A cells also increased over time (Fig 4E–4H). A comparison of the microscopic images of both cells revealed that the Zn-S-NVC complex was distributed in the cytosol of the PC3 cells, whereas in PNT1A cells, it was confined to the membrane. After 12 h of incubation, the PC3 cells started to exhibit membrane "blebbing," an indicator of cell death by apoptosis, whereas PNT1A cells remained healthy. This result was later confirmed using the MTT assay.

A haemolytic assay was conducted to study the haemocompatibility of the Zn-S-NVC complex. The haemolytic activity of peptides is a crucial parameter to estimate their therapeutic index. Strong membrane binding and the penetration ability of peptides into cancer cells can also pose a threat to RBC *via* similar membrane-disruption mechanisms. Thus, refining the

peptides will decrease these undesired side effects. Fig 4I illustrates that the highest applied concentration of Zn-S-NVC (500 nM) triggered haemolysis of only approximately 7.4% (in relation to Triton X-100 as a positive control). Thus, Zn-S-NVC can be applied with minimal effects on blood circulation.

The cytotoxicity of the Zn-S-NVC complex was examined in PC3 and PNT1A cell lines using the MTT assay. As shown in Fig 4J and 4K, NVC alone induced high toxicity in both PC3 (Fig 4J) and PNT1A (Fig 4K) cell lines, reducing cell viability by 50% at a concentration of 16 nM and by 100% at 63 nM after 24 h. The Zn-S complex without peptide also showed significant toxicity toward both cell lines compared with NVC alone, reducing cell viability by 40% at a concentration of 125 nM and by 100% at 250 nM after 24 h. After the application of the Zn-S-NVC complex to the PC3 cell line (Fig 4J), cell viability was reduced by 65% at a concentration of 46 nM. However, in PNT1A cells, the complex had negligible cytotoxicity, even at a concentration of 500 nM (Fig 4K).

Expression of genes associated with zinc stress in PCa cells

Human prostate PC3 cancer cells and PNT1A normal cells were incubated with Zn-S-NVC complex at a concentration of 150 μM. Before the treatment with Zn-S-NVC, the concentration of total zinc in cells was determined by AAS as 35.3 $\mu g \cdot mL^{-1}$. After treatment, the zinc concentration dropped to ~26.4 $\mu g \cdot mL^{-1}$ in the PC3 culture and to ~27.3 $\mu g \cdot mL^{-1}$ in the PNT1A culture. Assuming each confluent culture contained 8.4 million cells for both cell lines, the amount of zinc consumed was approximately 5.3 pg per PC3 cell and 4.8 pg per PNT1A cell. Although these numbers are not greatly different from each other, they support the notion that, with the Zn-S-NVC delivery system, PNT1A cells more efficiently exclude zinc than the PC3 cells.

Several studies have reported changes in the regulation of MT isoforms, zinc transport (ZnT), and tumor protein 53 (p53) in human prostate cells and tissues[8,27,28]. Western blot analysis revealed an absence of p53 protein in PC3 cells. However, there were no visible differences in p53 protein expression in PNT1A cells (Fig 5A). To evaluate the effect of Zn-S-NVC complex delivery on PCa cells, the gene expression in PC3 and PNT1A cells was assessed using quantitative RT-PCR. Three independent experiments were conducted to assess 5 genes after treatment with Zn-S-NVC complex: *SP1*, *p53*, *MT-1X*, *MT-2A* and *ZnT-1*, as shown in Fig 5B.

The expression levels of *p53* increased two-fold in PNT1A cells and five-fold in PC3 cells after treatment. *SP1* transcription factor expression levels remained relatively unchanged after treatment in both normal and tumor cells. Two MT isoforms genes (*MT-1X and MT-2A*) showed variable expression levels, with *MT-2A* expression levels that were 2.2-fold higher in treated PC3 cells compared with treated PNT1A cells. Interestingly, the expression of the zinc transporter *ZnT-1* was increased nearly two-fold after treatment in both PNT1A and PC3 cells.

Identification of cancer genes expression associated with Zn-S-NVC complex in prostate cell lines by microarray

Further investigation of cancer biomarkers affected by Zn-S-NVC complex treatment was performed. The employed DNA microarray consists of 4×2 k oligonucleotide probes specific to each type of cancer. For this study, we used a commercial chip (Human Cancer 3711 ElectraSense 4×2 k array slides) from CombiMatrix (Custom Array, Bothell, WA, USA) to identify cancer biomarkers that were expressed in PC3 cells treated with Zn-S-NVC complex.

In the present study, we used four different treatments: PNT1A (PNT1A cell line before treatment with Zn-S-NVC complex); PNT1A-Zn-S-NVC (PNT1A cell line after treatment); PC3 (PC3 cell line before treatment); and PC3-Zn-S-NVC (PC3 cell line after treatment). To evaluate the results, we determined the fold ratio or relative expression of genes in all possible

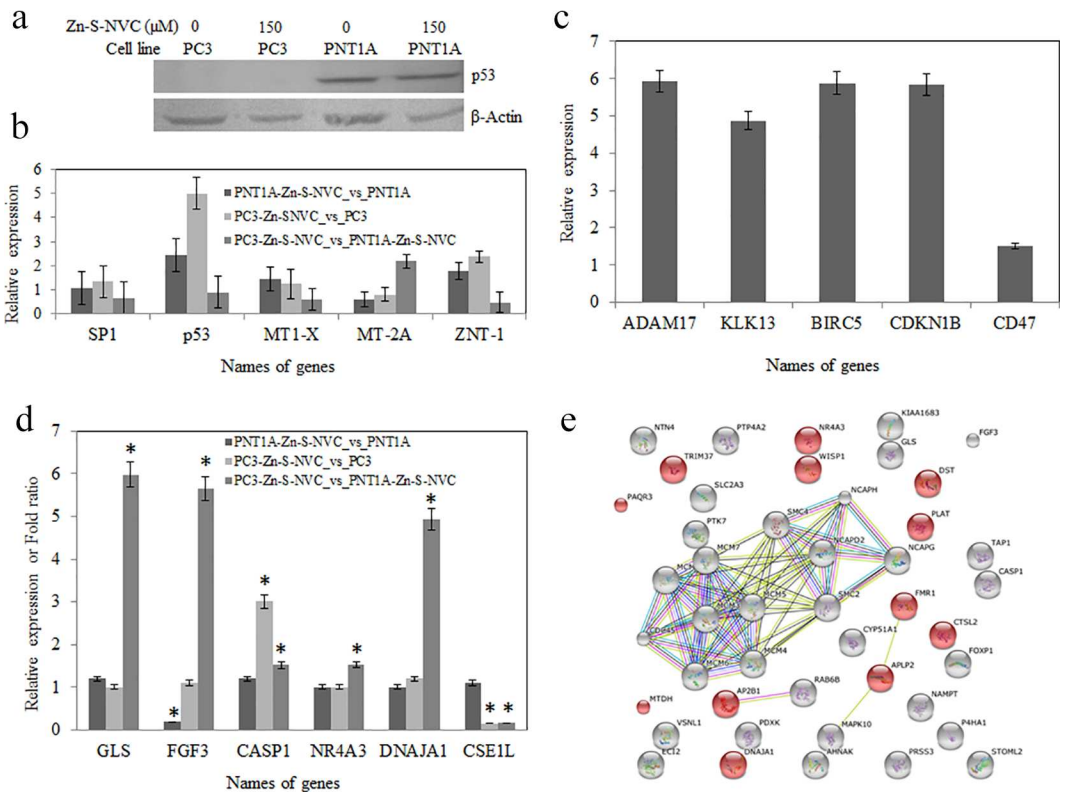

Fig 5. Gene expression analysis. A) Western blot analysis of p53 protein expression revealed no expression in PC3 cells and no change in PNT1A cells. Western blot analysis using anti-p53 (sc-126) after treatment with 150 μM Zn-S-NVC complex for 40 min. Anti-β-Actin (sc-130657) was used as an internal control. B) Change in the gene expression in PC3 and PNT1A cells assessed by qRT-PCR. Relative expression or fold change in genes after treatment with 150 μM Zn-S-NVC complex for 40 min. The qRT-PCR data were normalized to the internal control *18S rRNA*. The mean change is shown for two independent experiments (bars represent the standard deviation). C) Up-regulated genes in PC3 cells before treatment with Zn-S-NVC complex by microarray (PC3_vs_PNT1). D) Relative expression or fold change in genes in response to different treatments after application of Zn-S-NVC complex in PC3 and PNT1A cells by ElectraSense CombiMatrix microarray (bars represent the error standard, * indicates significant differences between treatments). E) Globally up-regulated genes in PC3 and PNT1A cells after treatment with Zn-S-NVC complex assessed using KEGG 10 software (Known and Predicted Protein-Protein Interactions). The red-colored genes indicate genes that negatively regulate cellular processes (metabolic, cell death or apoptotic processes). Different line colors represent the types of evidence for the association (neighborhood, gene fusion, co-occurrence and co-expression).

doi:10.1371/journal.pone.0163983.g005

combinations between treatments: the effect of Zn-S-NVC complex in PC3 cells (PC3-Zn-S-NVC *vs*. PC3) and in PNT1A cells (PNT1A-Zn-S-NVC *vs*. PNT1A) and the global effect between PC3 and PNT1A cells after treatment with Zn-S-NVC complex (PC3-Zn-S-NVC *vs*. PNT1A-Zn-S-NVC).

The image of the ElectraSense array with a gray scale representing the intensity of expression, number of regulated genes and an overview of regulated genes (up and down-regulation) in the PNT1A and PC3 cell lines in response to the different treatments (after and/or before Zn-S-NVC complex application) are shown in Figure A and Table B in S1 File, respectively.

Our control was the variant PC3 *vs*. PNT1A (before treatment with Zn-S-NVC) to verify the expression of general cancer genes and specific genes related to PCa in our samples (Table B in S1 File). Fig 5C shows the specific genes that were up-regulated in PC3 cells compared with PNT1A cells before treatment with Zn-S-NVC complex, which included *ADAM17*, *KLK13*, *BIRC5*, *CDKN1B*, and *CD47* genes.

Tables C and D in S1 File shows the list of processes and/or pathways of gene regulation in PC3 and PNT1A cells lines comparing different treatments using gene ontology (GO) annotations and KEGG 10 software, respectively. The most important and interesting comparison was the global effect between PC3 and PNT1A cells after treatment with the complex (PC3-Zn-S-NVC *vs*. PNT1A-Zn-S-NVC). Moreover, this comparison revealed the overexpression of different genes from biological pathways related to cell proliferation and cell differentiation (Fig 5D): *GLS* (glutaminase) is a key enzyme that converts glutamine to glutamate and couples glutaminolysis of the tricarboxylic acid cycle (TCA) with elevated glucose uptake and consequently the growth of PCa cells[29]; and *FGF3* (fibroblast growth factor 3) elevates the levels of *FGFRs*, which have been found in numerous human cancers, such as cancers of the brain, head and neck, lung, breast, stomach, and prostate, sarcomas and multiple myeloma [30,31]. Many genes responsible for the negative regulation of cellular metabolic processes and the positive regulation of programmed cell death were up-regulated (*CASP1*, *NR4A3* and *DNAJA1*). These results indicated that genes that induce cell death or apoptosis were activated in PC3 cells after applying the Zn-S-NVC complex (Fig 5E).

Discussion

Targeting the zinc metabolic pathway to induce apoptosis is a progressive field in PCa therapy. Here, we investigated a novel drug delivery system composed of a membrane-penetrating peptide and a Schiff base as a zinc carrier. Targeting the zinc pathway for PCa treatment has been a research interest of many investigators over the past decade. We believe that developing zinc delivery systems should be the next step for PCa treatment. The versatility of cell-penetrating peptides and Schiff bases will allow development of highly selective and potent therapeutic compounds in the future. In the current study, a NVC conjugate with a Schiff base-zinc complex was synthesized and evaluated for its apoptosis-inducing activity in human PCa cells. This zinc complex potently induced apoptosis in a dose- and time-dependent manner. Our findings reinforce the notion that peptide-carrying zinc compounds have great potential for the development of novel anticancer drugs. This new complex was successfully tested for stability, biocompatibility, cancer specificity, potency and mechanism of action in the PC3 cell line.

The molecular structure of NVC and Schiff base allows a compatible interaction. The NVC peptide is composed of alternating neutral and basic amino acids (Fig 1A). The *C*-terminal carboxylic group forms a negatively charged pocket surrounded by two aromatic rings (Fig 1B). Alternatively, the flexible structure of the Schiff base (Fig 1C) allows the zinc ion to be geometrically coordinated but rather accessible to the NVC carboxylic group from one of two opposing sides (Fig 1D). The two aromatic rings of the Schiff base provide a compatible electron clouds that can interact via π-π stacking with the aromatic rings of Phe and Tyr amino acids and increase the stability of the zinc-Schiff base-NVC complex.

The composition, interactions and stability of the Zn-S-NVC complex was investigated using mass spectrometry (Fig 2), FTIR (Fig 3A), fluorescence spectrometry (Fig 3B), and voltammetric methods (Fig 3C and 3D). The results support the formation of a complex with zinc ion that remains available for interactions within the complex.

Furthermore, we investigated the cytotoxicity of the NVC, Schiff base and delivery system. Our results revealed a decreased toxicity of Zn-S-NVC in the normal PNT1A cell line. A recent study investigating the cytotoxic antimicrobial activity of Melittin and NVC suggested an explanation for the decreased cytotoxicity in some cases [14]. In the presence of low fractions of negatively charged elements in the membrane, the free energy of the interaction between NVC and the membrane increased, leads to decreased cytotoxicity. Similarly, cancer cells

display more negatively charged elements on their membrane, thus decreasing the free energy of incorporation and increase the cytotoxicity, as was observed in our experiment [32].

It is unknown whether the Schiff base exerts oxidative stress effects while conjugated to zinc and NVC. Our preliminary analysis using the ratio of gallic acid equivalents per mg of protein (GAE/mg) revealed a change of 113.3% after treatment in PNT1A cells and 125.9% in PC3 [using the Antioxidant Assay Kit (Sigma), and BS-400 Chemistry Analyzer (Mindray Medical International Limited, China)]. This slight increase in gallic acid equivalents supports the notion that oxidative stress is not the main cause of cell death, which indicates that the Schiff base is not the main toxic component of the delivery system.

To study the effects of zinc stress in PNT1A and PC3 cell lines and its role in apoptosis, the expression of several genes was investigated. The transcription factor *SP1* plays a dual role in regulating stress to heavy metals and inducing apoptosis, possibly as a competitor antagonist toward other transcription factors involved in ion stress and apoptosis. Previous studies have reported that overexpression of the transcription factor Sp1 leads to cell cycle inhibition at the G_1 phase before the onset of apoptosis [33]. SP1 and mutant p53 were found to directly interact, forming a hetero-complex and leading to alterations in downstream target genes of both *SP1* and *p53*. In the case of decreasing *p53* expression due to growth factor deprivation, SP1 is released, leading to apoptosis [34]. It is possible that the SP1-p53 interaction leads to the blockade of DNA binding domains, and thus, p53 and SP1 can be regarded as antagonists [35]. In contrast, SP1 overexpression in tumor cells has been suggested to induce apoptosis by increasing the expression of *p53* and regulating apoptosis-related gene expression. SP1 overexpression also regulates global chromatin condensation and packaging stress that leads to apoptosis [36]. Our results show that the *p53* but not the *SP1* gene was activated by more than two-fold within 40 min of exposure to Zn-S-NVC. PC3 cells carry a mutant *p53* gene with a 1-bp deletion in codon 138 that produces a truncated protein due to the formation of a stop codon at position 169 *via* a frame shift [37], which was undetected by the antibody used herein (clone sc-126). Regarding PNT1A cells, there was no visible change in p53 protein levels after treatment with Zn-S-NVC. Previously, Chuang *et al*. showed that overexpression of the SP1 protein resulted in apoptosis through the overexpression of the p53 protein [36]. This result is consistent with our findings, in which p53 protein expression did not change in PNT1A cells and thus did not lead to apoptosis. Although the *p53* gene was activated at the mRNA level in our experiment, p53 activation at the protein level is a multistep post-translational process resulting in many modifications, in which DNA binding and protein-protein interactions confer stabilization, anti-repression and promoter-specific transcriptional activation [38].

As a part of the dual role of *SP1* in the regulation of heavy metal stress, *SP1* regulates the activity of MT. Li *et al*. showed that *MT-1* is activated by a complex of proteins involving MTF-1, SP1 and p300/CBP [39]. Other reports have shown that SP1 binds to the metallothionein-2A (*MT-2A*) gene and is likely to regulate transcription by competing with the transcriptional activator MTF-1 [40,41]. The MT family of proteins chelates heavy metal ions through their cysteine-rich motifs. Each molecule of MT is capable of binding seven divalent metal ions with variable affinities, with copper having the highest and zinc having the weakest affinity [42]. Our results revealed an increase in expression in one of two MT genes, namely *MT-2A*, upon exposure to Zn-S-NVC complex. MTs are located in the membrane of the Golgi apparatus [43]. Qin *et al*. showed that free zinc ions are mostly concentrated in the cytoplasm (80 pM in HeLa cells) and less concentrated in the endoplasmic reticulum (0.9 pM) and Golgi apparatus (0.6 pM) [44]. One can hypothesize that MTs and other chelating proteins in the ER and Golgi apparatus store zinc and heavy metal ions prior to extracellular secretion. Meplan *et al*. showed that MTs regulate the p53 conformation through their zinc-chelating properties [45]. The p53 DNA binding domain requires zinc for its wild type conformation, and thus, the overexpression of MTs leads

to a conformational change in p53 DNA binding domain folding and results in the modulation of p53 transcriptional activity.

However, the regulation of free zinc transport from the cytoplasm to organelles, the nucleus and extracellularly is regulated by specialized zinc transporter proteins. PCa cells accumulate reduced levels of zinc due to a down-regulation of the hormone-responsive zinc transporter *ZIP1* [46]. Normal prostate cells take up zinc either in free or chelated form, e.g., with citrate [47]. A study by Hasumi *et al*. investigating the *ZnT-1* zinc transporter in tumor prostate cell lines showed increased expression of both *ZnT-1* mRNA and protein in the presence of zinc [8]. In the absence of zinc, the authors reported a lower expression level of ZnT-1 in cancer cells compared with normal prostate cells, thus casting more doubt on the role of this protein as a zinc exporter in PCa cells. Our results revealed increased expression levels of *ZnT-1* in both cell lines following treatment. Unfortunately, the regulation of *ZnT-1* remains unclear, e.g., it is unclear whether this gene is hormone-responsive like the *ZIP1* transporter [8]. Cousins and McMahon also noted the variability in *ZnT-1* expression at the mRNA *vs*. the protein level [48]. They studied the role of the energy-independent zinc transporter *ZnT-1* in the detoxification (export) of zinc from cells exposed to high extracellular levels of zinc. Recent reports have also shown discrepancies in the levels of *ZnT-1* in PCa cell lines [49]. Additional studies are required to shed light on the regulation of this zinc transporter and its physiological role in PCa cells. In contrast to our microscopy findings showing peptide confined to the membrane of PNT1A cells, *ZnT-1* expression provided evidence supporting the delivery of zinc in both cell lines. This finding was confirmed by the zinc concentration measured using AAS. It is possible that the peptide component of the complex is only internalized by PC3 cells due to structural differences in their membranes, while Zn-Schiff base is internalized in both PC3 and PNT1A cells.

Microarray was employed to identify cancer biomarkers that are generally over-expressed in the PC3 cell line. The use of this method and its respective apparatus has been previously reported [50]. However, the obtained data do not provide information regarding what happens during cellular metabolism because the chip only identifies general and specific cancer biomarker that are regulated in human samples, i.e., prostate, gastric, lung and brain. Here, we reported the over-expression of several genes: *ADAM17*, *KLK13*, *BIRC5*, *CDKN1B* (p27Kip1) and *CD47*. *ADAM17* over-expression promotes PCa cell proliferation by activating the EGFR/PI3K/AKT pathway [51]. Lose *et al*. showed that the regulation of *KLK13* appears to be more complex in PCa cells depending on the tissue, tumor or cell line [52]. *BIRC5* up-regulation encodes negative regulatory proteins that prevent apoptotic cell death in the lung, pancreas, colon, breast, and PCa [53]. Different studies have suggested that the up-regulation of *CDKN1B* is a prognostic marker in PCa [54]. CD47 is a transmembrane protein that is encoded by the *CD47* gene in humans and is up-regulated in the PC3 cell line. The expression of *CD47* is a general mechanism used by which human solid tumor cells evade phagocytosis. *CD47* expression has been detected on most PCa cells and other cancer cells from primary and xenografted patient tumor samples [55]. Therefore, these results (Fig 5C) verified the expression of specific PCa genes in our samples.

The microarrays results could shed some light on the genes and biomarkers involved in inducing cellular death in PC3 cells after applying the Zn-S-NVC complex. Normal prostate cells accumulate zinc and contain high levels of cellular zinc. In contrast, PCa cells have lost the ability to accumulate zinc and contain low zinc concentrations. Zinc has been reported to induce apoptosis in many mammalian cell types, including prostate epithelial cells [56]. The influence of zinc on apoptosis is a well-known phenomenon [57]. However, *CASP1* overexpression has been shown to induce apoptosis in mammalian cells. *CASP1* is involved in the signal transduction pathways underlying apoptosis, necrosis and inflammation [58]. *CASP1* is a

caspase initiator that was originally characterized as cleaving inactive prointerleukin-1 to generate the active proinflammatory cytokine interleukin-1 [59]. Truong-Tran *et al*. examined the cytoprotective functions of zinc, which suppresses the major pathways leading to apoptosis, as well as the more direct influence of zinc on apoptotic regulators, particularly the CASP family of enzymes [60]. In our study, in comparing PC3 cells treated with the Zn-S-NVC complex (PC3-Zn-S-NVC *vs*. PC3) and in comparing the global effect between PC3 and PNT1A after treatment with the Zn-S-NVC complex (PC3-Zn-S-NVC *vs*. PNT1A-Zn-S-NVC), a clear suppression of proliferation was observed. These results may be due to an increase in *CASP1* gene expression, as shown in the Fig 5D. The up-regulation of *CASP1* can be induced to increase intracellular zinc in PC3 cells after treatment with the Zn-S-NVC complex. *CASP1* activation during apoptosis is an important underlying theme in PCa therapy and in recent therapeutic strategies aimed at specifically targeting these proteases in relation to PCa. In addition, the *NR4A3* gene was up-regulated in the global effect between PC3 and PNT1A cell lines after treatment with Zn-S-NVC complex (PC3-Zn-S-NVC *vs*. PNT1A-Zn-S-NVC) (Fig 5D). Neuron-derived orphan receptor 1 (*NOR1*) is a protein that is encoded by the *NR4A3* gene in humans [61]. Shan *et al*. provided the first direct evidence in PC3 that *NOR1* overexpression can lead to apoptosis induction by altering the expression of apoptosis-related genes through the MAPK signaling pathway [62]. Therefore, over-expression of the *NR4A3* gene can be activated by Zn-S-NVC complex in our PC3 cells. Additionally, the microarray results from our samples showed over-expression of the *DNAJA1* gene in the global effect between PC3 and PNT1A cell lines after treatment with Zn-S-NVC (PC3-Zn-S-NVC *vs*. PNT1A-Zn-S-NVC). The *DNAJA1* gene plays an important role in programmed cell death. Stark *et al*. showed that *DNAJA1* overexpression reduces PCa cell survivability under stress, and the J-domain of *DNAJA1* itself may be a valuable biological target for the treatment of PCa as part of a combination therapy [63]. Prior results had not shown the *DNAJA1* gene in the PC3 cell line. Therefore, we report the first information regarding the over-expression of this gene in PC3 cells after treatment with Zn-S-NVC complex. We also can assume that this gene induces apoptosis in PCa cells. However, the *CSE1L* (cellular apoptosis susceptibility protein) gene was down-regulated in response to all treatments in PC3 cells after treatments with Zn-S-NVC (PC3-Zn-S-NVC *vs*. PC3 and PC3-Zn-S-NVC *vs*. PNT1A-Zn-S-NVC) (Fig 5D). Zhu *et al*. showed that *CSE1L* expression was significantly inhibited in a human colon cancer cell line, causing a delay in cell proliferation and induction of apoptosis [64]. Therefore, we can suggest that this down-regulation of *CSE1L* by the Zn-S-NVC complex may be a potential therapeutic approach for PCa.

All presented data strongly suggest that Zn-S-NVC complex can be used as a potent inducer of apoptosis in PCa cells, revealing great potential for its development as a novel anticancer therapy.

Methods

Chemicals and reagents

Chemicals and solvents were supplied by Sigma-Aldrich (St. Louis, MO, USA) with ACS purity and used without further purification.

Synthesis of Schiff base (S), Schiff base complex Zn-S, Novicidin peptide and Zn-S-NVC complex

Schiff base [(2-[(E)-2-pyridylmethyleneamino]-N-[2-[(E)-2-pyridylmethylene-amino]ethyl]ethanamine)] was prepared by mixing 2-pyridinecarboxaldehyde (1902 μL) and diethylenetriamine

(1080 μL) with stirring and heating under reflux in methanol (35 mL) for 6 h. The color turned to orange; after cooling, methanol was added to 50 mL.

Zinc perchlorate hexahydrate (0.372 g) was dissolved in 50 mL of water, and Schiff base S (5 mL) was added with stirring to obtain Zn-S Schiff base complex. The light orange solution was heated at 80°C for 2 h, the solution was then filtered, and water was added to 100 mL.

To synthesize NVC peptide, Liberty Blue peptide synthesizer was used (CEM, Matthews, NC, USA). The sequences and monoisotopic molecular weight of the synthesized peptide were as follows, respectively: KNLRRIIRKGIHIIKKYF and—2296 Da.

A stock solution of NVC peptide (1 mM) was mixed with Zn-S (1 mM) at a 1:1 ratio. The final concentration of the complex in PBS buffer was 1 mM. The sample was incubated for 60 min at 25°C. After incubation, unbound Zn-S was removed using the fluorescein fast protein liquid chromatography (FPLC) system, Biologic DuoFlow (Bio-Rad, Philadelphia, PA, USA).

Characterization of Zn-S, NVC and Zn-S-NVC complex

Mass spectrometry experiments were performed using a MALDI-TOF MS Bruker Ultraflextreme (Bruker Daltonik GmbH, Bremen, Germany) equipped with a laser operating at a wavelength of 355 nm with an accelerating voltage of 25 kV, cooled with nitrogen, with a maximum energy of 43.2 μJ and a repetition rate of 2000 Hz in linear and positive mode. Data were acquired and processed using mass spectra flexControl version 3.4 and flexAnalysis version 2.2 software. The 2,5-dihydroxybenzoic acid matrix (DHB) was used for MALDI-TOF (Bruker Daltonik GmbH).

The interactions between Zn-S and NVC were determined using the multifunctional microplate reader, Tecan Infinite 200 PRO (Tecan, Maennedorf, Switzerland). The absorbance spectra were measured within the range from 230–850 nm. For the fluorescence spectra, 230 nm was used as the excitation wavelength, and the fluorescence scan was measured within the range from 260–650 nm. The complex stability was determined by spectra recorded within the range from 190–850 nm using quartz cuvettes (1 cm, Hellma, Essex, UK) on a SPECORD 210 spectrophotometer (Analytik Jena, Germany) at 20°C. Spectra were recorded after 0, 1, 3 and 7 days of incubation. The FTIR spectra (4000–400 cm^{-1}) were recorded on a Bruker Tensor 27 spectrometer (Bruker Daltonik GmbH) equipped with a platinum-ATR accessory with a diamond crystal.

Electrochemical measurements were performed with the AUTOLAB Analyzer (EcoChemie, Netherlands) connected to VA-Stand 663 (Metrohm, Switzerland), using a standard cell with three electrodes. Stability experiments for the Zn-S-NVC complex were performed using cyclic voltammetry in acetate buffer (0.2 M CH_3COONa + CH_3COOH, pH 5).

Cultivation of prostatic cell lines

Two human prostatic cell lines were used in this study: the PNT1A human cell line and the PC3 human cell line were purchased from Health Protection Agency Culture Collections (Salisbury, UK). PNT1A cells were cultured in RPMI-1640 with 10% FBS. PC3 cells were cultured in Ham's F12 medium with 7% FBS. All media were supplemented with penicillin (100 U/mL) and streptomycin (0.1 mg/mL), and the cells were maintained at 37°C in a humidified incubator (Sanyo, Moriguchi, Japan) with 5% CO_2. The total cell content was analyzed using the Casy model TT system (Roche Applied Science, Penzberg, Germany). To prepare a viable cell standard, a 100-μL cell suspension was mixed with 10 mL of Casy Tone. All subsequent measurements were performed with a 100-μL cell suspension diluted 100×. The background was subtracted prior to each measurement.

Determination of complex cytotoxicity—MTT assay

The suspension of approximately 5000 cells was added to each well of microtiter plates (E-plates 16). Cultures were incubated for 2 days at 37°C to ensure cell growth. The medium was replaced with medium containing Zn-S-NVC complex (2–500 nM), and medium without agents served as a control. The plates were incubated for 24 h, and the medium was replaced with fresh medium three times daily. Additionally, the medium was replaced with 200 μL of fresh medium containing 50 μL of 3-(4,5-dimethylthiazol-2-yl)-2,5-diphenyltetrazolium bromide (MTT [5 $mg{\cdot}mL^{-1}$ in PBS]) and incubated for 4 h at 37°C. The MTT-containing medium was replaced with 200 μL of 99.9% dimethyl sulfoxide to dissolve MTT-formazan crystals. Then, 25 μL of glycine buffer was added to all wells, and the absorbance was determined at 570 nm (VersaMax microplate reader, Molecular Devices, Sunnyvale, CA, USA). Six replicates were used to assess the Zn-S-NVC complex, and four replicates were used for Zn-S.

Hemolysis evaluation

Human blood was obtained from the Department of Physiology, Faculty of Medicine, Masaryk University, Czech Republic. We analysed the samples of healthy volunteers (n = 2), whereas the written consent of blood donors was granted. The research has been approved by the Independent ethics committee at University Hospital, Brno, Czech Republic. Red blood cells (RBCs) were obtained from whole blood according to Evans *et al.* [65]. RBC suspensions were washed three times with iso-osmotic PBS (pH 7.4) and then diluted. Five hundred microliters of erythrocyte suspension was interacted with Zn-S-NVC complex at various doses and then incubated for 1 h at 37°C. The degree of hemolysis was determined by measuring the absorbance of the supernatant at 540 nm after centrifugation and calculated according to the following equation: $\%hemolysis = [(A_t\text{-}A_c)/A_{100\%}\text{-}A_c)]\times 100$, where A_t is the absorbance of the supernatant from samples incubated with Zn-S-NVC; A_c is the absorbance of the supernatant from the negative control (PBS, pH 7.4); $A_{100\%}$ is the absorbance of the supernatant from the positive control (0.1% Triton X-100), which causes complete RBC lysis.

Microscopy of complexes in ambient light

Zinc-Schiff base-Novicidin complex was conjugated to fluorescent dye [5(6)-carboxyfluorescein *N*-hydroxysuccinimide ester] and purified by FPLC prior to microscopy. An inverted microscope system, Olympus UIS2 series (Tokyo, Japan), was used to image complex internalization into the cells. The CPlanFLN 10× objective was used for 100× magnification, and the LUCPlanFLN 40× objective was used for 400× magnification. The images were captured using a Camera Olympus DP73 and processed with Stream Basic 1.7 Software.

Atomic absorption spectrometry (AAS)

The total content of zinc in the samples was determined using a 280Z Agilent Technologies atomic absorption spectrometer (Agilent, USA) with electro-thermal atomization. An arsenic ultrasensitive hollow cathode lamp (Agilent) was used as the radiation source (lamp current 10 mA). The spectrometer was operated at a resonance of 193.7 nm with a spectral bandwidth of 0.5 nm.

RNA extraction and quantitative RT-PCR

The medium was discarded, and the cells were washed with 2 mL of PBS. Approximately 2 mL of either PBS or PBS/Zn-S-NVC was added for both types of cell lines to a final concentration

of 150 μM Zn-S-NVC complex. The four cultures were incubated for 40 min with occasional shaking. RNA was isolated using the RNeasy Mini Kit (Qiagen, Venlo, Netherlands).

Gene expression was studied by quantitative RT-PCR using the SYBR Green Quantitative RT-PCR Kit (Sigma-Aldrich, USA) and the Mastercycler pro S instrument (Eppendorf, Hamburg, Germany). The primer sets used to amplify the coding regions of different genes are shown in Table A in S1 File. Each 20-μL reaction contained 2 μL of RNA and a final concentration of 2 μM of each primer. The PCR program consisted of an RT step (44°C/30 min), followed by (94°C/2 min), 35 cycles of (94°C/15 s, 60°C/1 min) and a final extension (68°C/7 min). The specificity of the PCR product was checked by melting curve analysis and 1% agarose gel electrophoresis. The results obtained in triplicates were standardized to the *18S ribosomal RNA* (GenBank Accession X03205.1). The relative levels of transcription were calculated using the $2^{-\Delta\Delta CT}$ method.

Protein extraction, SDS-PAGE and Western blotting

Proteins were lysed directly in culture plates with 2 mL of lysis buffer (150 mM NaCl, 1.0% Triton X-100, 50 mM Tris, pH 8.0, and 10 μL of protease inhibitor cocktail (Sigma-Aldrich, USA)) for 30 min. Proteins were electrophoresed in 12.5% polyacrylamide gel at 200 V for 33 min using a Mini Protean Tetra apparatus (Bio-Rad, USA). For Western blotting, PVDF membranes and blotting buffer (25 mM Tris-base, 150 mM glycine and 10% (*v/v*) methanol) were used. The transfer was performed for 1 h at a voltage of 0.9 mA per 1 cm^2 of the membrane. Anti-β-Actin (sc-130657) and anti-p53 (sc-126) primary antibodies were purchased from Santa Cruz Biotechnology (Dallas, TX, USA) and diluted 1:200. Secondary antibodies were diluted 1:1000. The solution used for calorimetric detection for 1 membrane consisted of 5 mL of 0.01 M acetate buffer pH 5.4, 5 μL of hydrogen peroxide and 50 μL of 3-Amino-9-ethyl-carbazole in DMF.

Microarray analyses

The cDNA was obtained from 1 μg of total DNase-treated RNA in a 20-μL reaction volume containing 200 units of Super-Script II Reverse Transcriptase (Invitrogen, Carlsbad, CA, USA) and 100 ng of random hexamers. The obtained cDNA was biotinylated at its 3' end using the Biotin 3' End DNA labeling kit (Thermo Scientific, Waltham, MA, USA). Microarray was conducted according to Roth *et al.* [66]. For hybridization, Human Cancer 3711 ElectraSense 4×2k array slides were utilized with 1609 DNA probes (Custom Array, Bothell, WA, USA). The detection kit employed for hybridization was CombiMatrix ElectraSense™ and contained Biotin Blocking Solution, Biotin Wash Solution, 3, 3′, 5, 5′-tetramethylbenzidine (TMB) Rinse, and TMB Substrate (CombiMatrix Corporation, USA). The ElectraSense™ application software was used to create a microarray image in gray scale for visualization purposes (Figure A and Table B in S1 File). The list of processes and pathways (Tables C and D in S1 File) of gene regulation in PC3 and PNT1A cell lines showing the comparisons between different treatments was created by gene ontology (GO) annotations and KEGG (Known and Predicted Protein-Protein Interactions) 10 software, respectively.

Supporting Information

S1 File. Fig A. ElectraSense Array Image. Graphic showing the number of genes regulated in the PC3 and PNT1A cell lines in response to different treatments. PNT1A (PNT1A cell line before treatment with Zn-S-NVC complex), PNT1A-Zn-S-NVC (PNT1A cell line after treatment with Zn-S-NVC complex), PC3 (PC3 cell line before treatment with Zn-S-NVC complex) and PC3-Zn-S-NVC (PC3 cell line after treatment with Zn-S-5-NVC complex). **Fig**

B. Stability testing of Zinc-Schiff base-Novicidin complex over one week under different pH conditions. A) pH = 3.8. B) pH = 6. C) pH = 7.2. D) pH = 9. **Table A. Primers used for quantitative RT-PCR. Table B. Lists of up- and/or down-regulated genes in all possible combinations between treatments:** A) PC3 *vs*. PNT1A. B) PNT1A-Zn-S-NVC *vs*. PNT1A. C) PC3-Zn-S-NVC *vs*. PC3. D) PC3-Zn-S-NVC *vs*. PNT1A-Zn-S-NVC. **Table C. Lists of up- and/or down-regulated genes in biological processes in PC3 and PNT1A cell lines after treatment with Zn-S-NVC complex by gene ontology (GO) annotations.** A) PC3 *vs*. PNT1A. B) PNT1A-Zn-S-NVC *vs*. PNT1A. C) PC3-Zn-S-NVC *vs*. PC3. D) PC3-Zn-S-NVC *vs*. PNT1A-Zn-S-NVC. **Table D. Lists of up- and/or down-regulated genes in various pathways in PC3 and PNT1A cell lines after treatment with Zn-S-NVC complex by KEGG 10 software.** A) PC3 *vs*. PNT1A. B) PNT1A-Zn-S-NVC *vs*. PNT1A. C) PC3-Zn-S-NVC *vs*. PC3. D) PC3-Zn-S-NVC *vs*. PNT1A-Zn-S-NVC.
(DOCX)

Acknowledgments

This research was performed under project CEITEC 2020 (LQ1601) with financial support from the Ministry of Education, Youth and Sports of the Czech Republic under the National Sustainability Programme II and GACR 16-18917S.

Author Contributions

Conceptualization: VM.

Formal analysis: VM YH MAMR AM HP DH ZH PK.

Methodology: VM YH.

Resources: PK VA.

Supervision: VA.

Writing – original draft: VM.

Writing – review & editing: PK ZH.

References

1. Jemal A, Bray F, Center MM, Ferlay J, Ward E, et al. (2011) Global Cancer Statistics. CA-Cancer J Clin 61: 69–90. doi: 10.3322/caac.20107 PMID: 21296855
2. de Bono JS, Oudard S, Ozguroglu M, Hansen S, Machiels JP, et al. (2010) Prednisone plus cabazitaxel or mitoxantrone for metastatic castration-resistant prostate cancer progressing after docetaxel treatment: a randomised open-label trial. Lancet 376: 1147–1154. doi: 10.1016/S0140-6736(10)61389-X PMID: 20888992
3. Biancardi MF, Santos FCA, Madi-Ravazzi L, Goes RM, Vilamaior PSL, et al. (2010) Testosterone Promotes an Anabolic Increase in the Rat Female Prostate (Skene's Paraurethral Gland) Which Acquires a Male Ventral Prostate Phenotype. Anat Rec 293: 2163–2175. doi: 10.1002/ar.21250. Epub 2010 Sep 9 PMID: 20830685
4. Lodemann U, Einspanier R, Scharfen F, Martens H, Bondzio A (2013) Effects of zinc on epithelial barrier properties and viability in a human and a porcine intestinal cell culture model. Toxicol Vitro 27: 834–843. doi: 10.1016/j.tiv.2012.12.019. Epub 2012 Dec 27 PMID: 23274768
5. Costello LC, Franklin RB (1998) Novel role of zinc in the regulation of prostate citrate metabolism and its implications in prostate cancer. Prostate 35: 285–296. doi: 10.1002/(sici)1097-0045(19980601)35:4%3C285::aid-pros8%3E3.0.co;2-f PMID: 9609552
6. Kambe T, Hashimoto A, Fujimoto S (2014) Current understanding of ZIP and ZnT zinc transporters in human health and diseases. Cell Mol Life Sci 71: 3281–3295. doi: 10.1007/s00018-014-1617-0 PMID: 24710731

7. Krizkova S, Kepinska M, Emri G, Rodrigo MAM, Tmejova K, et al. (2016) Microarray analysis of metallothioneins in human diseases-A review. J Pharm Biomed Anal 117: 464–473. doi: 10.1016/j.jpba.2015.09.031 PMID: 26454339
8. Hasumi M, Suzuki K, Matsui H, Koike H, Ito K, et al. (2003) Regulation of metallothionein and zinc transporter expression in human prostate cancer cells and tissues. Cancer Lett 200: 187–195. doi: 10.1016/s0304-3835(03)00441-5 PMID: 14568174
9. Franklin RB, Feng P, Milon B, Desouki MM, Singh KK, et al. (2005) hZIP1 zinc uptake transporter down regulation and zinc depletion in prostate cancer. Mol Cancer 4: 1–10. doi: 10.1186/1476-4598-4-32 PMID: 16153295
10. Costello LC, Franklin RB, Zou J, Feng P, Bok R, et al. (2011) Human prostate cancer ZIP1/zinc/citrate genetic/metabolic relationship in the TRAMP prostate cancer animal model. Cancer Biol Ther 12: 1078–1084. doi: 10.4161/cbt.12.12.18367 PMID: 22156800
11. Johnson LN, Cashman SM, Kumar-Singh R (2008) Cell-penetrating peptide for enhanced delivery of nucleic acids and drugs to ocular tissues including retina and cornea. Mol Ther 16: 107–114. doi: 10.1038/sj.mt.6300324 PMID: 17923842
12. Gaspar D, Veiga AS, Castanho MRB (2013) From antimicrobial to anticancer peptides. A review. Front Microbiol 4: 1–24. doi: 10.3389/fmicb.2013.00294 PMID: 24101917
13. Regberg J, Srimanee A, Langel U (2012) Applications of cell-penetrating peptides for tumor targeting and future cancer therapies. Pharmaceuticals 5: 991–1007. doi: 10.3390/ph5090991 PMID: 24280701
14. Dorosz J, Gofman Y, Kolusheva S, Otzen D, Ben-Tal N, et al. (2010) Membrane Interactions of Novicidin, a Novel Antimicrobial Peptide: Phosphatidylglycerol Promotes Bilayer Insertion. J Phys Chem B 114: 11053–11060. doi: 10.1021/jp1052248 PMID: 20690652
15. Osowole AA, Kolawole GA, Fagade OE (2008) Synthesis, characterization and biological studies on unsymmetrical Schiff-base complexes of nickel(II), copper(II) and zinc(II) and adducts with 2,2 '-dipyridine and 1,10-phenanthroline. J Coord Chem 61: 1046–1055. doi: 10.1080/00958970701482446
16. Kostova I, Saso L (2013) Advances in Research of Schiff-Base Metal Complexes as Potent Antioxidants. Curr Med Chem 20: 4609–4632. doi: 10.2174/09298673113209990149 PMID: 23834186
17. Allam A, Maigre L, Alimi M, de Sousa RA, Hessani A, et al. (2014) New Peptides with Metal Binding Abilities and Their Use as Drug Carriers. Bioconjugate Chem 25: 1811–1819. doi: 10.1021/bc500317u PMID: 25192490
18. Fonseca SB, Pereira MP, Kelley SO (2009) Recent advances in the use of cell-penetrating peptides for medical and biological applications. Adv Drug Deliv Rev 61: 953–964. doi: 10.1016/j.addr.2009.06.001 PMID: 19538995
19. Cermakova S, Herchel R, Travnicek Z, Sebela M (2010) Syntheses and magnetic properties of trinuclear trithiocyanurato-bridged manganese(II) complexes involving bidentate aromatic N-donor heterocycles. Inorg Chem Commun 13: 778–781. doi: 10.1016/j.inoche.2010.03.045
20. Kopel P, Wawrzak D, Langer V, Cihalova K, Chudobova D, et al. (2015) Biological Activity and Molecular Structures of Bis(benzimidazole) and Trithiocyanurate Complexes. Molecules 20: 10360–10376. doi: 10.3390/molecules200610360 PMID: 26053490
21. Barth A (2007) Infrared spectroscopy of proteins. Biochim Biophys Acta-Bioenerg 1767: 1073–1101. doi: 10.1016/j.bbabio.2007.06.004 PMID: 17692815
22. Kopel P, Sindelar Z, Klicka R (1998) Complexes of iron(III) salen and saloph Schiff bases with bridging dicarboxylic and tricarboxylic acids. Transit Met Chem 23: 139–142.
23. Maxim C, Pasatoiu TD, Kravtsov VC, Shova S, Muryn CA, et al. (2008) Copper(II) and zinc(II) complexes with Schiff-base ligands derived from salicylaldehyde and 3-methoxysalicylaldehyde: Synthesis, crystal structures, magnetic and luminescence properties. Inorg Chim Acta 361: 3903–3911. doi: 10.1016/j.ica.2008.03.013
24. Shit S, Chakraborty J, Samanta B, Rosair GM, Mitra S (2009) Synthesis, Structure and Fluorescence Properties of a Trinuclear Zn(II) Complex with N,N,O-donor Schiff Base Ligands and Bridging Acetates. Z Naturforsch (B) 64: 403–408. doi: 10.1515/znb-2009-0408
25. Voicescu M, Heinrich M, Hellwig P (2009) Steady-State and Time Resolved Fluorescence Analysis on Tyrosine-Histidine Model Compounds. J Fluoresc 19: 257–266. doi: 10.1007/s10895-008-0411-5 PMID: 18766301
26. Guzow K, Ganzynkowicz R, Rzeska A, Mrozek J, Szabelski M, et al. (2004) Photophysical properties of tyrosine and its simple derivatives studied by time-resolved fluorescence spectroscopy, global analysis, and theoretical calculations. J Phys Chem B 108: 3879–3889. doi: 10.1021/jp036721c

27. Rivlin N, Brosh R, Oren M, Rotter V (2011) Mutations in the p53 Tumor Suppressor Gene: Important Milestones at the Various Steps of Tumorigenesis. Genes Cancer 2: 466–474. doi: 10.1177/1947601911408889 PMID: 21779514

28. Krizkova S, Ryvolova M, Hrabeta J, Adam V, Stiborova M, et al. (2012) Metallothioneins and zinc in cancer diagnosis and therapy. Drug Metab Rev 44: 287–301. doi: 10.3109/03602532.2012.725414 PMID: 23050852

29. Pan TJ, Gao L, Wu GJ, Shen GQ, Xie S, et al. (2015) Elevated expression of glutaminase confers glucose utilization via glutaminolysis in prostate cancer. Biochem Biophys Res Commun 456: 452–458. doi: 10.1016/j.bbrc.2014.11.105 PMID: 25482439

30. Beenken A, Mohammadi M (2009) The FGF family: biology, pathophysiology and therapy. Nat Rev Drug Discov 8: 235–253. doi: 10.1038/nrd2792 PMID: 19247306

31. Haugsten EM, Wiedlocha A, Olsnes S, Wesche J (2010) Roles of Fibroblast Growth Factor Receptors in Carcinogenesis. Mol Cancer Res 8: 1439–1452. doi: 10.1158/1541-7786.MCR-10-0168 PMID: 21047773

32. Riedl S, Rinner B, Asslaber M, Schaider H, Walzer S, et al. (2011) In search of a novel target—Phosphatidylserine exposed by non-apoptotic tumor cells and metastases of malignancies with poor treatment efficacy. Biochim Biophys Acta-Biomembr 1808: 2638–2645. doi: 10.1016/j.bbamem.2011.07.026 PMID: 21810406

33. Deniaud E, Baguet J, Chalard R, Blanquier B, Brinza L, et al. (2009) Overexpression of Transcription Factor Sp1 Leads to Gene Expression Perturbations and Cell Cycle Inhibition. PLoS One 4: 1–13.

34. Borellini F, Glazer RI (1993) Induction of SP1-P53 DNA-binding heterocomplexes during granulocyte-macrophage colony-stimulating factor-dependent proliferation in human erythroleukemia cell line TF-1. J Biol Chem 268: 7923–7928. PMID: 8463313

35. Wang LW, Wei DY, Huang SY, Peng ZH, Le XD, et al. (2003) Transcription factor Sp1 expression is a significant predictor of survival in human gastric cancer. Clin Cancer Res 9: 6371–6380. PMID: 14695137

36. Chuang JY, Wu CH, Lai MD, Chang WC, Hung JJ (2009) Overexpression of Sp1 leads to p53-dependent apoptosis in cancer cells. Int J Cancer 125: 2066–2076. doi: 10.1002/ijc.24563 PMID: 19588484

37. Jackson P, Grimm MO, Kingsley EA, Brosius U, Antalis T, et al. (2002) Relationship between expression of KAI1 metastasis suppressor gene, mRNA levels and p53 in human bladder and prostate cancer cell lines. Urol Oncol 7: 99–104. doi: 10.1016/s1078-1439(01)00175-2 PMID: 12474542

38. Brooks CL, Gu W (2010) New insights into p53 activation. Cell Res 20: 614–621. doi: 10.1038/cr.2010.53 PMID: 20404858

39. Li Y, Kimura T, Huyck RW, Laity JH, Andrews GK (2008) Zinc-induced formation of a coactivator complex containing the zinc-sensing transcription factor MTF-1, p300/CBP, and sp1. Mol Cell Biol 28: 4275–4284. doi: 10.1128/MCB.00369-08 PMID: 18458062

40. Gong PF, Ogra Y, Koizumi S (2000) Inhibitory effects of heavy metals on transcription factor Sp1. Ind Health 38: 224–227. doi: 10.2486/indhealth.38.224 PMID: 10812846

41. Ogra Y, Suzuki K, Gong PF, Otsuka F, Koizumi S (2001) Negative regulatory role of Sp1 in metal responsive element-mediated transcriptional activation. J Biol Chem 276: 16534–16539. doi: 10.1074/jbc.M100570200 PMID: 11279094

42. Coyle P, Philcox JC, Carey LC, Rofe AM (2002) Metallothionein: The multipurpose protein. Cell Mol Life Sci 59: 627–647. doi: 10.1007/s00018-002-8454-2 PMID: 12022471

43. Sigel A, Sigel H, Sigel RKO (2009) Metallothioneins and Related Chelators.

44. Qin Y, Dittmer PJ, Park JG, Jansen KB, Palmer AE (2011) Measuring steady-state and dynamic endoplasmic reticulum and Golgi Zn2+ with genetically encoded sensors. Proc Natl Acad Sci U S A 108: 7351–7356. doi: 10.1073/pnas.1015686108 PMID: 21502528

45. Meplan C, Richard MJ, Hainaut P (2000) Metalloregulation of the tumor suppressor protein p53: zinc mediates the renaturation of p53 after exposure to metal chelators in vitro and in intact cells. Oncogene 19: 5227–5236. doi: 10.1038/sj.onc.1203907 PMID: 11077439

46. Costello LC, Feng P, Milon B, Tan M, Franklin RB (2004) Role of zinc in the pathogenesis and treatment of prostate cancer: critical issues to resolve. Prostate Cancer Prostatic Dis 7: 111–117. doi: 10.1038/sj.pcan.4500712 PMID: 15175662

47. Franklin RB, Ma J, Zou J, Guan Z, Kukoyi BI, et al. (2003) Human ZIP1 is a major zinc uptake transporter for the accumulation of zinc in prostate cells. J Inorg Biochem 96: 435–442. doi: 10.1016/s0162-0134(03)00249-6 PMID: 12888280

48. Cousins RJ, McMahon RJ (2000) Integrative aspects of zinc transporters. J Nutr 130: 1384S–1387S. PMID: 10801948

49. Franz MC, Anderle P, Burzle M, Suzuki Y, Freeman MR, et al. (2013) Zinc transporters in prostate cancer. Mol Asp Med 34: 735–741. doi: 10.1016/j.mam.2012.11.007 PMID: 23506906

50. Rodrigo MAM, Zitka O, Krejcova L, Hynek D, Masarik M, et al. (2014) Electrochemical Microarray for Identification Pathogens: A Review. Int J Electrochem Sci 9: 3431–3439.

51. Lin P, Sun XC, Feng T, Zou HF, Jiang Y, et al. (2012) ADAM17 regulates prostate cancer cell proliferation through mediating cell cycle progression by EGFR/PI3K/AKT pathway. Mol Cell Biochem 359: 235–243. doi: 10.1007/s11010-011-1018-8 PMID: 21837402

52. Lose F, Batra J, O'Mara T, Fahey P, Marquart L, et al. (2013) Common variation in Kallikrein genes KLK5, KLK6, KLK12, and KLK13 and risk of prostate cancer and tumor aggressiveness. Urol Oncol-Semin Orig Investig 31: 635–643. doi: 10.1016/j.urolonc.2011.05.011 PMID: 21741862

53. Hodgson MC, Deryugina EI, Suarez E, Lopez SM, Lin D, et al. (2014) INPP4B suppresses prostate cancer cell invasion. Cell Commun Signal 12: 1–14. doi: 10.1186/s12964-014-0061-y PMID: 25248616

54. Sirma H, Broemel M, Stumm L, Tsourlakis T, Steurer S, et al. (2013) Loss of CDKN1B/p27Kip1 expression is associated with ERG fusion-negative prostate cancer, but is unrelated to patient prognosis. Oncol Lett 6: 1245–1252. doi: 10.3892/ol.2013.1563 PMID: 24179503

55. Willingham SB, Volkmer JP, Gentles AJ, Sahoo D, Dalerba P, et al. (2012) The CD47-signal regulatory protein alpha (SIRPa) interaction is a therapeutic target for human solid tumors. Proc Natl Acad Sci U S A 109: 6662–6667. doi: 10.1073/pnas.1121623109 PMID: 22451913

56. Franklin RB, Costello LC (2009) The Important Role of the Apoptotic Effects of Zinc in the Development of Cancers. J Cell Biochem 106: 750–757. doi: 10.1002/jcb.22049 PMID: 19160419

57. Sunderman FW (1995) The influence of zinc on apoptosis. Ann Clin Lab Sci 25: 134–142. PMID: 7785963

58. Eroglu C, Secme M, Bagci G, Dodurga Y (2015) Assessment of the anticancer mechanism of ferulic acid via cell cycle and apoptotic pathways in human prostate cancer cell lines. Tumor Biol 36: 9437–9446. doi: 10.1007/s13277-015-3689-3 PMID: 26124008

59. Coffey RNT, Watson RWG, Fitzpatrick JM (2001) Signaling for the caspases: Their role in prostate cell apoptosis. J Urol 165: 5–14. doi: 10.1097/00005392-200101000-00003 PMID: 11125352

60. Truong-Tran AQ, Carter J, Ruffin RE, Zalewski PD (2001) The role of zinc in caspase activation and apoptotic cell death. Biometals 14: 315–330. doi: 10.1007/978-94-017-3728-9_7 PMID: 11831462

61. Safe S, Jin UH, Hedrick E, Reeder A, Lee SO (2014) Minireview: Role Of Orphan Nuclear Receptors in Cancer and Potential as Drug Targets. Mol Endocrinol 28: 157–172. doi: 10.1210/me.2013-1291 PMID: 24295738

62. Shan ZJ, Hou QL, Zhang N, Guo L, Zhang XH, et al. (2014) Overexpression of oxidored-nitro domain containing protein 1 induces growth inhibition and apoptosis in human prostate cancer PC3 cells. Oncol Rep 32: 1939–1946. doi: 10.3892/or.2014.3407 PMID: 25118646

63. Stark JL, Mehla K, Chaika N, Acton TB, Xiao R, et al. (2014) Structure and Function of Human DnaJ Homologue Subfamily A Member 1 (DNAJA1) and Its Relationship to Pancreatic Cancer. Biochemistry 53: 1360–1372. doi: 10.1021/bi401329a PMID: 24512202

64. Zhu JH, Hong DF, Song YM, Sun LF, Wang ZF, et al. (2013) Suppression of Cellular Apoptosis Susceptibility (CSE1L) Inhibits Proliferation and Induces Apoptosis in Colorectal Cancer Cells. Asian Pac J Cancer Prev 14: 1017–1021. doi: 10.7314/APJCP.2013.14.2.1017 PMID: 23621178

65. Evans BC, Nelson CE, Yu SS, Beavers KR, Kim AJ, et al. (2013) Ex Vivo Red Blood Cell Hemolysis Assay for the Evaluation of pH-responsive Endosomolytic Agents for Cytosolic Delivery of Biomacromolecular Drugs. J Vis Exp 2013: 1–6. doi: 10.3791/50166 PMID: 23524982

66. Roth KM, Peyvan K, Schwarzkopf KR, Ghindilis A (2006) Electrochemical detection of short DNA oligomer hybridization using the CombiMatrix ElectraSense Microarray reader. Electroanalysis 18: 1982–1988. doi: 10.1002/elan.200603603

5.2.2. Research article III

Amitava Moulick, Zbynek Heger, **Vedran Milosavljevic**, Lukas Richtera, Joaquin Barroso-Flores, Miguel Angel Merlos Rodrigo, Hana Buchtelova, Robert Podgajny, David Hynek, Pavel Kopel and Vojtech Adam. Visualization of Cell Membrane Damage by Using Quantum Dots Modified with a Gadolinium-Schiff Base Complex. PNAS (Submitted - 2017).

Participation in the work of the author Vedran Milosavljevic: experimental part 30%.

The exchange of metabolic products between the cytoplasm and cellular organelles or intra- and intercellular transfer depends on biological activity of membranes [204]. It is also well known that wounded eukaryotic cells have ability to fast repair their damaged membrane very fast [205]. Cell penetrating peptides have a great ability to deliver various types of biologically active molecules, including nucleic acids, proteins or drugs agents, by direct membrane penetration or pore formation [23]. Transport of CPPs trough cell membrane by direct penetration may induce some serious membrane injuries. Investigation of such injuries is important, due to evaluation of CPP activity used in drug delivery and determination of cell membrane recovery level.

The aim of this study was to design a novel fluorescence agent CdTe, surface modified with gadolinium-Schiff base complex (Gd-SB) used for imaging purposes. Fluorescence characterization of new imaging agent was conducted by spectroscopy and fluorescence microscopy analysis. Structural characterization of product was done by MALDI-TOF MS, HR-TEM, FTIR and electrochemical analysis. Study of membrane integrity was performed under unfavorable conditions (including osmolysis), by application of CPP Hecate.

Based on obtained results, a novel fluorescence agent has been successfully designed - CdTe QDs with Gd-SB (GdQDs) surface modification in aqueous medium. The novel fluorescence agent shows great potential in real time imaging of membrane injuries. After inflicting an injury to membrane by sonication, protein membrane becomes highly available for interaction with designed fluorescence agent, which can be confirmed by staining of cellular debris by the GdQDs. Together with cytosol staining, fluorescence agent shows good bounding to nuclear membranes,

after Hoechst counterstaining of nuclei. Hecate-induced membrane damage and binding of GdQDs was analyzed using Cryo-electron microscopy. Results show that increasing peptide concentration causes membrane disruption in the size of hundreds of nm and cytosol leaking, while the GdQDs stain only the part of cell membrane damaged by peptide, indicating inability of GDQDs to translocate over cell membrane. These results lead to conclusion that GdQDs can serve as a unique tool for evaluation of CPP activity and determination of cell membrane integrity in various undesirable conditions.

Visualization of Cell Membrane Damage by Using Quantum Dots Modified with a Gadolinium-Schiff Base Complex

Amitava Moulick[a,b], Zbynek Heger[a,b], Vedran Milosavljevic[a,b], Lukas Richtera[a,b], Joaquin Barroso-Flores[c], Miguel Angel Merlos Rodrigo[a,b], Hana Buchtelova[a,b], Robert Podgajny[d], David Hynek[a,b], Pavel Kopel[a,b] and Vojtech Adam[a,b]*

[a]*Department of Chemistry and Biochemistry, Mendel University in Brno, Zemedelska 1, CZ-613 00 Brno, Czech Republic*

[b] *Central European Institute of Technology, Brno University of Technology, Purkynova 123, CZ-612 00 Brno, Czech Republic*

[c] *Centro Conjunto de Investigación en Química Sustentable UAEM-UNAM, Carretera Toluca–Atlacomulco Km 14.5, Unidad San Cayetano, CP-50200 Toluca, Estado de Méxicod*

[d]*Faculty of Chemistry, Jagiellonian University, Ingardena 3, PL-30060 Krakow, Poland*

***Corresponding author**

Vojtech Adam, Department of Chemistry and Biochemistry, Mendel University in Brno, Zemedelska 1, CZ-613 00 Brno, Czech Republic; E-mail: vojtech.adam@mendelu.cz, Tel.: +420-5-4513-3350; Fax: +420-5-4521-2044

Classification

PHYSICAL SCIENCES, Chemistry

Abstract

Despite the indispensability of cell membranes, there is still a lack of methods that allow simple real-time spatial visualization of their integrity. Herein, we describe novel hybrid nanostructures formed from a CdTe core and gadolinium-Schiff base shell (GdQDs) and possessing a diameter of 11±2 nm with an inter-planar distance of 0.31 nm. GdQDs have exceptional colloidal stability (ζ potential, -43.6±0.13 mV) and bright red fluorescence (quantum yield of up to 40.5%). We show that GdQDs can label cellular membrane damage, as shown for damages induced by exposure to cell-penetrating peptides (CPPs), cytostatic agents, mechanical puncture or starvation. The GdQDs preferentially interacted with NHE-RF2 localized on endomembrane systems and nuclear membranes, and thus becoming available for interaction after membrane disruption. Overall, GdQDs could serve as a unique and versatile tool for applications requiring real-time observations of membrane damage, including the testing of CPPs and drugs and observing host-pathogen interactions.

Keywords: Cell-penetrating peptides; Core-shell; Fluorescence labelling; Nanotechnologies; NHE-RF2

Significance

The submitted manuscript deals with discovering, testing and optimizing of novel assay for studying of a cell injury. Particularly, we developed a novel core-shell structure formed from CdTe QDs with Gd-SB surface modification with the capability of real-time spatial imaging of membrane injuries. Our synthetic strategy allows for direct synthesis of core-shell GdQDs in an aqueous medium instead of in organic solvents, making the synthesis simple and environmentally friendly. Based on the results discussed in the manuscript, we anticipate that GdQDs can be applied as an inexpensive, versatile and fast tool for studying the integrity of cell membranes.

\body

Biological membranes play a pivotal role in various cellular processes as they control the flux of metabolites between the cytoplasm and cellular organelles. Mitochondrial and chloroplast thylakoid membranes are indispensable for the energy supply of most cells (1). Membranes also participate in intra- and intercellular communication and control the transfer of information between organs in the form of action potentials.

Although it has been known for several decades that wounded eukaryotic cells tend to repair their membranes within a few seconds (2), many pathological states result from membrane injury. For instance, bacterial toxins (e.g., haemolysins produced by *Staphylococcus aureus*, *Escherichia coli* or *Streptococcus* spp. and many others(3)) or non-enveloped viruses (e.g., *Adenoviridae* and *Picornaviridae*) directly penetrate the host membranes(4). A few reports have also provided evidence of a link between the conformational changes in amyloid-β that are accompanied by oligomerization and neuronal membrane penetration and the development of Alzheimer's disease (5-7). Notably, membrane penetration and pore formation is a specific effect of a large group of cell-penetrating peptides (CPPs) with a broad spectrum of applications, including delivery of nucleic acids, proteins or contrast agents into the cell(8). Moreover, CPPs are considered a potent alternative to conventional antimicrobial and antiviral agents (9). This short overview indicates the importance of the investigation of membrane injuries. However, to the best of our knowledge, methods applicable for such purposes are lacking, and the few existing methods have specific drawbacks. For instance, Martinez and colleagues reported a high-resolution approach to the spatial visualization of adenovirus entry to cells. However their method relies on the stable expression of galectin-3 fused to a fluorophore, and thus lacks versatility(10). Membrane penetration can be further studied using electron and probe

microscopy techniques(11) but without the possibility of the real-time imaging of living cells. Hence, novel sensitive probes with broad applicability are currently of a high interest.

Advanced nanomaterials are a fast evolving group of structures with multifunctional properties. Semiconductor nanocrystals called quantum dots (QDs) are among the most promising advanced nanomaterials. Currently, a wide range of forming materials, functional coatings, and bioconjugate techniques are available for QDs, demonstrating their applicability (12). The synthesis of core-shell QDs is highly desirable because the core is stabilized with various surface ligands or caps to promote solubility in aqueous media and specific functionalities (13). Therefore, surface modification is vital for QDs in biological applications, and surface-modified QDs have been used for a myriad of applications, including *in vitro* diagnostics, energy transfer-based sensing, drug delivery, theranostics and *in vivo* imaging(14-16). However, to the best of our knowledge, QDs have not been applied to living cells imaging of membrane injuries.

Hence, the aim of our study was to design and synthesize QDs formed from CdTe surface-modified with a novel gadolinium-Schiff base complex (Gd-SB) for use in living cells imaging. The resulting nanostructure (hereinafter abbreviated as GdQDs) demonstrated clear red emission and exceptional colloidal properties. Fluorescence microscopy experiments in various unfavourable conditions, including osmolysis or the administration of the CPP Hecate(17) or platinum cytostatics (carboplatin, cisplatin), revealed that GdQDs are highly suitable not for specifically and sensitively visualizing cellular membrane damage. Further fragmentation by matrix-assisted laser desorption/ionization time-of-flight mass spectrometry (MALDI-TOF MS) indicated that these GdQDs preferentially interact with the Na^+/H^+ exchange regulatory cofactor NHE-RF2, which is a scaffold protein that supports the actin cytoskeleton(18). We anticipate that our novel GdQDs will be applicable to a broad range of applications, such as evaluation of

CPP activity, determination of cell membrane status and recovery in various undesirable conditions, and observation of host-pathogen interactions.

Results

Characterization of GdQDs

Fig. 1a shows the absorbance and fluorescence spectra of the GdQDs. The fluorescence emission maximum of the GdQDs was observed at 630 nm. Under UV transillumination (λ = 312 nm), the GdQDs solution displayed a dark red colour. The highest photoluminescence quantum yield for the prepared GdQDs was 40.5%. The average particle size and the particle size distribution of the prepared GdQDs were analysed by high-resolution transmission electron microscopy (HR-TEM, Fig. 1b and 1c) and dynamic light scattering (DLS, Fig. 1d). The HR-TEM images revealed the crystallinity of GdQDs, in which the distinct planes of the crystal structure can be observed. The inter-planar distance was found to be 0.31 nm, which is in accordance with the inter-planar spacing of CdTe QDs(19). The diameter of the GdQDs (11±2 nm) was clearly larger than the diameter of the CdTe QDs (7±2 nm), which is in agreement with the assumed surface modification of the QDs with Gd-SB. The modification also led to a change in the ζ potential from -35±0.17 mV (for CdTe QDs) to -43.6±0.13 mV (for GdQDs), reflecting the higher stability of GdQDs. The prepared GdQDs showed good stability in aqueous solution for several months.

The FTIR spectrum of the GdQDs is shown in Fig. 1e. The medium intensity peaks near 652 cm^{-1} and 842 cm^{-1} are characteristic of thiol-containing compounds and attributable to the ν(C-S) vibration of mercaptosuccinic acid (MSA) on the GdQDs surface. The very intense peaks near 1566 and 1381 cm^{-1} are attributed to ν_{as}(COO) and ν_{s}(COO) vibrations, respectively; however,

the peak near 1566 cm^{-1} probably overlaps with the ν(C=N) vibration of the Schiff base. A weak peak near 1250 cm^{-1} is attributed to the ν(C-N) vibration of heterocyclic rings (20).

We also sought to demonstrate the presence of gadolinium in the sample and to explore its possible utilization for magnetic resonance imaging. The DC moment (*H*) curve measured in the range -7 to +7 T is presented in Fig. 1f (open circles). Its shape is reminiscent of the presence of paramagnetic species in the measured sample, and its course is reproduced well by the simulated curve (blue line) based on equations 1-3, including the Brillouin function B_S for S = 7/2, the Landé factor g = 1.95 (expected for the almost isotropic character of GdQDs) and a scaling factor of 0.047. The DC moment (*T*) curve (Fig. 1g) is reproduced well by Curie's law (eq. 4-5), including a term for the diamagnetic contribution (foil and intrinsic diamagnetism of the material) and the relevant scaling factor. These results suggest that the Gd^{3+} ions are incorporated in the GdQDs material.

$$\text{DC moment } (H) \sim M = Ng\beta SBS(y) \qquad \text{(eq. 1)}$$

$$BS(y) = \frac{2S+1}{2S}\coth\left(\frac{2S+1}{2S}y\right) - \frac{1}{2S}\coth\left(\frac{1}{2S}y\right) \qquad \text{(eq. 2)}$$

$$y = g\beta SH/kT \qquad \text{(eq. 3)}$$

$$\text{DC moment } (T) \sim \chi = \frac{para}{T} - \frac{diam}{T} \qquad \text{(eq. 4)}$$

$$para \sim 0.125g2S(S+1) \qquad \text{(eq. 5)}$$

where *N* is the Avogadro constant, *g* is the Landé factor, *S* is the spin, *β* is the Bohr magneton, *H* is the magnetic field, *k* is the Boltzmann constant, *T* is the temperature, and *para* and *diam* are the paramagnetic and diamagnetic contributions, respectively, to the measured magnetic moment.

Energy dispersive X-ray (EDX) analysis confirmed the presence of all elements forming the GdQDs (*SI Appendix*, Fig. S1). Furthermore, the electrochemical responses of the GdQDs were

studied by using the Brdicka reaction. The strongest electrochemical signals of the CdTe QDs or GdQDs are attributed to their surface modification by MSA (characteristic peaks MSA1 and MSA2, Fig. 1h-I, *SI Appendix* Fig. S2 and S3). After surface passivation of the CdTe QDs with MSA, peak MSA2 (−1.55 V) disappeared (Fig. 1h-ii), indicating that the –SH groups of MSA had become electrochemically inactive. The voltammogram of Gd-SB (no –SH moieties) contains two relatively weak signals (Gd-SB1 and Gd-SB2, Fig. 1h-iii). Notably, Gd-SB modification is likely to cause the -SH moieties of MSA to become electrochemically active, which was observed as an increase in signal at -1.55 V (Fig. 1h-iv). The Cd peak of the CdTe QDs shifted from −0.83 V to −0.80 V after modification with Gd-SB.

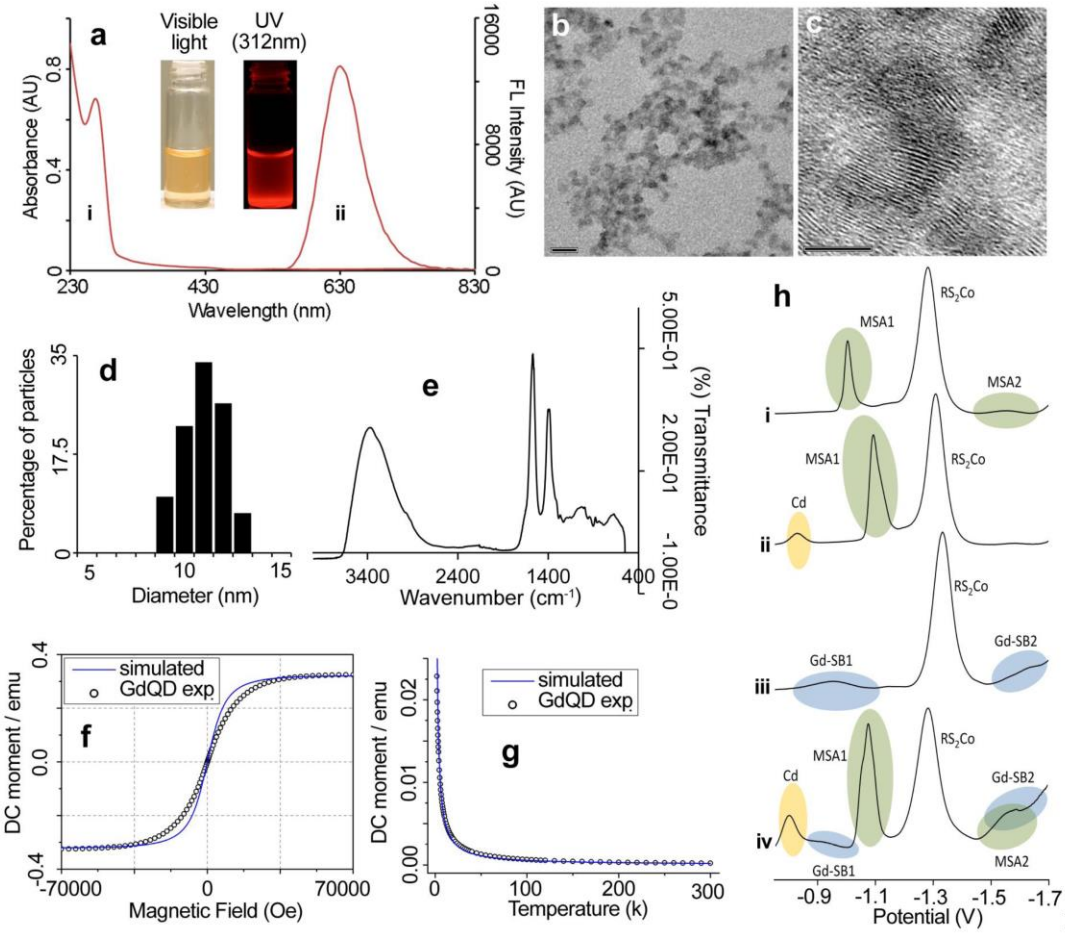

Figure 1

Fig. 1. Characterization of GdQDs. (**a**) Absorption (**i**) and fluorescence (**ii**) spectra of the GdQDs. Photographs of the GdQDs under visible and UV (312 nm) light are shown in the inset. (**b**) and (**c**) HR-TEM images of the GdQDs; scale bars are 20 and 5 nm, respectively. (**d**) DLS measurements of the GdQDs. Column charts indicate the size of the GdQDs. (**e**) FTIR spectra of the GdQDs. (**f** and **g**) Magnetic characteristics of the GdQDs: (**f**) magnetic field dependence of the DC moment (T = 2 K) and (**g**) thermal dependence of the DC moment (H = 1 kOe) (**o** - experimental points, **–** simulated curves). (**h**) Comparison of the electrochemical signals of MSA (**i**), CdTe QDs (**ii**), Gd-SB (**iii**) and GdQDs (**iv**). RS_2Co: typical signal from Brdicka electrolyte; MSA1 and 2: signals from MSA; Cd: signal from Cd^{2+} in the QDs (CdTe or GdQDs); Gd-SB1 and 2: signals from Gd-SB.

Molecular Modelling of GdQDs structure

Gd-SB is not planar but rather resembles a dextrorotatory helicene. Calculation of the Wiberg bond indexes (WBIs)(21) for Gd-SB indicated that the cation is held in the cavity by electrostatic interactions since no WBI involving Gd^{3+} exhibited a value close to 1.0, which would be indicative of a covalent bond. The highest WBIs calculated for Gd^{3+} were 0.16; 0.21 and 0.17 with the neighbouring N atoms. The molecular electrostatic potential mapped onto the isodensity surface is shown in *SI Appendix* Fig. S4a. The HOMO (*SI Appendix* Fig. S4b) in Gd-SB is mainly composed of the $2sp^3$ orbitals of electron lone pairs on the amino groups and the π orbitals on both pyridine rings, and the LUMO (*SI Appendix* Fig. S4c) consists mainly of the empty 5*d* orbital on Gd. Only those orbitals corresponding to the alpha density are shown in the figures for the sake of clarity. An MSA molecule was placed on the 100 face of a 2×2×1 CdTe cell and optimized at the M06-2X/lanl2dz level of theory while all Cd and Te atoms remained frozen in order to assess their coordination to the surface both in their neutral (*SI Appendix* Fig. S4d) and anionic (*SI Appendix* Fig. S4e) forms, with the latter are being the relevant deprotonated form at physiological pH. In the neutral state, MSA binds to CdTe through a single carboxylic group, whereas both carboxylate groups bind to CdTe in the anionic form, leaving the mercapto group to interact through available electron lone pairs with two Cd atoms on the

surface, which is indicative of its Lewis acidity. In both cases, the sulphur atom interacts closely with the surface through its basic electron lone pairs.

The complete system under study, consisting of a frozen layer of CdTe (100 face), two MSA molecules and the pre-optimized Gd-SB, was further optimized with the PM6 semiempirical Hamiltonian, and the final geometry is shown in *SI Appendix* Fig. S4f. Both MSA anions retain their original binding towards the CdTe surface and retain the Gd-SB exclusively through electrostatic interactions, allowing for strong binding of the complex on the surface.

GdQDs fluorescence spatially indicate the exact point of the plasma membrane damage

After pre-incubation of cells with CPP Hecate, the GdQDs showed the exact point of the damage on the plasma membrane by fluorescing bright red (Fig. 2). The extent of membrane injury was observed to increase with increasing concentration of Hecate. We also stained cells without Hecate treatment, and no fluorescence was observed, which showed that the GdQDs can only bind to the damaged portion of the plasma membrane. The fluorescence spectra of 5000 cells pre-incubated with Hecate and stained with GdQDs are shown in Fig. 2. The fluorescence intensity of the GdQDs attached to the damaged plasma membrane increased with increasing concentration of Hecate. The same experiment was also carried out using CdTe QDs, and we did not detect any fluorescent signal from the cells pre-incubated with Hecate (data not shown). The membrane integrity of the Hecate-untreated and -treated cells was also assessed by double staining with fluorescein diacetate (FDA) and propidium iodide (PI). The untreated cells fluoresced bright green and were thus considered viable, and the red fluorescence emitted by the cells treated with Hecate confirmed the damages to the plasma membrane caused by the treatment. The cytotoxicity of the characterized GdQDs was further evaluated using XTT assay

cells and compared to the unmodified CdTe QDs (*SI Appendix* Fig. S5). The formation of the Gd-SB shell resulted in a pronounced increase in the biocompatibility of the QDs, which is pivotal for applications in living cell cultures.

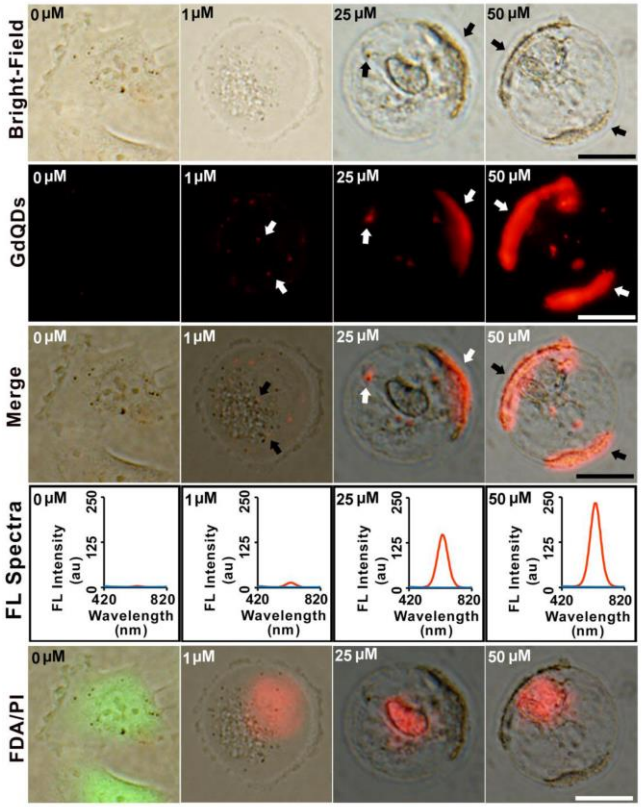

Fig. 2. Detection of plasma membrane damage to cells using GdQDs. Cells were treated with different concentrations (indicated at the top of each figure) of Hecate to damage the plasma membrane and subsequently stained with GdQDs. Pictures of the cells were taken with a fluorescence microscope. Arrows indicate some of the damaged areas of the plasma membrane. The fluorescence spectra of 5000 Hecate-untreated and -treated cells (stained by GdQDs) are shown in the fourth row. The blue and red lines indicate the control (without GdQDs staining) and sample (with GdQDs staining) cells, respectively. The membrane integrity of the PC-3 cells was assessed by double staining with FDA (green) and PI (red). The merged FDA/PI-staining and bright-field images are shown in the fifth row. The length of scale bar is 20 µm.

We further analysed the Hecate-induced membrane damage and subsequent binding of GdQDs using Cryo-electron microscopy. Representative Cryo-FIB-SEM micrograph of membrane of intact non-treated cell is depicted in Fig. 3a. Pre-incubation with Hecate caused obvious signs of

membrane disruptions in the size of hundreds of nm (Fig. 3b), which corresponds to the size of spots determined by GdQDs labeling. Moreover, Cryo-TEM micrographs (Fig. 3c and 3d) revealed a significant clustering of GdQDs within the disrupted regions.

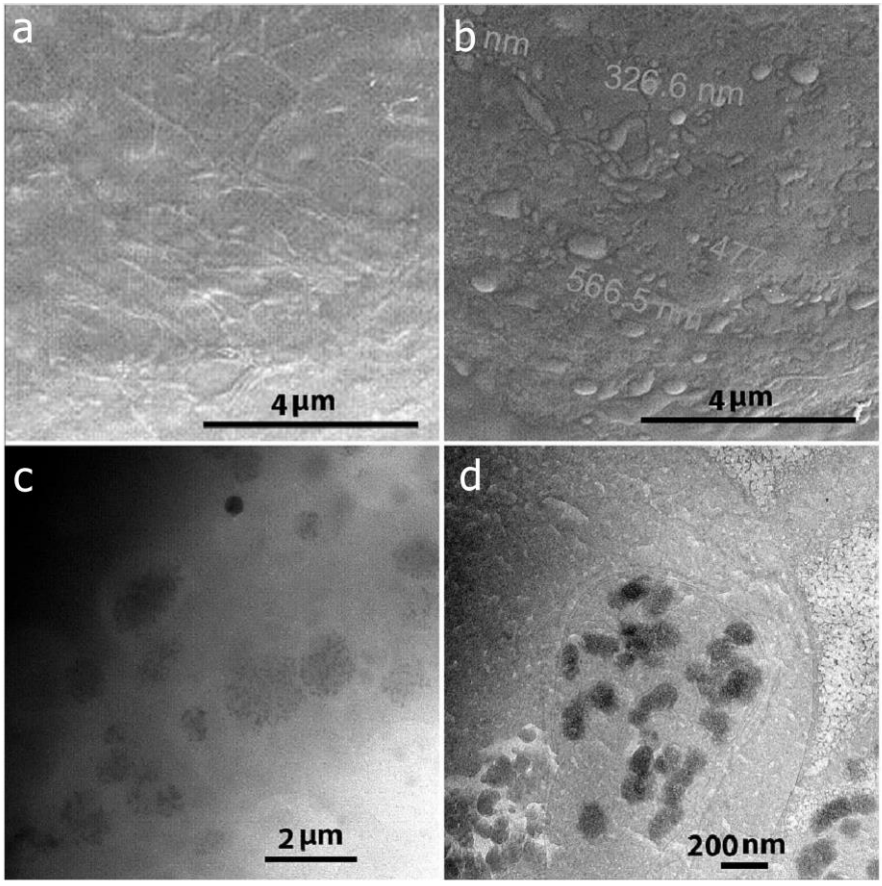

Fig. 3. Cryo-electron microscopy of membrane damage. Cryo-FIB-SEM micrographs of a membrane of (**a**) Hecate-untreated and (**b**) Hecate-treated (25 µM) cell showing obvious signs of membrane damages. (**c**) and (**d**) Cryo-TEM micrographs of GdQDs clustering within the membrane damage caused due to Hecate pre-incubation.

To check that the fluorescent signals from the GdQDs did not arise from any influence of the pre-incubation with Hecate, we punctured the cells mechanically with a glass capillary and subsequently stained them with the GdQDs. Fig. 4a clearly shows that the GdQDs were attached to the damaged portion of the cell. The bright red fluorescence denotes the exact area of penetration of the cell membrane.

Furthermore, approximately 5000 cells were completely disrupted by sonication, and the cell debris was then air-dried on a glass slide and stained with the GdQDs (Fig. 4b). The bright red fluorescence emitted from the cell debris confirmed that the GdQDs directly binds to almost all fragments of disrupted cells.

In a separate experiment, the cells were partially disrupted by osmosis induced by placing the cells in deionized autoclaved water. The cells were stained with the GdQDs and counterstained with Hoechst 33342. The red fluorescence-emitting GdQDs bound strongly to the nuclear membrane and to the cytoplasm (Fig. 4c).

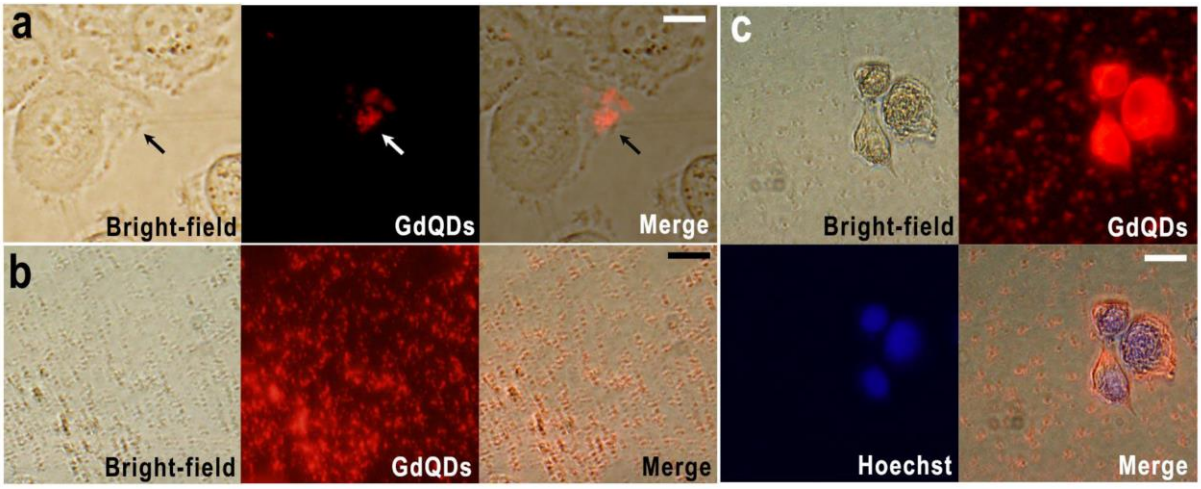

Fig. 4. GdQDs-based visualization of mechanical damage and destruction. (**a**) Micrograph of PC-3 cells that had been mechanically punctured using a glass capillary and stained with GdQDs. The damaged portion of the cells is indicated by an arrow. (**b**) Micrograph of the debris of PC-3 cells stained by GdQDs. The PC-3 cells were disrupted by sonication without Hecate treatment. (**c**) PC-3 cells semi-disrupted by osmosis, stained with GdQDs, and counterstained with Hoechst 33342. The length of scale bar is 20 μm.

NHE-RF2 sequence motif GEQGYGFHLHGE is a preferential target for GdQDs binding

To investigate which component or biomolecule in the cells was responsible for binding to the GdQDs, a graphene oxide (GO) film was prepared on a glass coverslip and fully covered by GdQDs. Then, the cell suspension was incubated with the GdQDs immobilized on the GO film

and analysed by MALDI-TOF in LIFT mode (Fig. 5a). The results revealed the presence of a GEQGYGFHLHGE (*m/z* 1329.806 Da) sequence motif belonging to the Na(+)/H(+) exchange regulatory cofactor protein (NHE-RF2, Mass Score 48.6, Swissport No. SLC9A3R2), which is localized on endomembrane systems, the nucleus, the apical cell membrane and the peripheral membrane (Fig. 5b).

We NHE-RF2 synthesized the GEQGYGFHLHGE and incubated it with GdQDs immobilized on a GO film. After washing, we confirmed the presence of the NHE-RF2 protein motif, showing its specific affinity for GdQDs. No significant interactions with GdQDs were identified for other tested peptides (GFHIDPEALKGF, LARLPVEPHIGK, TIRFTVWLHGV, GSSQHLEHIPPK, PRSIYLCRHGE, and HSPELTTPPGHGE).

The GEQGYGFHLHGE was further manually docked on top of the optimized GdQDs and optimized using molecular mechanics (Gaussian 09) with the universal force field (UFF) considering all atoms in the GdQDs to be fixed in rigid spheres in order to provide a rough description of the interaction between this peptide and the GdQDs. Both ends of the peptide interacted weakly with the GdQDs surface, whereas the middle portion of the peptide wrapped around the Gd-SB, presumably mostly through electrostatic interactions (Fig. 5c). The NHE-RF2 sequence motif appears to interact preferentially with the GdQDs through the electron-rich and hydrophobic residues located in the middle, namely Tyr and Phe.

Finally, anti-NHE-RF2 antibodies confirmed the presence of NHE-RF2 within membrane damage, caused by pre-incubation with Hecate. Fig. 5d demonstrates that both, GdQDs and anti-NHE-RF2 staining resulted in similar fluorescence patterns.

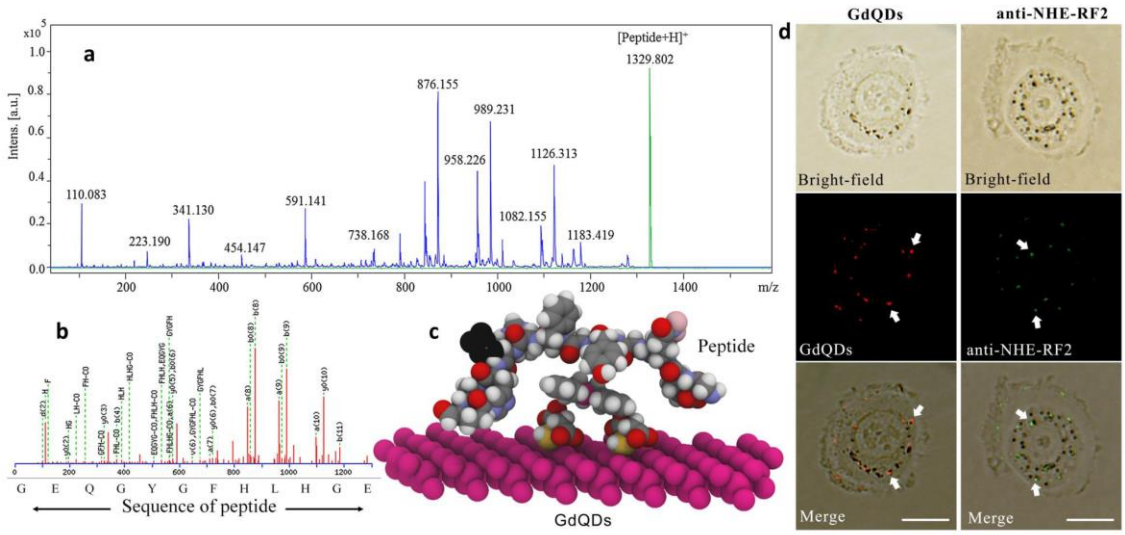

Fig. 5. GdQDs bind to NHE-RF2 scaffold protein. (**a**) MALDI-TOF MS spectrum of the peptide, part of NHE-RF2 sequence, bound to GdQDs (green line) and spectrum of the peptide (*m/z* 1329.826 Da) after MALDI-TOF fragmentation. Spectra were measured in a DHB matrix in TA30 at a maximum energy of 43.2 µJ with a repetition rate of 2000 Hz and 20 sub spectra. (**b**) LIFT-TOF/TOF spectrum and peptide mass fingerprint of *m/z* 1329.826 Da with assignment of the identified sequence: GEQGYGFHLHGE. The LIFT mass spectra were acquired in positive ion mode. (**c**) Peptide sequence that had been manually docked on top of the optimized GdQDs ensemble and optimized using molecular mechanics with the UFF, considering all atoms in the GdQDs as fixed and rigid spheres in order to provide a rough description of the interaction between the peptide and the GdQDs. (**d**) Comparison between post-Hecate pre-incubation GdQDs staining (*left*) and anti-NHE-RF2 immunostaining (*right*), which shows similar damage patterns. The length of scale bar is 20 µm.

GdQDs are applicable for visualization of the status of cell membrane

Cells were grown without changing the medium to deplete the nutrients and stained with GdQDs. Under a microscope, we observed small injuries to the plasma membrane of the cells, which were probably caused by cells starvation in unfavourable environmental conditions (Fig. 6a). This information helped us determine the membrane integrity status of the cells.

In the next experiment, cells were pre-incubated with two different conventional chemotherapeutic agents, carboplatin and cisplatin. GdQDs staining revealed significantly different effects of these two chemotherapeutic agents on the plasma membrane (Fig. 6b and 6c).

We anticipate that GdQDs could be thus applicable for simple and fast screening of plasma membrane health status of cells exposed to various unfavourable conditions.

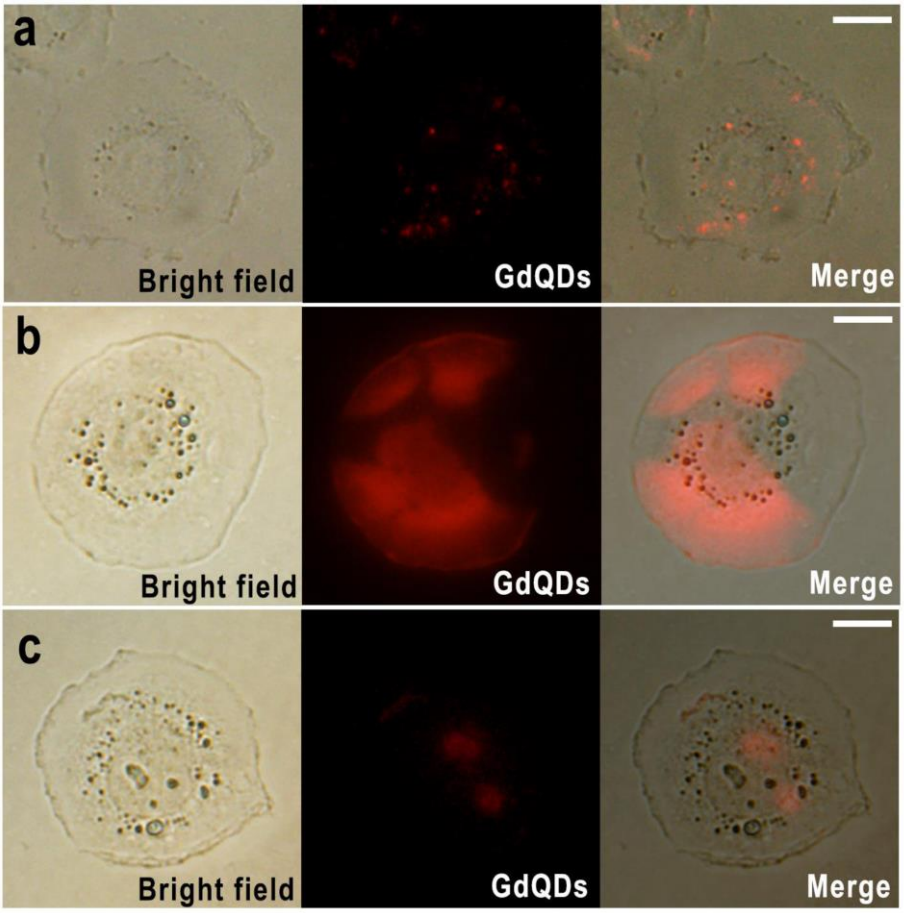

Fig. 6. Utilization of GdQDs for visualization of membrane damage caused by unfavourable conditions. (**a**) Micrographs of PC-3 cells that had been cultured in medium without exchange for 7 days and stained with GdQDs. The red fluorescent spots indicate the presence of damage on the plasma membrane caused by the depleted medium, in which most of the nutrients had already been consumed by the cells. Micrographs of cells treated with (**b**) carboplatin (10 μM) or (**c**) cisplatin (10 μM) for 12 h and subsequently stained with GdQDs. Different amounts of red fluorescence indicate distinct effects of the chemotherapeutic drugs on the plasma membrane. The length of scale bar is 20 μm.

Discussion

We developed a novel core-shell structure formed from CdTe QDs with Gd-SB surface modification with the capability of real-time spatial imaging of membrane injuries. Our synthetic strategy allows for direct synthesis of core-shell GdQDs in an aqueous medium instead of in organic solvents, making the synthesis simple and environmentally friendly. Similar core-shell nanostructured materials have recently received increasing attention owing to their exceptional properties and broad range of biological applications, including *in vivo* imaging(22), magnetic resonance imaging(23), drug delivery and tissue engineering(24). Nevertheless, to the best of our knowledge, there are no such methods for the visualization of membrane disruptions. Notably, we successfully designed and used GdQDs to visualize membrane damage caused by the CPP Hecate, mechanical puncturing, osmosis, starvation and conventional cytostatics. Thus, we anticipate that GdQDs will be applicable as an inexpensive, versatile and fast tool for studying the integrity of cell membranes.

Compared with other existing methods for studying membrane disruptions, including electron and probe microscopy(11) or methods utilizing cellular systems with the stable expression of fluorophores(10), our approach has several immediately identifiable advantages. First, no genetic manipulations are required, thus saving money and time. Second, our core-shell nanostructure can be easily exploited through a very simple and fast staining procedure. Third, GdQDs can be used for sensitive real-time spatial imaging using fluorescence microscopy, which is inexpensive compared to electron or probe microscopic techniques. Moreover, we have also shown that the fluorescence signal from the injured portions of membranes can be directly quantified in harvested cells.

Plasma membranes contain permanently anchored integral membrane proteins and temporarily attached peripheral membrane proteins(25). During injury to the membrane, the proteins attached to the intracellular portion of membranes become available to interact with the extracellular environment. Indeed, after complete disruption of cells by sonication, the cellular debris was widely stained by the GdQDs, indicating a specific interaction with the cytosol. Similarly, after partial disruption and Hoechst counterstaining of nuclei, we found that GdQDs bound very well to nuclear membranes. Hence, the next step was to identify the preferential binding target of GdQDs. A series of experiments using a cell suspension immobilized on a GO film revealed that the GdQDs surface specifically interacts with the sequence motif of the Na(+)/H(+) exchange regulatory cofactor (NHE-RF2), a protein localized on endomembrane systems, nuclei, apical cell membranes and peripheral membranes(26). NHE-RF2 connects plasma membrane proteins with proteins from the ezrin/moesin/radixin family, helping to link these latter proteins to the actin cytoskeleton(27). Moreover, NHE-RF2 also acts as scaffold protein in the nucleus(28). Molecular mechanics confirmed that the middle portion of the GEQGYGFHLHGE sequence of NHE-RF2 wraps around the Gd-SB preferentially through electron-rich and hydrophobic residues (Tyr and Phe). As NHE-RF2 is ubiquitously expressed in all eukaryotic cell types, we believe that it is an excellent target for similar labelling applications. It is worth noting that we also successfully optimized the NHE-RF2 labeling by anti-NHE-RF2 antibodies (Fig. 5d), with the results comparable to GdQDs staining. Despite that when comparing the complexity of both methods, immunostaining has several drawbacks, including variability, reliability and cost of primary antibodies, photodegradability of fluorophore conjugated to secondary antibody, or ability to penetrate deeper into the cytoplasm, which results in biased results.

Our development of GdQDs core-shell nanostructures affords a unique opportunity to spatially assess membrane injuries in a simple, fast, real-time manner, which can be otherwise challenging with other techniques. To explore this opportunity, we successfully evaluated the applicability of these structures to visualizing the membrane disruption caused by various exogenous stresses, including exposure to a CPP, puncturing, starvation and treatment with cytostatics. Taking our results together, we expect that these novel GdQDs will serve as a unique and versatile tool for a broad range of applications, such as evaluation of CPP activity, determination of cell membrane integrity in various undesirable conditions and recovery from injury, and the observation of host-pathogen interactions.

Materials and Methods

The experimental and computational methodologies used in this work are described in the *SI Appendix*. The methods includes preparation and characterization of GdQDs, molecular modelling, peptide synthesis, detection procedure of the damage of plasma membrane using GdQDs, Cryo-electron microscopy, Fragmentation of GdQDs-bound proteins by MALDI-TOF MS and Immunofluorescence without permeabilization. 2-Pyridinecarboxaldehyde, diethylenetriamine, gadolinium nitrate, cadmium acetate, MSA, sodium tellurite, sodium borohydride and all other chemicals used in this experiment were obtained from Sigma Aldrich (St. Louis, MO, USA) with ACS purity unless noted otherwise.

Acknowledgement

Financial support from CEITEC 2020 (LQ 1601) of the Ministry of Education, Youth and Sports of the Czech Republic under the National Sustainability Programme II and GACR 16-18917S is

acknowledged. The authors are grateful to Dr. Dawid Pinkowicz (Jagiellonian University) for the magnetic measurements (Large Research Infrastructure Fund of the Polish Ministry of Science and Higher Education, 6350/IA/158/2013.1) and to Dr. Paulina Indyka (Jagiellonian University) for the HR-TEM study (European Regional Development Fund in the framework of the Polish Innovation Economy Operational Program (POIG.02.01.00-12-023/08). We also acknowledge the CF CEITEC - Cryo-electron Microscopy and Tomography supported by the CIISB research infrastructure (LM2015043) for Cryo-SEM and Cryo-TEM analyses.

References

1. Licausi F, *et al.* (2011) Oxygen sensing in plants is mediated by an N-end rule pathway for protein destabilization. (Translated from English) *Nature* 479(7373):419-422 (in English).
2. Andrews NW, Almeida PE, & Corrotte M (2014) Damage control: cellular mechanisms of plasma membrane repair. (Translated from English) *Trends Cell Biol.* 24(12):734-742 (in English).
3. Gurnev PA & Nestorovich EM (2014) Channel-Forming Bacterial Toxins in Biosensing and Macromolecule Delivery. (Translated from English) *Toxins* 6(8):2483-2540 (in English).
4. Suomalainen M & Greber UF (2013) Uncoating of non-enveloped viruses. (Translated from English) *Curr. Opin. Virol.* 3(1):27-33 (in English).
5. Ronnback A, *et al.* (2016) Mitochondrial dysfunction in a transgenic mouse model expressing human amyloid precursor protein (APP) with the Arctic mutation. (Translated from English) *J. Neurochem.* 136(3):497-502 (in English).
6. Williams TL & Serpell LC (2011) Membrane and surface interactions of Alzheimer's A beta peptide - insights into the mechanism of cytotoxicity. (Translated from English) *Febs J.* 278(20):3905-3917 (in English).
7. Curtain CC, *et al.* (2001) Alzheimer's disease amyloid-beta binds copper and zinc to generate an allosterically ordered membrane-penetrating structure containing superoxide dismutase-like subunits. (Translated from English) *J. Biol. Chem.* 276(23):20466-20473 (in English).
8. Milletti F (2012) Cell-penetrating peptides: classes, origin, and current landscape. (Translated from English) *Drug Discov. Today* 17(15-16):850-860 (in English).
9. Skalickova S, *et al.* (2015) Perspective of Use of Antiviral Peptides against Influenza Virus. (Translated from English) *Viruses-Basel* 7(10):5428-5442 (in English).
10. Martinez R, Burrage AM, Wiethoff CM, & Wodrich H (2013) High Temporal Resolution Imaging Reveals Endosomal Membrane Penetration and Escape of Adenoviruses in Real Time. *Virus-Host Interactions: Methods and Protocols*, Methods in Molecular Biology, eds Bailer SM & Lieber D (Humana Press Inc, Totowa), Vol 1064, pp 211-226.

11. Angle MR, Wang A, Thomas A, Schaefer AT, & Melosh NA (2014) Penetration of Cell Membranes and Synthetic Lipid Bilayers by Nanoprobes. (Translated from English) *Biophys. J.* 107(9):2091-2100 (in English).
12. Algar WR, Susumu K, Delehanty JB, & Medintz IL (2011) Semiconductor Quantum Dots in Bioanalysis: Crossing the Valley of Death. (Translated from English) *Anal. Chem.* 83(23):8826-8837 (in English).
13. Medintz IL, Uyeda HT, Goldman ER, & Mattoussi H (2005) Quantum dot bioconjugates for imaging, labelling and sensing. (Translated from English) *Nat. Mater.* 4(6):435-446 (in English).
14. Wagner MK, Li F, Li JJ, Li XF, & Le XC (2010) Use of quantum dots in the development of assays for cancer biomarkers. (Translated from English) *Anal. Bioanal. Chem.* 397(8):3213-3224 (in English).
15. Mattoussi H, Palui G, & Na HB (2012) Luminescent quantum dots as platforms for probing in vitro and in vivo biological processes. (Translated from English) *Adv. Drug Deliv. Rev.* 64(2):138-166 (in English).
16. Heger Z, *et al.* (2015) Paramagnetic nanoparticles as a platform for FRET-based sarcosine picomolar detection. *Sci. Rep.* 5(8868):1-7.
17. Rivero-Müller A, *et al.* (2007) Use of hecate–chorionic gonadotropin β conjugate in therapy of lutenizing hormone receptor expressing gonadal somatic cell tumors. *Mol. Cell. Endocrinol.* 269(1–2):17-25.
18. Kim JH, *et al.* (2002) Ca2+-dependent inhibition of Na+/H+ exchanger 3 (NHE3) requires an NHE3-E3KARP-alpha-actinin-4 complex for oligomerization and endocytosis. (Translated from English) *J. Biol. Chem.* 277(26):23714-23724 (in English).
19. Dutta P, Saikia D, Adhikary NC, & Sen Sarma N (2015) Macromolecular Systems with MSA-Capped CdTe and CdTe/ZnS Core/Shell Quantum Dots as Superselective and Ultrasensitive Optical Sensors for Picric Acid Explosive. (Translated from English) *ACS Appl. Mater. Interfaces* 7(44):24778-24790 (in English).
20. Kopel P, Travnicek Z, Zboril R, & Marek J (2004) Synthesis, X-ray and Mossbauer study of iron(II) complexes with trithiocyanuric acid (ttcH(3)). The X-ray structures of Fe(bpy)(3) (ttcH) center dot 2bpy center dot 7H(2)O and Fe(phen)(3) (ttcH(2))(ClO4) center dot 2CH(3)OH center dot 2H(2)O. (Translated from English) *Polyhedron* 23(14):2193-2202 (in English).
21. Wiberg KB (1968) Application of the pople-santry-segal CNDO method to the cyclopropylcarbinyl and cyclobutyl cation and to bicyclobutane. *Tetrahedron* 24(3):1083-1096.
22. Choi JH, *et al.* (2007) Core-shell silica nanoparticles as fluorescent labels for nanomedicine. (Translated from English) *J. Biomed. Opt.* 12(6):1-12 (in English).
23. Varchi G, *et al.* (2015) Engineered porphyrin loaded core-shell nanoparticles for selective sonodynamic anticancer treatment. (Translated from English) *Nanomedicine* 10(23):3483-3494 (in English).
24. Perez RA & Kim HW (2015) Core-shell designed scaffolds for drug delivery and tissue engineering. (Translated from English) *Acta Biomater.* 21:2-19 (in English).
25. Johnson JE & Cornell RB (1999) Amphitropic proteins: regulation by reversible membrane interactions (review). (Translated from English) *Mol. Membr. Biol.* 16(3):217-235 (in English).

26. Padanyi R, *et al.* (2010) Apical Scaffolding Protein NHERF2 Modulates the Localization of Alternatively Spliced Plasma Membrane Ca2+ Pump 2B Variants in Polarized Epithelial Cells. (Translated from English) *J. Biol. Chem.* 285(41):31704-31712 (in English).
27. Yang JB, *et al.* (2015) The NHERF2 sequence adjacent and upstream of the ERM-binding domain affects NHERF2-ezrin binding and dexamethasone stimulated NHE3 activity. (Translated from English) *Biophys. J.* 470:77-90 (in English).
28. Kunkel MT, Garcia EL, Kajimoto T, Hall RA, & Newton AC (2009) The Protein Scaffold NHERF-1 Controls the Amplitude and Duration of Localized Protein Kinase D Activity. (Translated from English) *J. Biol. Chem.* 284(36):24653-24661 (in English).

5.3. Cell penetrating peptide interaction with functionalized carbon nanocarriers

Undesired toxicity and lack of specificity for intracellular target are limiting the application of drugs in advanced therapy. Application of nanocarriers is a promising way, how too safely deliver drug and reduce the potential toxicity. Advantage of nanocarriers can be found in high drug loading capacities, providing excellent opportunity for use of this material in drug delivery. The next step of the study demonstrated that carbon based nanocarriers modified with drugs and delivery by CPPs are the ideal and promising technique for advanced therapy.

5.3.1. Research article IV

Vedran Milosavljevic, Ludmila Krejcova, Roman Guran, Hana Buchtelova, Dorota Wawrzak, Lukas Richtera, Zbynek Heger, Pavel Kopel, Vojtech Adam. Exceptional Release Kinetics and Cytotoxic Selectivity of Oxidized MWCNTs Double-Functionalized with Doxorubicin and Prostate-Homing Peptide. Colloids and surfaces B Biointerfaces (2016-Submitted).

Participation in the work of the author Vedran Milosavljevic: experimental part 60% and manuscript preparation 60%.

MWCNTs with their large surface area and ability for surface modification by bioactive molecules, due to π electrons represent excellent transporters for cellular delivery [206]. Modification of MWCNTs can be improved by application of inorganic acids, resulting in production of carboxylic moieties on the surface. A significant amount of drug and peptide can be bound on multiple binding sites on oxidized MWCNT walls [207].

In the presented study, MWCNTs (*o*MWCNTs) were oxidized and used as carriers in delivery of doxorubicin (DOXO) for treatment of prostate cancer. To avoid the potential toxicity to normal prostate cells, *o*MWCNTs were modified with prostate-homing peptide (SMSIARL), in order to improve specificity of therapeutic agent.

Functionalization of MWCNTs was conducted by oxidative approach, using concentrated HNO_3. Surface defects and carboxyl group production on MWCNTs were

caused by strong oxidation process, resulting in formation of *o*MWCNTs. Oxidations of MWCNTs were confirmed by ATR-FTIR and TGA analysis. MALDI-TOF MS and electrochemical analysis confirmed formation of *o*MWCNTs-DOXO-PEPTIDE complexes. XTT assay confirmed lack of toxicity effect in both cell lines (PC3 and PNT1A) after treatment by peptide or MWCNTs. However, presence of doxorubicin complex shows the same toxicity effect on PC3 cell line as doxorubicin applied alone. On the other hand, PNT1A shows intolerance to doxorubicin alone, while after application of *o*MWCNTs-DOXO-PEPTIDE complex, toxicity effect is missing, proving the specificity of peptide for PC3 cell line. Release of doxorubicin from MWCNTs was simulated in acidic intracellular and human plasma environment, using specially prepared buffers. The obtained results indicate that release of doxorubicin in plasma condition after 24 hours is at 13 %, while in acidic condition after 24 hours 60 % of doxorubicin is released. This confirmed that doxorubicin release is pH dependent.

In this study, the considerable potential of *o*MWCNTs-DOXO- Pep was demonstrated. The validity of the results requires however further evaluation by *in vivo* experiments. Despite that, it was demonstrated that *o*MWCNTs can serve as an exceptional platform for simple, stable and efficient immobilization of bioactive compounds.

Exceptional Release Kinetics and Cytotoxic Selectivity of Oxidised MWCNTs Double-Functionalised with Doxorubicin and Prostate-Homing Peptide

Vedran Milosavljevic[a], Ludmila Krejcova[a,b], Roman Guran[a], Hana Buchtelova[a], Dorota Wawrzak[c], Lukas Richtera[a,b], Zbynek Heger[a,b], Pavel Kopel[a,b], Vojtech Adam[a,b]

[a]*Department of Chemistry and Biochemistry, Mendel University in Brno, Zemedelska 1, CZ-613 00 Brno, Czech Republic*

[b]*Central European Institute of Technology, Brno University of Technology, Purkynova 123, CZ-612 00 Brno, Czech Republic*

[c]*Institute of Chemistry, Environmental Protection and Biotechnology, Jan Dlugosz University of Czestochowa, Armii Krajowej 13/15, PL-42-201 Czestochowa, Poland*

***Corresponding author**

Vojtech Adam, Department of Chemistry and Biochemistry, Mendel University in Brno, Zemedelska 1, CZ-613 00 Brno, Czech Republic, European Union; E-mail: vojtech.adam@mendelu.cz; phone: +420-5-4513-3350; fax: +420-5-4521-2044

Abstract

Multiwall carbon nanotubes (MWCNTs) are among the frequently studied carbon materials, particularly because of their physical and chemical properties and high potential for application in materials chemistry, industry, and medicine. MWCNTs are very promising as transporters of bioactive molecules because of their π electrons and large surface area, which can be easily modified, mostly by the application of inorganic acids for the introduction of carboxylic moieties on the surface. In the present study, we designed an oxidised MWCNTs (*o*MWCNTs) transporter for the targeted delivery of doxorubicin (Dox). The modification of *o*MWCNTs with prostate-homing peptide (SMSIARL) promotes increased cytotoxicity for prostate cancer cells. Using advanced analytical techniques, we studied the loading efficiency, stability, and release kinetics of Dox from a *o*MWCNTs-Dox-Pep nanoconstruct. We show that pH strictly drives Dox release, and imitating the pH of intracellular acidic compartments, 60% of Dox is released from *o*MWCNTs-Dox-Pep, while in plasma conditions, only a 14% release of Dox was found during 24 hours. The nanoconstruct displayed no cytotoxicity in non-malignant prostate cells (PNT1A), while in metastatic prostate cancer cells (LNCaP), the cytotoxic effects were close to the cytotoxicity of free Dox. This indicates that peptide modification promotes interactions with malignant cells, resulting in efficient internalisation into the intracellular region. Overall, we show that *o*MWCNTs are exceptional platforms for simple and stable non-covalent modification with bioactive molecules.

Keywords: Carbon nanomaterial; prostate-homing peptide; drug delivery; nanomedicine

Introduction

Carbon nanotubes (CNTs) are among the most studied carbon materials. CNTs are described as single (single-wall carbon nanotube, SWCNT) or multiwall cylindrical layers of graphene (multi-wall carbon nanotube, MWCNT) with no overlapping edges [1]. Usually, the length of CNTs ranges between 1 and 100 nm with a typical diameter from 0.8 to 2 nm. However, in some cases, their lengths can range from 100 nm up to several micrometres with a diameter of 5 to 20 nm. In the case of MWCNTs, it is reported that the length of tubes can reach tens of micrometres with a diameter between 0.7 and 100 nm [2, 3]. The unique physical and chemical properties of CNTs increase their potential application in various fields, from electronic devices and sensors to therapeutic purposes [4, 5]. The therapeutic application of CNTs is especially attracting a great deal of attention because of their high cell membrane penetrability, high drug capacity, pH-dependent releasing, prolonged circulating time, and photo-thermal activity [6, 7].

Various types of drugs containing aromatic groups in their structure can be covalently or non-covalently bonded with CNTs. Such binding mostly results from strong π–π interactions [8, 9]. However, several works have described the transport of cargo inside the CNT cylinder through defects of sidewall sites or in the process of CNTs' synthesis [10, 11]. In contrast, interactions between drugs and CNTs are often limited by the chemical route available to create covalent or non-covalent bonds [12]. This limitation can be overcome by oxidising CNTs with concentrated acid (e.g., nitric acid). This leads to strong oxidation on CNTs' surface, resulting in the incorporation of carboxyl groups at the ends of CNTs. The production of carboxylated CNTs increases the range of chemical species that can be conjugated (e.g., through amide linkages, hydrazone bond, carbamate, or esterification) [13-15]. Strong oxidation also causes local defects on the walls, increasing the chemical reactivity of the CNT wall [16].

Delivery of drugs to specific intracellular targets and a reduction in their undesired toxicity is the main hallmark of advanced therapeutic applications. Utilising nanotransporters for drug delivery can represent a promising method for safe drug delivery with a minimal toxicity effect [17]. CNTs have great membrane penetration qualities and high drug loading capacities as a drug container, providing excellent opportunities for use of this material in drug delivery [18]. However, despite CNTs' excellent properties, their application range can be limited by non-targeted cytotoxicity, limited control, and the potential to cause inflammatory and fibrotic reactions [19, 20].

The use of bioactive peptides in cellular targeting is a promising strategy for the development of novel therapeutics. Because of their biochemical properties, peptides can deliver various cell-impermeable covalently or non-covalently conjugated cargos to a wide range of intracellular targets [21]. MWCNTs can be used to simultaneously harbour significant amounts of drugs and peptides because of the multiple binding sites on MWCNT walls. MWCNTs, with their large surface area, tuneable surface chemistry, and excellent drug loading capacity via π–π stacking interactions open the possibility to use these tubes as a promising delivery system candidate [22, 23]. However, non-functionalised MWCNTs often show limitations because of traces of amorphous carbon obtained from catalysts in the process of synthesis. This results in the synthesis of MWCNTs with carbon molecule defects (sp3-hybridised C atoms and other carbon) [24]. This limitation can be avoided by the purification and functionalisation of MWCNTs by using hot nitric acid [25]. MWCNTs, which are oxidised with nitric acid, have oxygen-containing moieties that can be easily modified with various organic and inorganic compounds. However, it is also reported that oxidation with nitric acid leads to increasing solubility and shortening of MWCNTs' length, which broadens their application, especially in drug delivery [3, 26, 27].

Hence, the purpose of this work was to design and construct a doxorubicin (Dox) loaded nanocarrier composed of oxidised MWCNTs (*o*MWCNTs) conjugated with the prostate-homing peptide (SMSIARL; final construct referred to as *o*MWCNTs-Dox-Pep). We characterised Dox loaded onto *o*MWCNTs to determine the *o*MWCNTs' loading efficiency. Further, Dox release kinetics from *o*MWCNTs were investigated under conditions corresponding to the extracellular and intracellular environments. Finally, the cytotoxic effects of *o*MWCNT-Dox-Pep were analysed using androgen-dependent metastatic human prostate adenocarcinoma cells (LNCaP) and normal human prostatic epithelial cells (PNT1A).

Materials and Methods

Chemicals

Chemicals used in this study were purchased from Sigma-Aldrich (St. Louis, MO, USA) in ACS purity.

Fmoc solid phase synthesis of prostate-homing peptide

For synthesis of the prostate-homing peptide (SMSIARL), Liberty Blue peptide synthesiser was employed (CEM, Matthews, NC, USA). The monoisotopic molecular weight of the peptide was 776.42 g/mol. Deblock of Fmoc protecting groups was performed with 20% piperidine (*v/v*) in *N*,*N*-dimethylformamide (DMF). Coupling was achieved using *N,N,N′,N′*-tetramethyl-*O*-(1*H*-benzotriazol-1-yl)uronium hexafluorophosphate (HBTU), *N*,*N*-diisopropylethylamine (DIEA), and DMF. Cleavage of side chain protecting groups was performed by treating the peptide resin with 95% trifluoroacetic acid (TFA, *v/v*), 2.5% H_2O (*v/v*), and 2.5% triisopropylsilane *v/v* for 30 min at 38°C under microwave irradiation.

Acidic oxidation of MWCNT surface using HNO_3

1 mg of commercially available MWCNTs (Sigma-Aldrich, St. Louis, MO, USA) was mixed with 0.5 mL of concentrated HNO_3. The mixture was then heated on a Thermo-mixer (Eppendorf, Hamburg, Germany) for 20 min at 80°C at 800 rpm. Subsequently, the mixture was sonicated using an ultrasonic bath (Bandelin, Berlin, Germany) for 15 min and centrifuged at 25,000 rpm at 20°C for 10 min using a table-top centrifuge (Eppendorf, Hamburg, Germany). The supernatant was discarded and the product was washed by centrifugation with MilliQ water until the pH became neutral. Finally, the volume was made up to 1 mL using MilliQ water.

Modification of oMWCNTs using Dox and SMSIARL

The stock solution of peptide (SMSIARL) was prepared in a concentration of 1 mg/mL. The Dox concentration was set at the clinical trial dose of 54.3 μg/mL [28]. After centrifugation and removal of water from the *o*MWCNTs, 1 mL of Dox (54.3 μg/mL) was added and mixed for 24 hours at 25°C. Then the prepared conjugate was washed three times with MilliQ water to remove unbound Dox. After that, 1 mL of SMSIARL solution (1 mg/mL) was added and mixed for 24 hours at 25°C. The prepared conjugate (referred to as *o*MWCNTs-Dox-Pep) was washed three times by centrifugation (6,000 rpm at 20°C for 10 min) with MilliQ water to remove unbound chemicals. The resulting *o*MWCNTs-Dox-Pep was photographed using a scanning electron microscope (SEM) MIRA3 LMU (Tescan a.s., Brno, Czech Republic) with accelerating voltage of 15 kV and a beam current of 1 nA.

Attenuated total reflectance-Fourier transform infrared spectroscopy (ATR-FT-IR)

FT-IR spectra were collected using a Nicolet iS10 FT-IR spectrometer with a diamond ATR attachment (Thermo Electron Inc., San Jose, USA). IR spectra were recorded from 4,000 to 650 cm^{-1} at a resolution of 4 cm^{-1}. Each spectrum was acquired by adding together 32

interferograms. Spectra were taken at 22°C. The OMNIC™ software was used for IR spectra recording, and the JDXview v0.2 software was used for further spectra evaluation.

Optical analyses

Fluorescence and absorbance were investigated by a multifunctional microplate reader, the Tecan Infinite 200 PRO (Tecan, Männedorf, Switzerland). For Dox analysis, λ_{ex} was set to 480 nm. The emission scans for Dox were recorded within the range from 400–850 nm with 2 nm steps. The sample (100 μL) was placed in transparent 96 well microplates with flat bottoms (Thermo Scientific, Waltham, MA, USA).

Matrix-assisted laser desorption/ionisation-time-of-flight mass spectrometry (MALDI-TOF MS) analysis

The experiments were performed on a MALDI-TOF mass spectrometer, the Bruker ultrafleXtreme (Bruker Daltonik GmbH, Bremen, Germany), using 2,5-dihydroxybenzoic acid (DHB) or α-cyano-4-hydroxycinnamic acid (HCCA). The saturated matrix solution was prepared in 30% acetonitrile and 0.1% TFA. All measurements were performed in reflectron positive mode in the *m/z* range 0-4 kDa. The mass spectra were typically acquired by averaging 2,000 sub-spectra from a total of 2,000 laser shots per spot. Laser power was set 5–10% above the threshold.

Adsorptive transfer technique coupled with differential pulse voltammetry (AdT-DPV)

Electrochemical analyses were performed with a 663 VA Stand instrument (Metrohm, Switzerland). The three-electrode setup consisted of a hanging mercury drop electrode involved as the working electrode, an Ag/AgCl/3M KCl reference electrode, and a platinum auxiliary electrode. Brdicka supporting electrolyte containing 1 mM $[Co(NH_3)_6]Cl_3$ and 1 M ammonia buffer ($NH_3(aq)$ and NH_4Cl, pH = 9.6) was used for all AdT-DPV analyses. The parameters of the measurement were as follows: initial potential −0.50 V, end potential −1.75

V, adsorption time 60 s; modulation time 0.03 s; interval time 0.8 s; step potential 3.5 mV; and modulation amplitude 25 mV.

Thermogravimetric analysis of oxidised MWCNTs

Thermogravimetric analysis (TGA) was performed by thermal decomposition of the MWCNTs and oxidised MWCNTs groups under an oxidative atmosphere. TGA was performed using a temperature ramp of 10°C/min to 1,000°C/min on a TA Q500 instrument.

Haemolysis of human red blood cells (RBCs)

RBCs were obtained from whole blood according to Evans *et al*. [29]. RBC suspensions were washed three times by 150 mM NaCl and then diluted in washing solution to the volume of 1 mL and stored at 4°C for no more than 24 hours. 1 mL of erythrocyte suspension was interacted with the complex at various doses (6, 12, 25, and 50 µg/mL) and then incubated for 1 hour at 37°C. The degree of haemolysis was determined by measuring the absorbance of the supernatant at 540 nm after centrifugation and calculated according to the following equation: $\% \ haemolysis = [(A_t - A_c)/A_{100\%} - A_c)] \times 100$, where A_t is the absorbance of the supernatant from samples incubated with the complexes; A_c is the absorbance of the supernatant from the negative control (PBS, pH 7.4); $A_{100\%}$ is the absorbance of the supernatant of the positive control (0.1% Triton X-100), which causes complete lysis of RBCs.

Evaluation of release kinetics of Dox from oMWCNTs

The method for release kinetics studies was adopted from Dostalova *et al*. [30]. Samples were incubated for 24 hours at 37°C, and release kinetics were analysed using a multifunctional microplate reader, the Tecan Infinite 200 PRO (Tecan, Männedorf, Switzerland). Sampling and measurements were conducted at different time points for 24 hours. Evaluation of Dox release was carried out in Ringer's solution, as it imitates the human plasma environment and

the intracellular acidic compartments, according to Corazzari *et al*. [31]. Dox release was further and more precisely studied using DPV within the parameters described above.

Cultivation of prostatic cell lines

The two human prostatic cell lines used in this study, the PNT1A and the LNCaP, were both purchased from Health Protection Agency Culture Collections (Salisbury, UK). The cells were cultured in RPMI-1640 medium at 10%. All media were supplemented with penicillin (100 U/mL) and streptomycin (0.1 mg/mL), and the cells were maintained at 37°C in a humidified incubator (Galaxy 170r, Eppendorf, Hamburg, Germany) with 5% CO_2. Total cell content was analysed using Countess IIFL Automated Cell Counter (Life Technologies, Carlsbad, CA). To prepare a viable cell standard, 10 µL of cell suspension was mixed with 10 µL of trypan blue.

Determination of cytotoxicity – XTT proliferation assay

Cell viability was estimated using the XTT assay. A suspension of 5,000 cells in 50 µL medium was added to each well of microtiter plates (E-plates 96), followed by incubation for 24 hours at 37°C with 5% CO_2 to ensure cell growth. The treatments were normalised to Dox concentrations (0–25 µg/mL). After treatment, cells were incubated for 24 hours. Then, 25 µL of solution containing XTT [(2,3-bis-(2-methoxy-4-nitro-5-sulfophenyl)-2*H*-tetrazolium-5-carboxanilide)] and phenazine methosulfate was added directly to each well, and the mixture was incubated for 2 hours at 37°C. Finally, the absorbance was determined at 450 nm (Infinite 200PRO, Tecan, Männedorf, Switzerland).

Microscopy of oMWCNTs-PEPTIDE localisation in cell lines

An inverted system microscope in the Olympus UIS2 series (Olympus, Tokyo, Japan) was used for the imaging of applied sample internalisation into the cells *in ambient light*. The LUCPlanFLN 40× was used for magnification of 400×. The images were captured by a Camera Olympus DP73 and processed by the Stream Basic 1.7 software.

Fluorescence microscopy of live/dead cells using SYTO9 and propidium iodide (PI)

A microscopic assay for the evaluation of live/dead cells was performed using an inverted Olympus IX 71S8F-3 fluorescence microscope (Olympus, Tokyo, Japan) equipped with Olympus UIS2 series objective LUCPlanFLN 40× (N.A. 0.6, WD 2.7–4 mm, F.N. 22) and a mercury arc lamp, the X-cite 12 (120 W, Lumen Dynamics, Mississauga, Canada), for illumination. Dyes used for the assay included PI to stain cells with damaged membranes and SYTO9 (Invitrogen AG, Basel, Switzerland) to permeate both intact and damaged cell membranes [32]. Images were processed using the Stream Basic 1.7 software (Olympus Soft Imaging Solutions GmbH, Münster, Germany) with a software resolution of 1600 × 1200 pixels.

Descriptive statistics

The results are expressed as the mean ± standard deviation unless noted otherwise. Differences between groups were analysed using the paired t-test and analysis of variance (ANOVA). Unless noted otherwise, the threshold for significance was $p < 0.05$. The Statistica 12 software (StatSoft, Tulsa, OK, USA) was employed for the analyses.

Results and Discussion

Characterisation of oMWCNTs-Dox-Pep

Generally, the loading of drugs on/into MWCNTs can be carried out through covalent bond or non-covalent adsorption. Molecules containing aromatic groups such as Dox can be easily bound to MWCNTs non-covalently by physical adsorption, enabling hydrophobic interaction (including strong π–π stacking) between molecules and MWCNTs [33].

In the present study, surface functionalisation of pristine MWCNTs was performed by harsh oxidative processes using concentrated HNO_3. The strong oxidation process leads to surface defects and the introduction of end cap carboxyl groups to the *o*MWCNTs, as shown in our previous study dealing with *o*MWCNTs and VP-16 [34]. Formed carboxyl groups can serve

as anchor moieties, enabling the simple loading of Dox on the *o*MWCNT surface (a schematic depiction is shown in **Fig. 1A**). The efficiency of *o*MWCNT modifications with prostate-homing peptide, and Dox loading was investigated by ATR-FTIR (**Fig. 1B**). The addition of peptide to the *o*MWCNTs resulted in an increase in O−H, C−H, and N−H moiety signals in the 2,600–3,600 cm^{-1} region. A significant change can be observed at the Amide I peptide band (original position at 1,650 cm^{-1}), which is shifted to the lower frequency of 1,618 cm^{-1} and leads to the increase and broadening of the overall signal in this region. Similarly, the slight increase in overall intensity around 1,500 cm^{-1} can be connected with the shifting of the peptide band originally found at 1,530 cm^{-1} (Amide II peptide band) [35]. Such observed shifting can be explained by strong interactions between peptide functional groups with the *o*MWCNT surface. The addition of Dox to *o*MWCNTs leads to analogous changes in spectra, especially in the region of C=O bands and in the fingerprint region. The recorded spectra do not correspond to a simple mixture of the discussed substances, and the existence of a strong interaction can be suggested based on significant band shifts and changes in spectra character (e.g., instead of generally well-differentiated and resolved doxorubicin bands at 1,661; 1,617; 1,580; and 1,524 cm^{-1}, only two broad signals at 1,633 and 1,524 cm^{-1} can be observed). The formation of *o*MWCNTs-Dox-Pep resulted in IR spectra with attributes of both *o*MWCNTs-Pep and *o*MWCNTs-Dox. Most significant bands can be found at 1,623; 1,549; 1,439; 1,201; 1,181; 1,135; and 1,048 cm^{-1}. To evaluate the efficiency of MWCNT oxidation and possible structural damage, a TGA analysis was performed. The results of the thermogravimetric analysis of the pristine MWCNTs and oxidised *o*MWCNTs are plotted in supplementary Fig. 1A. The pristine MWCNTs show a minor weight loss (<1%) below 150°C, which is usually caused by loss of the physic-adsorbed water [36]. However, significant weight losses in pristine MWCNTs start around 500°C as a result of the degradation of amorphous or disordered carbon (supplementary Fig.

1B) [37]. However, *o*MWCNTs show early weight losses, which is evidence of structural damage to tubes caused by harsh acid treatment (supplementary Fig. 2C). The continuous decreasing of the curve from 150 to 350°C results from the decarboxylation of the carboxylic groups (7.5%), which is an early sign of the thermal degradation of *o*MWCNT walls [38]. Thermal degradation of *o*MWCNTs between 350°C and 500°C usually contributes to the elimination of hydroxyl functionalities from the *o*MWCNT walls [39]. Similarly, the case of pristine MWCNTs at temperatures higher than 500°C involves the degradation of the remaining highly ordered carbon.

Surface modifications of *o*MWCNTs with prostate-homing peptide and Dox (the SEM micrograph inserted in **Fig. 1C** shows characteristic *o*MWCNTs morphology) were further confirmed by optical analysis. First, the binding efficiency of Dox within *o*MWCNTs-Dox-Pep was estimated. **Fig. 1C** illustrates that the *o*MWCNTs-Dox interaction is strong enough to withstand three washing steps without any Dox being prematurely released. Further, the loading efficiency was studied to compare the Dox in concentration used for *o*MWCNT modification (54.3 μg/mL) with the intermediate (*o*MWCNTs-Dox) and final products (*o*MWCNTs-Dox-Pep) of synthesis. **Fig. 1D** illustrates that, during the synthesis steps, there were significant ($p < 0.05$) losses of Dox. Despite that, we confirmed that the final product still retains more than 63% of the Dox and is thus suitable for further applications. We also analysed the bare prostate-homing peptide and oMWCNTs, and the results revealed no fluorescence when using the employed λ_{exc} and λ_{em} for Dox.

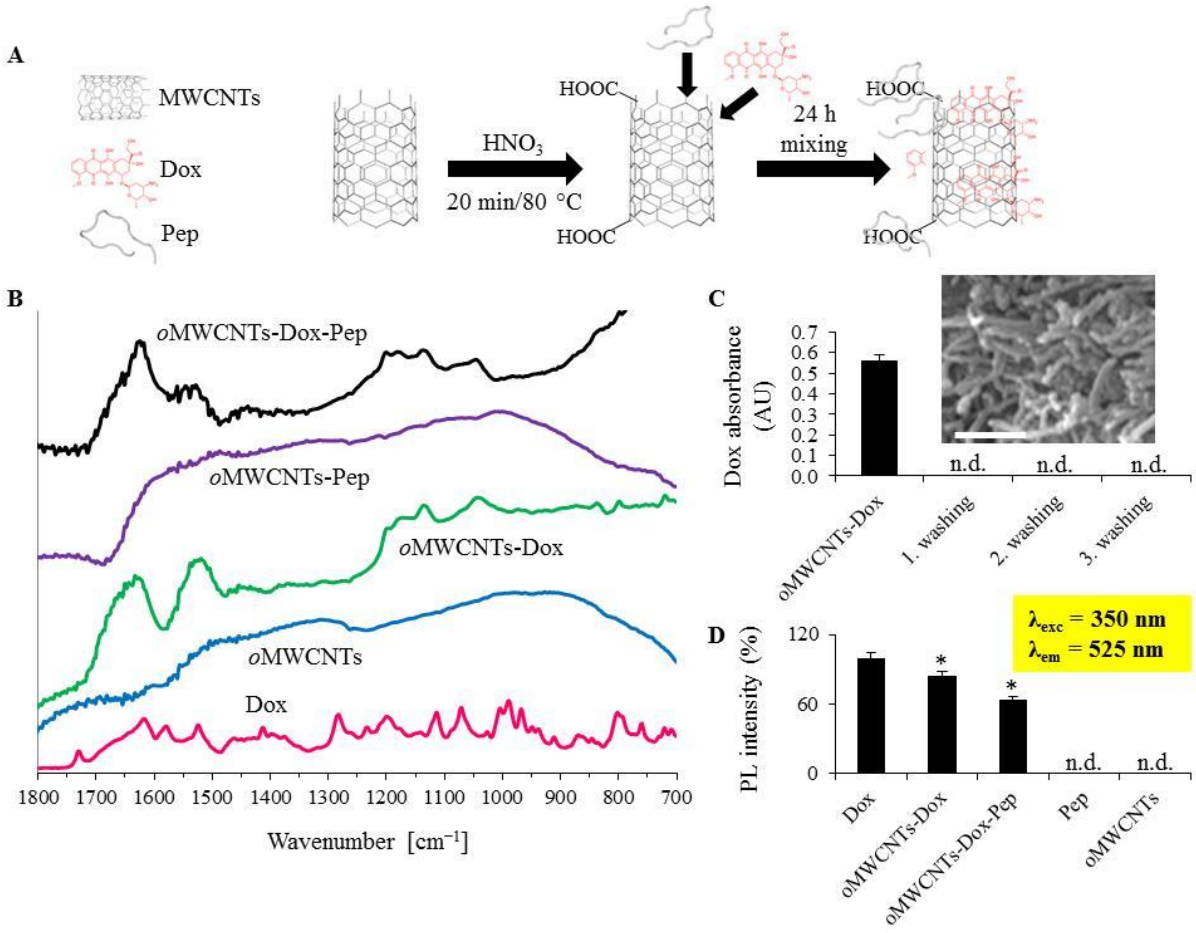

Figure 1: (A) Overall schematic workflow of the multi-step preparation of oMWCNTs-Dox-Pep. HNO3 oxidation introduces end-cap COOH moieties on pristine MWCNTs. (B) IR spectra of oMWCNTs, Dox, oMWCNTs-Dox, oMWCNTs-Pep, and oMWCNTs-Dox-Pep recorded by a spectrometer equipped with platinum-ATR accessory with diamond crystal. (C) Optical characterisation of binding strength between oMWCNTs and Dox. The absorbance of Dox in oMWCNTs-Dox-Pep was estimated directly after preparation and then gradually after three washing steps (MilliQ water). Insert shows representative SEM micrograph of oMWCNTs-Dox-Pep. The length of scale bar is 100 nm. (D) Loading efficiency of Dox within oMWCNTs-Dox-Pep analysed by fluorescence spectroscopy and compared to Dox in concentration exploited for oMWCNTs-Dox-Pep preparation, n.d. (not detected). Values are means of three independent replicates (n = 3). Vertical bars indicate standard error. Asterisks (*) indicate statistical significance ($p < 0.05$). Significance is relative to initial Dox concentration (54.3 µg/mL)

To further characterise the *o*MWCNTs-Dox-Pep, we employed MALDI-TOF-MS. **Figs. 2A–C** show mass spectra of *o*MWCNTs, prostate-homing peptide (*m/z* = 776.40 Da, corresponding to its theoretical monoisotopic molecular weight, 776.42 Da), and Dox (*m/z* = 537 Da, corresponding to its theoretical monoisotopic molecular weight, 537.17 Da). **Fig. 2D**

shows a newly formed peak observed at *m/z* = 1,313.79 Da, denoting a quasi-molecular ion of *o*MWCNTs-Dox-Pep. Overall, the MS analyses confirmed the successful formation of complex.

We further utilised AdT-DPV using the Brdicka catalytic reaction to study the interaction between components in *o*MWCNTs-Dox-Pep (**Fig 2E**). The Brdicka reaction has been widely used for polarographic determination of proteins that contain thiol moieties [40-42], but some other electrochemically active species can provide specific signals using this reaction (e.g., Cd^{2+}, Ni^{2+}, polyethylene glycol, polyvinylpyrrolidone, mercaptosuccinic acid, and Dox) [43, 44]. For such measurements, the potential range must be adjusted with respect to the signals of the analysed compounds (initial potential was set to −0.50 V and end potential to −1.75 V; see below). The pure Brdicka solution gives a characteristic signal at −1.30 ± 0.01 V that is present in all other voltammograms at position ± 0.08 V. The addition of Dox to Brdicka solution results in a slight shift and decrease of the electrolyte signal and the display of a characteristic double peak at potentials −0.63 V and −0.68 V (Fig. 2C, solid blue line). In the voltammogram of *o*MWCNTs in Brdicka solution (Fig. 2C, solid green line), a broad overlapping double peak at potentials −1.55 V and −1.65 V can be observed together with a pronounced decrease in electrolyte response. The addition of prostate-homing peptide to the electrolyte resulted in a characteristic voltammogram shape with peaks at potentials −1.40 V and −1.50 V. In the *o*MWCNTs-Dox voltammogram, a shift and a change in the shape of the Dox double peak was identified. The double peak shape became less noticeable, and potential was shifted to the more negative potential −1.02 V and ±0.05 V. This corresponds to a higher energy demand for Dox reduction. Analogous alterations were found in *o*MWCNTs-Pep.

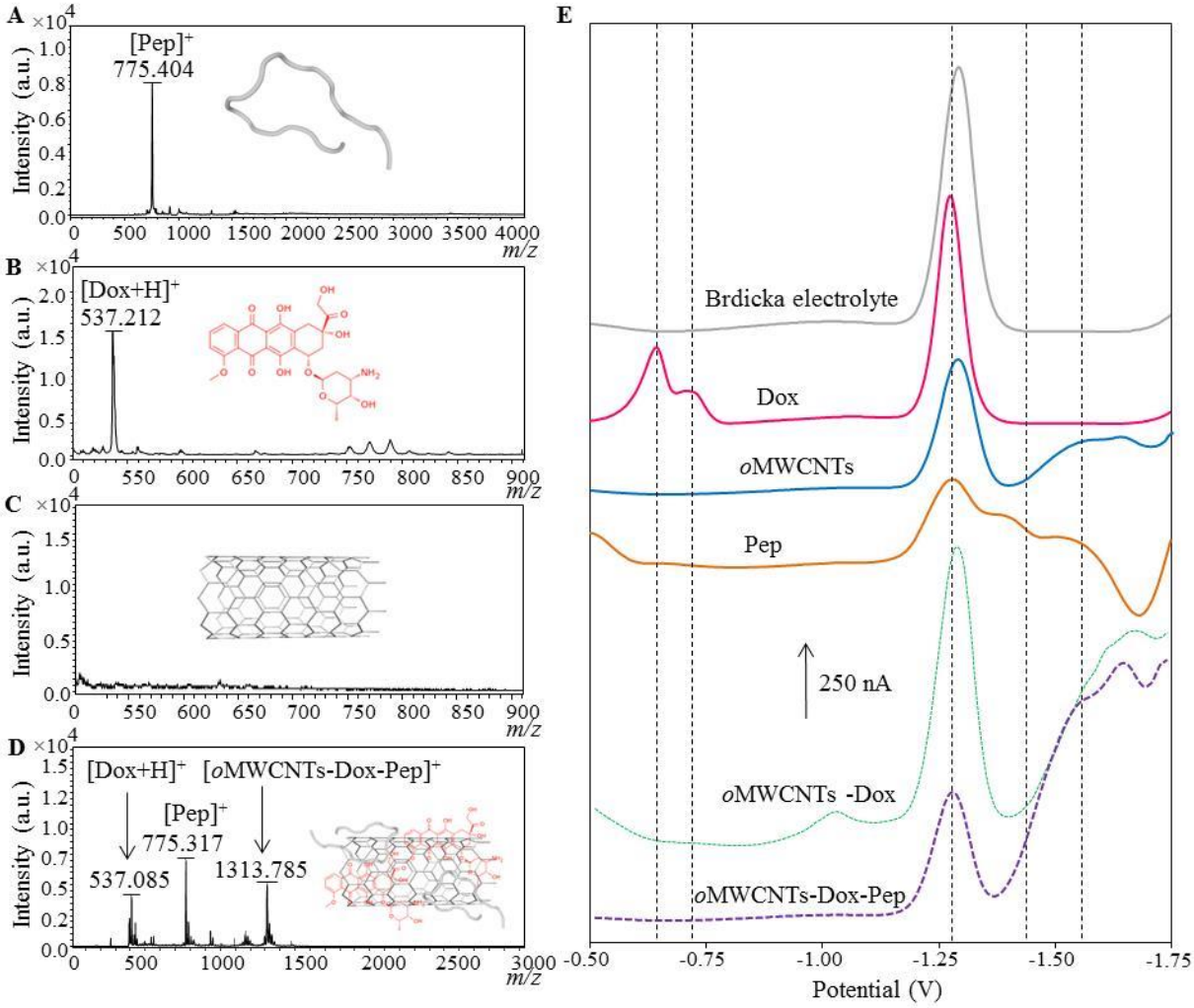

Figure 2: MALDI-TOF MS showing spectra for (**A**) prostate-homing peptide, (**B**) Dox, (**C**) oMWCNTs, and (**D**) *o*MWCNTs-Dox-Pep. Inserted are representative structures for individual components. All spectra were obtained with 2,5-dihydroxybenzoic acid matrix in TA30 with a maximum energy of 43.2 µJ with the repetition rate 2,000 Hz and were averaged from 2,000 sub-spectra. (**E**) Representative DP voltammograms of bare *o*MWCNTs, Dox, prostate-homing peptide, *o*MWCNTs-Dox, *o*MWCNTs-Dox-Pep, and Brdicka electrolyte. All samples were analysed by AdT-DPV.

Haemocompatibility and kinetics of Dox release in plasma and intracellular environments

The haemolytic activity of drugs and drug carriers is a crucial parameter to estimate their therapeutic index. The strong membrane binding and insertion ability of complexes to cancer cells could also threaten RBCs *via* similar membrane-disruption mechanisms. **Fig. 3A** illustrates that the highest applied concentration of Dox triggered haemolysis of about 48%, while at the lowest concentration, haemolysis was around 17%. In contrast, the *o*MWCNTs-

Dox-Pep haemolytic effect decreased significantly ($p < 0.05$) within all tested concentrations. Thus, it is worth noting that complexes show lower haemotoxicity than Dox, which can be the result of the slower release of Dox from *o*MWCNTs. These *in vitro* results suggest that the use of complexes in drug delivery could lead to minimisation of Dox's toxic effects on blood circulation.

Further, Dox release from *o*MWCNTs-Dox-Pep was estimated in conditions imitating acidic intracellular compartments and the human plasma environment. Incubation in the human plasma environment resulted in a 14% release of Dox after 3 hours, and during 24 hours, the oMWCNTs-Dox-Pep remained relatively stable without any pronounced premature release (**Fig. 3B**). In contrast, the acidic intracellular compartment environment caused a linear release of Dox, and after 24 hours, 60% of the Dox was released (**Fig. 3C**). Similar results were achieved by Heister *et al.*, who reported that the kinetics of Dox release from CNTs in acidic conditions is higher than 50% within 24 hours, but neutral pH resulted in the release of only 10% of the Dox [45]. Gu *et al*. also identified a very low rate of Dox release kinetics (about 14%) from SWCNTs and a significant increase (> 50%) of Dox release in slightly acidic conditions [12].

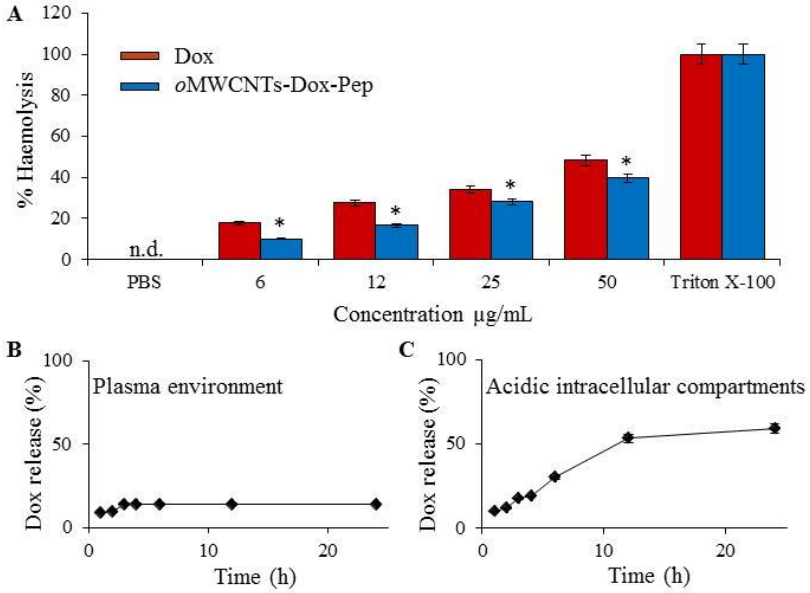

Figure 3: (**A**) Haemocompatibility of Dox compared to haemocompatibility of *o*MWCNTs-Dox-Pep in selected Dox concentration range of 0–50 μg/mL, n.d. (not detected). Values are expressed as the mean of three independent replicates ($n = 3$). Vertical bars indicate standard error. Data with asterisks (*) indicate statistical significance ($p < 0.05$) related to haemotoxicity of Dox. Release kinetics of Dox in (**B**) Ringer's solution imitating the human plasma environment and (**C**) buffer imitating the intracellular acidic compartments. Release profiles were determined with entire constructs (*o*MWCNTs-Dox-Pep). PBS (pH 7.4) and 0.1% Triton X-100 were employed as negative and positive controls, respectively.

We further employed AdT-DPV, which can simultaneously detect bound and free forms of Dox. As demonstrated, the free Dox double peak appeared at a more positive potential than the peak of bound Dox. Such a separation of signals enabled the monitoring of time and pH dependence on the release of Dox from *o*MWCNTs-Dox-Pep. **Figs. 4A** and **4B** illustrate the time dependence of Dox release in both plasma and acidic intracellular compartment environments. It is obvious that the release of Dox is faster at a mildly acidic pH ~5.5 (characteristic of the hypoxic environment of tumour tissue) compared to physiological pH ~7.4. Free Dox peak heights decreased with an increasing time of incubation (0 → 7 h), while the peaks of bound Dox behaved conversely. Our results are in good agreement with the findings of Qi *et al*., who described the pH-dependent sustained release of Dox from chitosan-grafted CNTs [46]. Focusing on the sum of relative peak heights of free and bound Dox with each other (black squares), it is apparent that, at pH 5.5, an increase in free and total Dox peaks occurred. The explanation is simple: free Dox is reduced more easily and efficiently than bound Dox. To complete the illustration, voltammograms of free, partly bound, and completely bound Dox are shown in **Figs. 4C** and **4D**. Overall, it must be noted that the non-covalent binding of Dox to *o*MWCNTs can overcome the burst effect of the free drug and provides sustained release of Dox in more acidic environments, such as early/late endosomes or hypoxic regions common in solid tumours.

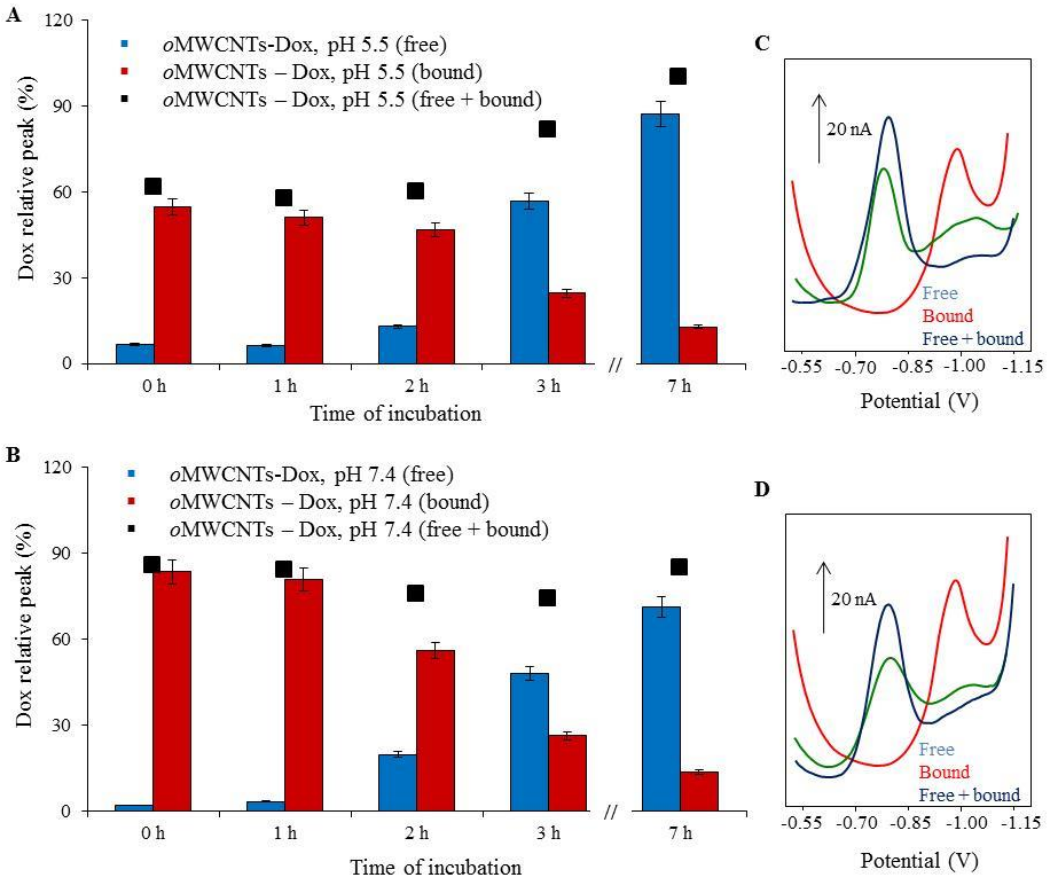

Figure 4: AdT-DPV estimation of Dox bound in *o*MWCNTs-Dox-Pep and Dox released from oMWCNTs-Dox-Pep in (**A**) buffer imitating intracellular acidic compartments (pH 5.5) and (**B**) Ringer's solution (pH 7.4). (**C**) and (**D**) represent characteristic DP voltammograms for free, bound, and total Dox in solution.

Estimation of the in vitro cytotoxicity of oMWCNTs-Dox-Pep in prostate cells

In drug delivery, it is expected that the drug carrier will have a low or no toxic effect. The toxicity of CNTs is an important attribute that needs to be considered in each biomedical application. It depends on various parameters, including structure (SWCNTs *vs.* MWCNTs), length, purity, agglomeration, and surface functionalisation [47, 48]. In our experiment workflow, the cytotoxicity of individual components and the entirely of *o*MWCNTs-Dox-Pep was examined in human non-malignant (PNT1A) and metastatic (LNCaP) prostatic cell lines. As shown in **Fig. 5A**, prostate-homing peptide alone induces only low cytotoxic effects (about 10%) in the case of the highest applied concentration in LNCaP cells. In the case of

PNT1A cells, no cytotoxic effects were identified. These results are in good conformity with the results obtained by Arap and coworkers [49], who showed that the primary role of prostate-homing peptide is the delivery of therapeutic agents to prostate cancer cells. Similarly, the application of *o*MWCNTs did not display any cytotoxic effects in both tested cell lines and mostly significantly ($p > 0.05$) stimulated cells to proliferate (**Fig. 5B**).

We further proceeded to test whole constructed *o*MWCNTs-Dox-Pep and compared the cytotoxicity with adequate Dox. **Fig. 5C** shows cytotoxicity in LNCaP cells, where Dox exhibited stronger cytotoxicity than *o*MWCNTs-Dox-Pep. Despite that, at the highest applied concentration, the cytotoxic effects of free Dox and *o*MWCNTs-Dox-Pep were similar (56% *vs.* 59% viability). We anticipate that the lower cytotoxicity of *o*MWCNTs-Dox-Pep is due to the limited exposure time (24 hours), which in combination with a neutral environment of cultivation media does not enable the complete release of Dox. Despite that, we succeeded in confirming that, in higher concentrations, Dox and *o*MWCNTs-Dox-Pep can have similar antiproliferative activity. In the case of PNT1A cells, Dox displayed pronounced cytotoxic effects, which resulted in a reduction of cell viability in all applied concentrations from 10% at 0.1 µg/mL to 80% at 25 µg/mL (**Fig. 5D**). It is noteworthy that *o*MWCNTs-Dox-Pep had no cytotoxic effects after 24 hours of exposure, which corresponds to the cytotoxicity of bare *o*MWCNTs.

The results show that the utilisation of prostate-homing peptide can significantly affect the interactions between *o*MWCNTs-Dox-Pep and metastatic/non-malignant cells and can thus increase the selectivity of Dox delivery. The prostate-homing peptide influence on the internalisation of *o*MWCNTs into metastatic/non-malignant cells was additionally confirmed by optical microscopy. The internalisation of *o*MWCNTs modified with homing peptide and *o*MWCNTs without peptide modification was observed under ambient light conditions on PC3 and PNT1A cell lines at a *o*MWCNT concentration of 50 µg/ mL (supplementary Fig.

2). The results show that oMWCNTs modified with peptide after 4 hours of incubation successfully internalised the PC3 cell line with localisation in cytoplasm. It is obvious that *o*MWCNTs without peptide modification are localised on the PC3 cell line surface and do not enter the cell line. In contrast to the obtained results, it is obvious that *o*MWCNTs modified with peptide and *o*MWCNTs without modification do not internalise in the PNT1A cell line after 4 hours. Samples are localised on the cell membrane surface in the case of both samples. Other authors have reported that the internalisation of *o*MWCNTs to cell lines required incubation between 24 and 48 hours [50, 51]. Our results obviously suggest that homing peptide increases the speed of internalisation and selectivity of doxorubicin delivery.

As mentioned above regarding the XTT proliferation assay results and results obtained from release kinetics studies, it is clear that they are in good agreement. This leads to the conclusion that the effect of pH has the main role in drug release from *o*MWCNTs. In a similar study, Zhang *et al*. modified the surface of SWCNTs with Dox [52]. They reported that, in conditions of lysosomal pH, the release of Dox is around 40% after 72 hours, while in conditions of neutral pH, the release of Dox is around 5% after 72 hours. Cao *et al*. reported that the release rate of Dox from polyethyleneimine (PEI) modified MWCNTs at pH 5.8 was 54.6% after 48 hours [53]. It is noteworthy that, at pH 7.4, Dox release was around 40% after 48 hours. Plausibly, the main reason for such behaviour of Dox is its partial protonation, which does not favour the π–π stacking in which Dox can be easily released from PEI-MWCNTs. Overall, it can be concluded that CNTs can bind Dox strongly and can thus effectively protect non-target cells from the side effect of Dox toxicity.

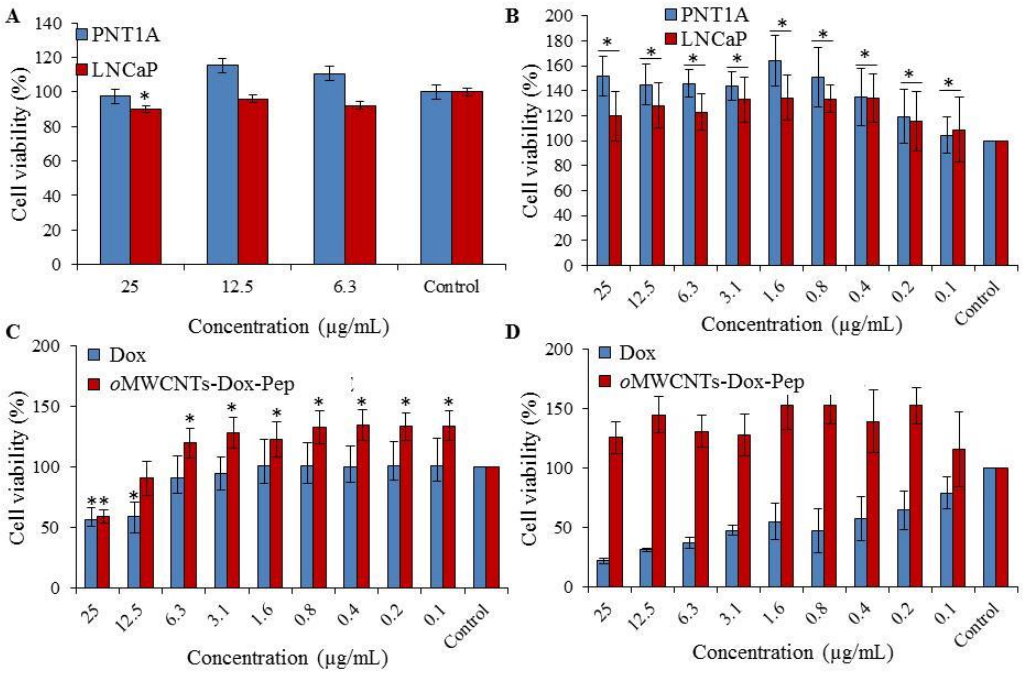

Figure 5: Evaluation of cytotoxicity using XTT proliferation assay showing cytotoxic effects of (A) prostate-homing peptide and (B) cytotoxicity of oMWCNTs. Further, cytotoxic effects of whole oMWCNTs-Dox-Pep were tested on (C) LNCaP cells and (D) PNT1A cells. Values are expressed as the mean of three independent replicates (n = 3). Vertical bars indicate standard error. Data with asterisks (*) indicate statistical significance ($p < 0.05$) related to non-treated cells. The applied concentration refers to the concentration of doxorubicin in complex.

To further evaluate the cytotoxic effects, the LNCaP cells were monitored 45 min after treatments using fluorescence microscopy (PI/SYTO9 assay). When no complexes were applied (**Fig. 6A**), the SYTO9 staining indicated a very strong signal because of the presence of living cells. The same result was obtained after the treatment of cells with *o*MWCNTs (**Fig. 6B**). The application of free Dox showed a high percentage of LNCaP cell death (**Fig. 6C**). Next, we have shown a concentration-dependent manner of dead and living LNCaP cells after exposure to 6, 12.5, and 25 µg/mL of Dox in *o*MWCNTs-Dox-Pep (**Figs. 6D**, **6E** and **6F**), which confirms the results obtained from the XTT assay.

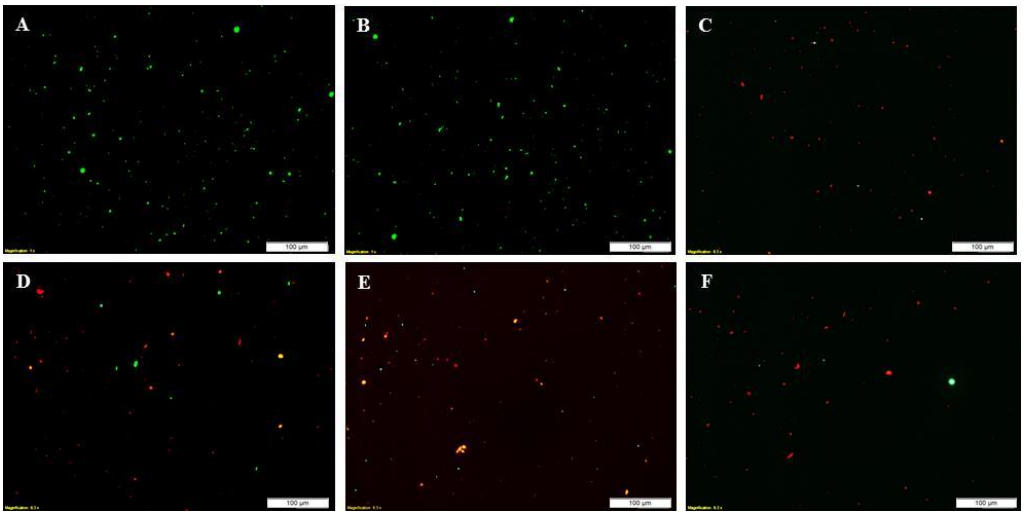

Figure 6: Evaluation of cytotoxicity of individual components and the whole *o*MWCNTs-Dox-Pep on LNCaP cells carried out using PI/SYTO9 live/dead cell microscopic assay. (**A**) Control – live, non-treated cells; (**B**) *o*MWCNTs; (**C**) Dox. Applications of *o*MWCNTs-Dox-Pep at following Dox concentrations: (**D**) 6 µg/mL; (**E**) 12 µg/mL, and (**F**) 25 µg/mL. The length of the scale bar is 100 µm.

Conclusion

We have developed and characterised an efficient Dox delivery system based on prostate-homing peptide-functionalised *o*MWCNTs. The role of prostate-homing peptide was to improve the drug targeting and internalisation through the cell membrane. Several techniques confirmed the successful formation of *o*MWCNTs-Dox-Pep. We have shown exceptional release kinetics profiles of Dox, which was primarily released in acidic pH, while in neutral conditions, only minor Dox release was found. In summary, this study demonstrates the considerable potential of *o*MWCNTs-Dox-Pep. It should be mentioned that the system is versatile and that many well-known homing peptides could be utilised to switch the applicability from prostate cancer to any other malignant disease. The validity of our results, however, requires further evaluation by *in vivo* experiments. Despite that, we demonstrate that *o*MWCNTs can serve as an exceptional platform for simple, stable, and efficient immobilisation of bioactive compounds.

Acknowledgements

This work is financially supported by IGA MENDELU IP_07_2016 and CEITEC 2020 (LQ1601) with financial support from the Ministry of Education, Youth and Sports of the Czech Republic under the National Sustainability Programme II.

Conflicts of interest

The authors declare no conflicts of interest.

References

[1] E.J. Petersen and T.B. Henry, Methodological considerations for testing the ecotoxicity of carbon nanotubes and fullerenes: Review, Environ.Toxicol. Chem., 31 (2012) 60-72.
[2] N. Roy, R. Sengupta and A.K. Bhowmick, Modifications of carbon for polymer composites and nanocomposites, Prog. Polym. Sci., 37 (2012) 781-819.
[3] N. Saifuddin, A.Z. Raziah and A.R. Junizah, Carbon Nanotubes: A Review on Structure and Their Interaction with Proteins, J. Chem., (2013) 1-18.
[4] A.J. Andersen, P.P. Wibroe and S.M. Moghimi, Perspectives on carbon nanotube-mediated adverse immune effects, Adv. Drug Deliv. Rev., 64 (2012) 1700-1705.
[5] A.A. Yazdi, L. D'Angelo, N. Omer, G. Windiasti, X.N. Lu and J. Xu, Carbon nanotube modification of microbial fuel cell electrodes, Biosens. Bioelectron., 85 (2016) 536-552.
[6] F. Karchemski, D. Zucker, Y. Barenholz and O. Regev, Carbon nanotubes-liposomes conjugate as a platform for drug delivery into cells, J. Control. Release, 160 (2012) 339-345.
[7] L.J. Meng, X.K. Zhang, Q.H. Lu, Z.F. Fei and P.J. Dyson, Single walled carbon nanotubes as drug delivery vehicles: Targeting doxorubicin to tumors, Biomaterials, 33 (2012) 1689-1698.
[8] H.X. Wu, H.L. Shi, H. Zhang, X. Wang, Y. Yang, C. Yu, C.Q. Hao, J. Du, H. Hu and S.P. Yang, Prostate stem cell antigen antibody-conjugated multiwalled carbon nanotubes for targeted ultrasound imaging and drug delivery, Biomaterials, 35 (2014) 5369-5380.
[9] S.Y. Madani, N. Naderi, O. Dissanayake, A. Tan and A.M. Seifalian, A new era of cancer treatment: carbon nanotubes as drug delivery tools, Int. J. Nanomed., 6 (2011) 2963-2979.
[10] M. Raoof, B.T. Cisneros, A. Guven, S. Phounsavath, S.J. Corr, L.J. Wilson and S.A. Curley, Remotely triggered cisplatin release from carbon nanocapsules by radiofrequency fields, Biomaterials, 34 (2013) 1862-1869.
[11] R. Marega and D. Bonifazi, Filling carbon nanotubes for nanobiotechnological applications, New J. Chem., 38 (2014) 22-27.
[12] Y.J. Gu, J.P. Cheng, J.F. Jin, S.H. Cheng and W.T. Wong, Development and evaluation of pH-responsive single-walled carbon nanotube-doxorubicin complexes in cancer cells, Int. J. Nanomed., 6 (2011) 2889-2898.
[13] C.B. Dong, A.S. Campell, R. Eldawud, G. Perhinschi, Y. Rojanasakul and C.Z. Dinu, Effects of acid treatment on structure, properties and biocompatibility of carbon nanotubes, Appl. Surf. Sci., 264 (2013) 261-268.
[14] Z.Y. Zhao, Z.H. Yang, Y.W. Hu, J.P. Li and X.M. Fan, Multiple functionalization of multi-walled carbon nanotubes with carboxyl and amino groups, Appl. Surf. Sci., 276 (2013) 476-481.
[15] B.S. Wong, S.L. Yoong, A. Jagusiak, T. Panczyk, H.K. Ho, W.H. Ang and G. Pastorin, Carbon nanotubes for delivery of small molecule drugs, Adv. Drug Deliv. Rev., 65 (2013) 1964-2015.
[16] C. Punckt, M.A. Pope, J. Liu, Y.H. Lin and I.A. Aksay, Electrochemical Performance of Graphene as Effected by Electrode Porosity and Graphene Functionalization, Electroanalysis, 22 (2010) 2834-2841.
[17] J. Zugazagoitia, C. Guedes, S. Ponce, I. Ferrer, S. Molina-Pinelo and L. Paz-Ares, Current Challenges in Cancer Treatment, Clin. Ther., 38 (2016) 1551-1566.
[18] K. Bhattacharya, S.P. Mukherjee, A. Gallud, S.C. Burkert, S. Bistarelli, S. Bellucci, M. Bottini, A. Star and B. Fadeel, Biological interactions of carbon-based nanomaterials: From coronation to degradation, Nanomed.-Nanotechnol. Biol. Med., 12 (2016) 333-351.

[19] J. Muller, F. Huaux, N. Moreau, P. Misson, J.-F. Heilier, M. Delos, M. Arras, A. Fonseca, J.B. Nagy and D. Lison, Respiratory toxicity of multi-wall carbon nanotubes, Toxicol. Appl. Pharmacol., 207 (2005) 221-231.
[20] C.P. Firme and P.R. Bandaru, Toxicity issues in the application of carbon nanotubes to biological systems, Nanomed.-Nanotechnol. Biol. Med., 6 (2010) 245-256.
[21] F.H. Wang, Y. Wang, X. Zhang, W.J. Zhang, S.R. Guo and F. Jin, Recent progress of cell-penetrating peptides as new carriers for intracellular cargo delivery, J. Control. Release, 174 (2014) 126-136.
[22] V.S. Thakare, M. Das, A.K. Jain, S. Patil and S. Jain, Carbon nanotubes in cancer theragnosis, Nanomedicine, 5 (2010) 1277-1301.
[23] A. Bianco, K. Kostarelos and M. Prato, Opportunities and challenges of carbon-based nanomaterials for cancer therapy, Expert Opin. Drug Deliv., 5 (2008) 331-342.
[24] L. Stobinski, B. Lesiak, L. Kover, J. Toth, S. Biniak, G. Trykowski and J. Judek, Multiwall carbon nanotubes purification and oxidation by nitric acid studied by the FTIR and electron spectroscopy methods, J. Alloy. Compd., 501 (2010) 77-84.
[25] H. Kong, C. Gao and D.Y. Yan, Controlled functionalization of multiwalled carbon nanotubes by in situ atom transfer radical polymerization, J. Am. Chem. Soc., 126 (2004) 412-413.
[26] P.H. Matter and U.S. Ozkan, Non-metal catalysts for dioxygen reduction in an acidic electrolyte, Catal. Lett., 109 (2006) 115-123.
[27] I.D. Rosca, F. Watari, M. Uo and T. Akaska, Oxidation of multiwalled carbon nanotubes by nitric acid, Carbon, 43 (2005) 3124-3131.
[28] J.L. Misset, V. Dieras, G. Gruia, H. Bourgeois, E. Cvitkovic, S. Kalla, L. Bozec, P. Beuzeboc, C. Jasmin, J.P. Aussel, A. Riva, N. Azli and P. Pouillart, Dose-finding study of docetaxel and doxorubicin in first-line treatment of patients with metastatic breast cancer, Ann. Oncol., 10 (1999) 553-560.
[29] B.C. Evans, C.E. Nelson, S.S. Yu, K.R. Beavers, A.J. Kim, H. Li, H.M. Nelson, T.D. Giorgio and C.L. Duvall, Ex Vivo Red Blood Cell Hemolysis Assay for the Evaluation of pH-responsive Endosomolytic Agents for Cytosolic Delivery of Biomacromolecular Drugs, J. Vis. Exp., (2013) 1-5.
[30] S. Dostalova, T. Cerna, D. Hynek, Z. Koudelkova, T. Vaculovic, P. Kopel, J. Hrabeta, Z. Heger, M. Vaculovicova, T. Eckschlager, M. Stiborova and V. Adam, Site-Directed Conjugation of Antibodies to Apoferritin Nanocarrier for Targeted Drug Delivery to Prostate Cancer Cells, ACS Appl. Mater. Inferfaces, 8 (2016) 14430-14441.
[31] I. Corazzari, A. Gilardino, S. Dalmazzo, B. Fubini and D. Lovisolo, Localization of CdSe/ZnS quantum dots in the lysosomal acidic compartment of cultured neurons and its impact on viability: Potential role of ion release, Toxicol. Vitro, 27 (2013) 752-759.
[32] M. Berney, F. Hammes, F. Bosshard, H.U. Weilenmann and T. Egli, Assessment and interpretation of bacterial viability by using the LIVE/DEAD BacLight kit in combination with flow cytometry, Appl. Environ. Microbiol., 73 (2007) 3283-3290.
[33] H.C. Tsai, J.Y. Lin, F. Maryani, C.C. Huang and T. Imae, Drug-loading capacity and nuclear targeting of multiwalled carbon nanotubes grafted with anionic amphiphilic copolymers, Int. J. Nanomed., 8 (2013) 4427-4440.
[34] Z. Heger, A. Moulick, H.V. Nguyen, M. Kremplova, P. Kopel, D. Hynek, T. Eckschlager, M. Stiborova, O. Zitka, V. Adam and R. Kizek, Characterization of Multi-Walled Carbon Nanotubes Double-Functionalization with Cytostatic Drug Etoposide and Phosphorothioate Oligodeoxynucleotides, Int. J. Electrochem. Sci., 10 (2015) 7707-7719.
[35] V. Milosavljevic, Y. Haddad, M.A.R. Merlos, A. Moulick, H. Polanska, D. Hynek, Z. Heger, P. Kopel and V. Adam, The zinc-Schiff base-novicidin complex as a potential prostate cancer therapy, PLoS ONE, 11 (2016) 1-19.

[36] F. Aviles, J.V. Cauich-Rodriguez, L. Moo-Tah, A. May-Pat and R. Vargas-Coronado, Evaluation of mild acid oxidation treatments for MWCNT functionalization, Carbon, 47 (2009) 2970-2975.
[37] V. Datsyuk, M. Kalyva, K. Papagelis, J. Parthenios, D. Tasis, A. Siokou, I. Kallitsis and C. Galiotis, Chemical oxidation of multiwalled carbon nanotubes, Carbon, 46 (2008) 833-840.
[38] M.H. Tang, H.J. Dou and K. Sun, One-step synthesis of dextran-based stable nanoparticles assisted by self-assembly, Polymer, 47 (2006) 728-734.
[39] S. Grandi, A. Magistris, P. Mustarelli, E. Quartarone, C. Tomasi and L. Meda, Synthesis and characterization of SiO2-PEG hybrid materials, J. Non-Cryst. Solids, 352 (2006) 273-280.
[40] V. Adam, I. Fabrik, V. Kohoutkova, P. Babula, J. Hubalek, R. Vrba, L. Trnkova and R. Kizek, Automated Electrochemical Analyzer as a New Tool for Detection of Thiols, Int. J. Electrochem. Sci., 5 (2010) 429-447.
[41] S. Krizkova, P. Blahova, J. Nakielna, I. Fabrik, V. Adam, T. Eckschlager, M. Beklova, Z. Svobodova, V. Horak and R. Kizek, Comparison of Metallothionein Detection by Using Brdicka Reaction and Enzyme-Linked Immunosorbent Assay Employing Chicken Yolk Antibodies, Electroanalysis, 21 (2009) 2575-2583.
[42] R. Brdička, Polarographic studies with the dropping mercury kathode. Part XXXI. A new test for proteins in the presence of cobalt salts in ammoniacal solutions of ammonium chloride, Collect. Czech. Chem. Comm., 5 (1933) 112-128.
[43] J. Kudr, L. Richtera, L. Nejdl, I. Blazkova, V. Milosavljevic, Z. Moravec, D. Wawrzak, P. Kopel, B. Ruttkay-Nedecky, V. Adam and R. Kizek, Characterization of Carbon Dots Covered with Polyvinylpyrrolidone and Polyethylene Glycol, Int. J. Electrochem. Sci., 10 (2015) 8243-8254.
[44] K. Tmejova, D. Hynek, P. Kopel, S. Dostalova, K. Smerkova, M. Stanisavljevic, H.V. Nguyen, L. Nejdl, M. Vaculovicova, S. Krizkova, R. Kizek and V. Adam, Electrochemical Behaviour of Doxorubicin Encapsulated in Apoferritin, Int. J. Electrochem. Sci., 8 (2013) 12658-12671.
[45] E. Heister, V. Neves, C. Lamprecht, S.R.P. Silva, H.M. Coley and J. McFadden, Drug loading, dispersion stability, and therapeutic efficacy in targeted drug delivery with carbon nanotubes, Carbon, 50 (2012) 622-632.
[46] X. Qi, Y. Rui, Y. Fan, H. Chen, N. Ma and Z. Wu, Galactosylated chitosan-grafted multiwall carbon nanotubes for pH-dependent sustained release and hepatic tumor-targeted delivery of doxorubicin in vivo, Colloid Surf. B-Biointerfaces, 133 (2015) 314-322.
[47] K. Kostarelos, The long and short of carbon nanotube toxicity, Nat. Biotechnol., 26 (2008) 774-776.
[48] S. Lanone, P. Andujar, A. Kermanizadeh and J. Boczkowski, Determinants of carbon nanotube toxicity, Adv. Drug Deliv. Rev., 65 (2013) 2063-2069.
[49] W. Arap, W. Haedicke, M. Bernasconi, R. Kain, D. Rajotte, S. Krajewski, H.M. Ellerby, D.E. Bredesen, R. Pasqualini and E. Ruoslahti, Targeting the prostate for destruction through a vascular address, Proc. Natl. Acad. Sci. U. S. A., 99 (2002) 1527-1531.
[50] Q.X. Mu, D.L. Broughton and B. Yan, Endosomal Leakage and Nuclear Translocation of Multiwalled Carbon Nanotubes: Developing a Model for Cell Uptake, Nano Lett., 9 (2009) 4370-4375.
[51] R.B. Li, X. Wang, Z.X. Ji, B.B. Sun, H.Y. Zhang, C.H. Chang, S.J. Lin, H. Meng, Y.P. Liao, M.Y. Wang, Z.X. Li, A.A. Hwang, T.B. Song, R. Xu, Y. Yang, J.I. Zink, A.E. Nel and T. Xia, Surface Charge and Cellular Processing of Covalently Functionalized Multiwall Carbon Nanotubes Determine Pulmonary Toxicity, ACS Nano, 7 (2013) 2352-2368.

[52] X.K. Zhang, L.J. Meng, Q.H. Lu, Z.F. Fei and P.J. Dyson, Targeted delivery and controlled release of doxorubicin to cancer cells using modified single wall carbon nanotubes, Biomaterials, 30 (2009) 6041-6047.
[53] X. Cao, L. Tao, S. Wen, W. Hou and X. Shi, Hyaluronic acid-modified multiwalled carbon nanotubes for targeted delivery of doxorubicin into cancer cells, Carbohydr. Res., 405 (2015) 70-77.

5.3.2. Research article V

S. Dostalova, A. Moulick, **V. Milosavljevic**, R. Guran, M. Kominkova, K. Cihalova, Z. Heger, L. Blazkova, P. Kopel, D. Hynek, Antiviral activity of fullerene C60 nanocrystals modified with derivatives of anionic antimicrobial peptide maximin H5, Monatshefte für Chemie-Chemical Monthly, 147 (2016) 905-918.

Participation in the work of the author Vedran Milosavljevic: experimental part 30% and manuscript preparation 25%.

Fullerenes or fullerene C60 nanocrystals are large spherical hollow cages structured from 60 to hundreds of carbon atoms [208]. Functionalization of fullerene C60 nanocrystals with various types of inorganic acids involves formation of carboxylic groups on the surface of cage. Carboxylic surface modification increases the bonding rate between different drugs and the fullerene C60 nanocrystal surface. Functionalized fullerene C60 nanocrystals can be modified with a variety of drugs, including chemotherapeutics, antiviral and antibacterial agents [209].

The aim of this study was to synthesize a novel carbon based nanocarrier modified with highly antiviral peptides. Six different mutants of maximin H5 were synthesized by replacing aspartic amino acid with asparagine, histidine, tyrosine, alanine, glycine, or valine at position 11, showing increasing antiviral and antibacterial activity. Functionalization of fullerene C60 nanocrystals was done by treatment with concentrated nitric acid and trimesic acid (benzene-1,3,5-tricarboxylic acid). Oxidation of fullerene was studied by gas chromatography (CHNS) analysis. Formation of bonds between fullerenes and maximin derivated peptides was studied by MALDI-TOF MS and SEM techniques. The antiviral activity was tested on model organism bacteriophage, by using the plaque assay. The antibacterial activity was tested on its *E. coli*, using the growth curves method.

The obtained results show that peptides have very low activity, which was improved by attaching them to suitable nanocarrier, fullerene C60 nanocrystals. The trimesic acid functionalization of fullerenes introduced more carboxyl groups on the surface of fullerene C60 nanocrystals, in comparison to nitric acid. The tests have shown that maximin derivate have higher antiviral activity than the original peptide. Maximin H5 with exchanged aspartic amino acid at position 11 with asparagine, valine

or tyrosine shows better antiviral activity. Moreover, the antiviral activity was in correlation with the amount of peptide conjugated on the fullerene surface.

To conclude, in this study the considerable potential of fullerene C60 nanocrystals modified with antimicrobial peptide maximin H5 was demonstrated. Fullerene C60 nanocrystals functionalized with acids increase the binding potential and can serve as an exceptional platform for simple, stable and efficient immobilization of peptides and increase of their antiviral or antibacterial potential.

Monatsh Chem (2016) 147:905–918
DOI 10.1007/s00706-016-1675-0

ORIGINAL PAPER

Antiviral activity of fullerene C_{60} nanocrystals modified with derivatives of anionic antimicrobial peptide maximin H5

Simona Dostalova[1,2] · Amitava Moulick[1,2] · Vedran Milosavljevic[1,2] · Roman Guran[1,2] · Marketa Kominkova[1,2] · Kristyna Cihalova[1,2] · Zbynek Heger[1,2] · Lucie Blazkova[1,2] · Pavel Kopel[1,2] · David Hynek[1,2] · Marketa Vaculovicova[1,2] · Vojtech Adam[1,2] · Rene Kizek[1,2]

Received: 2 December 2015 / Accepted: 14 January 2016 / Published online: 1 March 2016

Abstract Many active antiviral substances come from natural sources. In this way, peptides, isolated from Asian toad *Bombina maxima*, called maximins, are very promising. Most of them have good antimicrobial activity; however, derivatives of anionic 20 amino acids-long maximin H5 show also promising antiviral activity. The effect can be enhanced by binding to suitable nanocarriers such as fullerenes. In the present study, six mutants of maximin H5 were designed where aspartic acid at position 11 was replaced by asparagine, histidine, tyrosine, alanine, glycine, or valine. The binding yield of each peptide to fullerene C_{60} nanocrystals was studied by derivatization with fluorescent reagent fluorescamine. The antiviral activity of these peptides and peptides bound to fullerene C_{60} nanocrystals was studied using bacteriophage λ as a model virus. All of the designed peptides had higher antiviral activity compared to maximin H5. The highest antiviral activity was observed in case of maximin variants H5N, H5V, or H5Y. Moreover, the antiviral activity was dependent on the amount of peptide bound on the surface of fullerene C_{60} nanocrystals, which was enhanced by trimesic acid (benzene-1,3,5-tricarboxylic acid) treated fullerene C_{60} nanocrystals.

Graphical abstract

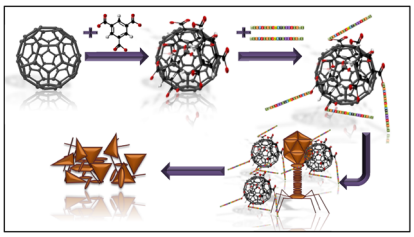

Keywords Carbon nanomaterials · Maximin H5 · Nanocarrier · Nanomedicine · Viral infections

Introduction

Nanomaterials provide unique properties compared with bulk materials of the same chemical composition [1]. They differ in some basic properties like melting temperature, magnetic properties, or color [2]. Using nanoparticles called nanocarriers, it is possible to dissolve insoluble drugs in desired solvents and transport them selectively to target cells or virions which can increase its efficiency or decrease the negative side effects associated with many therapeutics. The nanocarriers help to decrease the amount of administered drug [1]. In addition, the specificity, biocompatibility, and storage lifetime can be enhanced by encapsulation of the drug into the nanocarrier [3, 4].

The nanocarriers can be made from various materials: inorganic or organic (lipid, polymeric, or protein based). Inorganic nanocarriers can be made up of metal, metalloid,

Electronic supplementary material The online version of this article (doi:10.1007/s00706-016-1675-0) contains supplementary material, which is available to authorized users.

✉ Rene Kizek
kizek@sci.muni.cz

[1] Laboratory of Metallomics and Nanotechnologies, Department of Chemistry and Biochemistry, Mendel University in Brno, Zemedelska 1, 613 00 Brno, Czech Republic

[2] Central European Institute of Technology, Brno University of Technology, Technicka 3058/10, 616 00 Brno, Czech Republic

non-metal [5]. In addition, carbon nanoparticles, such as nanotubes, graphene, or fullerenes, are often studied [6]. Fullerenes or fullerene C_{60} nanocrystals are self-assembly cages containing 30 to hundreds of carbon atoms [7]. It is possible to functionalize fullerene C_{60} nanocrystals with carboxylic groups, which enable the covalent bond between different drugs and the fullerene C_{60} nanocrystal surface [8]. They can bind a variety of drugs, including chemotherapeutics [9, 10], antiviral [11] or antibacterial agents [12].

Viral infections are a growing problem both in developed and developing countries, reminded by recent Ebola virus epidemic [13] or HIV virus, infecting more than 35 million people [14]. These are just two of numerous viral diseases with very complicated treatment, often inaccessible for wide population, especially in developing countries [15, 16]. Many substances with antimicrobial or antiviral effect are naturally occurring in plants or animals [17]. They are, in the form of peptides, usually a part of innate immune system of amphibians [18], highly evolved especially on their skin due to the high exposition of amphibian skin to microbes from various environments [19]. However, these peptides are also present in the brains of amphibians [20]. They are usually composed of cationic and hydrophobic amino acids allowing them to selectively interact with bacterial membranes [21]. They are also efficient against fungi and even some types of cancer cells [22].

Peptides, isolated from various Asian toads [23] such as *Bombina maxima*, are significant to study. These peptides are called maximins or maximins H. Maximin H5 is an anionic peptide with antimicrobial activity only towards Gram-positive bacteria such as *Staphylococcus aureus*. On the other hand, Gram-negative bacteria, such as *Escherichia coli* (*E. coli*), are not significantly inhibited by this peptide [24]. The sequence of this peptide is composed of 20 amino acids and includes acidic aspartic acid at positions 11, 14, and 15 and hydrophobic amino acids, glycine and isoleucine at positions 18 and 19. This phenomenon distinguishes maximin H5 from other maximins containing basic amino acids at these positions [24].

Recent research shows a promising antiviral activity of basic derivatives of H5, although the exact mechanism is still unknown [25]. Generally, three different mechanisms of the antiviral activity of the peptide have been described: (a) it can interact with the viral capsid or envelope, thus inhibit the adhesion to host cell and its entering; (b) it can disrupt the lipid layer of the viral envelope and lyse the virion; and (c) it can inhibit the replication of the viral nucleic acid [26]. Moreover, some of the previous works have indicated that the mice injected with maximin peptides can develop neurotoxic symptoms [27]. Binding of the peptide to some nanocarrier can lower the negative side effects and increase their effectivity [28].

In the present work, a novel nanocarrier with high antiviral activities was developed. Six different mutants of maximin H5 were synthesized. As a nanocarrier, fullerene C_{60} nanocrystals were activated with nitric acid or modified by trimesic acid (benzene-1,3,5-tricarboxylic acid) and their ability to conjugate with maximin peptides was studied, as along with antiviral and antibacterial properties. The antiviral activity was tested on model organism bacteriophage λ using the plaque assay. The antibacterial activity was tested on its host bacteria using the growth curves method.

Results and discussion

Interaction of maximins and fullerene C_{60} nanocrystals

Abundant antimicrobial peptides can be found in the skin and brain of an Asian toad: *B. maxima*. Its skin and brain contains 27 and 52 maximin peptides, respectively [20, 29]. In the present study, we proposed that the derivatives of 20-amino acid long H5 maximin can be used as antiviral drugs which can inhibit the growth of bacteriophage λ in *E. coli* colonies. We synthesized six different mutants with the replacement of aspartic acid at the position 11 by alanine, glycine, histidine, asparagine, valine, or tyrosine. The designated H5N and H5G maximin have the same sequence as maximin H37 and H41, respectively, and both of them were also found in the toad, *B. maxima* [20]. The synthesized peptides were characterized using matrix-assisted laser desorption/ionization–time of flight mass spectrometric analysis (MALDI–TOF–MS; Supplementary data 1–7) according to [30]. The MS analysis confirmed the successful synthesis of the designed peptides. The high-performance liquid chromatography with electrospray ionization quadrupole time of flight mass spectrometry analysis showed that the purity of the synthesized peptides was approx. 70 %. The influence of the amino acid mutation on the theoretical prediction of secondary structures showed that the replacement of the central amino acid could have a significant influence on the secondary structure of the peptide (Fig. 1). The biggest change was observed in the case of H5N. The structure of H5N mutant changed from partly helical structure of H5 maximin to a completely helical structure. Another significant change was observed in the case of H5V mutant where the structure changed to two partly helical parts.

Pristine fullerenes, such as C_{60} or C_{70}, are widely used in biomedicine as drug delivery systems [9, 31–33]. To attach a drug to fullerene or fullerene C_{60} nanocrystals, it is

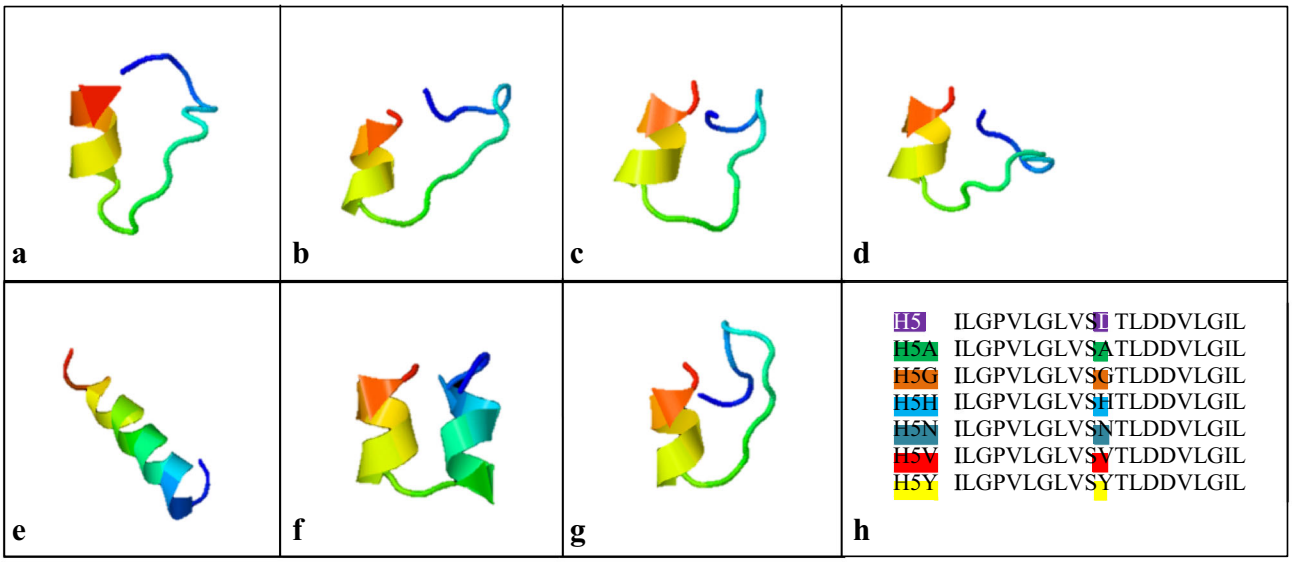

Fig. 1 Software prediction of maximin H5 mutants secondary structure using the PEP-FOLD online software (http://bioserv.rpbs.univ-paris-diderot.fr/services/PEP-FOLD/). **a** Maximin H5, **b** maximin H5A, **c** maximin H5G, **d** maximin H5H, **e** maximin H5N, **f** maximin H5V, **g** maximin H5Y, **h** the sequences of maximin H5 peptides with *highlighted* amino acid changes

needed to activate their surface either electrochemically [34] or with various active groups, such as palladium [35], amines [33], esters [36], or hydroxyl groups [37]. In this work, we examined two ways of activating the fullerene C_{60} nanocrystal surface by treatment with nitric acid or trimesic acid (TMA). Nitric acid can be used for the oxidation of the carbon nanostructures to enable covalent binding of the drug molecules; however, the oxidation rate is usually very low [8, 9]. Moreover, because of their structure, fullerene C_{60} nanocrystals are also able to bind non-covalently with different molecules containing aromatic rings via π–π stacking interactions [38, 39]. We used trimesic acid to modify fullerenes by π–π interactions of its aromatic ring. Such π–π interactions were proved by X-ray analyses [40] and many examples of trimesate hydrogen bonding with formation of networks can be also found in the literature [41, 42]. The presence of trimesic acid should improve the bonding of the peptide by H-bonding between the electron pairs of oxygen atoms from carboxylate groups and the hydrogens of amide peptide groups.

After the activation or modification of the surface of fullerene C_{60} nanocrystals, they were purified from excess molecules of nitric and trimesic acid by several times washing with water and centrifugation according to [9]. The size distribution, zeta potential, and content of elements were studied. The size distribution and zeta potential of fullerene C_{60} nanocrystals activated with either nitric acid or trimesic acid (F-HNO_3 or F-TMA) and dissolved in cultivating medium of pH 7.4 were determined by dynamic light scattering and Doppler micro-electrophoresis. The average size and zeta potential of F-HNO_3 were 50 nm and −18.6 mV, respectively. The sizes of these nanocrystals were not uniform; a number of particles were also around 122 nm (4 %) in diameter. The F-TMA had an average size of 295 nm (with uniform size distribution) and zeta potential of −22.7 mV [43]. The more negative zeta potential indicated higher presence of negative groups on the surface of fullerene C_{60} nanocrystals, which was probably due to the presence of the trimesic carboxylate groups attached to the fullerene C_{60} nanocrystal surface via the π–π stacking interactions [38].

These results were further confirmed by the elemental analysis of fullerene C_{60} nanocrystals with calculated percentage of oxygen. F-HNO_3 contained only 0.1 % of hydrogen and 98.9 % of carbon and this proportion did not change with increasing applied concentration of nitric acid. In case of F-TMA, the amounts of hydrogen and carbon were found to be 0.2 and 92.0 %, respectively. In this preparation we used a very high concentration of trimesic acid and it was found that the ratio remained the same and it was not dependent on the concentration of trimesic acid. According to calculations, the fullerene:TMA ratio was 9:6 in all cases (calculated H = 0.2 %, C = 92.3 %). The presence of the trimesic acid molecules on the fullerene C_{60} nanocrystal surface can enable the binding of other active molecules, such as peptides. This interaction is possible not only via hydrophobic interactions of peptides with fullerene C_{60} nanocrystal surface [44] (as is the case of C_{60} nanocrystals activated with nitric acid), but also via hydrogen bonding of trimesic acid with peptide [45]. Even though the amount of trimesic acid attached on the surface is low, the fullerene C_{60} nanocrystals modified with

trimesic acid are more suitable as a nanocarrier for antiviral maximins than the fullerene C_{60} nanocrystals activated with nitric acid. The schematic representation of the proposed nanocarriers is shown in Fig. 2a, b.

The surface of fullerene C_{60} nanocrystals was modified with the maximin H5 mutants. The fullerene C_{60} nanocrystals were purified from the excess molecules of peptides by a filtration through Amicon 3K centrifugal columns [10] and the binding yield of the peptides to fullerene C_{60} nanocrystals was measured by the derivatization of the peptides' amino groups with fluorescamine (Fig. 2c). The results showed different binding properties of F-HNO_3 and F-TMA. F-TMA was able to bind the peptides in average two times more than F-HNO_3. It is presumably caused by the presence of carboxylate groups on the surface of fullerene C_{60} nanocrystals. The binding of each peptide also varied. The concentration of maximin H5 peptide bound on fullerene C_{60} nanocrystals was very low in comparison with other mutants with the same applied concentration (0.18 mg cm^{-3} in H5 and F-TMA). The highest binding was achieved with maximins H5A (0.79 mg cm^{-3} with F-TMA), H5N (0.70 mg cm^{-3}), H5V (0.71 mg cm^{-3}), and H5Y (0.90 mg cm^{-3}).

The surface modification of fullerene C_{60} nanocrystals with maximin H5 mutants was further confirmed using the scanning electron microscopy. Figure 3a shows fullerene C_{60} nanocrystals without modification. Approximately 2 µm long nanocrystals with very sharp edges can be observed. Similar results have been published by Abe et al. [46]. Significant changes in the fullerene C_{60} nanocrystals can also be observed for both F-HNO_3 (Fig. 3b) and F-TMA (Fig. 3d) and these variants modified with the

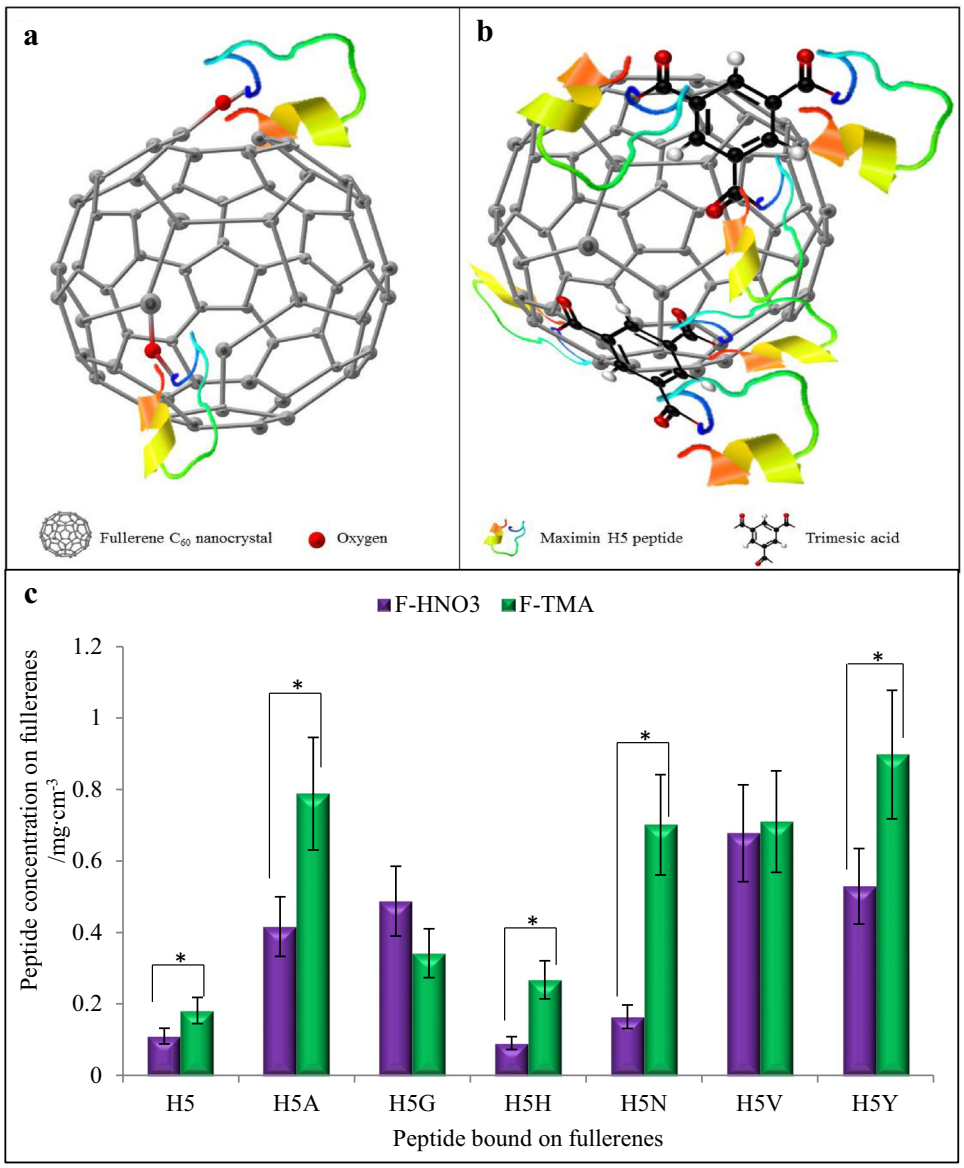

Fig. 2 **a** The schematic representation of fullerene C_{60} nanocrystal activated with nitric acid and modified by maximin H5 peptide, **b** the schematic representation of fullerene C_{60} nanocrystal modified by trimesic acid and maximin H5 peptide, **c** the amount of peptides bound to fullerene C_{60} nanocrystals activated by nitric (F-HNO_3) or trimesic acid (F-TMA) determined by derivatization with 30 mm^3 of 1 mM fluorescamine per 50 mm^3 of peptide-modified fullerene C_{60} nanocrystals (for details see "Experimental" section). *Asterisks* indicate significant difference at $p < 0.05$ (*)

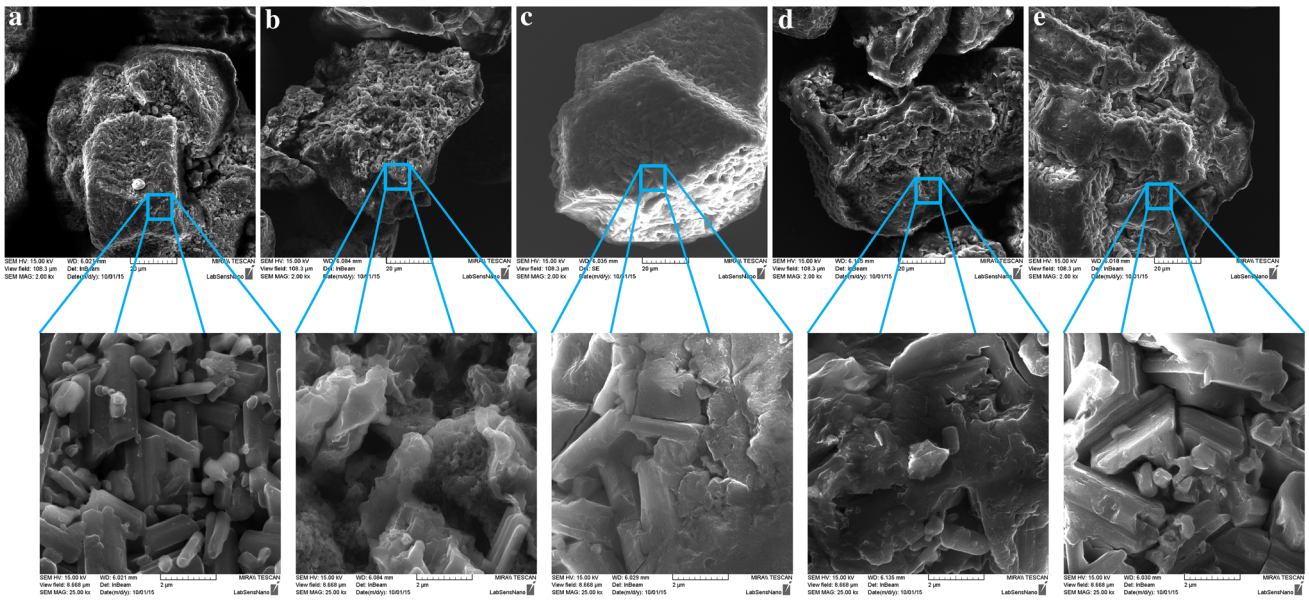

Fig. 3 The structural changes of fullerene C_{60} nanocrystals revealed by scanning electron microscopy. **a** Fullerene C_{60} nanocrystals without activation; **b** fullerene C_{60} nanocrystals activated with nitric acid (F-HNO_3), **c** fullerene C_{60} nanocrystals activated with nitric acid (F-HNO_3) and modified with maximin H5N peptide, **d** fullerene C_{60} nanocrystals activated with trimesic acid (F-TMA), **e** fullerene C_{60} nanocrystals activated with trimesic acid (F-TMA) and modified with maximin H5N peptide. The length of *scale bar* is 20 μm in *upper line* and 2 μm in *lower line*, respectively

maximin H5N peptide (Fig. 3c, e). After modification with HNO_3 and TMA, the fullerenes became bulkier and their edges became smoother. Modification with maximin H5N peptide further enhanced these changes, creating fuzzier and bulkier fullerene C_{60} nanocrystals.

The influence of each component on *E. coli*

The antibacterial activity was determined using the growth curves method of host bacteria, indicator *E. coli* according to [47]. The application of the highest concentration of the peptides had no observed inhibition activity on the bacteria (Fig. 4a). The maximin H5 peptide is an anionic peptide, which is mainly active against Gram-positive bacteria with reduced activity towards Gram-negative bacteria [48], thus limited activity should be expected against the Gram-negative *E. coli*. Next, we studied the influence of fullerene C_{60} nanocrystals on the host bacteria *E. coli* (Fig. 4b) to determine whether the stimulation of bacteriophage λ plaque formation was caused by the antibacterial activity of fullerene C_{60} nanocrystals. Neither F-HNO_3 nor F-TMA had any observed antibacterial activity towards the tested strain of *E. coli*. The obtained results showed that neither fullerene C_{60} nanocrystals nor designed peptides by themselves had any observed antiviral or antibacterial activity ($p < 0.05$).

Finally, the conjugates of the mutants with the F-HNO_3 or F-TMA were investigated and as shown in Fig. 4c, d, no significant ($p < 0.05$) inhibition of the *E. coli* growth was observed. This was further confirmed by the live/dead bacterial cell analysis [49] of control (untreated *E. coli*, Fig. 4e) and *E. coli* treated with the maximin H5N mutant (Fig. 4f), F-HNO_3 (Fig. 4g), F-TMA (Fig. 4h), F-HNO_3 modified with the maximin H5N mutant (Fig. 4i), and F-TMA modified with the maximin H5N mutant (Fig. 4j).

The influence of peptide-modified fullerene C_{60} nanocrystals on bacteriophage λ

Bacteriophage λ is a temperate phage of bacteria *E. coli* [50]. It is the key model organism of molecular biology [51] with discoveries ranging from the control of gene expression [52], through SDS-PAGE [53] to DNA site-specific recombination [54]. Therefore, it is an ideal model organism for the investigation of new compounds with antiviral activity. Multiple potential antiviral agents or disinfectants have been tested on bacteriophage lambda in the past, including nitrogen mustard [55], Virkon-S [56], or *N*-methylisatin β-thiosemicarbazone–copper complexes [57].

Firstly, the bacteriophage was characterized. During the lytic pathway, around 100 phage particles can be produced in one host cell [51]. The SDS-PAGE experiment showed a 37 kDa protein, gpE of bacteriophage λ (Fig. 5a left). Each capsid of bacteriophage λ contains 420 copies of this protein which made it the major capsid protein [58]. The

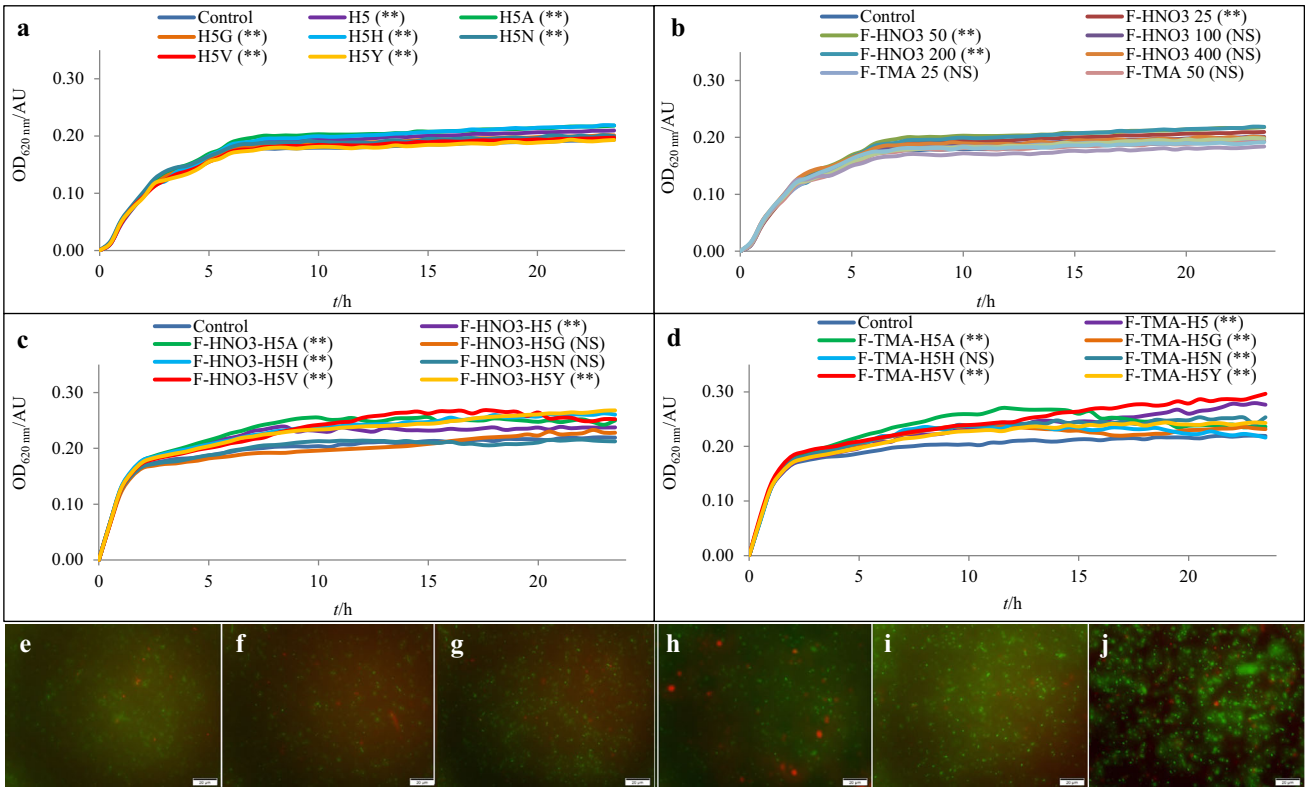

Fig. 4 **a** Growth curves of indicator *E. coli* with maximin H5 derivatives measured (every 30 min for 24 h) at absorbance 620 nm during cultivation at 37 °C, **b** growth curves of indicator *E. coli* with fullerene C_{60} nanocrystals oxidized (F-HNO_3) or modified by trimesic acid (F-TMA) measured (every 30 min for 24 h) at absorbance 620 nm during cultivation at 37 °C. Antibacterial activity of fullerene C_{60} nanocrystals activated with nitric (**c**) or trimesic (**d**) acid and modified with maximin H5 mutants investigated using the growth curves method (absorbance at 620 nm during cultivation at 37 °C each 30 min for 24 h). [*Asterisks* indicated significantly increased growth of *E. coli* at $p < 0.05$ (**). NS indicate non-significantly different growth of *E. coli*. The statistical evaluation was performed on the absorbance values after 24 h of incubation of *E. coli* with fullerene C_{60} nanocrystals, peptides or peptide-modified fullerene C_{60} nanocrystals], **e** live/dead bacterial cell analysis of control *E. coli*, **f** live/dead bacterial cell analysis of *E. coli* treated with the H5N mutant, **g** live/dead bacterial cell analysis of *E. coli* treated with F-HNO_3, **h** live/dead bacterial cell analysis of *E. coli* treated with F-TMA, **i** live/dead bacterial cell analysis of *E. coli* treated with F-HNO_3 modified with the H5N mutant, **j** live/dead bacterial cell analysis of *E. coli* treated with F-TMA modified with the H5N mutant

results showed a constant yield of bacteriophage λ virions during cultivation.

The presence of bacteriophage λ was subsequently observed using AFM (Fig. 5a right). The image showed the icosahedral capsid of bacteriophage λ with approximately 60 nm in diameter and the whole length of bacteriophage was determined as 130 nm. This corresponds to known literatures [59].

The representative photographs of observed plaques after cultivation of bacteriophage λ in indicator *E. coli* in the presence of F-HNO_3 modified with maximin H5 or F-TMA modified with mutant H5N are shown in Fig. 5b left, right, respectively. The plaques are marked with arrows.

Next, we evaluated the antiviral activity of the designed mutants and F-HNO_3 or F-TMA. The antiviral activity was determined by using plaque assay method with bacteriophage λ as a model virus. For the assessment of the antiviral activity of the peptides, we used five concentrations of each designed peptide (Fig. 5c). The number of plaques was relatively compared to control (maximin H5), which was determined as 100 %. The lower relative number of plaques showed a lower amount of mature bacteriophage λ and thus a higher antiviral activity of the peptides. The relative number of plaques in comparison with control was not significantly lower at the different applied concentrations of the peptides.

For the assessment of antiviral activity of fullerene C_{60} nanocrystals, we have used five different concentrations of F-HNO_3 or F-TMA (Fig. 5d). The lower relative number of plaques can be caused by a lower amount of mature bacteriophage λ and thus a higher antiviral activity of the fullerene C_{60} nanocrystals. However, higher concentrations of fullerene C_{60} nanocrystals showed no observed antiviral activity; and instead more bacteriophage λ plaques were formed. Fullerene C_{60} nanocrystals stimulated the

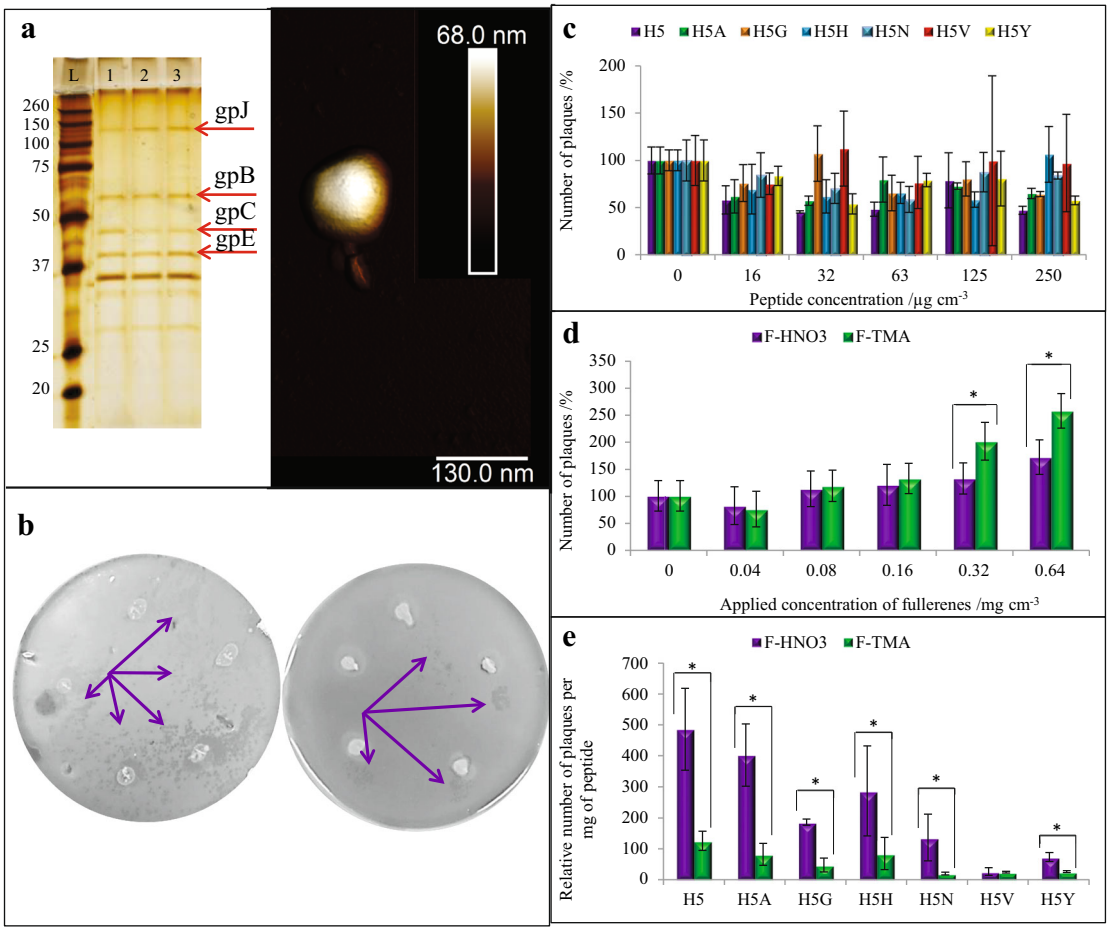

Fig. 5 (**a** *left*) Main capsid protein gpE (37 kDa) of bacteriophage λ after multiple cultivation and subsequent purification (*lanes 1*, *2* and *3*) separated on 12.5 % SDS PAGE gel at 200 V for 57 min and visualized with silver staining. Experion Pro260 Ladder was used as a molecular marker (*lane L*); (**a** *right*) AFM image of 5 mm of bacteriophage λ on freshly cleaved mica acquired in liquid phase employed with SiNi AFM probe using wedge tip with 12 μm overall tip height (>800 nm effective tip height) with a double tip spacing of 4.5 μm, **b** Representative photographs of plaques observed after the cultivation of bacteriophage λ in the indicator *E. coli* in the presence of F-HNO_3 modified with maximin H5 (*left*) or F-TMA modified with maximin mutant H5N (*right*), **c** Plaque assay for the assessment of antiviral activity of maximin H5 mutants, **d** Plaque assay for the assessment of antiviral activity of pure fullerene C_{60} nanocrystals activated with nitric or trimesic acid, **e** plaque assay for the assessment of antiviral activity of fullerene C_{60} nanocrystals modified with maximin H5 derivatives. *Asterisks* indicate significant difference at $p < 0.05$ (*)

bacteriophage λ growth and this stimulating effect was even more enhanced with F-TMA in comparison with F-HNO_3.

The combined antiviral activity of the peptide-modified fullerene C_{60} nanocrystals was evaluated using the plaque assay method. To remove the possibility of maximin peptides causing the bacteriophage λ to only enter lysogenic state instead of killing it, the indicator *E. coli* with bacteriophage λ was induced with UV light to enter the lytic replication state. The relative number of plaques was compared to control (fullerene C_{60} nanocrystal conjugated with H5) and recalculated using the amount of peptide bound on fullerene C_{60} nanocrystals and thus applied on bacteriophage λ (Fig. 5e). The lower relative number of plaques indicated at the lower amount of mature virulent bacteriophage λ and thus a higher antiviral activity of the peptide-modified fullerene C_{60} nanocrystals. The antiviral activity of all designed mutants was significant in comparison with the H5 maximin. The highest antiviral activity was observed when F-TMA and H5N mutant were used. A very good antiviral activity was also observed after the modification of F-TMA with H5V and H5Y maximin.

The replacement of acidic amino acids in peptide was shown to enhance the antiviral activity of H5 peptide to the HIV virus. Wang et al. [25] replaced the aspartic acid in H5 peptide by a basic amino acid arginine. In this work, we replaced the aspartic acid on the position 11 by a basic amino acid histidine, which helped to enhance the antiviral activity of the peptide, although some other modifications of the peptide showed even higher antiviral activity.

To understand the mechanism of the action of fullerene C_{60} nanocrystal–peptides conjugates in more details, the investigation at the nucleic acid level was carried out. At first, the number of virions was determined using the quantitative PCR analysis (Fig. 6a). It was found out that the number of virions differed according to the type of peptide mutants as well as according to the type of fullerene C_{60} nanocrystals ($p < 0.05$). In case of F-HNO_3, the biggest decrease in number of virions (compared to H5 conjugated F-HNO_3) was determined in case of conjugates with H5H (17 orders of magnitude) followed by H5G (15 orders of magnitude) and H5A (10 orders of magnitude).

The conjugates of peptides with the F-TMA exhibited lower number of virions even in the control H5-conjugated group (8 orders of magnitude). From all H5 mutants, the lowest number of virions was determined in the group of F-TMA coupled with H5N. The decrease of 19 orders of magnitude was observed. From these results, it was also concluded that the highest antiviral activity possess the F-TMA modified with H5N peptide.

The number of virions was determined as a number of DNA copies in each tested group. However, not all DNA molecules have to be transcribed to RNA and therefore the next level of the process has to be tested in terms of gene expression. The expression of two main genes of bacteriophage λ (capsid E gene, tail J gene) was investigated to assess whether the peptide–fullerene C_{60} nanocrystal conjugates restrict the transcription process. The results were statistically evaluated at the level of significance $p < 0.05$ in comparison with un-mutated H5-fullerene C_{60} nanocrystals conjugate. It was found that the expression of the tail J protein was not significantly influenced by the application of any of the studied peptide mutants conjugated with F-HNO_3, compared to the control H5-modified F-HNO_3. However, the capsid E gene was significantly overexpressed when the H5A-, H5G-, H5H-, H5N-, and H5V-modified F-HNO_3 were applied (Fig. 6b). The highest increase was observed in case of H5N group. On the other hand, the application of F-TMA conjugated with all H5 derivatives exhibited only a slight, but insignificant ($p < 0.05$), overexpression of the capsid E gene and minor influence on tail J gene (Fig. 6c).

Even though the RNA transcription is an essential process, the protein translation may also be affected by the presence of peptide-fullerene C_{60} nanocrystal conjugates. Therefore, the protein composition was investigated by the SDS-PAGE. The main capsid protein E with the molecular mass of 37 kDa was observed as the most intense band in each lane. It can be seen that the treatment with the H5 mutant conjugated fullerene C_{60} nanocrystals led to changes in protein E expression. These changes are not so visible in case of F-HNO_3 (Fig. 6d); however, in case of F-TMA, the more pronounced effect was observed (Fig. 6e). Even though the capsid E gene was overexpressed after exposure to peptide conjugates with F-HNO_3, no significant increase in protein E translation was observed. In case of F-TMA, the expression of the capsid E gene was not so increased; however, the protein translation was reduced in all H5 mutants except the H5N variant. These results led us to conclude that the peptide–fullerene C_{60} nanocrystal conjugates affect mainly the translation part of the whole infection process. Even though the protein E content in F-TMA conjugated with H5N peptide exhibited almost the same value as the control (F-TMA with H5), the number of plaques obtained at this variant was the lowest. This may be explained by the fact that although the proteins are expressed at the sufficient quantity, their structure or function is altered and the virions assembled from these proteins are significantly less infectious.

Conclusion

In summary, we evaluated the antiviral activity of six different mutants of maximin H5 peptide. The peptides showed very low antiviral activity, which was enhanced by their binding to suitable nanocarrier, fullerene C_{60} nanocrystals. For the binding of the peptides, the surface of fullerene C_{60} nanocrystals was activated with nitric acid or trimesic acid. The modification with trimesic acid was able to introduce more carboxyl groups on the surface of fullerene C_{60} nanocrystals, thus enabling higher amount of peptide bound to the fullerene C_{60} nanocrystals. The proposed mutants of maximin H5 had higher antiviral activity than the original peptide. The highest antiviral activity was observed using mutants of maximin H5 with aspartic acid at position 11 exchanged for asparagine, valine or tyrosine.

Experimental

All chemicals of American Chemical Society (ACS) purity were obtained from Sigma-Aldrich (St. Louis, MO, USA) unless stated otherwise.

The formulation for Luria–Bertani (LB) broth was as follows: 1 % tryptone, 0.5 % yeast extract, and 0.5 % sodium chloride. The formulation for LB bottom agar was as follows: 1 % tryptone, 0.5 % yeast extract, 0.5 % sodium chloride, and 1.5 % agar bacteriological. The formulation for soft agar was as follows: 0.5 % peptone, 0.3 % meat extract, and 0.5 % agar bacteriological. The formulation for SM medium was as follows: 0.58 % sodium chloride, 0.2 % magnesium sulfate heptahydrate, and 0.61 % Trizma base pH 7.5.

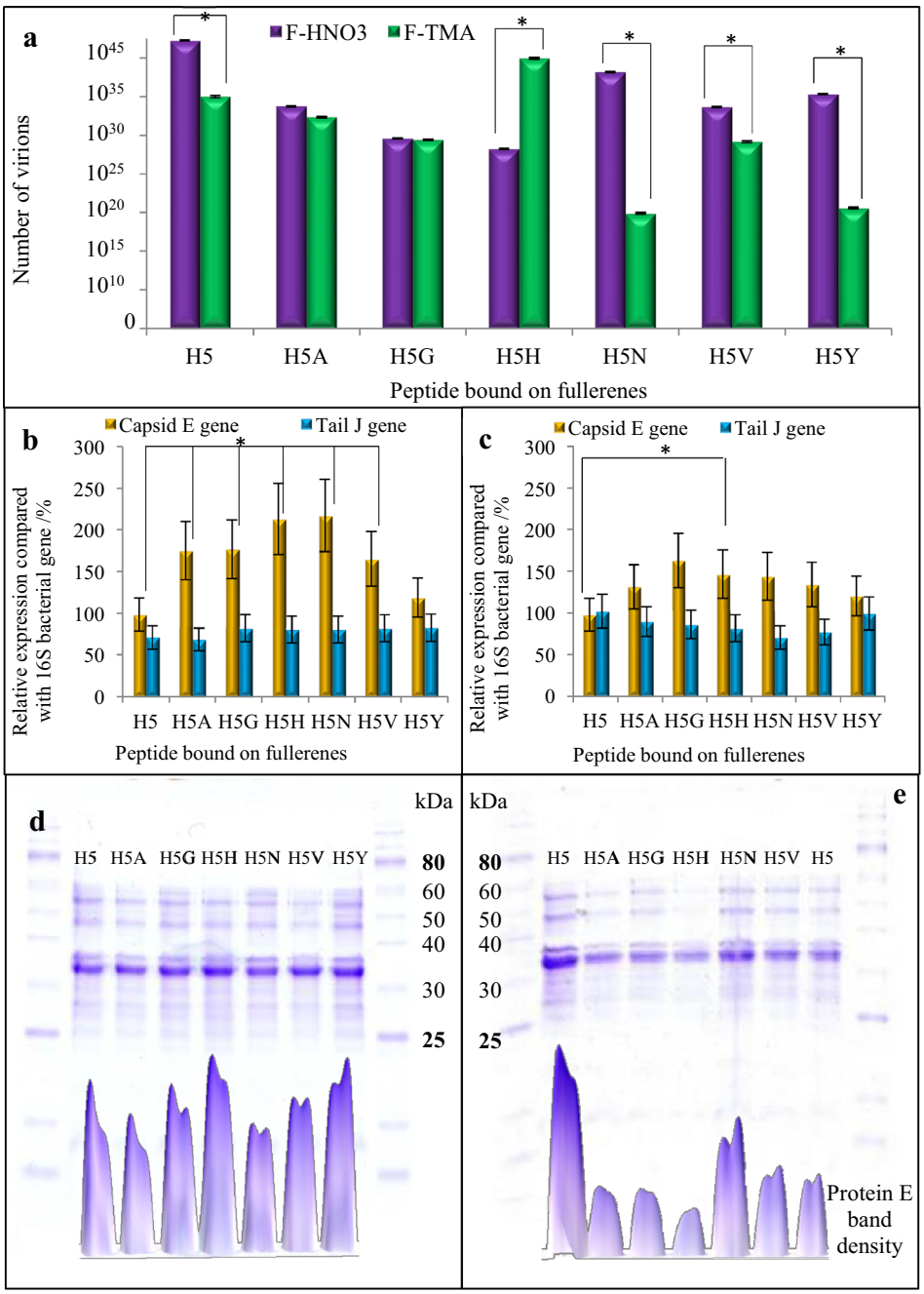

Fig. 6 **a** Number of virions in plaque assay samples of phage cultivated in the presence of fullerene C_{60} nanocrystals activated with nitric (F-HNO_3) or trimesic acid (F-TMA) and modified with maximin H5 mutants. The plaques were released in SM medium with chloroform and phage was purified using ultracentrifugation. The number of virions was evaluated using qPCR with Sybr Green labelling and calculated using the realplex software with the best R^2 values, **b** expression of phage genes for major capsid protein E and major tail protein J in host bacteria *E. coli* cultivated in the presence of fullerene C_{60} nanocrystals activated with nitric (F-HNO_3) and modified with maximin H5 mutants, **c** expression of phage genes for major capsid protein E and major tail protein J in host bacteria *E. coli* cultivated in the presence of fullerene C_{60} nanocrystals activated with trimesic acid (F-TMA). RT-PCR was performed using 88 ng of isolated RNA and subsequently 5 mm^3 of transcribed cDNA was used for each of the amplification of the genes of interest. The amplified genes were visualized on agarose gel and the fluorescence intensity was compared with the intensity of reference bacterial 16S gene, determined as 100 %. *Asterisks* indicate significant difference at $p < 0.05$, **d** Tris–glycine SDS-PAGE of phage λ purified from plaques formed after cultivation of phage in the indicator *E. coli* in the presence of fullerene C_{60} nanocrystals activated with nitric acid and modified with maximin H5 derivatives, **e** Tris–Glycine SDS-PAGE of phage λ purified from plaques formed after the cultivation of phage in indicator *E. coli* in the presence of fullerene C_{60} nanocrystals activated with trimesic acid and modified with maximin H5 derivatives. (Densitometry of the major capsid protein E was performed and the band intensity was compared with intensity of protein E in samples modified with maximin H5, dedicated as 100 %)

The bacteriophage λ producing and indicator strains of *E. coli* (GY 5027 and GY 4015, respectively) were kindly provided by Ljubica Svobodova (Department of Biology, Faculty of Medicine, Masaryk University in Brno, Brno, Czech Republic). Both the producing and indicator strains of *E. coli* were cultivated in a media containing 0.2 % maltose.

Preparation of activated fullerene C_{60} nanocrystals

Fullerene C_{60} nanocrystals (C_{60}, 2 mg) were mixed with 0.5 cm^3 of concentrated HNO_3 or 4 mg of trimesic acid in 0.5 cm^3 of water and incubated and washed according to [9] until the pH became 7. Finally, the volume was made up to 2 cm^3 using MilliQ water. The final concentration of activated or modified fullerenes was 1 mg cm^{-3}.

Characterization of fullerene C_{60} nanocrystal size and composition

The average particle size and size distribution were determined by quasi-elastic laser light scattering with a Malvern Zetasizer (NANO-ZS, Malvern Instruments Ltd., Worcestershire, United Kingdom). The zeta potential in cultivating medium of pH 7.4 was determined by laser Doppler micro-electrophoresis with a Malvern Zetasizer. Nanoparticles in 1.5 cm^3 solution containing 0.5 % peptone and 0.3 % meat extract were put into a polystyrene latex cell and measured at a detector angle of 173°, a wavelength of 633 nm, temperature of 25 °C, refractive index of 0.30, and a real refractive index of 2.2.

The elemental analyses were carried by CHNS organic elemental analyzer Flash 2000 (Thermo-Fisher Scientific Inc., Waltham, MA, USA). Fullerene C_{60} nanocrystals modified with trimesic acid or oxidized with nitric acid in solid state (2 mg) were placed into soft tin containers and burnt in a furnace at 950 °C.

The mass spectrometry experiments were performed using a MALDI–TOF mass spectrometer Bruker ultrafleXtreme (Bruker Daltonik GmbH, Bremen, Germany) according to [60] with a reflector positive mode in a mass range 400–6000 Da, 2,5-dihydroxyacetophenone (15.2 mg cm^{-3}) as a matrix and the samples prepared following the dried-droplet method: the solutions of fullerene C_{60} nanocrystals were mixed with matrix solution in a ratio of 1:1 v/v. After being homogeneous, 1 mm^3 of the solution was applied on the MTP 384 polished steel target plate and dried under atmospheric pressure at 20 °C. Finally, the mass spectra were made from 6000 laser shots within different regions of a sample spot. The laser power was set to 35 %.

Synthesis of maximin peptides

Six different derivatives of maximin H5 peptide were prepared replacing aspartic acid on the position 11 by different amino acids—asparagine, glycine, histidine, alanine, valine, and tyrosine. The synthesis process was carried out using Liberty Blue peptide synthesizer (CEM, Matthews, NC, USA). The sequences and molecular weights of synthesized peptides were as follows: maximin H5: ILGPVLGLVSD TLDDVLGIL—2021.17 Da; maximin H5A: ILGPVLGLV SATLDDVLGIL—1977.18 Da; maximin H5G: ILGPVL GLVSGTLDDVLGIL—1963.16 Da; maximin H5H: ILGP VLGLVSHTLDDVLGIL—2043.20 Da; maximin H5N: ILGPVLGLVSNTLDDVLGIL—2020.18 Da; maximin H5V: ILGPVLGLVSVTLDDVLGIL—2005.21 Da; maximin H5Y: ILGPVLGLVSYTLDDVLGIL—2069.20 Da.

The deblocking of Fmoc protecting group was performed with 20 % piperidine *v/v* in *N*,*N*-dimethylformamide (DMF). The couplings of the amino acids were achieved using *N*,*N*,*N*′,*N*′-tetramethyl-*O*-(1*H*-benzotriazol-1-yl)uronium hexafluorophosphate (HBTU), *N*,*N*-diisopropylethylamine (DIEA), and DMF. The cleavage of the side chain protecting groups was performed by treating the peptides resin with 95 % trifluoroacetic acid (TFA) v/v, 2.5 % H_2O v/v, and 2.5 % triisopropylsilane v/v for 30 min at 38 °C under microwave irradiation.

Analysis of maximin peptides

To predict the secondary structures of the peptides, software PEP-FOLD (http://bioserv.rpbs.univ-paris-diderot.fr/services/PEP-FOLD/) was used. The MALDI-TOF MS analysis of maximin peptides was performed according to [60, 61] with the 2,5-dihydroxybenzoic acid (DHB) used as a matrix. The saturated matrix solution was prepared in 30 % acetonitrile and 0.1 % TFA. The mixture was thoroughly vortexed and ultrasonicated using Bandelin 152 Sonorex Digital 10P ultrasonic bath (Bandelin electronic, Berlin, Germany) for 2 min at 50 % of intensity and 20 °C. The sample deposition method was same as in the case of fullerene C_{60} nanocrystals. All the measurements were performed in the reflector positive mode in the *m/z* range of 0–8000 Da.

For the analysis of peptide purity, a high-performance liquid chromatography (HPLC) system coupled with quadrupole time-of-flight detector (Q-TOF) mass spectrometer was used. The HPLC system consisted of two chromatographic pumps Model 582 ESA (ESA Inc., Chelmsford, MA, USA) and chromatographic column with reverse phase Kinetex 5 μm EVO C18 (150 × 4.6 mm, Phenomenex, Inc., Torrance, CA, USA). The flow rate of mobile phase was 1 cm^3 min^{-1}. The mobile phase con-

sisted of A: 0.01 % TFA and B: acetonitrile with 0.01 % TFA. The compounds of interest were separated by the following linear gradient 15 min 0–100 % B. For the measurements Bruker Maxis Impact Q-TOF mass spectrometer (Bruker Daltonik GmbH, Bremen, Germany) was employed. The electrospray ionization source was operated in a positive mode. The voltage of the electrospray capillary was set to 2900 V with nebulizing gas (N_2) flow rate of 12 dm^3 min^{-1} and the drying gas temperature was set at 250 °C. The scanning was carried out in the range of $m/z = 30–3800$.

Modification of fullerene C_{60} nanocrystals with peptides

Different derivatives of maximin H5 peptide were used in this experiment to check their antiviral properties. 0.5 mg of these peptides were dissolved in 100 mm^3 of DMF by mixing using a programmable rotator-mixer Multi RS-60 (Biosan, Riga, Latvia) at 600 rpm and 20 °C for 1 h. 200 mm^3 of the fullerene C_{60} nanocrystals was added to the dissolved peptides and mixed for 24 h using a rotator. Then they were filtered by centrifugation (6000*g* at 20 °C for 15 min) using Amicon Ultra 3K Centrifugal Filters (Merck Millipore Ltd., Darmstadt, Germany). The products were washed three times with MilliQ water by centrifugation. The final volumes of these products were adjusted to 1 cm^3 with MilliQ water.

The amount of the peptide, bound on fullerene C_{60} nanocrystals, was determined by derivatization with fluorescamine according to Kocdan and Basan [62]. 50 mm^3 of the peptide-modified fullerene C_{60} nanocrystals was mixed with 30 mm^3 of 1 mM fluorescamine on a microtiter plate and incubated for 5 min at 20 °C. The fluorescence of bound fluorescamine was measured using Microplate reader Infinite 200 PRO (Tecan Group Ltd., Männedorf, Switzerland) with excitation at 390 nm and emission from 420 to 850 nm.

The structures of fullerene C_{60} nanocrystals were observed using scanning electron microscopy (FE Tescan Mira II LMU, Brno, Czech Republic) under the following conditions: work distance of 5 mm, high vacuum mode (10^{-3} Pa) and voltage of 15 kV.

Characterization of bacteriophage λ

After cultivation of bacteriophage λ in phosphate buffered saline (PBS), the virions were released from soft agar into SM medium mixed with chloroform at 6:1 ratio and incubated for 1 h at 25 °C to kill the producing *E. coli*. The samples were centrifuged at 5200*g* and 4 °C for 10 min to remove *E. coli* cells and then at 10,000*g* and 4 °C for 6 min to remove remaining contaminants. Next, the supernatant containing phage was ultracentrifuged at 130,000*g* and 4 °C for 3 h. The pellet containing phage was resuspended in PBS at a protein concentration of 15 μg cm^{-3} and stored at 4 °C.

The characterization of the bacteriophage λ was carried out using polyacrylamide gel electrophoresis (PAGE), both native and with sodium dodecyl sulfate (SDS), and atomic force microscopy (AFM). The electrophoresis was performed according to Cernei et al. [63] using non-reducing sample buffer in 2:1 ratio. Experion Pro260 Ladder (BioRad, Hercules, CA, USA) was used to determine the molecular mass. The electrophoresis was run at 200 V for 35 min at 20 °C (Power Basic, BioRad, Hercules, CA, USA) in Tris–glycine running buffer (0.025 M Trizma base, 0.19 M glycine, and 0.0035 M SDS in case of SDS-PAGE). After separation, the gels were stained with silver staining according to Krizkova et al. [64].

The AFM images of bacteriophage λ were acquired in liquid phase with a Dimension Icon AFM (Bruker Nano GmbH, Berlin, Germany), employed with silicon nitride (SiNi) AFM probe, using wedge tip with 12 μm overall tip height (>800 nm effective tip height), with a double tip spacing of 4.5 μm. The samples were prepared by pipetting 5 mm^3 of bacteriophage solution onto freshly cleaved mica. The samples were incubated for 3 min, 50 mm^3 of PBS buffer was applied and the PeakForce Tapping™ mode analysis was performed.

Assessment of antibacterial activity by growth curves measurement and live/dead Baclight assay

The antibacterial activity of fullerene C_{60} nanocrystals and peptides was evaluated by the measurement of the indicator *E. coli* growth curves using Multiskan EX (Thermo-Fisher Scientific Inc., Waltham, MA, USA) according to Chudobova et al. [47]. 280 mm^3 of the culture diluted to $OD_{600nm} = 0.1$ was mixed with 10 mm^3 of various concentrations of fullerene C_{60} nanocrystals or peptides and PBS as a control for the measurement. The used concentrations of fullerene C_{60} nanocrystals were 0.64, 0.32, 0.16, 0.08, and 0.04 mg cm^{-3}. In case of the peptides the used concentration was 2 mg cm^{-3}. Total volume in the microplate wells was always 300 mm^3.

The microscopic assay for the evaluation of live/dead bacterial cells was performed using an inverted Olympus IX 71S8F-3 fluorescence microscope (Olympus, Tokyo, Japan) equipped with Olympus UIS2 series objective LUCPlanFLN 40 × (N.A. 0.6, WD 2.7–4 mm, F.N. 22) and a mercury arc lamp X-cite 12 (120 W, Lumen Dynamics, Mississauga, Canada) for illumination. Two fluorescent dyes were used for the assay: propidium iodide for staining of cells with damaged membranes and SYTO9 (Invitrogen AG, Basel, Switzerland) permeating both intact

and damaged membranes of the cells [49]. 5 mm^3 of 10× diluted bacterial suspension after 24 h growth was stained with 0.5 mm^3 of fluorescent dye. The fluorescence mirror used for the visualization of the SYTO9 staining had excitation wavelengths of 460–495 nm, emission wavelengths of 510–550 nm and dichroic mirror of 505 nm. The fluorescence mirror used for the visualization of the propidium iodide staining had excitation wavelengths of 545–580 nm, emission wavelength of 610 nm and dichroic mirror of 600 nm. The images were captured using a Camera Olympus DP73 (Olympus, Tokyo, Japan) and processed by Stream Basic 1.7 software (Olympus Soft Imaging Solutions GmbH, Münster, Germany) with the software resolution of 1600 × 1200 pixels.

Assessment of antiviral activity by plaque assay

The producing *E. coli* cells were inoculated into Luria–Bertani (LB) broth and cultivated for 24 h at 37 °C and 600 rpm using Incubator Hood TH 15 (Edmund Bühler GmbH, Hechingen, Germany) according to [65]. After the cultivation, the *E. coli* cells were inoculated by 5 punctures into LB bottom agar on each Petri dish and cultivated for 24 h at 37 °C in an Incubator MIR-162 (Sanyo Electric Co., Ltd., Osaka, Japan). At the same time, the indicator *E. coli* was inoculated into LB broth and cultivated for 24 h at 37 °C and 600 rpm. After cultivation, the producing *E. coli* on Petri dish was killed by the exposure to chloroform fumes for 30 min. The bacteriophage λ on Petri dish was covered with 3 cm^3 of soft agar, 1 cm^3 of indicator *E. coli*, and 0.25 cm^3 of peptide-modified fullerene C_{60} nanocrystals. PBS served as a control. The growth of bacteriophage λ was induced with UV light to enter the lytic replication state.

The antiviral activity of peptide-modified fullerene C_{60} nanocrystals was checked after 16 h of cultivation by counting observed bacteriophage λ plaques. The results were recalculated relatively to the amount of the peptides bound on the surface of fullerene C_{60} nanocrystals.

The plaques were collected in 0.5 cm^3 of chloroform and 3 cm^3 of SM medium (0.58 % sodium chloride; 0.2 % magnesium sulfate heptahydrate, and 0.6057 % Tris–HCl pH 7.5) and incubated for 1 h to lyse the host *E. coli* and release the virions in the medium. The samples were centrifuged at 6000*g* and 20 °C for 10 min to remove the agar. The supernatants were centrifuged at 10,000*g* and 20 °C for 6 min to remove the *E. coli* cells. The supernatants were ultracentrifuged at 130,000*g* and 4 °C for 3 h. The pellets were resuspended in PBS buffer and used for other analyzes.

Protein analysis of bacteriophage λ after treatment

The protein content of purified bacteriophage λ in PBS was verified by Tris–glycine SDS electrophoresis on 12.5 % w/v running gels. Prior to analysis, the samples of bacteriophage λ in PBS were mixed with the non-reducing sample buffer in 2:1 ratio. 10–250 kDa Protein Ladder (New England Biolabs, Ipswich, MA, USA) was used to determine the molecular mass. The electrophoresis was run at 200 V and 20 °C for 35 min in Tris–glycine running buffer. After separation, the gels were stained with Coomassie blue. The densitometry of major capsid protein E (38 kDa) was performed using the Bruker MI SE software (Bruker Daltonik GmbH, Bremen, Germany). The protein intensity in samples with maximin derivatives was compared with the maximin H5.

Quantitative polymerase chain reaction analysis

Quantitative PCR was performed using the SYBR Green Quantitative RT-PCR Kit (Sigma-Aldrich, St. Louis, MO, USA) with 0.2 μM of each primer for the amplification of bacteriophage λ *xis* gene (the sequences of the forward and reverse primers were chosen 5′-CCTGCTCTGCCGCT TCACGC-3′ and 5′-TCCGGATAAAAACGTCGATGA CATTTGC-3′ respectively [66, 67]) and 11.5 mm^3 of purified bacteriophage λ samples. The conditions of the PCR reaction were as follows: 94 °C for 2 min and 40 cycles of 94 °C for 15 s and 60 °C for 1 min with detection of SYBR Green fluorescence after every cycle. A commercial λ phage DNA of known concentration was used as a standard. After the amplification, automatic melting curves measurement was performed. The number of phage λ virions was calculated using the *realplex* software with the best R^2 values. The expression of genes for the major capsid protein E and major tail protein J was studied. RNA was isolated from 200 mm^3 of supernatant prior to ultracentrifugation using MagNA Pure Compact (Roche, Basel, Switzerland) and RNA Isolation Kit with the addition of DNAse (Roche, Basel, Switzerland). 88 ng of isolated RNA was used for RT-PCR using Transcriptor First Strand cDNA Synthesis Kit (Roche, Basel, Switzerland). 5 mm^3 of transcribed cDNA was used for each of the subsequent amplification of the genes of interest. For the amplification of reference bacterial 16S gene, the used primers were as follows: forward primer 5′-GAGTTT-GATCCTGGCTCAG-3′ and reverse primer 5′-GGTTACCTTGTTACGACTT-3′. For the amplification of the major capsid protein E, the primers were as follows: forward primer 5′-GTACGTTTCGCCGATTGTTT-3′ and reverse primer 5′-ATCCTGAATGCAGCCATAGG-3′. For the amplification of the major tail protein J, the primers were as follows: forward primer 5′-ACCACCT-CAAAGGGTGACAG-3′ and reverse primer 5′-CTGGCATGTCAACAATACGG-3′. The amplified genes were visualized on 1 % agarose gel with ethidium bromide after an electrophoretic separation at 100 V and 20 °C for 60 min. The fluorescence intensity was measured using

Bruker MI SE software (Bruker Daltonik GmbH, Bremen, Germany). The fluorescence intensity was compared with the intensity of reference bacterial 16S gene, determined as 100 %.

Acknowledgments The financial support from IGA FULERENE_MAXIMIN IP_31_2015 is highly acknowledged. The authors wish to express their thanks to Adela Jarosova, Radek Chmela, Michaela Docekalova and Dita Munzova for perfect technical assistance; to Lukas Richtera for data consultation and Ljubica Svobodova from Masaryk University for providing *E. coli* strains.

References

1. Park K (2013) ACS Nano 7:7442
2. Leonard B (2009) Cancer nanotechnology: going small for big advances: using nanotechnology to advance cancer diagnosis, prevention and treatment. DIANE, Philadelphia
3. Gu FX, Karnik R, Wang AZ, Alexis F, Levy-Nissenbaum E, Hong S, Langer RS, Farokhzad OC (2007) Nano Today 2:14
4. Chomoucka J, Drbohlavova J, Huska D, Adam V, Kizek R, Hubalek J (2010) Pharmacol Res 62:144
5. Peer D, Karp JM, Hong S, FaroKhzad OC, Margalit R, Langer R (2007) Nat Nanotechnol 2:751
6. Dunk PW, Kaiser NK, Hendrickson CL, Quinn JP, Ewels CP, Nakanishi Y, Sasaki Y, Shinohara H, Marshall AG, Kroto HW (2012) Nat Commun 3:1
7. Yamamoto S, Ohkita H, Benten H, Ito S (2012) Adv Funct Mater 22:3075
8. Heister E, Neves V, Tilmaciu C, Lipert K, Beltran VS, Coley HM, Silva SRP, McFadden J (2009) Carbon 47:2152
9. Blazkova I, Nguyen HV, Kominkova M, Konecna R, Chudobova D, Krejcova L, Kopel P, Hynek D, Zitka O, Beklova M, Adam V, Kizek R (2014) Electrophoresis 35:1040
10. Heger Z, Kominkova M, Cernei N, Krejcova L, Kopel P, Zitka O, Adam V, Kizek R (2014) Electrophoresis 35:3290
11. Shetti NP, Malode SJ, Nandibewoor ST (2012) Bioelectrochemistry 88:76
12. Tollas S, Bereczki I, Sipos A, Roth E, Batta G, Daroczi L, Keki S, Ostorhazi E, Rozgonyi F, Herczegh P (2012) Eur J Med Chem 54:943
13. Anonymous (2014) Nat Rev Drug Discov 13:644. doi:10.1038/nrd4424
14. Mojola SA (2014) Signs 39:341
15. Krejcova L, Hynek D, Kopel P, Rodrigo MAM, Adam V, Hubalek J, Babula P, Trnkova L, Kizek R (2013) Viruses-Basel 5:1719
16. Turner C (2014) Nursing 44:68
17. Epand RM, Vogel HJ (1999) Biochim Biophys Acta Biomembr 1462:11
18. Boman HG (2000) Immunol Rev 173:5
19. Clarke BT (1997) Biol Rev Camb Philos Soc 72:365
20. Liu R, Liu HA, Ma YF, Wu J, Yang HL, Ye HH, Lai R (2011) J Proteome Res 10:1806
21. Matsuzaki K (2001) Biochem Soc Trans 29:598
22. Lee WH, Zhang H, Zhang YX, Jin Y, Lai R, Zhang Y (2005) FEBS Lett 579:4443
23. Ortega G, Rhee DS, Papandria DJ, Yang J, Ibrahim AM, Shore AD, Makary MA, Abdullah F (2012) J Surg Res 174:33
24. Lai R, Liu H, Lee WH, Zhang Y (2002) Biochem Biophys Res Commun 295:796
25. Wang GS, Watson KM, Peterkofsky A, Buckheit RW (2010) Antimicrob Agents Chemother 54:1343
26. Yang J, Li MM, Shen XT, Liu SW (2013) Viruses-Basel 5:352
27. Lai R, Zheng YT, Shen JH, Liu GJ, Liu H, Lee WH, Tang SZ, Zhang Y (2002) Peptides 23:427
28. Solaro R, Chiellini F, Battisti A (2010) Materials 3:1928
29. Lee WH, Li Y, Lai R, Li S, Zhang Y, Wang W (2005) Eur J Immunol 35:1220
30. Kominkova M, Michalek P, Guran R, Cernei N, Ruttkay-Nedecky B, Anyz J, Zitka O, Stepankova O, Pikula J, Adam V, Beklova M, Kizek R (2014) Chromatographia 77:609
31. Rastogi V, Yadav P, Bhattacharya SS, Mishra AK, Verma N, Verma A, Pandit JK (2014) J Drug Deliv 2014:670815–670838
32. Wang J, Hu ZB, Xu JX, Zhao YL (2014) NPG Asia Mater 6:1
33. Yang XL, Ebrahimi A, Li J, Cui QJ (2014) Int J Nanomed 9:77
34. Palanisamy S, Thirumalraj B, Chen S-M, Ali MA, Al-Hemaid FMA (2015) J Colloid Interface Sci 448:251
35. Zhou DB, Wang GW (2015) Org Lett 17:1260
36. Lens M, Medenica L, Citernesi U (2008) Biotechnol Appl Biochem 51:135
37. Murray RW, Iyanar K (1997) Tetrahedron Lett 38:335
38. Chen BX, Wilson SR, Das M, Coughlin DJ, Erlanger BF (1998) Proc Natl Acad Sci USA 95:10809
39. Sawamura M, Kawai K, Matsuo Y, Kanie K, Kato T, Nakamura E (2002) Nature 419:702
40. Cheng DP, Khan MA, Houser RP (2001) Inorg Chem 40:6858
41. Liang SW, Li MX, Shao M, Liu HJ (2007) Inorg Chem Commun 10:1347
42. Mrozinski J, Bienko A, Kopel P, Langer V (2008) Inorg Chim Acta 361:3723
43. Dostalova S, Milosavljevic V, Guran R, Kominkova M, Cihalova K, Cernei N, Kopel P, Vaculovicova M, Adam V, Kizek R (2015) Antiviral activity of fullerenes modified with maximin H5 derivatives. Paper presented at the MendelNet 2015, Mendel University in Brno, Czech Republic, pp 579–584
44. Xie LG, Luo Y, Lin DD, Xi WH, Yang XJ, Wei GH (2014) Nanoscale 6:9752
45. Jung JE, Yoon SS (2002) Bull Korean Chem Soc 23:1483
46. Abe S, Hyono A, Nakayama K, Takada T, Yonezawa T (2013) Jpn J Appl Phys 52:1
47. Chudobova D, Dostalova S, Ruttkay-Nedecky B, Guran R, Rodrigo MAM, Tmejova K, Krizkova S, Zitka O, Adam V, Kizek R (2015) Microbiol Res 170:147
48. Vizioli J, Salzet M (2002) Trends Pharmacol Sci 23:494
49. Berney M, Hammes F, Bosshard F, Weilenmann HU, Egli T (2007) Appl Environ Microbiol 73:3283
50. Dostalova S, Munzova D, Vaculovicova M, Kizek R (2014) J Metallomics Nanotech 1:34
51. Murray NE, Gann A (2007) Curr Biol 17:R305
52. Herskowi I (1973) Annu Rev Genet 7:289
53. Weber K, Osborn M (1969) J Biol Chem 244:4406
54. Signer ER, Weil J (1968) Cold Spring Harbor Symp Quant Biol 33:715
55. Fraser MJ, Ainley K, Parish JH (1982) Mut Res 88:76
56. Clark EM, Wright H, Lennon KA, Craik VA, Clark JR, March JB (2012) Appl Environ Microbiol 78:3033
57. Levinson W, Helling R (1976) Antimicrob Agents Chemother 9:160
58. Bayer ME, Bocharov AF (1973) Virology 54:465
59. Dokland T, Murialdo H (1993) J Mol Biol 233:682
60. Heger Z, Michalek P, Guran R, Cernei N, Duskova K, Vesely S, Anyz J, Stepankova O, Zitka O, Adam V, Kizek R (2015) Oncol Rep 34:3247
61. Nguyen HV, Heger Z, Kominkova M, Michalek P, Gumulec J, Guran R, Pridal A, Fernandez C, Hynek D, Adam V, Kizek R (2015) Int J Electrochem Sci 10:1249
62. Kocdan D, Basan H (2013) Luminescence 28:961

63. Cernei N, Dostalova S, Heger Z, Kopel P, Zitka O, Adam V, Kizek R (2015) J Metallomics Nanotech 1:57
64. Krizkova S, Adam V, Eckschlager T, Kizek R (2009) Electrophoresis 30:3726
65. Dostalova S, Vaculovicova M, Kizek R (2014) J Metallomics Nanotech 1:64
66. Smerkova K, Dostalova S, Skutkova H, Ryvolova M, Adam V, Provaznik I, Kizek R (2013) Chromatographia 76:329
67. Smerkova K, Dostalova S, Vaculovicova M, Kynicky J, Trnkova L, Kralik M, Adam V, Hubalek J, Provaznik I, Kizek R (2013) J Pharm Biomed Anal 86:65

6. CONCLUSION

Side effects and inability to reach intracellular target are limiting the application of drugs in advanced therapy. Application of cell penetrating peptides is a promising way to safely deliver various types of biologically active molecules and to reduce their potential toxicity. The advantage of cell penetrating peptides can be found in prolonged activity, localization, targeting and protection of drugs from environment, providing excellent opportunity for use of peptides as drug delivery system. Application of cell penetrating peptides for drug delivery has been illustrated in this work.

The first step in this work was to optimize both synthesis of cell penetrating peptides and method for characterization of the final product. The cell penetrating peptides are successfully synthetized by the Fmoc strategy, using onium salt (HBTU) as activator. However, the HBTU's high reactivity has the tendency to terminate peptide chain trough guanidine side product. This was the reason to apply *N*,*N*-diisopropylethylamine (DIEA) as activator base, in order to protect amino acid activated ester state from α-proton abstraction. To increase the rate of reactions between amino acids, the microwave assisted method has been used. Through characterization of synthesized peptide by MALDI-TOF MS and spectroscopic methods, its purity was tested and established to be more than 96 %. It has been found that possible impurities belong to short sequences of synthetized peptide due to chain breakage. The Fmoc strategy has been proven as a promising technique for synthesis of cell penetrating peptides, as it enables production of highly pure peptides with lower side reactions occurrence.

The optimized method for rapid and cheap characterization of peptide-molecules interactions has been developed, which may be important pathway for development of new therapeutic agents. Electrochemical analysis has been used for detection of interactions between synthetized peptide and various nanoconstructs (Zn-Schiff base, MWCNTs, fullerenes and Gd-Schiff base quantum dots). Electrochemical analysis confirms the high potential of peptides to bind other molecules. The data presented in this work also highlighted the potential of cell penetrating peptides for cell delivery and localization of known and potentially new drugs, using nanocarrier or directly peptides. It was discovered that interaction of peptide with specific molecules influences the penetrating properties of peptides. Novicidin modified with Zn-Schiff base shows high affinity towards prostate cancer cells, while non-cancerous prostate cells stay

unaffected, due to structural differences in their membranes. On the other side, peptide with high specificity to target will deliver the cargo, regardless of modification. Homing peptide can deliver therapeutic agents to prostate cancer cells, increasing the selectivity of drugs. Evaluation of the antiviral activity of maximin H5 peptide shows low antiviral activity, however binding to fullerene C60 enhances the antiviral activity. Fullerene C60 nanocrystals do not have antiviral activity, indicating the amount of peptide bound on the surface of fullerene plays the main role in antiviral activity. Modified fullerene increases the number of peptides used in the treatment of virus. The presented study demonstrates therapeutically approaches to employing cell penetrating peptides in treatments of diseases and their advantages over the other currently used methods.

7. ABBREVIATIONS

ATR-FTIR: attenuated total reflectance
AMPs: antimicrobial peptides
AAA: amino acid analysis
APA2: Aspartic proteinase A2
AdTS-DPV: adsorptive stripping differential pulse voltammetry
A549: adenocarcinoma human alveolar basal epithelial cells
ACN: acetonitrile
AAS: atomic absorption spectroscopy
BBB: blood-brain barrier
Boc: *tert*-butyloxycarbonyl
BOP: benzotriazol-1-yloxy)tris(dimethylamino)phosphonium hexafluorophosphate
CPPS: cell penetrating peptides
CHO: Chinese hamster ovary
CDK9: cyclin-dependent kinase 9
Calu-3: cultured Human Airway Epithelial Cells
Cbz: carbobenzoxy
cDNA: complementary deoxyribonucleic acid
CASP1: caspase-1
CdTe: cadmium telluride
DMF: dimethylformamide
DNA: deoxyribonucleic acid
DHB: 2,5-dihydroxybenzoic acid matrix
DNAJA1: DnaJ Heat Shock Protein Family (Hsp40) Member A1
DOXO: doxorubicin
DIEA: *N*,*N*-diisopropylethylamine
EL-4: mouse lymphoma cell line
ESI: electrospray ionization
EGFP: enhanced green fluorescent protein
EDTA: ethylenediaminetetraacetic acid
FIA: flow injection analysis
FGF12: fibroblast growth factor-12
FPLC: fast protein liquid chromatography
Fmoc: fluorenylmethyloxycarbonyl chloride
FT-IR: Fourier transform infrared spectroscopy
FBS: fetal bovine serum
GAGs: glycosaminoglycan's
GLP-1: glucagon-like peptide-1
GTPase: guanosine triphosphate family of hydrolase enzymes
gp120: glycoprotein 120
Gd-SB: gadolinium-Schiff base complex
HCCA: α-cyano-4-hydroxycinnamic acid
HT-1080: fibrosarcoma cell line
H1299: human non-small cell lung carcinoma
HIV: human Immunodeficiency Virus
HMDE: hanging mercury drop electrode
HEK293: human embryonic kidney cells

HPLC: high-performance liquid chromatography
HMPA: hexamethylphosphoramide
HR-TEM: high-resolution transmission electron microscopy
hCT: human calcitonin
HBTU: 2-(1H-benzotriazol-1-yl)-1,1,3,3-tetramethyluronium hexafluorophosphate
HOBt: Hydroxybenzotriazole
HOAt: 1-Hydroxy-7-azabenzotriazole
HNO_3: nitric acid
IEC6: rat intestinal epithelial cell line
IEC: ion exchange chromatography
IFN-β: interferon-β
KIF20A: Kinesin-like protein
K562: human immortalised myelogenous leukemia cell line
LB: Luria-Bertani medium
LDH: lactate dehydrogenase leakage
MALDI-TOF: matrix assisted laser desorption/ionization-time of flight mass spectrometric
MTS: membrane translocation sequence
MCF-7: Michigan Cancer Foundation-7
MTX: Methotrexate
MTs: metallothioneins
MTF: metal-responsive transcription factor
MDR: multidrug resistance
MDA-MB-231: human breast adenocarcinoma
MPM: motif from Kaposi fibroblast growth factor
mRNA: messenger ribonucleic acid
MDCK: Madin Darby Canine Kidney cell culture
MTT: 3-(4,5-dimethylthiazol-2-yl)-2,5-diphenyltetrazolium bromide
MWCNTs: multi-walled carbon nanotube
*o*MWCNTs: oxidized MWCNTs
NBs: nanobubbles
NH_4Cl: ammonium chloride
NH_3: ammonia
NLSs: nuclear localization sequences
NaCl: sodium chloride
NR4A3: neuron-derived orphan receptor 1
PCR: polymerase chain reaction
PTD: protein transduction domain
PMF: peptide mass fingerprinting
pGL3: luciferase-encoding plasmid
pAntp: Antennapedia homeodomain protein
p53: tumor suppressor protein
PyBOP: benzotriazol-1-yl-oxytripyrrolidinophosphonium hexafluorophosphate
PNT1A: normal prostate epithelium cell line
PC3: human prostate cancer cell lines
PBS: phosphate-buffered saline
q-RT-PCR: quantitate real time polymerase chain reaction
RBCs: red blood cells
SPPS: solid phase peptide synthesis
siRNA: small interference ribonucleic acid

S40: transformed human alveolar epithelial cells
SH-SY5Y: neuroblast from neural tissue
TA30: (30:70 [*v/v*] acetonitrile : TFA 0.1% in water)
TFA: trifluoroacetic acid
TAT: Trans-activator of transcription protein
Th2: T helper 2 cell
TA3/St: mammary adenocarcinoma
TLM: translocation motif
TP10: transportan 10
TCD: thermal conductive detector
TBTU: O-(Benzotriazol-1-yl)-N,N,N′,N′-tetramethyluronium tetrafluoroborate
TGA: thermogravimetric analysis
U2OS: Human Bone Osteosarcoma Epithelial Cells
UV: ultraviolent
U87:human primary glioblastoma cell
XTT: [(2,3-bis-(2-methoxy-4-nitro-5-sulfophenyl)-2H-tetrazolium-5-carboxanilide)]
ZnT-1: zinc-transporter 1

7. LITERATURE

[1] F.H. Wang, Y. Wang, X. Zhang, W.J. Zhang, S.R. Guo, F. Jin, Recent progress of cell-penetrating peptides as new carriers for intracellular cargo delivery, Journal of Controlled Release, 174 (2014) 126-136.
[2] S. Deshayes, M.C. Morris, G. Divita, F. Heitz, Cell-penetrating peptides: tools for intracellular delivery of therapeutics, Cellular and Molecular Life Sciences, 62 (2005) 1839-1849.
[3] D. Gaspar, A.S. Veiga, M.R.B. Castanho, From antimicrobial to anticancer peptides. A review, Frontiers in Microbiology, 4 (2013).
[4] A.D. Frankel, C.O. Pabo, CELLULAR UPTAKE OF THE TAT PROTEIN FROM HUMAN IMMUNODEFICIENCY VIRUS, Cell, 55 (1988) 1189-1193.
[5] E.L. Snyder, S.F. Dowdy, Cell penetrating peptides in drug delivery, Pharmaceutical research, 21 (2004) 389-393.
[6] P. Lundberg, U. Langel, A brief introduction to cell-penetrating peptides, Journal of Molecular Recognition, 16 (2003) 227-233.
[7] J. Regberg, A. Srimanee, Ü. Langel, Applications of cell-penetrating peptides for tumor targeting and future cancer therapies, Pharmaceuticals, 5 (2012) 991-1007.
[8] F. Heitz, M.C. Morris, G. Divita, Twenty years of cell-penetrating peptides: from molecular mechanisms to therapeutics, British Journal of Pharmacology, 157 (2009) 195-206.
[9] I. Nakase, G. Tanaka, S. Futaki, Cell-penetrating peptides (CPPs) as a vector for the delivery of siRNAs into cells, Molecular Biosystems, 9 (2013) 855-861.
[10] H. Bai, Y. You, H. Yan, J.R. Meng, X.Y. Xue, Z. Hou, Y. Zhou, X. Ma, G.J. Sang, X.X. Luo, Antisense inhibition of gene expression and growth in gram-negative bacteria by cell-penetrating peptide conjugates of peptide nucleic acids targeted to rpoD gene, Biomaterials, 33 (2012) 659-667.
[11] M. Lindgren, K. Rosenthal-Aizman, K. Saar, E. Eiriksdottir, Y. Jiang, M. Sassian, P. Ostlund, M. Hallbrink, U. Langel, Overcoming methotrexate resistance in breast cancer tumour cells by the use of a new cell-penetrating peptide, Biochemical Pharmacology, 71 (2006) 416-425.
[12] B.R. Liu, J.S. Liou, Y.J. Chen, Y.W. Huang, H.J. Lee, Delivery of Nucleic Acids, Proteins, and Nanoparticles by Arginine-Rich Cell-Penetrating Peptides in Rotifers, Marine Biotechnology, 15 (2013) 584-595.
[13] S. Santra, H. Yang, J.T. Stanley, P.H. Holloway, B.M. Moudgil, G. Walter, R.A. Mericle, Rapid and effective labeling of brain tissue using TAT-conjugated CdS: Mn/ZnS quantum dots, Chemical Communications, (2005) 3144-3146.
[14] M. Lewin, N. Carlesso, C.H. Tung, X.W. Tang, D. Cory, D.T. Scadden, R. Weissleder, Tat peptide-derivatized magnetic nanoparticles allow in vivo tracking and recovery of progenitor cells, Nature Biotechnology, 18 (2000) 410-414.
[15] E. Vives, J. Schmidt, A. Pelegrin, Cell-penetrating and cell-targeting peptides in drug delivery, Biochimica Et Biophysica Acta-Reviews on Cancer, 1786 (2008) 126-138.
[16] D. Raucher, J.S. Ryu, Cell-penetrating peptides: strategies for anticancer treatment, Trends in Molecular Medicine, 21 (2015) 560-570.
[17] E. Koren, V.P. Torchilin, Cell-penetrating peptides: breaking through to the other side, Trends in Molecular Medicine, 18 (2012) 385-393.
[18] F. Wang, Y. Wang, X. Zhang, W. Zhang, S. Guo, F. Jin, Recent progress of cell-penetrating peptides as new carriers for intracellular cargo delivery, Journal of Controlled Release, 174 (2014) 126-136.

[19] M. Green, M. Ishino, P.M. Loewenstein, Mutational analysis of HIV-1 Tat minimal domain peptides: Identification of trans-dominant mutants that suppress HIV-LTR-driven gene expression, Cell, 58 (1989) 215-223.
[20] D. Derossi, S. Calvet, A. Trembleau, A. Brunissen, G. Chassaing, A. Prochiantz, Cell internalization of the third helix of the antennapedia homeodomain is receptor-independent, Journal of Biological Chemistry, 271 (1996) 18188-18193.
[21] J. Ruczynski, P.M. Wierzbicki, M. Kogut-Wierzbicka, P. Mucha, K. Siedlecka-Kroplewska, P. Rekowski, Cell-penetrating peptides as a promising tool for delivery of various molecules into the cells, Folia Histochemica Et Cytobiologica, 52 (2014) 257-269.
[22] L.M. Traub, Tickets to ride: selecting cargo for clathrin-regulated internalization, Nat Rev Mol Cell Biol, 10 (2009) 583-596.
[23] F. Milletti, Cell-penetrating peptides: classes, origin, and current landscape, Drug Discovery Today, 17 (2012) 850-860.
[24] A. Ziegler, J. Seelig, High affinity of the cell-penetrating peptide HIV-1 Tat-PTD for DNA, Biochemistry, 46 (2007) 8138-8145.
[25] W.J. Gehring, M. Affolter, T. Bürglin, Homeodomain proteins, Annual Review of Biochemistry, 63 (1994) 487-526.
[26] G. Gouridis, S. Karamanou, I. Gelis, C.G. Kalodimos, A. Economou, Signal peptides are allosteric activators of the protein translocase, Nature, 462 (2009) 363-367.
[27] M. Magzoub, S. Sandgren, P. Lundberg, K. Oglecka, J. Lilja, A. Wittrup, L.E. Göran Eriksson, U. Langel, M. Belting, A. Gräslund, N-terminal peptides from unprocessed prion proteins enter cells by macropinocytosis, Biochemical and Biophysical Research Communications, 348 (2006) 379-385.
[28] P. Lundberg, M. Magzoub, M. Lindberg, M. Hällbrink, J. Jarvet, L.E.G. Eriksson, U. Langel, A. Gräslund, Cell membrane translocation of the N-terminal (1-28) part of the prion protein, Biochemical and Biophysical Research Communications, 299 (2002) 85-90.
[29] S. Liu, F. Zhou, M. Höök, D.D. Carson, A heparin-binding synthetic peptide of heparin/heparan sulfateinteracting protein modulates blood coagulation activities, Proceedings of the National Academy of Sciences of the United States of America, 94 (1997) 1739-1744.
[30] Y.J. Choi, J.Y. Lee, J.H. Park, J.B. Park, J.S. Suh, Y.S. Choi, S.J. Lee, C.-P. Chung, Y.J. Park, The identification of a heparin binding domain peptide from bone morphogenetic protein-4 and its role on osteogenesis, Biomaterials, 31 (2010) 7226-7238.
[31] C. De Coupade, A. Fittipaldi, V. Chagnas, M. Michel, S. Carlier, E. Tasciotti, A. Darmon, D. Ravel, J. Kearsey, M. Giacca, F. Cailler, Novel human-derived cell-penetrating peptides for specific subcellular delivery of therapeutic biomolecules, Biochemical Journal, 390 (2005) 407-418.
[32] R. Reeves, M.S. Nissen, The AT-DNA-binding domain of mammalian high mobility group I chromosomal proteins. A novel peptide motif for recognizing DNA structure, Journal of Biological Chemistry, 265 (1990) 8573-8582.
[33] I. Nakase, H. Hirose, G. Tanaka, A. Tadokoro, S. Kobayashi, T. Takeuchi, S. Futaki, Cell-surface accumulation of flock house virus-derived peptide leads to efficient internalization via macropinocytosis, Molecular Therapy, 17 (2009) 1868-1876.
[34] R. Tan, A.D. Frankel, Structural variety of arginine-rich RNA-binding peptides, Proceedings of the National Academy of Sciences, 92 (1995) 5282-5286.
[35] S. Balayssac, F. Burlina, O. Convert, G. Bolbach, G. Chassaing, O. Lequin, Comparison of penetratin and other homeodomain-derived cell-penetrating peptides: Interaction in a membrane-mimicking environment and cellular uptake efficiency, Biochemistry, 45 (2006) 1408-1420.

[36] H. Noguchi, M. Matsushita, S. Matsumoto, Y.F. Lu, H. Matsui, S. Bonner-Weir, Mechanism of PDX-1 protein transduction, Biochemical and Biophysical Research Communications, 332 (2005) 68-74.
[37] L. Chaloin, P. Vidal, A. Heitz, N. Van Mau, J. Méry, G. Divita, F. Heitz, Conformations of primary amphipathic carrier peptides in membrane mimicking environments, Biochemistry, 36 (1997) 11179-11187.
[38] K. Sadler, K.D. Eom, J.L. Yang, Y. Dimitrova, J.P. Tam, Translocating proline-rich peptides from the antimicrobial peptide bactenecin 7, Biochemistry, 41 (2002) 14150-14157.
[39] L. Otvos Jr, M. Cudic, B.Y. Chua, G. Deliyannis, D.C. Jackson, An insect antibacterial peptide-based drug delivery system, Mol Pharm, 1 (2004) 220-232.
[40] H. Raghuraman, A. Chattopadhyay, Melittin: a membrane-active peptide with diverse functions, Bioscience reports, 27 (2007) 189-223.
[41] S. Kobayashi, K. Takeshima, C.B. Park, S.C. Kim, K. Matsuzaki, Interactions of the novel anfimicrobial peptide buforin 2 with lipid bilayers: Proline as a translocation promoting factor, Biochemistry, 39 (2000) 8648-8654.
[42] S. Lu, L.A. Tager, S. Chitale, L.W. Riley, A cell-penetrating peptide derived from mammalian cell uptake protein of Mycobacterium tuberculosis, Analytical Biochemistry, 353 (2006) 7-14.
[43] S. Oess, E. Hildt, Novel cell permeable motif derived from the PreS2-domain of hepatitis-B virus surface antigens, Gene Therapy, 7 (2000) 750-758.
[44] J. Oehlke, E. Krause, B. Wiesner, M. Beyermann, M. Bienert, Extensive cellular uptake into endothelial cells of an amphipathic β-sheet forming peptide, FEBS Letters, 415 (1997) 196-199.
[45] M. Lindgren, M. Hällbrink, A. Prochiantz, Ü. Langel, Cell-penetrating peptides, Trends in Pharmacological Sciences, 21 (2000) 99-103.
[46] M. Pooga, M. Hällbrink, M. Zorko, Cell penetration by transportan, The FASEB Journal, 12 (1998) 67-77.
[47] S.S. Sidhu, G.A. Weiss, CHAPTER 13 - DNA-ENCODED PEPTIDE LIBRARIES AND DRUG DISCOVERY A2 - Baguley, Bruce C, in: D.J. Kerr (Ed.) Anticancer Drug Development, Academic Press, San Diego, 2002, pp. 237-248.
[48] S. Gao, M.J. Simon, C.D. Hue, B. Morrison, S. Banta, An unusual cell penetrating peptide identified using a plasmid display-based functional selection platform, ACS Chemical Biology, 6 (2011) 484-491.
[49] H. Kamada, T. Okamoto, M. Kawamura, H. Shibata, Y. Abe, A. Ohkawa, T. Nomura, M. Sato, Y. Mukai, T. Sugita, S. Imai, K. Nagano, Y. Tsutsumi, S. Nakagawa, T. Mayumi, S.I. Tsunoda, Creation of novel cell-penetrating peptides for intracellular drug delivery using systematic phage display technology originated from tat transduction domain, Biological and Pharmaceutical Bulletin, 30 (2007) 218-223.
[50] P.M. Watt, Screening for peptide drugs from the natural repertoire of biodiverse protein folds, Nature Biotechnology, 24 (2006) 177-183.
[51] G. Tünnemann, G. Ter-Avetisyan, R.M. Martin, M. Stöckl, A. Herrmann, M.C. Cardoso, Live-cell analysis of cell penetration ability and toxicity of oligo-arginines, Journal of Peptide Science, 14 (2008) 469-476.
[52] S. Gao, M.J. Simon, C.D. Hue, B. Morrison III, S. Banta, An unusual cell penetrating peptide identified using a plasmid display-based functional selection platform, ACS Chemical Biology, 6 (2011) 484-491.
[53] M.C. Morris, J. Depollier, J. Mery, F. Heitz, G. Divita, A peptide carrier for the delivery of biologically active proteins into mammalian cells, Nature Biotechnology, 19 (2001) 1173-1176.
[54] J. Oehlke, A. Scheller, B. Wiesner, E. Krause, M. Beyermann, E. Klauschenz, M. Melzig, M. Bienert, Cellular uptake of an α-helical amphipathic model peptide with the potential to deliver polar compounds into the cell interior non-endocytically, Biochimica et Biophysica Acta - Biomembranes, 1414 (1998) 127-139.

[55] L. Crombez, G. Aldrian-Herrada, K. Konate, Q.N. Nguyen, G.K. McMaster, R. Brasseur, F. Heitz, G. Divita, A new potent secondary amphipathic cell–penetrating peptide for siRNA delivery into mammalian cells, Molecular Therapy, 17 (2009) 95-103.
[56] S. Nishimura, S. Takahashi, H. Kamikatahira, Y. Kuroki, D.E. Jaalouk, S. O'Brien, E. Koivunen, W. Arap, R. Pasqualini, H. Nakayama, A. Kuniyasu, Combinatorial targeting of the macropinocytotic pathway in leukemia and lymphoma cells, Journal of Biological Chemistry, 283 (2008) 11752-11762.
[57] B.P. Meloni, L.M. Brookes, V.W. Clark, J.L. Cross, A.B. Edwards, R.S. Anderton, R.M. Hopkins, K. Hoffmann, N.W. Knuckey, Poly-arginine and arginine-rich peptides are neuroprotective in stroke models, Journal of Cerebral Blood Flow & Metabolism, 35 (2015) 993-1004.
[58] M. Lindgren, U. Langel, Classes and prediction of cell-penetrating peptides, Methods in molecular biology (Clifton, N.J.), 683 (2011) 3-19.
[59] I. Nakase, T. Takeuchi, G. Tanaka, S. Futaki, Methodological and cellular aspects that govern the internalization mechanisms of arginine-rich cell-penetrating peptides, Advanced Drug Delivery Reviews, 60 (2008) 598-607.
[60] S. Futaki, T. Suzuki, W. Ohashi, T. Yagami, S. Tanaka, K. Ueda, Y. Sugiura, Arginine-rich peptides. An abundant source of membrane-permeable peptides having potential as carriers for intracellular protein delivery, Journal of Biological Chemistry, 276 (2001) 5836-5840.
[61] M. Zahid, P. Robbins, Cell-Type Specific Penetrating Peptides: Therapeutic Promises and Challenges, Molecules, 20 (2015) 13055.
[62] A.D. Ragin, R.A. Morgan, J. Chmielewski, Cellular import mediated by nuclear localization signal peptide sequences, Chemistry and Biology, 9 (2002) 943-948.
[63] J. Mueller, I. Kretzschmar, R. Volkmer, P. Boisguerin, Comparison of cellular uptake using 22 CPPs in 4 different cell lines, Bioconjugate Chemistry, 19 (2008) 2363-2374.
[64] M.C. Morris, L. Chaloin, J. Méry, F. Heitz, G. Divita, A novel potent strategy for gene delivery using a single peptide vector as a carrier, Nucleic acids research, 27 (1999) 3510-3517.
[65] U. Langel, Cell-penetrating peptides: processes and applications, CRC press, 2002.
[66] S. Deshayes, T. Plénat, G. Aldrian-Herrada, G. Divita, C. Le Grimellec, F. Heitz, Primary amphipathic cell-penetrating peptides: structural requirements and interactions with model membranes, Biochemistry, 43 (2004) 7698-7706.
[67] Y.H. Nan, I.S. Park, K.S. Hahm, S.Y. Shin, Antimicrobial activity, bactericidal mechanism and LPS-neutralizing activity of the cell-penetrating peptide pVEC and its analogs, Journal of Peptide Science, 17 (2011) 812-817.
[68] H.J. Johansson, S. El-Andaloussi, T. Holm, M. Mäe, J. Jänes, T. Maimets, Ü. Langel, Characterization of a novel Cytotoxic cell-penetrating Peptide Derived from p14ARF protein, Molecular Therapy, 16 (2008) 115-123.
[69] M. Magzoub, S. Sandgren, P. Lundberg, K. Oglęcka, J. Lilja, A. Wittrup, L.G. Eriksson, Ü. Langel, M. Belting, A. Gräslund, N-terminal peptides from unprocessed prion proteins enter cells by macropinocytosis, Biochemical and Biophysical Research Communications, 348 (2006) 379-385.
[70] A. Eguchi, S.F. Dowdy, siRNA delivery using peptide transduction domains, Trends in Pharmacological Sciences, 30 (2009) 341-345.
[71] C. Plank, W. Zauner, E. Wagner, Application of membrane-active peptides for drug and gene delivery across cellular membranes, Advanced Drug Delivery Reviews, 34 (1998) 21-35.
[72] B.N. Taylor, R.R. Mehta, T. Yamada, F. Lekmine, K. Christov, A.M. Chakrabarty, A. Green, L. Bratescu, A. Shilkaitis, C.W. Beattie, T.K. Das Gupta, Noncationic peptides obtained from azurin preferentially enter cancer cells, Cancer Research, 69 (2009) 537-546.
[73] J.A. Gomez, V. Gama, T. Yoshida, W. Sun, P. Hayes, K. Leskov, D. Boothman, S. Matsuyama, Bax-inhibiting peptides derived from Ku70 and cell-penetrating pentapeptides, Biochemical Society Transactions, 35 (2007) 797-801.

[74] J.A. Gomez, J. Chen, J. Ngo, D. Hajkova, I.J. Yeh, V. Gama, M. Miyagi, S. Matsuyama, Cell-penetrating penta-peptides (CPP5s): Measurement of cell entry and protein-transduction activity, Pharmaceuticals, 3 (2010) 3594-3613.
[75] L.D. Walensky, A.L. Kung, I. Escher, T.J. Malia, S. Barbuto, R.D. Wright, G. Wagner, G.L. Verdine, S.J. Korsmeyer, Activation of apoptosis in vivo by a hydrocarbon-stapled BH3 helix, Science, 305 (2004) 1466-1470.
[76] F. Bernal, A.F. Tyler, S.J. Korsmeyer, L.D. Walensky, G.L. Verdine, Reactivation of the p53 tumor suppressor pathway by a stapled p53 peptide, Journal of the American Chemical Society, 129 (2007) 2456-2457.
[77] J.D. Ochocki, D.G. Mullen, E.V. Wattenberg, M.D. Distefano, Evaluation of a cell penetrating prenylated peptide lacking an intrinsic fluorophore via in situ click reaction, Bioorganic and Medicinal Chemistry Letters, 21 (2011) 4998-5001.
[78] L. Covic, A.L. Gresser, J. Talavera, S. Swift, A. Kuliopulos, Activation and inhibition of G protein-coupled receptors by cell-penetrating membrane-tethered peptides, Proceedings of the National Academy of Sciences of the United States of America, 99 (2002) 643-648.
[79] C. Gao, S. Mao, H.J. Ditzel, L. Farnaes, P. Wirsching, R.A. Lerner, K.D. Janda, A cell-penetrating peptide from a novel pVII–pIX phage-displayed random peptide library, Bioorganic & Medicinal Chemistry, 10 (2002) 4057-4065.
[80] F. Nakayama, T. Yasuda, S. Umeda, M. Asada, T. Imamura, V. Meineke, M. Akashi, Fibroblast Growth Factor-12 (FGF12) Translocation into Intestinal Epithelial Cells Is Dependent on a Novel Cell-penetrating Peptide Domain: INVOLVEMENT OF INTERNALIZATION IN THE IN VIVO ROLE OF EXOGENOUS FGF12, The Journal of Biological Chemistry, 286 (2011) 25823-25834.
[81] F. Madani, S. Lindberg, Ü. Langel, S. Futaki, A. Gräslund, Mechanisms of Cellular Uptake of Cell-Penetrating Peptides, Journal of Biophysics, 2011 (2011) 414729.
[82] S.B. Fonseca, M.P. Pereira, S.O. Kelley, Recent advances in the use of cell-penetrating peptides for medical and biological applications, Advanced Drug Delivery Reviews, 61 (2009) 953-964.
[83] S. Trabulo, A.L. Cardoso, M. Mano, M.C.P. de Lima, Cell-penetrating peptides-mechanisms of cellular uptake and generation of delivery systems, Pharmaceuticals, 3 (2010) 961-993.
[84] P.E.G. Thorén, D. Persson, P. Isakson, M. Goksör, A. Önfelt, B. Nordén, Uptake of analogs of penetratin, Tat(48–60) and oligoarginine in live cells, Biochemical and Biophysical Research Communications, 307 (2003) 100-107.
[85] J.B. Rothbard, T.C. Jessop, R.S. Lewis, B.A. Murray, P.A. Wender, Role of membrane potential and hydrogen bonding in the mechanism of translocation of guanidinium-rich peptides into cells, Journal of the American Chemical Society, 126 (2004) 9506-9507.
[86] S. Kawamoto, M. Takasu, T. Miyakawa, R. Morikawa, T. Oda, S. Futaki, H. Nagao, Inverted micelle formation of cell-penetrating peptide studied by coarse-grained simulation: Importance of attractive force between cell-penetrating peptides and lipid head group, The Journal of chemical physics, 134 (2011) 03B604.
[87] D. Sengupta, H. Leontiadou, A.E. Mark, S.-J. Marrink, Toroidal pores formed by antimicrobial peptides show significant disorder, Biochimica et Biophysica Acta (BBA) - Biomembranes, 1778 (2008) 2308-2317.
[88] L. Yang, T.A. Harroun, T.M. Weiss, L. Ding, H.W. Huang, Barrel-stave model or toroidal model? A case study on melittin pores, Biophysical Journal, 81 (2001) 1475-1485.
[89] H. Sato, J.B. Feix, Peptide–membrane interactions and mechanisms of membrane destruction by amphipathic α-helical antimicrobial peptides, Biochimica et Biophysica Acta (BBA) - Biomembranes, 1758 (2006) 1245-1256.
[90] M. Lindberg, H. Biverståhl, A. Gräslund, L. Mäler, Structure and positioning comparison of two variants of penetratin in two different membrane mimicking systems by NMR, European Journal of Biochemistry, 270 (2003) 3055-3063.

[91] Z.O. Shenkarev, A.S. Paramonov, E.N. Lyukmanova, A.K. Gizatullina, A.V. Zhuravleva, A.A. Tagaev, Z.A. Yakimenko, I.N. Telezhinskaya, M.P. Kirpichnikov, T.V. Ovchinnikova, Peptaibol Antiamoebin I: Spatial Structure, Backbone Dynamics, Interaction with Bicelles and Lipid-Protein Nanodiscs, and Pore Formation in Context of Barrel-Stave Model, Chemistry & biodiversity, 10 (2013) 838-863.
[92] K. Matsuzaki, S. Yoneyama, O. Murase, K. Miyajima, Transbilayer transport of ions and lipids coupled with mastoparan X translocation, Biochemistry, 35 (1996) 8450-8456.
[93] W.C. Wimley, Describing the mechanism of antimicrobial peptide action with the interfacial activity model, ACS Chemical Biology, 5 (2010) 905-917.
[94] Y. Shai, Mechanism of the binding, insertion and destabilization of phospholipid bilayer membranes by α-helical antimicrobial and cell non-selective membrane-lytic peptides, Biochimica et Biophysica Acta (BBA)-Biomembranes, 1462 (1999) 55-70.
[95] K. Matsuzaki, Why and how are peptide–lipid interactions utilized for self-defense? Magainins and tachyplesins as archetypes, Biochimica et Biophysica Acta (BBA)-Biomembranes, 1462 (1999) 1-10.
[96] J.P. Lim, P.A. Gleeson, Macropinocytosis: an endocytic pathway for internalising large gulps, Immunology and cell biology, 89 (2011) 836-843.
[97] I.M. Kaplan, J.S. Wadia, S.F. Dowdy, Cationic TAT peptide transduction domain enters cells by macropinocytosis, Journal of Controlled Release, 102 (2005) 247-253.
[98] S. Pujals, E. Giralt, Proline-rich, amphipathic cell-penetrating peptides, Advanced Drug Delivery Reviews, 60 (2008) 473-484.
[99] S.A. Mousavi, L. Malerød, B. Trond, R. Kjeken, Clathrin-dependent endocytosis, Biochemical Journal, 377 (2004) 1-16.
[100] H.T. McMahon, I.G. Mills, COP and clathrin-coated vesicle budding: different pathways, common approaches, Current opinion in cell biology, 16 (2004) 379-391.
[101] J.P. Richard, K. Melikov, H. Brooks, P. Prevot, B. Lebleu, L.V. Chernomordik, Cellular uptake of unconjugated TAT peptide involves clathrin-dependent endocytosis and heparan sulfate receptors, Journal of Biological Chemistry, 280 (2005) 15300-15306.
[102] C. Palm, M. Jayamanne, M. Kjellander, M. Hällbrink, Peptide degradation is a critical determinant for cell-penetrating peptide uptake, Biochimica et Biophysica Acta (BBA)-Biomembranes, 1768 (2007) 1769-1776.
[103] E. Vivès, J. Schmidt, A. Pèlegrin, Cell-penetrating and cell-targeting peptides in drug delivery, Biochimica et Biophysica Acta (BBA) - Reviews on Cancer, 1786 (2008) 126-138.
[104] A. El-Aneed, An overview of current delivery systems in cancer gene therapy, Journal of Controlled Release, 94 (2004) 1-14.
[105] S. Pujals, J. Fernández-Carneado, C. López-Iglesias, M.J. Kogan, E. Giralt, Mechanistic aspects of CPP-mediated intracellular drug delivery: relevance of CPP self-assembly, Biochimica et Biophysica Acta (BBA)-Biomembranes, 1758 (2006) 264-279.
[106] S. El-Andaloussi, T. Holm, U. Langel, Cell-penetrating peptides: mechanisms and applications, Current pharmaceutical design, 11 (2005) 3597-3611.
[107] Y. Li, X. Zheng, Z. Cao, W. Xu, J. Zhang, M. Gong, Self-assembled peptide (CADY-1) improved the clinical application of doxorubicin, International Journal of Pharmaceutics, 434 (2012) 209-214.
[108] S. Deshayes, M. Morris, F. Heitz, G. Divita, Delivery of proteins and nucleic acids using a non-covalent peptide-based strategy, Advanced Drug Delivery Reviews, 60 (2008) 537-547.
[109] F. Heitz, M.C. Morris, G. Divita, Twenty years of cell-penetrating peptides: from molecular mechanisms to therapeutics, British Journal of Pharmacology, 157 (2009) 195-206.
[110] W. Lin, X. Xie, J. Deng, H. Liu, Y. Chen, X. Fu, H. Liu, Y. Yang, Cell-penetrating peptide-doxorubicin conjugate loaded NGR-modified nanobubbles for ultrasound triggered drug delivery, Journal of drug targeting, 24 (2016) 134-146.

[111] E.A. Dubikovskaya, S.H. Thorne, T.H. Pillow, C.H. Contag, P.A. Wender, Overcoming multidrug resistance of small-molecule therapeutics through conjugation with releasable octaarginine transporters, Proceedings of the National Academy of Sciences of the United States of America, 105 (2008) 12128-12133.
[112] J.B. Rothbard, S. Garlington, Q. Lin, T. Kirschberg, E. Kreider, P.L. McGrane, P.A. Wender, P.A. Khavari, Conjugation of arginine oligomers to cyclosporin A facilitates topical delivery and inhibition of inflammation, Nature Medicine, 6 (2000) 1253-1257.
[113] M. Lindgren, K. Rosenthal-Aizman, K. Saar, E. Eiríksdóttir, Y. Jiang, M. Sassian, P. Östlund, M. Hällbrink, U. Langel, Overcoming methotrexate resistance in breast cancer tumour cells by the use of a new cell-penetrating peptide, Biochemical Pharmacology, 71 (2006) 416-425.
[114] N.-Q. Shi, W. Gao, B. Xiang, X.-R. Qi, Enhancing cellular uptake of activable cell-penetrating peptide-doxorubicin conjugate by enzymatic cleavage, Int J Nanomedicine, 7 (2012) 1613-1621.
[115] C. Rousselle, P. Clair, J.-M. Lefauconnier, M. Kaczorek, J.-M. Scherrmann, J. Temsamani, New advances in the transport of doxorubicin through the blood-brain barrier by a peptide vector-mediated strategy, Molecular pharmacology, 57 (2000) 679-686.
[116] E.A. Dubikovskaya, S.H. Thorne, T.H. Pillow, C.H. Contag, P.A. Wender, Overcoming multidrug resistance of small-molecule therapeutics through conjugation with releasable octaarginine transporters, Proceedings of the National Academy of Sciences, 105 (2008) 12128-12133.
[117] M. Lindgren, K. Rosenthal-Aizman, K. Saar, E. Eiríksdóttir, Y. Jiang, M. Sassian, P. Östlund, M. Hällbrink, Ü. Langel, Overcoming methotrexate resistance in breast cancer tumour cells by the use of a new cell-penetrating peptide, Biochemical Pharmacology, 71 (2006) 416-425.
[118] A.M. Storniolo, S.R. Allerheiligen, H.L. Pearce, Preclinical, pharmacologic, and phase I studies of gemcitabine, Seminars in oncology, 24 (1997) S7-2-S7-27.
[119] N. Suzuki, S. Hazama, T. Ueno, H. Matsui, Y. Shindo, M. Iida, K. Yoshimura, S. Yoshino, K. Takeda, M. Oka, A Phase I Clinical Trial of Vaccination With KIF20A-derived Peptide in Combination With Gemcitabine For Patients With Advanced Pancreatic Cancer, Journal of Immunotherapy (Hagerstown, Md. : 1997), 37 (2014) 36-42.
[120] C.T. McCusker, Y. Wang, J. Shan, M.W. Kinyanjui, A. Villeneuve, H. Michael, E.D. Fixman, Inhibition of experimental allergic airways disease by local application of a cell-penetrating dominant-negative STAT-6 peptide, Journal of Immunology, 179 (2007) 2556-2564.
[121] M. Hollstein, M. Hergenhahn, Q. Yang, H. Bartsch, Z.-Q. Wang, P. Hainaut, New approaches to understanding p53 gene tumor mutation spectra, Mutation Research/Fundamental and Molecular Mechanisms of Mutagenesis, 431 (1999) 199-209.
[122] E.L. Snyder, B.R. Meade, C.C. Saenz, S.F. Dowdy, Treatment of Terminal Peritoneal Carcinomatosis by a Transducible p53-Activating Peptide, PLoS Biology, 2 (2004) e36.
[123] J. Michl, B. Scharf, A. Schmidt, C. Huynh, R. Hannan, H. Von Gizycki, F.K. Friedman, P. Brandt-Rauf, R.L. Fine, M.R. Pincus, PNC-28, a p53-derived peptide that is cytotoxic to cancer cells, blocks pancreatic cancer cell growth in vivo, International journal of cancer, 119 (2006) 1577-1585.
[124] R.S. Hotchkiss, P.E. Swanson, B.D. Freeman, K.W. Tinsley, J.P. Cobb, G.M. Matuschak, T.G. Buchman, I.E. Karl, Apoptotic cell death in patients with sepsis, shock, and multiple organ dysfunction, Critical Care Medicine, 27 (1999) 1230-1251.
[125] R.S. Hotchkiss, K.W. McConnell, K. Bullok, C.G. Davis, K.C. Chang, S.J. Schwulst, J.C. Dunne, G.P.H. Dietz, M. Bähr, J.E. McDunn, I.E. Karl, T.H. Wagner, J.P. Cobb, C.M. Coopersmith, D. Piwnica-Worms, TAT-BH4 and TAT-Bcl-xL peptides protect against sepsis-induced lymphocyte apoptosis in vivo, Journal of Immunology, 176 (2006) 5471-5477.
[126] R.P. Bennett, B. Dalby, Protein delivery using VP22 [3], Nature Biotechnology, 20 (2002) 20.

[127] J. Bian, Z.B. Popović, C. Benejam, M. Kiedrowski, L.L. Rodriguez, M.S. Penn, Effect of cell-based intercellular delivery of transcription factor GATA4 on ischemic cardiomyopathy, Circulation Research, 100 (2007) 1626-1633.
[128] E. Bleifuss, T. Kammertoens, A. Hutloff, D. Quarcoo, M. Dorner, P. Straub, W. Uckert, E. Hildt, The translocation motif of hepatitis B virus improves protein vaccination, Cellular and Molecular Life Sciences, 63 (2006) 627-635.
[129] R. Kanasty, J.R. Dorkin, A. Vegas, D. Anderson, Delivery materials for siRNA therapeutics, Nature materials, 12 (2013) 967-977.
[130] C.E. Thomas, A. Ehrhardt, M.A. Kay, Progress and problems with the use of viral vectors for gene therapy, Nature Reviews Genetics, 4 (2003) 346-358.
[131] S. Trabulo, A.L. Cardoso, M. Mano, M.C.P. De Lima, Cell-penetrating peptides—mechanisms of cellular uptake and generation of delivery systems, Pharmaceuticals, 3 (2010) 961-993.
[132] S.D. Patil, D.G. Rhodes, D.J. Burgess, DNA-based therapeutics and DNA delivery systems: a comprehensive review, The AAPS journal, 7 (2005) E61-E77.
[133] S.F. Ye, M.M. Tian, T.X. Wang, L. Ren, D. Wang, L.H. Shen, T. Shang, Synergistic effects of cell-penetrating peptide Tat and fusogenic peptide HA2-enhanced cellular internalization and gene transduction of organosilica nanoparticles, Nanomedicine: Nanotechnology, Biology, and Medicine, 8 (2012) 833-841.
[134] D.J. Glover, H.J. Lipps, D.A. Jans, Towards safe, non-viral therapeutic gene expression in humans, Nature Reviews Genetics, 6 (2005) 299-310.
[135] A. Bolhassani, Potential efficacy of cell-penetrating peptides for nucleic acid and drug delivery in cancer, Biochimica et biophysica acta, 1816 (2011) 232-246.
[136] B.R. Liu, M.D. Lin, H.J. Chiang, H.J. Lee, Arginine-rich cell-penetrating peptides deliver gene into living human cells, Gene, 505 (2012) 37-45.
[137] K.-L. Veiman, I. Mäger, K. Ezzat, H. Margus, T.n. Lehto, K. Langel, K. Kurrikoff, P. Arukuusk, J. Suhorutšenko, K.r. Padari, PepFect14 peptide vector for efficient gene delivery in cell cultures, Molecular pharmaceutics, 10 (2012) 199-210.
[138] J.H. Lin, M. Yamazaki, Role of P-glycoprotein in pharmacokinetics, Clinical pharmacokinetics, 42 (2003) 59-98.
[139] A. Astriab-Fisher, D.S. Sergueev, M. Fisher, B.R. Shaw, R.L. Juliano, Antisense inhibition of P-glycoprotein expression using peptide–oligonucleotide conjugates, Biochemical Pharmacology, 60 (2000) 83-90.
[140] M. Antopolsky, E. Azhayeva, U. Tengvall, S. Auriola, I. Jääskeläinen, S. Rönkkö, P. Honkakoski, A. Urtti, H. Lönnberg, A. Azhayev, Peptide− oligonucleotide phosphorothioate conjugates with membrane translocation and nuclear localization properties, Bioconjugate Chemistry, 10 (1999) 598-606.
[141] S. Mocellin, M. Provenzano, RNA interference: learning gene knock-down from cell physiology, Journal of translational medicine, 2 (2004) 39.
[142] E.J. Sontheimer, Assembly and function of RNA silencing complexes, Nature Reviews Molecular Cell Biology, 6 (2005) 127-138.
[143] T.J. Davidson, S. Harel, V.A. Arboleda, G.F. Prunell, M.L. Shelanski, L.A. Greene, C.M. Troy, Highly efficient small interfering RNA delivery to primary mammalian neurons induces microRNA-like effects before mRNA degradation, Journal of Neuroscience, 24 (2004) 10040-10046.
[144] Y.L. Chiu, A. Ali, C.Y. Chu, H. Cao, T.M. Rana, Visualizing a correlation between siRNA localization, cellular uptake, and RNAi in living cells, Chemistry and Biology, 11 (2004) 1165-1175.
[145] S.A. Moschos, S.W. Jones, M.M. Perry, A.E. Williams, J.S. Erjefalt, J.J. Turner, P.J. Barnes, B.S. Sproat, M.J. Gait, M.A. Lindsay, Lung delivery studies using siRNA conjugated to TAT(48-

60) and penetratin reveal peptide induced reduction in gene expression and induction of innate immunity, Bioconjugate Chemistry, 18 (2007) 1450-1459.
[146] J. Fominaya, J. Bravo, A. Rebollo, Strategies to stabilize cell penetrating peptides for in vivo applications, Therapeutic delivery, 6 (2015) 1171-1194.
[147] E.J.B. Nielsen, S. Yoshida, N. Kamei, R. Iwamae, E.-S. Khafagy, J. Olsen, U.L. Rahbek, B.L. Pedersen, K. Takayama, M. Takeda-Morishita, In vivo proof of concept of oral insulin delivery based on a co-administration strategy with the cell-penetrating peptide penetratin, Journal of Controlled Release, 189 (2014) 19-24.
[148] E.-S. Khafagy, M. Morishita, N. Kamei, Y. Eda, Y. Ikeno, K. Takayama, Efficiency of cell-penetrating peptides on the nasal and intestinal absorption of therapeutic peptides and proteins, International Journal of Pharmaceutics, 381 (2009) 49-55.
[149] R. Rennert, C. Wespe, A.G. Beck-Sickinger, I. Neundorf, Developing novel hCT derived cell-penetrating peptides with improved metabolic stability, Biochimica et Biophysica Acta (BBA) - Biomembranes, 1758 (2006) 347-354.
[150] C. Foerg, K.M. Weller, H. Rechsteiner, H.M. Nielsen, J. Fernández-Carneado, R. Brunisholz, E. Giralt, H.P. Merkle, Metabolic cleavage and translocation efficiency of selected cell penetrating peptides: a comparative study with epithelial cell cultures, The AAPS journal, 10 (2008) 349-359.
[151] X. Jing, M.R. Kasimova, A.H. Simonsen, L. Jorgensen, M. Malmsten, H. Franzyk, C. Foged, H.M. Nielsen, Interaction of peptidomimetics with bilayer membranes: biophysical characterization and cellular uptake, Langmuir, 28 (2012) 5167-5175.
[152] X. Jing, M. Yang, M.R. Kasimova, M. Malmsten, H. Franzyk, L. Jorgensen, C. Foged, H.M. Nielsen, Membrane adsorption and binding, cellular uptake and cytotoxicity of cell-penetrating peptidomimetics with α-peptide/β-peptoid backbone: Effects of hydrogen bonding and α-chirality in the β-peptoid residues, Biochimica et Biophysica Acta (BBA) - Biomembranes, 1818 (2012) 2660-2668.
[153] K. Saar, M. Lindgren, M. Hansen, E. Eiríksdóttir, Y. Jiang, K. Rosenthal-Aizman, M. Sassian, Ü. Langel, Cell-penetrating peptides: A comparative membrane toxicity study, Analytical Biochemistry, 345 (2005) 55-65.
[154] M. Zorko, Ü. Langel, Cell-penetrating peptides: mechanism and kinetics of cargo delivery, Advanced Drug Delivery Reviews, 57 (2005) 529-545.
[155] U. Soomets, M. Lindgren, X. Gallet, M. Hällbrink, A. Elmquist, L. Balaspiri, M. Zorko, M. Pooga, R. Brasseur, Ü. Langel, Deletion analogues of transportan, Biochimica et Biophysica Acta (BBA)-Biomembranes, 1467 (2000) 165-176.
[156] S. El-Andaloussi, P. Järver, H.J. Johansson, Ü. Langel, Cargo-dependent cytotoxicity and delivery efficacy of cell-penetrating peptides: a comparative study, Biochemical Journal, 407 (2007) 285-292.
[157] A. Hansen, I. Schäfer, D. Knappe, P. Seibel, R. Hoffmann, Intracellular toxicity of proline-rich antimicrobial peptides shuttled into mammalian cells by the cell-penetrating peptide penetratin, Antimicrobial agents and chemotherapy, 56 (2012) 5194-5201.
[158] F.W. Lichtenthaler, Emil Fischer, his personality, his achievements, and his scientific progeny, European Journal of Organic Chemistry, 2002 (2002) 4095-4122.
[159] G.W. Anderson, A.C. McGregor, t-Butyloxycarbonylamino acids and their use in peptide synthesis, Journal of the American Chemical Society, 79 (1957) 6180-6183.
[160] R.B. Merrifield, Solid phase peptide synthesis. I. The synthesis of a tetrapeptide, Journal of the American Chemical Society, 85 (1963) 2149-2154.
[161] V.d. Vigneaud, C. Ressler, C.J.M. Swan, C.W. Roberts, P.G. Katsoyannis, S. Gordon, The synthesis of an octapeptide amide with the hormonal activity of oxytocin, Journal of the American Chemical Society, 75 (1953) 4879-4880.
[162] F. Liu, A.N. Zaykov, J.J. Levy, R.D. DiMarchi, J.P. Mayer, Chemical synthesis of peptides within the insulin superfamily, Journal of Peptide Science, (2016).

[163] K. Yoshiaki, M. YOSHIDA, T. KIMURA, Y. FUJIWARA, M. SHIMOKURA, K. AKAJI, Solution-Phase Synthesis of Porcine Brain Natriuretic Peptide (pBNP) Using S-Trimethylacetamido-methylcysteine, Chemical and Pharmaceutical Bulletin, 38 (1990) 1192-1199.
[164] D.M. Coe, R. Storer, Solution-phase combinatorial chemistry, in: Annual Reports in Combinatorial Chemistry and Molecular Diversity, Springer, 1999, pp. 1-8.
[165] V. Austel, Solution-phase combinatorial chemistry, Combinatorial Chemistry: Synthesis, Analysis and Screening, (1999).
[166] R. Gedye, F. Smith, K. Westaway, H. Ali, L. Baldisera, L. Laberge, J. Rousell, The use of microwave ovens for rapid organic synthesis, Tetrahedron letters, 27 (1986) 279-282.
[167] A. Loupy, Microwaves in organic synthesis, Wiley-VCh, 2006.
[168] L.A. Carpino, G.Y. Han, 9-Fluorenylmethoxycarbonyl function, a new base-sensitive amino-protecting group, Journal of the American Chemical Society, 92 (1970) 5748-5749.
[169] C.-C. Chen, B. Rajagopal, X.Y. Liu, K.L. Chen, Y.-C. Tyan, F. Lin, P.-C. Lin, A mild removal of Fmoc group using sodium azide, Amino acids, 46 (2014) 367-374.
[170] S. Routier, L. Saugé, N. Ayerbe, G. Coudert, J.-Y. Mérour, A mild and selective method for N-Boc deprotection, Tetrahedron letters, 43 (2002) 589-591.
[171] S. Chen, K.D. Janda, Total synthesis of naturally occurring prostaglandin F 2α on a non-cross-linked polystyrene support, Tetrahedron letters, 39 (1998) 3943-3946.
[172] B. Gutte, R. Merrifield, The synthesis of ribonuclease A, Journal of Biological Chemistry, 246 (1971) 1922-1941.
[173] M. Stawikowski, G.B. Fields, Introduction to peptide synthesis, Current protocols in protein science, (2012) 18.11. 11-18.11. 13.
[174] G.S. Vanier, Microwave-assisted solid-phase peptide synthesis based on the Fmoc protecting group strategy (CEM), Peptide Synthesis and Applications, (2013) 235-249.
[175] A. Basso, L. Sinigoi, L. Gardossi, S. Flitsch, Effect of microwave radiation on enzymatic and chemical peptide bond synthesis on solid phase, International journal of peptides, 2009 (2009).
[176] B. Hayes, Microwave Synthesis: Chemistry at the Speed of Light 2002, CEM: Matthews, NC, (2006).
[177] A. de la Hoz, A. Loupy, Microwaves in organic synthesis, 2 volume set, John Wiley & Sons, 2013.
[178] L.A. Carpino, G.Y. Han, 9-Fluorenylmethoxycarbonyl amino-protecting group, The Journal of Organic Chemistry, 37 (1972) 3404-3409.
[179] L.A. Carpino, The 9-fluorenylmethyloxycarbonyl family of base-sensitive amino-protecting groups, Accounts of Chemical Research, 20 (1987) 401-407.
[180] J.C. Sheehan, G.P. Hess, A new method of forming peptide bonds, Journal of the American Chemical Society, 77 (1955) 1067-1068.
[181] G. Windridge, E.C. Jorgensen, 1-Hydroxybenzotriazole as a racemization-suppressing reagent for the incorporation of im-benzyl-L-histidine into peptides, Journal of the American Chemical Society, 93 (1971) 6318-6319.
[182] D.H. Rich, J. Singh, The carbodiimide method, The peptides, 1 (2014) 241-261.
[183] C. Roche, M. Pucheault, M. Vaultier, A. Commerçon, Onium salt supported peptide synthesis, Tetrahedron, 66 (2010) 8325-8334.
[184] L.C. Chan, B.G. Cox, Kinetics of amide formation through carbodiimide/N-hydroxybenzotriazole (HOBt) couplings, The Journal of Organic Chemistry, 72 (2007) 8863-8869.
[185] L.A. Carpino, 1-Hydroxy-7-azabenzotriazole. An efficient peptide coupling additive, Journal of the American Chemical Society, 115 (1993) 4397-4398.
[186] B. Castro, J. Dormoy, " AZIDO-TRIS-DIMETHYLAMINOPHOSPHONIUM HEXAFLUOROPHOSPHATE-EXCELLENT REAGENT FOR PEPTIDE COUPLING, BULLETIN DE LA SOCIETE CHIMIQUE DE FRANCE PARTIE II-CHIMIE MOLECULAIRE ORGANIQUE ET BIOLOGIQUE, (1973) 3359-3361.

[187] J. Coste, D. Le-Nguyen, B. Castro, PyBOP®: A new peptide coupling reagent devoid of toxic by-product, Tetrahedron letters, 31 (1990) 205-208.
[188] S.-Y. Han, Y.-A. Kim, Recent development of peptide coupling reagents in organic synthesis, Tetrahedron, 60 (2004) 2447-2467.
[189] F. Albericio, J.M. Bofill, A. El-Faham, S.A. Kates, Use of Onium Salt-Based Coupling Reagents in Peptide Synthesis1, The Journal of Organic Chemistry, 63 (1998) 9678-9683.
[190] R. Behrendt, P. White, J. Offer, Advances in Fmoc solid-phase peptide synthesis, Journal of Peptide Science, 22 (2016) 4-27.
[191] M. Amblard, J.-A. Fehrentz, J. Martinez, G. Subra, Methods and protocols of modern solid phase peptide synthesis, Molecular biotechnology, 33 (2006) 239-254.
[192] B.C. Evans, C.E. Nelson, S.S. Yu, K.R. Beavers, A.J. Kim, H. Li, H.M. Nelson, T.D. Giorgio, C.L. Duvall, Ex Vivo Red Blood Cell Hemolysis Assay for the Evaluation of pH-responsive Endosomolytic Agents for Cytosolic Delivery of Biomacromolecular Drugs, Jove-Journal of Visualized Experiments, (2013) 1-5.
[193] K.M. Roth, K. Peyvan, K.R. Schwarzkopf, A. Ghindilis, Electrochemical detection of short DNA oligomer hybridization using the CombiMatrix ElectraSense Microarray reader, Electroanalysis, 18 (2006) 1982-1988.
[194] R. Wyatt, P.D. Kwong, E. Desjardins, R.W. Sweet, J. Robinson, W.A. Hendrickson, J.G. Sodroski, The antigenic structure of the HIV gp120 envelope glycoprotein, Nature, 393 (1998) 705-711.
[195] B. Stein, E. Engleman, Intracellular processing of the gp160 HIV-1 envelope precursor. Endoproteolytic cleavage occurs in a cis or medial compartment of the Golgi complex, Journal of Biological Chemistry, 265 (1990) 2640-2649.
[196] R.L. Willey, J.S. Bonifacino, B.J. Potts, M.A. Martin, R.D. Klausner, Biosynthesis, cleavage, and degradation of the human immunodeficiency virus 1 envelope glycoprotein gp160, Proceedings of the National Academy of Sciences, 85 (1988) 9580-9584.
[197] I. Douagi, M.N. Forsell, C. Sundling, S. O'dell, Y. Feng, P. Dosenovic, Y. Li, R. Seder, K. Loré, J.R. Mascola, Influence of novel CD4 binding-defective HIV-1 envelope glycoprotein immunogens on neutralizing antibody and T-cell responses in nonhuman primates, Journal of virology, 84 (2010) 1683-1695.
[198] C.T. Wild, D.C. Shugars, T.K. Greenwell, C.B. McDanal, T.J. Matthews, Peptides corresponding to a predictive alpha-helical domain of human immunodeficiency virus type 1 gp41 are potent inhibitors of virus infection, Proceedings of the National Academy of Sciences, 91 (1994) 9770-9774.
[199] J.S. De Bono, S. Oudard, M. Ozguroglu, S. Hansen, J.-P. Machiels, I. Kocak, G. Gravis, I. Bodrogi, M.J. Mackenzie, L. Shen, Prednisone plus cabazitaxel or mitoxantrone for metastatic castration-resistant prostate cancer progressing after docetaxel treatment: a randomised open-label trial, The Lancet, 376 (2010) 1147-1154.
[200] M.F. Biancardi, F.C. Santos, L. Madi-Ravazzi, R.M. Goes, P.S. Vilamaior, S.L. Felisbino, S.R. Taboga, Testosterone promotes an anabolic increase in the rat female prostate (Skene's paraurethral gland) which acquires a male ventral prostate phenotype, The Anatomical Record, 293 (2010) 2163-2175.
[201] A.S. Prasad, Zinc: an antioxidant and anti-inflammatory agent: role of zinc in degenerative disorders of aging, Journal of Trace Elements in Medicine and Biology, 28 (2014) 364-371.
[202] L. Costello, R. Franklin, Novel role of zinc in the regulation of prostate citrate metabolism and its implications in prostate cancer, The Prostate, 35 (1998) 285-296.
[203] L.C. Costello, R.B. Franklin, J. Zou, P. Feng, R. Bok, M.G. Swanson, J. Kurhanewicz, Human prostate cancer ZIP1/zinc/citrate genetic/metabolic relationship in the TRAMP prostate cancer animal model, Cancer biology & therapy, 12 (2011) 1078-1084.

[204] F. Licausi, M. Kosmacz, D.A. Weits, B. Giuntoli, F.M. Giorgi, L.A. Voesenek, P. Perata, J.T. van Dongen, Oxygen sensing in plants is mediated by an N-end rule pathway for protein destabilization, Nature, 479 (2011) 419-422.
[205] N.W. Andrews, P.E. Almeida, M. Corrotte, Damage control: cellular mechanisms of plasma membrane repair, Trends in cell biology, 24 (2014) 734-742.
[206] S.Y. Madani, N. Naderi, O. Dissanayake, A. Tan, A.M. Seifalian, A new era of cancer treatment: carbon nanotubes as drug delivery tools, Int J Nanomedicine, 6 (2011) 2963-2979.
[207] C. Punckt, M.A. Pope, J. Liu, Y. Lin, I.A. Aksay, Electrochemical performance of graphene as effected by electrode porosity and graphene functionalization, Electroanalysis, 22 (2010) 2834-2841.
[208] S. Yamamoto, H. Ohkita, H. Benten, S. Ito, Formation mechanism of fullerene cation in bulk heterojunction polymer solar cells, Advanced Functional Materials, 22 (2012) 3075-3082.
[209] E. Heister, V. Neves, C. Tîlmaciu, K. Lipert, V.S. Beltrán, H.M. Coley, S.R.P. Silva, J. McFadden, Triple functionalisation of single-walled carbon nanotubes with doxorubicin, a monoclonal antibody, and a fluorescent marker for targeted cancer therapy, Carbon, 47 (2009) 2152-2160.